uOttawa

L'Université canadienne
Canada's university

FACULTÉ DES ÉTUDES SUPÉRIEURES ET POSTOCTORALES

uOttawa

L'Université canadienne
Canada's university

FACULTY OF GRADUATE AND POSDOCTORAL STUDIES

Behnam Shadravan

AUTEUR DE LA THÈSE / AUTHOR OF THESIS

Ph.D. (Civil Engineering)

GRADE / DEGREE

Department of Civil Engineering

FACULTÉ, ÉCOLE, DÉPARTEMENT / FACULTY, SCHOOL, DEPARTMENT

Investigation of Surface Bond Behaviour of FRP Sheets on Concrete and Masonry Substrates

TITRE DE LA THÈSE / TITLE OF THESIS

Murat Saatcioglu

DIRECTEUR (DIRECTRICE) DE LA THÈSE / THESIS SUPERVISOR

CO-DIRECTEUR (CO-DIRECTRICE) DE LA THÈSE / THESIS CO-SUPERVISOR

Hassan Aoude

Khaled Galal (Concordia University)

Burkan Isgor

Beatriz Martin-Perez

Gary W. Slater

Le Doyen de la Faculté des études supérieures et postdoctorales / Dean of the Faculty of Graduate and Postdoctoral Studies

INVESTIGATION OF SURFACE BOND BEHAVIOUR OF FRP SHEETS ON CONCRETE AND MASONRY SUBSTRATES

By

Behnam Shadravan

A thesis submitted to
the Faculty of Graduate Studies and Research
in partial fulfillment of
the requirement for the degree of

DOCTOR OF PHILOSOPHY

in Civil engineering*

Department of Civil Engineering
University of Ottawa
Ottawa, Ontario, Canada

December 2009

*The Ph.D in civil engineering is a joint program with the Carleton University, administrated by the Ottawa-Carleton Institute for Civil Engineering

Your file Votre référence
ISBN: 978-0-494-69115-1
Our file Notre référence
ISBN: 978-0-494-69115-1

ACKNOWLEDGEMENT

I wish to thank my research supervisor Dr. Murat Saatcioglu for his technical guidance and the tremendous amount of time dedicated in the realization of this research project and thesis. My appreciation also extends to include the care, advice and financial support Dr Saatcioglu has provided throughout my doctoral studies. His constructive criticisms and suggestions were vital for the successful conclusion of this project.

I also wish to thank the Faculty of Graduate and Postdoctoral Studies at the University of Ottawa for providing me with an entrance scholarship. I particularly thank Dr. Gary Slater, the Dean of the Faculty, who supported me in every stage of the PhD program.

I wish to express my appreciation to the Faculty of Engineering and the personnel of the Department of Civil Engineering, especially to Mr. Muslim Majid, the Structures Laboratory technician, for his great help during the experimental work.

Furthermore, my warmest expressions go to my wonderful parents for providing their unconditional motivation and love during my studies in Canada.

Last, but not least, I wish to express my deepest gratitude to the person who has always provided unconditional support during the journey of my life, my best friend, my wife, and my love, Aida, who endured the demands of the doctoral program along with me.

ABSTRACT

The majority of non-ductile reinforced concrete buildings are vulnerable to extreme load effects, including those caused by strong earthquakes and blast shock waves. These buildings consist of reinforced concrete frames with and without infill masonry walls, and non-ductile shear walls. They often benefit from retrofit strategies at the system level because of the presence of a large number of poorly designed non-ductile elements. This indicates that a limited number of elements are strengthened and stiffened for deformation control, while the remaining elements remain within the elastic range of deformations during loading. One of the attractive retrofit techniques used to ensure deformation control is the use of surface bonded fibre-reinforced polymer (FRP) sheets or strips on masonry and non-ductile concrete walls for increased strength. Because FRP material itself does not possess ductility, its use in such applications is not intended for ductility enhancement.

The surface bond characteristics of FRP sheets have not been fully understood. The sheets exhibit brittle performance and often delaminate prematurely before they attain their material capacity. The current research is aimed at contributing towards the knowledge gap in this area. It consists of both experimental and analytical tasks. The experimental research consists of seventy one small-scale pull-out tests. The test variables includes, the width, length, and the number of layers of Carbon FRP (CFRP) strips; concrete compressive strength; substrate material consisting of concrete, brick and concrete blocks; and loading conditions as monotonic and cyclic loading.

The experimental data indicate that surface-bonded FRP strips on concrete and masonry substrates develop limited strength as governed by bond failure. The bond stress

shows a bell-shaped distribution, spreading over an effective bond length with a maximum bond stress that varies between 3.0 MPa and 7.0 MPa for the type of application considered in the current investigation. The FRP has an effective bond length beyond which any further increase in length does not result in a substantial increase in bond strength. This length was determined to vary between 90 mm and 115 mm for the specimens tested in this investigation. The effect of increased concrete strength on surface bond characteristics of FRP is to increase ultimate bond capacity and corresponding slip marginally, without much influence on the effective length. The effect of increased number of layers of FRP is to increase ultimate bond while decreasing slippage, with a small increase in effective bond length. The effect of the increase in FRP strip width is to increase ultimate bond force while decreasing ultimate bond strength and the corresponding slip, without much influence on the effective bond length. Cyclic loading improves surface bond characteristics of FRP, increasing ultimate load resistance by approximately a factor of 1.2 while also resulting in increases in ultimate bond stress and effective bond length. Surface bond characteristics of FRP on concrete and clay brick substrates are similar. Concrete block masonry tends to fail prematurely due to the material failure of block cell walls prior to developing bond failures.

The experimental results are used to generate and validate a new bond-slip model. Design expressions, in terms of effective bond length and ultimate load capacity, are suggested. Comparisons between the analytical and experimental results show good correlations. It is shown that the ultimate load capacity continues to increase, all be it marginally, with an increase in bond length between the effective length and twice the effective length. Therefore, it is recommended to use twice the effective length in design.

CONTENTS

LIST OF TABLES

LIST OF FIGURES

Chapter 1

INTRODUCTION

1.1. General

The main advantages of FRP sheets are their high strength to weight ratio and high corrosion resistance. The former property leads to ease in site handling, reduced labour cost, speed of construction and reductions in the interruption of existing services, while the later ensures durability and log term performance. FRP sheets are significantly stronger than steel plates, often reaching and sometimes exceeding 10 times the strength of steel with only 20% of the weight of steel (Darby, 1999).

The limited use of these materials in civil engineering applications has been due to their high cost. The cost has been coming down rapidly in recent years, enabling wider applications in the construction industry. For structural strengthening applications, where the material cost is only one consideration and may be only a small portion of the total project cost, FRP composites may provide the most cost effective solution (Hallaway and Leeming, 1999).

Wet-laid carbon FRP (CFRP) sheets and pre-cured plates have been the object of much interest in the civil engineering arena for applications on beams, slabs, and columns due to their excellent strength, durability and stiffness. Repair and strengthening with CFRP sheets or plates provides an attractive alternative to the use of steel plates, which is more labor- and equipment-intensive (Tripi *et al.* 2000).

External bonding of fibre reinforced polymer (FRP) plates or sheets has emerged over the past decade as a popular method and an efficient technique for structural

rehabilitation, repair and strengthening of deteriorated and deficient concrete components and systems (Karbhari *et al.* 2006, Meier 1997). The strengthening of reinforced concrete (RC) structures (Teng *et al.*, 2002c), and particularly seismic strengthening and retrofit applications (Shadravan *et al.*, 2007) have gain popularity in recent years.

The effectiveness of FRP repair and retrofit techniques is intrinsically dependent on the bond performance between the FRP and the substrate. For column wrapping applications, the FRP sheets often overlap and develop strong FRP to FRP bond, and the bond between the FRP and concrete becomes less important. However, surface bonded applications; as in the case of wall and beam repair, strengthening and retrofit; any failure in the bond interface can lead to the deterioration of composite action, resulting in a premature debonding failure (Karbhari *et al.* 2006).

The detailed understanding of different aspects of FRP bond characteristics on substrate material, such as failure initiation, interface bond mechanisms, and the properties of constituent materials still need to be developed in order to enable the development of cost-effective design procedures and models for service-life predictions (Karbhari *et al.* 2006). While the high tensile strength of FRP provides tremendous benefits to strengthen existing structural elements, lack of sufficient bond between the FRP and its substrate may pose design challenges because of the potential delamination of FRP prematurely. Therefore, it is essential to establish the bond characteristics of FRP sheets on substrate materials, like concrete and masonry (Shadravan *et al.*, 2007).

The behaviour of interface between FRP and concrete is a key factor in controlling debonding failures in FRP-strengthened RC structures. In such applications, the most important role of interface bond is to transfer shear stresses from existing concrete structures to externally bonded FRP sheets for both shear and flexural strengthening (Karbhari *et al.* 2006). The bond behaviour between concrete and externally glued reinforcement can be very brittle. Delamination starts at small relative displacements and may lead to local bond failures (Daus, 2004). Such failures, unless adequately considered in the design process, may significantly decrease the effectiveness of strengthening or repair application (Buyukozturk *et al.*, 2004).

1.2. Research Needs

Lack of clear understanding of interface characteristics of surface-bonded FRP sheets on concrete and masonry substrates hinders the widespread use of FRP in repair and retrofit applications. In particular, a reliable local bond–slip model is of fundamental importance for accurate modeling and understanding of FRP-strengthened RC structures (e.g. Teng *et al.* 2002c).

Most of the prior research on surface bonded FRP sheets concentrated on experimental investigations of selected parameters for modeling of bond behaviour of FRP on concrete and masonry materials. The test setup and specimen characteristics, as well as analytical approaches employed, varied among research programs. The stress state of the interface in some bond failure modes was found to be similar to that generated in pull-out test prisms on which an FRP sheet was bonded and subjected to tension. Such pull-out tests can be realized in laboratories in a number of different ways. Many bond-slip models have been developed as a result of such test programs. However, these models were typically developed on the basis of limited experimental data. A comprehensive experimental research program is needed to generate much needed test data, consisting of the parameters of surface bond conditions, including the variables that pertain to material characteristics and loading conditions. Such research program not only leads to a new behavioural model for bond strength of FRP on concrete and masonry but also provides an opportunity to complement and compare experimental data obtained earlier in similar research programs. It can also provide design recommendations for building codes and standards. Furthermore, a new standardized test procedure is needed to establish the bond behaviour of FRP on concrete, as the existing procedure outlined in CSA Standard S806 (2002) appears to be deficient. Therefore, there is need for a comprehensive test program. A thorough review of previous research and re-assessment of previously obtained test data are also needed. Such an effort can result in an analytical model, overcoming some of the shortcomings of the existing models on FRP surface bond stresses.

1.3. Objective

The objective of the current research is to investigate the performance of bond behaviour of CFRP sheets on concrete and masonry substrates, including clay brick and concrete block masonry, and to develop an analytical model for bond-slip relationship that can be used in structural engineering practice. The objective also includes the generation of design information for surface bonded FRP sheets for repair, strengthening and seismic retrofit applications.

1.4. Scope

The scope of the proposed project is as follows:

1) Literature review on previous experimental research, including test setups, methods and results.
2) Literature review on suggested analytical models and expressions for FRP bond on concrete and masonry substrates.
3) Design, construction and development of a test program for surface bonded FRP sheets and comparisons with tests conducted by others.
4) Development of a standard test setup and test procedure for surface mounted FRP bond tests.
5) Tests of concrete, clay brick and concrete block masonry prisms with surface bonded FRP sheets to generate test data on bond characteristics of FRP on different substrates.
6) Numerical evaluation of test data to establish the bond behaviour of FRP on concrete and masonry units.
7) Development of an analytical bond-slip model for FRP sheets on concrete and masonry substrates based on the experimental data generated in the current research program, as well as those collected by others.
8) Development of design recommendations for surface bonded FRP applications on concrete and masonry.

1.5. Research Contributions

The following contributions are made through the current project:

- A large volume of experimental test data on bond strength of surface bonded FRP sheets on concrete and masonry substrates has been generated, including those under cyclic loading, which is very rare in the literature.
- A new analytical model was developed for bond behaviour of FRP on concrete and masonry substrates.
- A new design methodology was devised for surface mounted FRP sheets for rehabilitation and retrofit projects.
- A new test setup and test procedure was developed for standard FRP bond tests for concrete and masonry substrates.

Chapter 2

PREVIOUS RESEARCH

Previous research conducted in the area of surface bonded FRP has been reviewed and summarized in this section. The literature review is first categorized under experimental and analytical research. The experimental research consists of two subsections, covering test methods and test results. The discussion of previously employed test methods is found to be especially relevant as test results may be influenced by the setup used. The previous analytical research is presented in terms of various methodologies employed in developing bond-slip models, as well as the design approaches recommended.

2.1. Experimental Research

Different researchers employed different test setups and methods of testing to investigate the bond behaviour and debonding failures of surface bonded FRP sheets experimentally. First, various setups used are discussed as different setups result in different loading conditions that change bond stress characteristics. Subsequently, the results of experimental research are presented, including important bond parameters, while emphasizing fundamental differences between surface-bonded FRP and conventional reinforcement embedded in concrete. The crack pattern and propagation are discussed, including other observations relevant to the experimental performance of specimens.

- **Test Setups and Methods**

The test setups previously used can be classified into four, on the basis of the type of stresses generated in concrete; i) tension ii) direct or pure shear, iii)combined shear and tension, and iv) bending. These test setups reflect the intended use of FRP for which bond behaviour is under investigation. In terms of combined bending and shear, it is difficult to directly estimate the bond characteristics of the concrete-fiber system, but it is simpler to have a shear bond test. Fig.2.1 shows some test setup types used in bond tests.

Test setups used for direct shear bond tests can be classified into two groups; Double Lap type and Single Lap type. The double lap type is implemented either as Double Shear Pull (Double Pull) tests, also called Far End Supported (FES) Double-Shear Tests, and Double Shear Push tests (Double Push), also called Near End Supported (NES) Double-Shear tests. Single lap type tests are conducted either as Single Shear Pull (Single Pull) tests, which may also be called Far End Supported (FES) Single-Shear tests, or Single Shear Pull push tests (Single Push), which may also be called near end supported (NES) single-shear tests. In all of these test setups the FRP sheet is pulled directly by a tensile force. Collectively, all these four tests may be referred to as pull tests, as the FRP is always directly pulled by a tensile force.

The "double shear pull test" and the "single shear push test" (shown as Types a and d in Fig.2.1) are the most commonly used test methods among researchers because of their simplicity (Chen *et al.* 2001, Ueda and Dai 2005, Yao *et al.* 2005, Nakaba *et al.* 2001b). However, the stress state in the concrete in each of these two test methods can be expected to be quite different. Therefore, significant difference exists between these two methods (Chen *et al.* 2001). The single shear push test offers savings in both material and labor because only one coupon is bonded to the concrete (Chen *et al.* 2001). The double pull tests are more suitable for standard universal testing machines, which enable the application of different loading procedures at different loading speeds, including cycling loading and fatigue tests. This is one reason why they are used more commonly among researchers (Van Gemert 1980; Kobatake *et al.* 1993; Autocon FORCA 1994; Yoshizawa *et al.*, 1996; Brosens and van Gemert 1997; Hiroyuki and Wu 1997; Maeda *et al.* 1997; Fuzukawa *et al.* 1997; Izumo *et al.* 1997;, Horiguchi and Saeki 1997; Ueda *et al.* 1999;

Casareto *et al.* 2003). In this test setup, two FRP sheets are bonded on opposing sides of a concrete block and equal tensile forces are applied to each sheet. These forces are balanced by a pulling force applied on concrete, which may be applied either through a steel bar embedded in concrete or through steel plates bonded on the sides of the concrete block (Chen *et al.* 2001).

The Single Push tests are the second most popular tests after the Double Pull tests. It was used by Täljsten (1994, 1997), Chajes *et al.* (1995, 1996), Bizindavyi and Neale (1997, 1999), Dai J. G., Yoshizawa *et al.* (1996), Oehlers and Seracino (2004), McSweeney and Lopez (2005), and Yao *et al.* (2005).

In a double push test (Fig.2.1b), the pushing force exerted on the concrete block is usually applied through a hydraulic jack (Swamy *et al.* 1986; Neubauer and Rostásy 1997). The stresses generated in this setup are applied through compressive forces applied on concrete, as opposed to tensile forces applied on FRP, as in the case of Double Pull test. This difference may lead to discrepancies among test results (Chen *et al.* 2001), as well as the mechanism of fracture.

The standard tests recommended in Annex P of the Canadian Standard Association's CSA S806 (2002) involves direct tension tests. Fig.2.2 shows test set-ups and tests methods recommended by CSA. Method A is a double shear pull out test. Method B is a push apart double shear test.

The Single Pull test, shown in Fig.2.1(c), has not been used in the past, though the test set-up was mentioned by Chen *et al.* (2001). In this case only one FRP sheet is bonded on one side of the concrete block. This leads, however, to a loss of symmetry, unlike the Double Pull tests (Chen *et al.* 2001).

In addition to the unidirectional tests discussed above, Fig.2.3 shows Beam Tests, conducted for the purpose of investigating the mechanism of bond in flexural members. One form of a beam test set-up, illustrated in Fig.2.3(a) consists of two pieces of concrete, connected together by a surface bonded material (steel or FRP), forming a simply supported beam, subjected to point loading. This set-up can simulate the effects of moment and shear variations along the length of the member. It was employed by van Gemert (1980) to investigate the bond behaviour of surface bonded steel plates on

concrete beams. Ziraba *et al.* (1995) also used a similar setup to investigate the effects of concrete compressive strength on steel-concrete bond strength. In this case, the researchers used a solid beam, cut a certain depth to create a weak section, with a steel sheet surface bonded over the cut as shown in Fig.2.3(b). They found no dependence of surface joint failure on concrete strength and concluded that the concrete-glue-plate interface behaviour was rather a surface phenomenon. However, this contradicted with other experimental observations (Chajes *et al.* 1996, Horiguchi and Saeki 1997, Lorenzis *et al.* 2001, Dai *et al.* 2005).

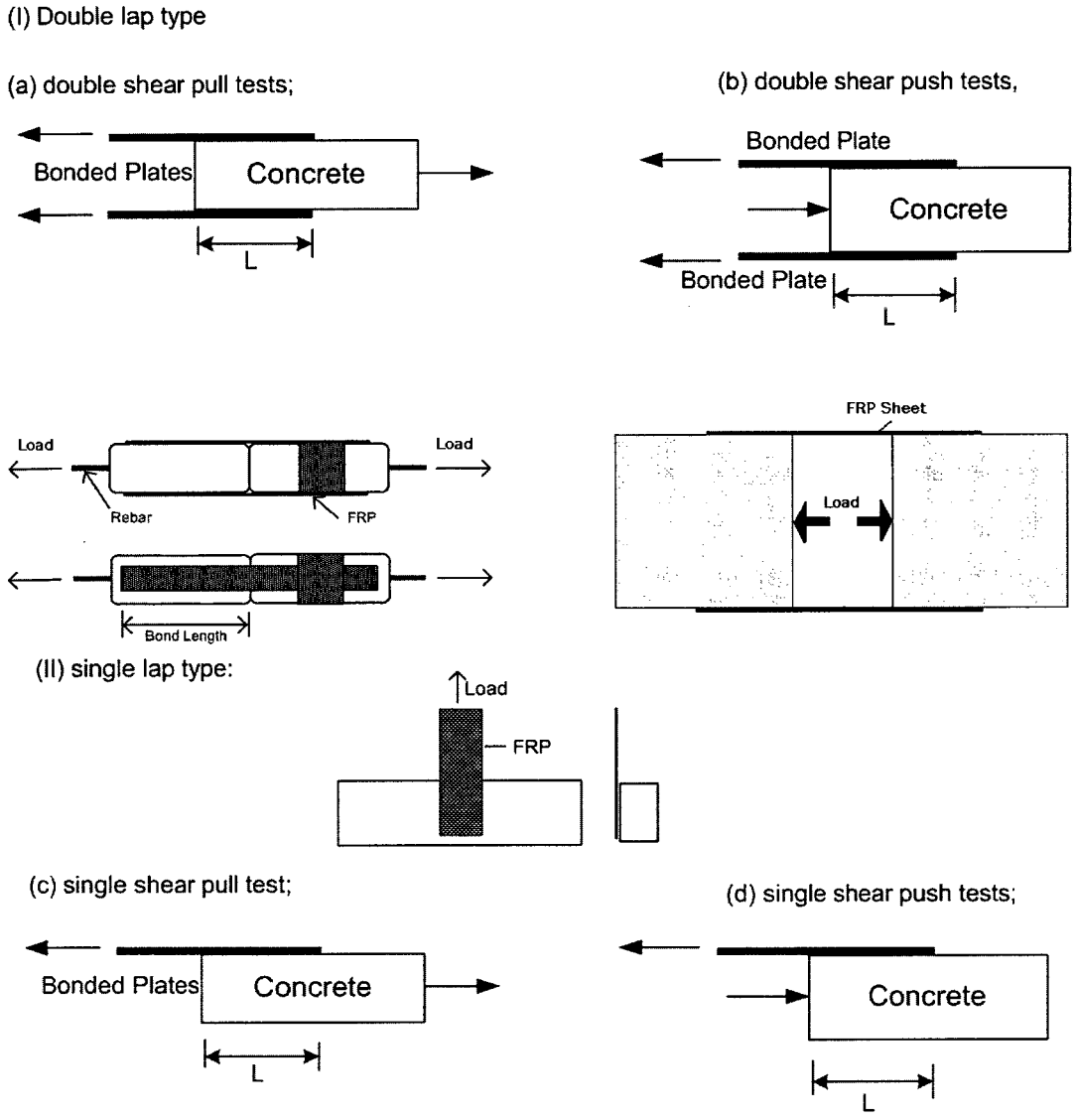

Fig. 2.1. Types of direct shear bond tests redrawn in Shadravan *et al.* 2007 (Yao *et al.* 2005, Nakaba *et al.* 2001b and Chen *et al.* 2001)

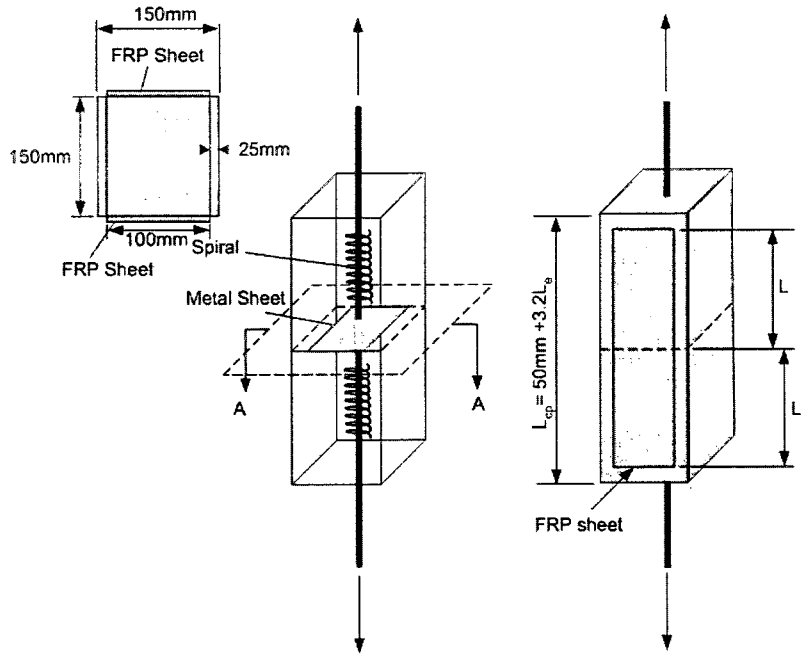

(a) Method A: double shear pull out test

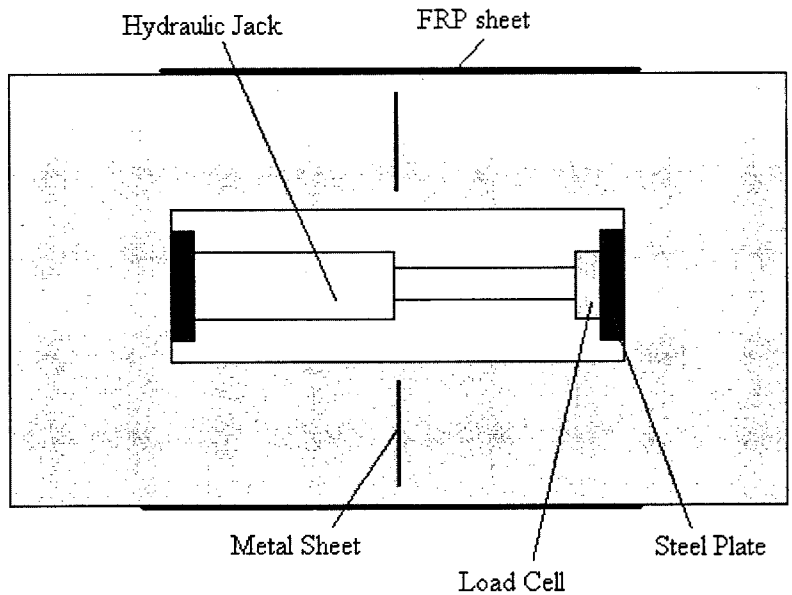

(b) Method B: push apart double shear test

Fig. 2.2. Concrete bond test (redrawn from Recommend in Annex P CSA S806-02)

In addition to the above setups and methods of testing, several other techniques were reported in the literature for subjecting interfaces to out-of-plane tension and combination of tension with shear (Chen *et al.*, 2001, Ueda *et al.*, 2003., Yao *et al.*, 2005, Nakaba, *et al.*, 2001b). The effects of test setups and testing techniques on bond were investigated in the past. Both numerical and experimental studies have been

conducted. The results indicated that the use of different test set-ups can lead to significantly different test results (Chen *et al.* 2001, Yao *et al.* 2005). Little difference can be expected between the double and single shear push tests, and between the double and single shear pull tests (Chen *et al.* 2001). Furthermore, it has also been reported that small variations in test setups within a selected method, such as the height of the support block, may also have significant effects on bond behaviour (Chen *et al.* 2001).

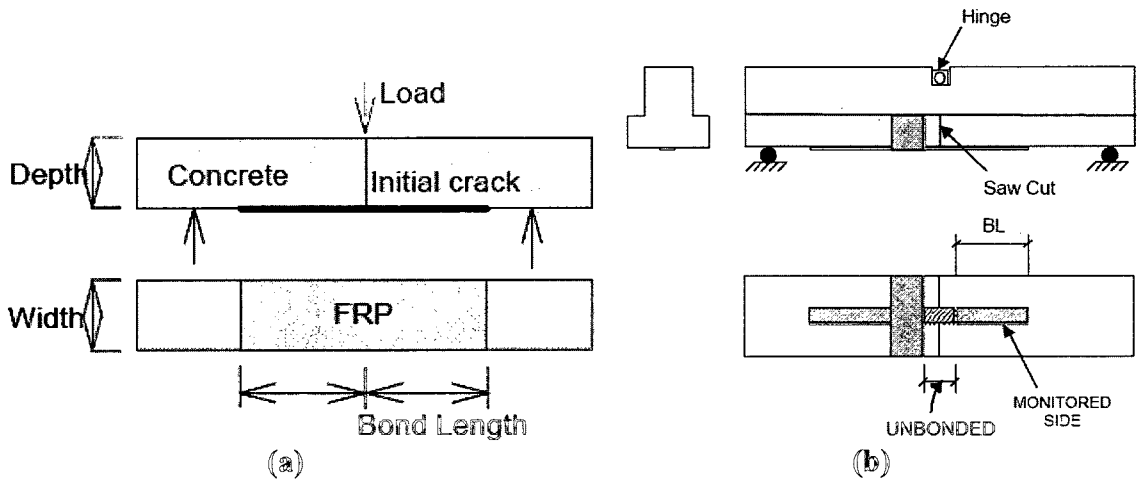

Fig. 2.3. Modified beam method re drawn from (a) Chen *et al.* (2001) (b) Lorenzis *et al.* (2001)

- **Test Results**

The bond characteristics of surface mounted FRP sheets have been a source of controversy in the past, since lack of sufficient bond between the high-strength FRP sheets and relatively low strength concrete substrate posed challenges in practical applications. A number of experimental research programs have been undertaken to assess the adequacy of bond strength. This section provides a summary of previous experimental findings, while also providing explanation of some of the behavioural aspects of surface bonded FRP sheets on concrete.

It is well established through previous experimental research that bond stresses that develop under in-plane shear are not evenly distributed throughout the bond area. Instead, higher stresses are taken up near the critical section with stresses decreasing exponentially with distance (Buyukozturk and Au, 2004). A very important aspect of the

behaviour of these bonded joints is that there exists an effective bond length beyond which an extension of the surface-bonded material length cannot increase the ultimate load resistance. This length is called "effective length" or "effective transfer length". This is the fundamental difference between externally bonded reinforcement (as in the case of surface bonded FRP) and internal reinforcement (as in internal re-bars embedded in concrete) for which a sufficiently long anchorage length can always be found to attain the full tensile strength of reinforcement. If the failure load recorded during bond tests is used to compute the average shear strength between the FRP and the concrete substrate, as was done in some of the early studies, it may result in incorrect interpretation of bond capacity as this would imply that increased bond area could lead to increased resistance, leading to the conclusion that the FRP tensile strength can always be developed if the anchorage length is long enough. In reality, tensile stresses in FRP are transferred to concrete mainly via bond stresses that develop in the adhesive (epoxy) within a short length near the applied force (Chen and Teng, 2001). Also, the existing studies suggest that the main failure mode of FRP-to-concrete joints is the bond failure of surface concrete that occurs generally within a few millimeters depth from the concrete-to-adhesive interface (Yuan *et al.* 2004). Therefore, some of the analytical research and the resulting bond strength expressions concentrated on concrete fracture mechanics and rupture energy. Bond stress-slip models play a significant role in such studies (Karbhari, *et al.* 2006). The ultimate load (i.e. the maximum transferable load) and the effective bond length of the joint depend on concrete strength. Concrete strengths; including compressive, tensile, and bond strength are used as parameters in some bond models. Indeed, the tests confirmed that the effective bond length tends to decrease with increasing concrete strength. The parameters related to FRP and the dimensions of the substrate (concrete) are considered to be less pronounced. In addition, the FRP sheet-to-substrate width ratio was found to affect bond performance (Lu *et al.* 2005a,b, Oehlers and Seracino 2004, Lu *et al.* 2004a,Ueda *et al.* 2003, Yuan *et al.* 2004, Teng *et al.* 2001, Chen and Teng 2001, Dai J.G.2006, Shadravan *et al.* 2007).

Van Gemert (1980) examined stresses in steel plates bonded to rectangular plain concrete prisms in double shear tests. The tensile force in a steel plate was found to decay exponentially toward the anchored end of the plate. At higher loads, the distribution of

tensile forces became more even within the loaded end of the bonded region. This means that practically no force was transferred from the plate to the concrete within this zone because the cracking of concrete near the applied load shifted the active bond zone to new areas farther away from the loading point. This phenomenon has been confirmed by other studies on steel-to-concrete bonded joints (Täljsten, 1997) and FRP-to-concrete bonded joints (Maeda *et al.*, 1997). Clearly, a very important aspect of the behaviour of these bonded joints is that there exists an effective bond length beyond which an extension of the bonded length of material cannot increase the ultimate load capacity. This is a fundamental difference between an externally bonded plate and an internally embedded reinforcing bar for which a sufficiently long anchorage length can always be found to develop the full tensile strength of reinforcement (Yuan *et al.* 2004).

Previous research also indicated that the shift in the active bond zone can occur under increasing tensile forces. This means that as cracking in concrete propagates, bond resistance gradually diminishes in regions near the load, but in the meantime it is activated farther away from the loaded end, as confirmed experimentally (Chajes *et al.* 1996; Maeda *et al.* 1997; Täljsten 1997) and analytically (Holzenkämpfer 1994; Yuan and Wu 1999; Yuan *et al.* 2001). However, a longer bond length may improve the ductility of the failure process. This phenomenon is believed to be the primary reason for the observed low stresses in bonded plates at anchorage failure (Chen and Teng, 2001). Existing studies have been mainly concerned with the prediction of ultimate load and the effective bond length (Chen and Teng, 2001), but much less attention has been given to the prediction of the entire debonding process of such bonded joints. Chen and Teng (2001) also found that the ultimate stress in FRP at failure σ_{fu} has an average value of 28% of the ultimate tensile strength of FRP f_{fu}, with a coefficient of variation (COV) of 40%. This ratio is substantially higher for steel-to-concrete joints with an average value of σ_{su} / f_{su} = 58%, but the degree of scatter is similar (COV = 37%). The corresponding ratio to steel yield stress is σ_{su} / f_{sy} = 71%. The researchers indicated that this phenomenon is substantially different from the bond behaviour of internal reinforcement for which a bond length can always be designed for its full tensile strength, emphasizing that this key aspect must be accounted for in the development of bond anchorage strength models.

The experimental research in the past has resulted in two major models describing FRP debonding failure in concrete structures; i) cohesive failure in the concrete surface layer, and ii) adhesion failure at the adhesive/concrete interface (Ouyang and Wan, 2008). In general, the debonding of FRP occurs within a thin layer of concrete adjacent to the concrete-to-adhesive interface unless the adhesive is weak. The thickness of this concrete layer is about 2~5mm (Lu *et al.* 2004b). McSweeney and Lopez (2005) investigated the sensitivity of FRP-concrete bond failure load to changes in geometric and material parameters. They illustrated the propagation of failure through gradual deterioration of bond. During the initial stages of loading, the specimens do not display signs of distress until the load becomes sufficiently high to cause cracking. At this stage popping sounds can be heard as the load continues to increase. As the final bond failure is approached, cracking sounds become louder and occur at shorter intervals. On occasion, just prior to complete failure, the cracking sound can be heard in a continuous string, analogous to an unzipping sound. This has been observed in other tests, such as those conducted by Lopez (2000). As the bond failure progresses small diagonal cracks begin to form along the edges of CFRP strips, as shown in Fig.2.4. These cracks appear at regular intervals, and never propagate significantly inward. The angle of cracks suggests an edge effect, affecting the crack propagation, as seen in the crack front of a GFRP strip bonded to steel in Fig.2.4. Each new crack in the CFRP strip appears when a shift in the crack front occurs as the substrate bond fails. McSweeney and Lopez (2005) reported that as the failure is approached, 86% of the 42 specimens that they tested developed cracks in the concrete substrate that ran from the edge of the FRP strip up to a point at the leading edge of the concrete block. Fig.2.5 depicts these cracks which resulted in a tooth-like appearance in concrete, near the surface. The angle, α in Fig. 2.5 increased as the bond width of the strip increased, but the distance x, remained the same, leading to a wider tooth of concrete at the free edge. Rarely did the tooth approach the edge of the shim plate used in the restraint setup – thus, the unrestrained edge distance of 25mm between the shim plate and the bonding surface was sufficient to prevent an unrealistic restraint of concrete against failure. The tooth did not displace visibly during testing, but upon final bond failure, the tooth remained bonded to the FRP strip. Concrete cover failure, as part

of overall bond failure, has been noted by several researchers (Lopez and Namaan 2003, Buyukozturk 1998).

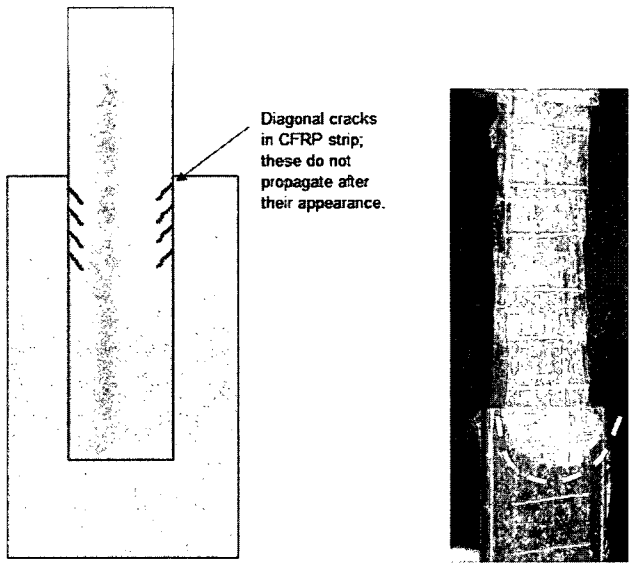

Fig. 2.4. Exaggerated sketch of edge cracking in CFRP during testing, compared to the edge effects observed in GFRP strips bonded to steel (McSweeney and Lopez, 2005)

The final bond failure of CFRP on concrete was reported by McSweeney and Lopez (2005) to be extremely brittle, and it was accompanied by a large release of energy. Other researchers confirmed this observation. Some of the FRP strips in test specimens were damaged by the energy release at final failure; exhibiting splitting in the longitudinal (fiber) direction, while the epoxy of other strips had post failure transverse cracking. Fragments of concrete often broke loose from the block when the strip broke free (Fig.2.6). Increased bond length, width, and thickness led to longer time to failure, but changes to the bond width had the greatest impact on time to failure. For the shortest bond length (76mm), there was little warning before the final failure. All other FRP strips provided some warning prior to final bond failure in the form of cracking sounds. While a few specimens experienced pull-out of an additional tooth of concrete at the end of bond length during failure, the vast majority only lost concrete tooth at the leading edge as discussed previously. The remainder of the bonded region, past the leading edge, was free of epoxy after failure, and the FRP strips did not exhibit a significant amount of paste left, clinging to the strip. However, the concrete surface was rough, with numerous

microcracks oriented in a manner indicative of the direction of bond failure. A pattern of regularly spaced microcracks was visible throughout the bonded area, with small pieces of paste peeled back by the propagation of bond failure as shown in Fig. 2.6.

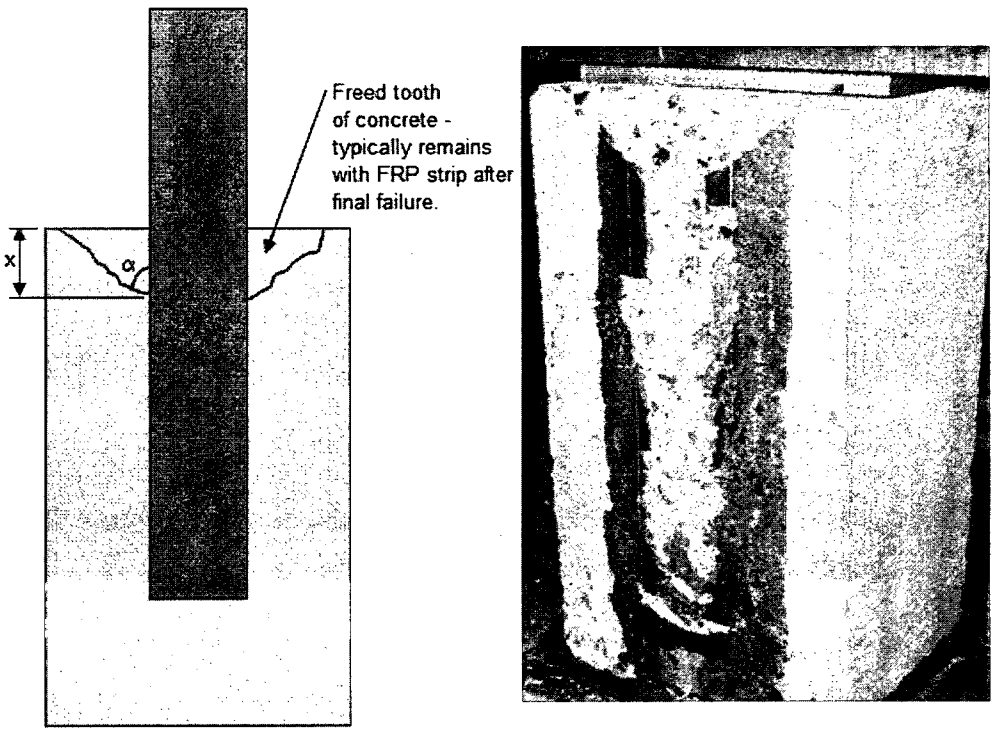

Fig. 2.5. Free edge failure of the concrete. (McSweeney and Lopez, 2005)

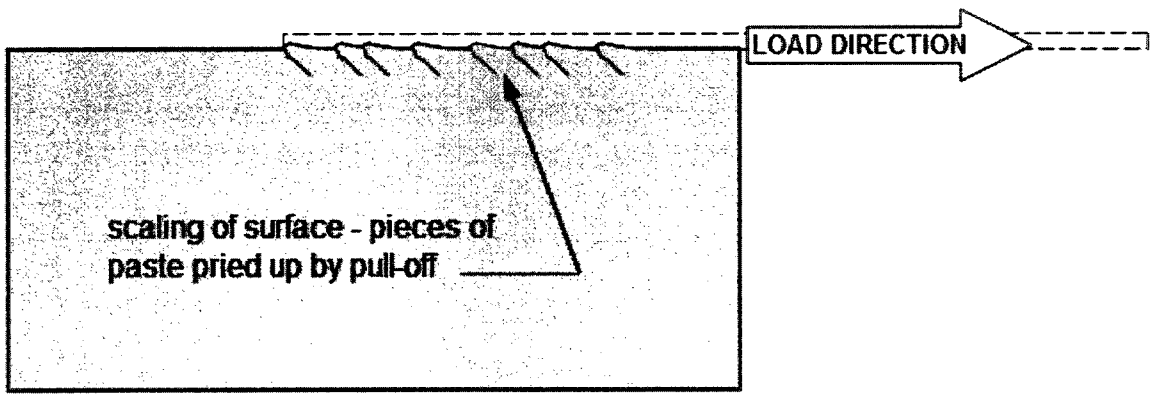

Fig. 2.6. Concrete surface scaling due to pull-off of the FRP strip. (McSweeney and Lopez, 2005)

Tommaso *et al.* (2001) evaluated the results of the influence of temperature on adhesively bonded plate-concrete joint systems on bond failure. Casareto *et al.* (2003)

tested standard hollow concrete blocks and clay brick specimens to investigate the bond behaviour of AFRP sheets on different types of masonry surface with a double shear pull push test (Fig.2.7).

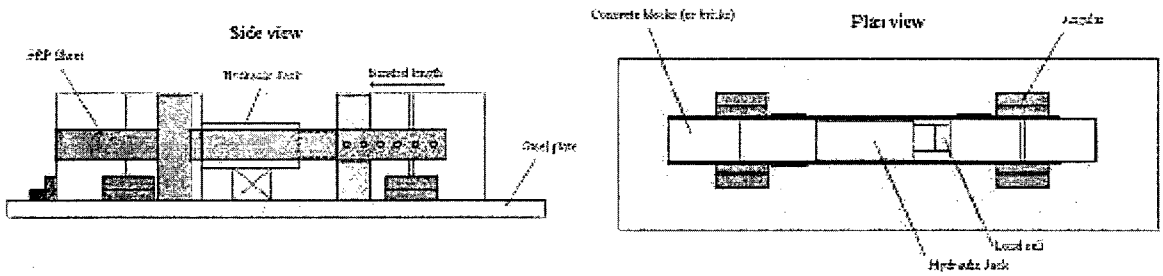

Fig. 2.7. Casareto *et al.* (2003) Setup for testing Brick specimens

Numerous researches investigated cyclic loading on large scale masonry and RC frames, walls, and beams (Chen and Pan 2006, Shalouf 2005, Serrato 2002). However, no cyclic loading test, involving small scale specimens or prisms was found in the literature. Zhao *et al.* (2007) conducted pull out and beam flexure tests and measured local slip at the interface between concrete and FRP. They used fiber optic sensors with 1 mm resolution for measurements of local slip at the interface. In flexure, the long gauge distributed sensors were found to provide more precise data, especially during deformation reversals.

Based on the previous research and observed behaviour of FRP bond failures, it may be concluded that the parameters that affect surface bond can be summarized as follows;

i. base material (type, strength, and surface roughness),

ii. FRP sheet (type, mechanical properties, thickness, number of layers, width),

iii. epoxy resin (strength, elongation, thickness), and

iv. loading history(monotonic, cyclic, dynamic: seismic, fatigue, blast).

Shadravan *et al.* (2007) also hypothesized that the test method and setup used in experimental studies change the loading conditions and the fracture mechanism, thereby affecting the effective length established by tests. Other researchers also pointed out that

environmental conditions, such as temperature, frosting, humidity, pollution etc. may also affect the bond characteristics of FRP strips.

2.2. Analytical Research

The effectiveness of the externally bonded FRP technique explicitly depends on the bond between the FRP and the concrete substrate, an accurate description of the interaction between these two materials across the interfaces is essential. Therefore, the emphasis on previous research has been on the development of analytical models for bond behaviour of surface-bonded FRP. A number of models have been developed and reported. The suggested models included equations for the ultimate load capacity, the interfacial bond stress distribution at the first attainment of capacity and the effective bond length for various interfacial bond–slip models. Chen and Teng (2001) conducted an extensive literature review on previous research, including the assessment of previously proposed analytical models. The researchers compared analytical predictions against available experimental data in the literature, and themselves developed expressions for the computation of ultimate load and effective bond length. The majority of empirical bond strength models were obtained through the use of test data and regression analysis of data on sets involving different constituent materials and different test conditions, and hence the resulting equations do not have broad-based applicability (Karbhari *et al.* 2006). Recognizing the difficulty in modeling bond strength of concrete/FRP interface, several investigators have taken the fracture mechanics approach by assuming a forward shear type debonding mechanism for CFRP sheets in various types of specimen configurations (Tripi *et al.* 2000). Several bond anchorage strength models have also been advanced. Classification of the modeling trends used in the past may not be possible as the models are usually based on empirical results.

Chen and Teng (2001) classified previous analytical models into four categories; i) empirical models based directly on the regression of test data, ii) fracture mechanics models, iii) finite element analysis, and iv) design proposals that generally make use of some simple assumptions. A discussion of previous models is presented in this Section.

2.2.1. Empirical Models

The majority of previously developed empirical expressions for models is summarized in Table 2.1. Van Gemert (1980) examined stresses in steel plates bonded to rectangular plain concrete prisms in double shear tests. He assumed a linear elastic stress distribution within the bond length, under service loads, followed by a symmetric bilinear distribution at ultimate load.

Table 2.1. Suggested empirical equations for bond behaviour of FRP sheets on concrete

Reference	Suggested Equation
Chajes *et al.* (1996)	$P_u \propto \sqrt{f_c'}$
Hiroyuki and Wu (1997)	$\tau_\upsilon = 5.88L^{-0.669}$ (MPa)
Tanaka (1996)	$\tau_\upsilon = 6.13\ln L$ (MPa) $P_u = \tau_u b_p L_b$
Maeda *et al.* (1997)	$L_e = \exp(6.134 - 0.58\ln(t_p E_p))$ $\tau = 110.2 \times 10^{-6} E_p t_p$(MPa)
ACI440.2.R- 02 (2008)	$L_e = \frac{23300}{(nt_p E_p)^{0.58}}, (SI)$
CSA, *S806-02,2002*	$L_e = \frac{25350}{(t_p E_p)^{0.58}}$
Miller and Nanni (1999)	$L_e = -0.432(t_p E_p) + 94.3$
Izumo (JCI, Rep 2003)	$L_e = 1.89(E_p t_p)^{0.4}$ $P_u = (3.8 f_c'^{2/3} c + 15.2) L E_p b_p t_p \times 10^{-3}$
Sato *et al.* (2001)	$P_u = 5.06 f_c'^{0.2} (E_p t_p)^{1.4} (b_P + 2\Delta b_p) L_b \times 10^{-5}$ $E_p t_p < 38.4 kN / mm$ $P_u = 1.95 f_c'^{0.2} (E_p t_p)^{0.4} (b_P + 2\Delta b_p) L_b \times 10^{-5}$ $E_p t_p > 38.4 kN / mm$
Sato (JCI,Report 2003)	$\tau_u = 2.68 . f_c'^{0.2} t_p E_p \times 10^{-5}$ $P_u = (b_P + 2\Delta b_p) L_e \tau_u$ Δb_p=3.7 mm
Dai *et al.* (2005),	$P_{max} = (b_P + 2\Delta b_p)\sqrt{2 E_p t_p G_f}$
M.Iso 2003 (JCI. Rep. 03)	$L_e = 0.125 (E_p t_p)^{0.57}$
Kamel.et al. (2004)	$P_u = 0.0016 b_p L_e + 0.75\sqrt{E_p t_p}$ $L_e = 0.25 b_p^{0.14}\sqrt{E_p t_p}$
Leung and Pan (2005)	$G_f = (-1.0053 a + 1.3432)(0.4245 f_{ctm} - 0.0163)$

Hiroyuki and Wu (1997) conducted double shear experiments on carbon fiber sheets (CFS) that strengthened RC members. The test data resulted in the following empirical relationship between the bond length L (cm) and the average bond shear stress at failure τ_u:

$$\tau_u = 5.88L^{-0.669} \text{ (MPa)} \tag{2.1}$$

Similarly, Tanaka (1996) presented another simple expression, as indicated below:

$$\tau_u = 6.13 - \ln L \text{ (MPa)} \tag{2.2}$$

Where, L is in millimeters. In the above two models, the ultimate bond strength of the joint P_u is given by:

$$P_u = \tau_u b_p L. \tag{2.3}$$

Maeda *et al.* (1997) developed a more robust model that considers the effective bond length. Their suggested expression is shown below:

$$\tau = 110.2 x10^{-6} E_p t_p \text{ (MPa)} \tag{2.4}$$

Where, τ is the surface bond stress and t_p (mm) and E_p (MPa) are thickness and Young's modulus of the bonded plate, respectively. The ultimate bond strength P_u can be obtained by multiplying the ultimate bond stress τ_u by the effective bond area $L_e b_p$. Maeda *et al.* (1997) also presented a relationship for the effective bond length, as shown below.

$$L_e = exp(6.134 - 0.58.\ell n(t_p E_p)) \tag{2.5}$$

The main variables are modulus of elasticity and thickness of FRP sheet, which represent the sheet stiffness. Recently developed relationships also use the same variables, but the variables appear in the numerator instead of the denominator as above. Therefore, they contradict with the above expressions. In spite of this contradiction, several researchers like Miller *et al.* (1999) accepted and used these expressions. Furthermore, several design guidelines also adopted them for use in design (ACI440.2.R- 02, 2002, CSA S806-02 2002).

Miller and Nanni (1999) suggested a simplified linear relationship for effective bond length based on their test results.

$$L_e = -0.432(t_p E_p) + 94.3 \quad (2.6)$$

The bond strength model proposed by Izumo is discussed in a JCI Report (2003), and is presented below:

$$P_u = (3.8 f'^{2/3}_c c + 15.2) L E_p b_p t_p \times 10^{-3} \text{ for carbon fibre (CFRP) sheets,} \quad (2.7)$$

and $$P_u = (3.4 f'^{2/3}_c + 69) L E_p b_p t_p \times 10^{-3} \text{ for aramid fibre (AFRP) sheets.} \quad (2.8)$$

Sato *et al.* (2001) suggested a shear softening stress slip model, consisting of;

$$L_e = 1.89(E_p t_p)^{0.4} \quad (2.9)$$

and $$P_u = 5.06 f'^{0.2}_c (E_p \ t_p)^{1.4} ((b_p + 2\Delta b_p) L_b \times 10^{-5} \quad \text{for} \quad E_p \ t_p < 38.4 \ kN/mm \quad (2.10)$$

$$P_u = 1.95 f'^{0.2}_c (E_p \ t_p)^{0.4} ((b_p + 2\Delta b_p) L_b \times 10^{-5} \quad \text{for} \quad E_p \ t_p > 38.4 \ kN/mm \quad (2.11)$$

The researchers subsequently proposed an expression for ultimate bond stress and the resulting ultimate load, while keeping their original expression for the effective length to be the same (JCI, Report 2003). The following are the new expressions suggested:

$$\tau_u = 2.68 . f'^{0.2}_c t_p E_p \times 10^{-5} \quad (2.12)$$

$$P_u = (b_P + 2\Delta b_p) L_e \tau_u \quad (2.13)$$

Where, $\Delta b_p = 3.7$ mm is assumed to be the width of concrete effective for bonding.

Dai *et al.* (2005), modified the above expression and presented a new formulation based on Täljsten's (1994) analytical model, as shown below:

$$P_{max} = (b_P + 2\Delta b_p) \sqrt{2 E_p t_p G_f} \quad (2.14)$$

Lorenzis *et al.* (2001) also followed Täljsten's (1996) analytical model but proposed an elastoplastic bond slip model based on their experimental data.

Sena Cruz and J. Barros (2003) combined two previously proposed expressions to describe experimentally observed bond stress-slip relationship for surface mounted CFRP:

$$\tau(s) = \begin{cases} \tau_{max}\left(\frac{s}{s_m}\right)^{a} & if\ s \le s_m \\ \tau_{max}\left(\frac{s}{s_m}\right)^{-a'} & if\ s > s_m \end{cases} \tag{2.15}$$

Where, τ_m and s_m are bond strength and corresponding slip, and α and α' are parameters defining the shape of the curve. The equation for $s \le s_m$ was originally developed by Eligehausen *et al.* (1983), and defines bond behaviour up to the peak stress (ascending branch). The equation for $s_m > s$ was adopted from Lorenzis and Nanni (2002) and provides post-peak bond behaviour (descending branch). The above expressions were selected due to their simplicity and ability to simulate the observed experimental phenomena fairly accurately. The researchers also discussed the difference in behaviour between near surface bonded CFRP and surface bonded CFRP sheets, and concluded that the near surface mounted CFRP behaviour is in between the behaviours of FRP bars and FRP sheets.

M. Iso(2003) suggested a formula for the computation of effective length of FRP (JCI. Report-2003) based on his experimental research. The expression is given below:

$$L_e = 0.125(E_P t_P)^{0.57} \tag{2.16}$$

Kamel *et al.* (2004) conducted experimental research to establish bond characteristics of FRP. The researchers developed empirical expressions based on the regression analysis of test data. The expressions are given below for effective length and ultimate bond load:

$$L_e = 0.25 b_p^{0.14} \sqrt{E_P t_P} \tag{2.17}$$

$$P_u = 0.0016 b_p L_e + 0.75\sqrt{E_p t_p} \tag{2.18}$$

Where, E_p, t_p, and b_p are the FRP sheet modulus of elasticity in MPa, thickness, and width in mm, respectively.

The experimental data not only provided much needed information for the derivation of analytical expressions for bond length, bond stress and ultimate bond force, but also provided insight for the development of a complete bond-slip models. Lu *et al.* (2005a) used pull tests for the generation of complete bond-slip model. Local bond–slip curves from pull tests are commonly determined in two ways; (a) from axial strains of the FRP plate measured with closely spaced strain gauges (e.g. Nakaba *et al.* 2001a); or (b) from load–displacement (slip at the loaded end) curves (e.g. Ueda *et al.* 2003). In the first method, the bond stress of a particular location along the FRP-to concrete interface can be found from strain readings, while the corresponding slip can be found through numerical integration of measured longitudinal strains of the plate. This method appears to be simple, but in reality cannot produce accurate local bond–slip curves. This is because the axial strains measured on a thin FRP plate generally show drastic variations as a result of the discrete nature of concrete cracks, the heterogeneity of concrete and the roughness of the underside of the debonded FRP plate. For example, a strain gauge located above a crack will have a much greater strain than that sitting above a large aggregate particle. Consequently, bond–slip curves found from different tests may differ substantially. The second method is an indirect method and has its own problems as well. In this approach, a local bond–slip curve is determined indirectly from the load–slip curve, but it is easy to show that different local bond–slip curves may lead to similar load–displacement curves (Lu *et al.* 2005a).

In addition to the purely empirical and experimental approached discussed above, several researchers used empirical data to supplement their theoretical approaches in developing their models. Among various theoretical approaches employed, many used the principles of fracture mechanics, and complemented their work through experimental data and observations. Leung and Pan (2005) developed an empirical approach by employing neural networks to investigate the effects of concrete surface tensile strength and aggregate content on fracture energy. As a result, they derived the following equation for fracture energy:

$$G_f = (-1.0053\,a + 1.3432)(0.4245\,f_{ctm} - 0.0163) \quad (2.19)$$

2.2.2. Fracture Mechanics Based Models

The use of a fracture mechanics-based approach is extremely attractive since, in principle, it can potentially capture the critical aspects related to interfacial mechanics and failure initiation and propagation. In spite of the powerful analytical tools that fracture mechanics offer, most existing theoretical models have been developed on the basis of simple bond tests (single-lap or double-lap tension tests of FRP-bonded concrete block, or idealized flexural test). That is why they can not replicate complicated stress conditions as affected by cracks that can be seen in actual structural systems. Experimentally obtained models also tend to involve too many parameters to be considered of practical use. In some cases these models were modified through the use of parameters that represent physical/mechanistic conditions, but derived empirically by curve fitting (Karbhari *et al.* 2006).

Vilnay (1988) was among the first researchers who adopted a theoretical approach to describe the bond behaviour of surface bonded FRP. He developed an analytical model and applied it to a composite beam with externally bonded steel plate. He obtained an expression for the maximum bond stress from the moment-deflection differential equation.

Several researchers presented analytical models using the principles of fracture mechanics. Among them are; Triantafillou and Plevris (1992), Holzenkämpfer (1994), Täljsten (1994), Brosens and van Gemert (1998), Yuan and Wu (1999), Yuan *et al.* (2001) and Wu *et al.*(2002). The fracture-mechanics based models are based on experimentally observed bond-slip relationships. Various empirical bond–slip relationships pertaining to the FRP-concrete interface were proposed based on specific sets of experimental observations, as discussed earlier. Some of the simplified bond-slip models are illustrated in Fig. 2.8. A number of analytical relationships were also developed based on mechanics. The variety of shapes used in describing the bond-slip phenomenon demonstrates the difficulty in defining a reliable and comprehensive relationship based on simplistic tests, short bond transfer length, and local geometric and

material variations. It is, however, noted that the use of fracture mechanics implicitly leads to a very simple generic expression for the determination of bond capacity, related only to the FRP stiffness and interfacial fracture energy (defined as the area beneath the bond stress–slip curve), no matter what type of interfacial constitutive law is adopted (Täljsten 1996, Yuan *et al.* 2001, Wu *et al.* 2002).

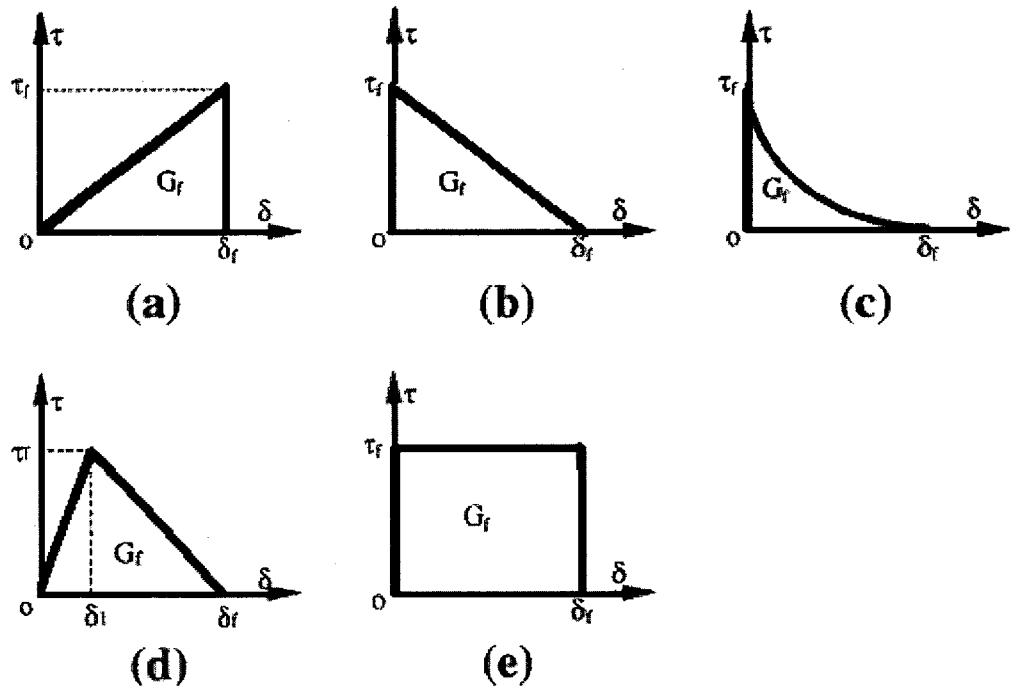

Fig. 2.8. Some Bond-Slip Models for Plate to Concrete Bonded Joints (Yuan and Wu 1999)

Holzenkämpfer (1994) investigated bond strength between a steel plate and concrete using nonlinear fracture mechanics. Holzenkämpfer solved the differential equation for surface bond that describes the structural behaviour of externally bonded reinforcement in general.

$$s'' - \frac{\tau(s)}{E_P t_P} = 0 \tag{2.20}$$

Holzenkämpfer used the Mohr–Coulomb failure criterion to derive the maximum bond stress, which is expressed as follows:

$$\tau_{max} = \frac{1}{2}\sqrt{f_c' f_t} \tag{2.21}$$

where f'_c and f_t are concrete compressive strength and tensile strength as measured by pull-off tests, respectively.

Täljsten (1994) analytically obtained the expression for ultimate load using a linear ascending bond–slip model. Subsequently, Täljsten (1996) and Holzenkämpfer (1994) used a nonlinear fracture mechanics bond slip model which is shown in Fig. 2.9. Täljsten simplified this model by assuming linear segments and used interfacial fracture energy to determine the maximum transferable load or bond capacity, P_{max}, in terms of interfacial fracture energy, G_f, and FRP reinforcing stiffness, $E_p t_p$, (Täljsten, 1994).

$$P_u = \sqrt{\frac{2E_p t_p G_f}{1+\alpha_T}} b_p \tag{2.22}$$

Where,

$$\alpha_T = \frac{E_p t_p}{E_c t_c} \tag{2.23}$$

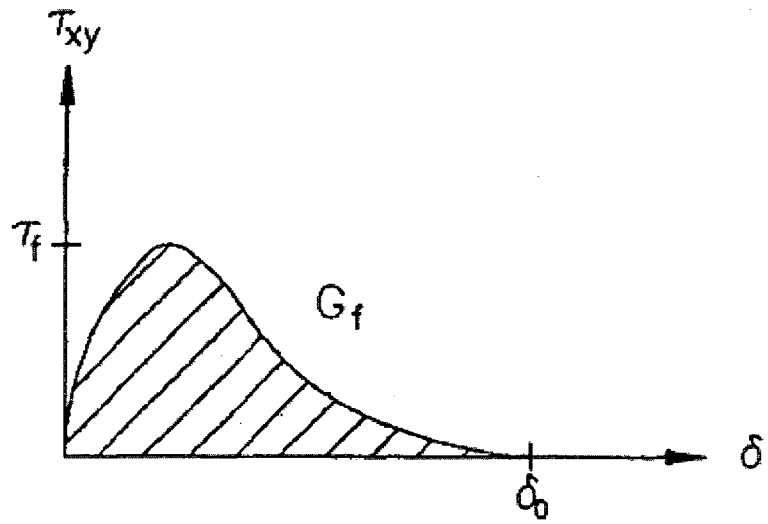

Fig. 2.9. Bond Displacement curve of an adhesive joint based on nonlinear fracture mechanics (Täljsten, 1996)

The researcher also presented the maximum normal strain as shown below (Täljsten 1994, 1997):

$$\varepsilon_{max} = \frac{P_{max}}{nt_p b_p E_p} \times 10^6 \tag{2.24}$$

and

$$\varepsilon_{ub} = \sqrt{\frac{2.G_f}{E_p t_p}} \tag{2.25}$$

The effective length was then represented as:

$$L_{e-exp} = \frac{\varepsilon_{max}}{\frac{d\varepsilon}{dx}}, \varepsilon_{max} = \frac{P_{max}}{nt_p b_p E_p} \times 10^6, l_e = \sqrt{\frac{2E_p t_p G_f}{\tau_m}} \tag{2.26}$$

Where,

$$\tau_m = 0.0184\sqrt{E_p . t_p} \tag{2.27}$$

The ultimate load is derived as:

$$P = \beta_l P_u \tag{2.28}$$

$$\beta_l = \begin{cases} 1.0 & if : L > L_e \\ sin\left(\frac{\pi}{2}\frac{L}{L_e}\right) & if : L \le L_e \end{cases} \tag{2.29}$$

These two basic models of Holzenkämpfer (1994) and Täljsten (1996) have been modified by various investigators, as will be shown in this section to provide a more comprehensive description of bond strength and related interfacial fracture phenomena. (Niedermeier 1996, Blaschko *et al.* 1996, Täljsten 1994, 1997, JCI. Report-2003, Kamel *et al.* 2004,)

Niedermeier (1996) and Blaschko *et al.* (1996) modified the model developed by Holzenkämpfer (1994). They calculated the bond strength by using nonlinear fracture mechanics, as illustrated below:

$$P_u = \begin{cases} 0.78 b_p \sqrt{2 G_f E_p t_p} & if L \geq L_e \\ 0.78 b_p \sqrt{2 G_f E_p t_p}\, \dfrac{L}{L_e}\left(2 - \dfrac{L}{L_e}\right) & if L < L_e \end{cases} \tag{2.30}$$

Where the effective bond length L_e and the fracture energy G_f are given by

$$G_f = k_p^2 C_f f_{ctm} \tag{2.31}$$

$$L_e = \sqrt{\frac{t_p E_p}{4.f_{ctm}}} (mm) \tag{2.32}$$

where f_{ctm} (MPa) is the average surface tensile strength of concrete determined in a pull-off test according to DIN1048 (Deutsches, 1991); c_f is a constant determined in a linear regression analysis using the results of double shear or similar tests; and k_p is a geometric factor related to the width of bonded plate b_p and the width of concrete member b_c.

$$k_p = \sqrt{1.125 \frac{2 - b_p / b_c}{1 + b_p / 400}} \tag{2.33}$$

The concept of geometrical factor was widely accepted and improved by other researchers to make sure the shape effects are taken into account. Neubauer and Rostásy (1997) conducted a series of double shear tests on carbon fiber reinforced polymer (CFRP)-to-concrete bonded joints. They used the linear bond slip model with a linear ascending branch and a sudden drop at a maximum slip of s_o, where s_o, is expressed below;

$$s_0 = k_p x\ 0.202 \tag{2.34}$$

The maximum bond stress, τ_{max}, was expressed in terms of the tensile strength of concrete, f_t, as expressed below:

$$\tau_{max} = 1.8 k_b f_t \tag{2.35}$$

Casareto et al. (2003) applied a methodology similar to Täljsten (1996) to derive the following effective length equation:

$$L_e = \frac{\varepsilon_{ub}}{d\varepsilon/dx} \tag{2.36}$$

$$L_e = \frac{\sqrt{2G_f E_p}}{\tau_{max}} \tag{2.37}$$

Casareto also suggested the expression shown below as average bond stress:

$$\tau(x) = t_p . E_p . \frac{d\varepsilon}{dx} \tag{2.38}$$

The normal strain of FRP ε in the above expressions can be computed by assuming the slip at the end of the laminate, s(0) is equal to zero, as it can be consider negligible prior to delamination.

$$\varepsilon = \frac{ds}{dx} \Rightarrow s(x) = s(0) + \int_0^x \varepsilon(x)dx \tag{2.39}$$

The ultimate strain prior to debonding can then be defined as:

$$\varepsilon_{ub} = \sqrt{\frac{2.G_f}{E_p t_p}} \tag{2.40}$$

Neubauer and Rostásy (1997) concluded that, for both concrete fracture failures and FRP delamination failures, the bond-slip relationship may be represented by the triangular model shown in Fig.2.8(d). The fracture energy, G_f, can then be calculated using;

$$G_f = c_f f_t \tag{2.41}$$

Where f_t is the tensile strength of concrete and c_f is a coefficient reported to be equal to a mean value of 0.202mm for the 72 specimens investigated. They presented a modified form of Holzenkämpfer's (1994) model. Therefore, it applies to both CFRP and steel plates:

$$P_u = \begin{cases} 0.64 k_p b_p \sqrt{E_p t_p f_t} & if L \geq L_e \\ 0.64 k_p b_p \sqrt{E_p t_p f_t}\, \dfrac{L}{L_e}\left(2 - \dfrac{L}{L_e}\right) & if L < L_e \end{cases}. \tag{2.42}$$

$$L_e = \sqrt{\frac{t_p E_p}{2.f_t}} \tag{2.43}$$

Where, E_p and f_t are measured in MPa, t_p and L_e are measured in millimeters, k_p is a geometric factor related to the width of bonded plate b_p, and the width of concrete member b_c (both measured in millimeters). The geometric factor k_p is expressed the same as Niedermeier (1996) and Blaschko *et al.* (1996) suggestion.

The maximum strain in FRP can then be expressed as;

$$\varepsilon_{max} = 0.64\sqrt{1.125\frac{2-b_p/b_c}{1+b_p/400}}\sqrt{\frac{f_t}{E_p t_p}} \tag{2.44}$$

Where, the concrete tensile strength is determined from measured compressive strength following the CEB-FIP Model Code (1993) given below.

$$f_t = 1.4\left(\frac{f_c' - 8}{10}\right)^{2/3} \tag{2.45}$$

Neubauer and Rostásy (1997) intrinsically neglected the thickness of the adhesive. Brosens and Van Gemert (1999), however, modified the models of Niedermeier (1996) and Blaschko *et al.* (1996) included the adhesive thickness in their formulation. Furthermore, they also incorporated the thickness of concrete substrate near the surface which is considered to be effective in developing bond. This is illustrated in Fig.2.10(a).

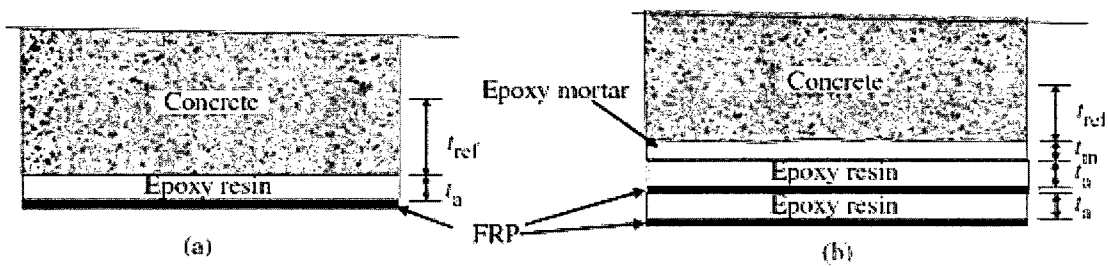

Fig. 2.10. Representative schematics of configurations of different layers used for the computation of bond slip: (a) Brosens and Van Gemert (1999) (b) Brosens (2001)

This layer, which essentially serves as an additional interface, can significantly affect both the bond transfer length and the level of bond strength. Brosens and van

Gemert (1999) derived expressions for the maximum transferable load at both the serviceability and the ultimate limit states. They modified Neubauer and Rostásy (1997) Equations to account for the effects of FRP width. The resulting expressions for maximum bond stress, τ_{max}, and interfacial fracture energy, G_f, are shown below:

$$\tau_{max} = 1.8 k_b f_t \tag{2.46}$$

and

$$G_f = k_b^2 C_f f_t \tag{2.47}$$

where

$$k_b = \sqrt{1.5 \frac{2 - b_p / b_c}{1 + b_p / 100}} \tag{2.48}$$

C_f above was found to be 0.3 from test data. For cases where the bond length L is larger than the effective bond length, L_e, the maximum transferable load, P_{max}, is expressed as expressed below.

$$P_u = b_p \sqrt{2 G_f E_p t_p} \tag{2.49}$$

Where, the effective bond length, L_e, is expressed as;

$$L_e = \frac{2\lambda + a\tan(\tanh(2)/\lambda)}{\lambda \omega} \tag{2.50}$$

The parameters λ and ω can be computed from the following expressions.

$$\lambda = \sqrt{\frac{s_0}{s_f - s_0}} \tag{2.51}$$

and

$$\omega = \sqrt{\frac{\tau_{max}(1 + (E_p A_p / E_c A_c))}{s_f - s_0}} \approx \sqrt{\frac{\tau_{max}}{s_0 E_p t_p}} \tag{2.52}$$

In the above equation, A_p is the cross-sectional area of externally bonded FRP plate. The slip, s_0, corresponding to the maximum bond stress is determined as the sum of the slip in the adhesive and the slip in concrete shown in Fig.2.10(b).

$$s_0 = \tau_{max}\left(\frac{t_a}{G_a}+\frac{t_{ref}}{G_c}\right)=\tau_{\max}\left(2.6\frac{t_a}{E_a}+2.32\frac{t_{ref}}{E_c}\right) \tag{2.53}$$

where t_a is the thickness of adhesive, estimated in their study to be 0.2 mm, G_a is the shear modulus of adhesive, expressed as $G_a=(E_a/2(1+\nu_a))$, where the Poisson's ratio ν_a is estimated to be 0.3 for ordinary epoxy resins and E_a is the Young's modulus of the adhesive. G_c is the shear modulus of concrete and it is expressed as $G_c=(E_c/2(1+\nu_c))$, where the Poisson's ratio ν_c was estimated to be 0.16 and E_c is the Young's modulus of concrete, expressed following the CEB FIP Model Code (1993) as shown below.

$$E_c = 2.15\times 10^4\left(\frac{f_c'}{10}\right)^{1/3} \tag{2.54}$$

The ultimate slip, s_f, corresponding to local bond failure was computed as shown below based on the bilinear bond-slip model.

$$s_f = \frac{2G_f}{\tau_{max}} \tag{2.55}$$

$$\tau_{max} = 1.8k_b f_t \tag{2.56}$$

The reference thickness t_{ref} in concrete, shown in Fig.2.10(a), is the reference distance in concrete over which stresses are influenced by FRP. This thickness can be taken as 2.5 – 3 times the maximum aggregate size, usually resulting in a depth of 40–50 mm. In the new configuration, the maximum strain in FRP is determined as

$$\varepsilon_{\max} = \sqrt{\frac{2G_f}{E_p t_p}} \tag{2.57}$$

Based on a microscopic study of the interfacial region, Brosens (2001) concluded that it was critical not only to consider size effects which could cause significant effect on bond level mechanisms through local irregularities, but also the effect of additional interfaces between layers of FRP as shown in Fig.2.10(b). In addition, through a re-evaluation of the bond stress model used by Holzenkämpfer (1994), it was hypothesized that a state of pure shear was responsible for maximum bond-stress leading to a modification of the Mohr–Coulomb envelope, shown in Fig.2.11.

$$\tau_{max} = \frac{f_c' f_t}{f_c' + f_t} \tag{2.58}$$

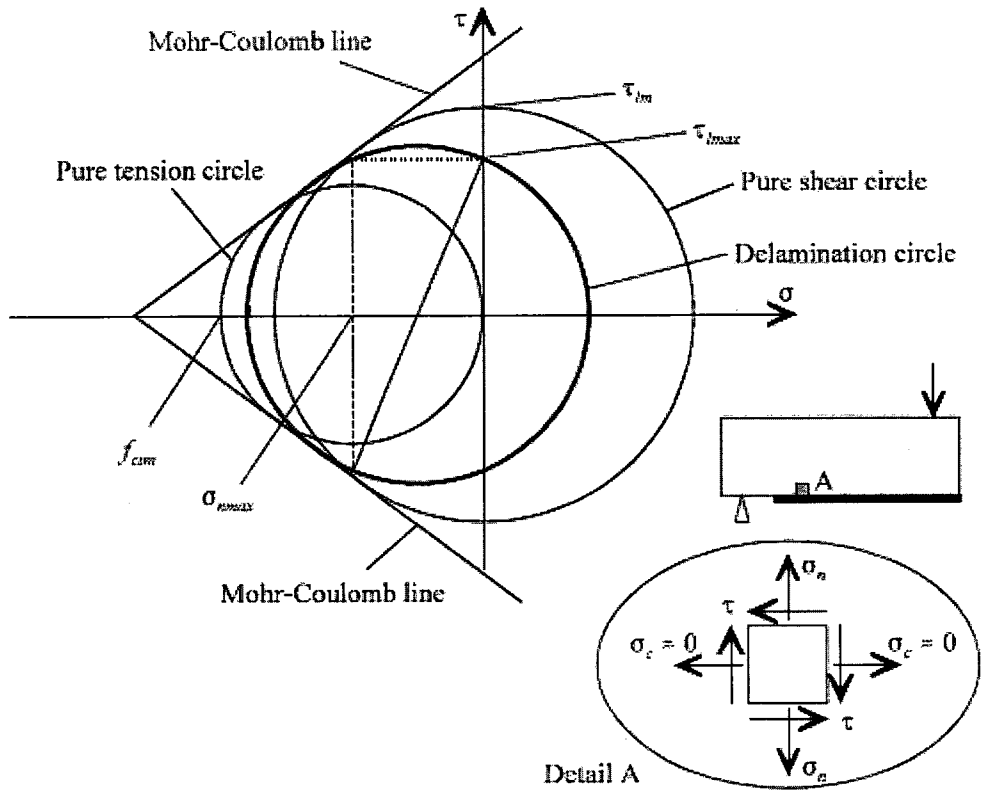

Fig. 2.11. Mohr-coulomb failure criterion , (Brosens, 2001)

Brosens (2001) modified the formulation as indicated below to introduce the size effect and local irregularities.

$$\tau_{\max} = k_b k_c \frac{f_c' f_t}{f_c' + f_t} \tag{2.59}$$

where

$$k_b = \sqrt{k \frac{2 - b_p / b_c}{1 + b_p / b_0}} \tag{2.60}$$

and

$$b_0 = \frac{t_{ref}}{k - 1}. \tag{2.61}$$

leading to

$$\tau_{max} = \sqrt{\frac{1.47(2-(b_p/b_c))}{1+(b_p/85)}} \cdot \frac{f_c' f_t}{f_c' + f_t} \tag{2.62}$$

It was also derived that,

$$s_0 = \tau_{\max}\left(2.4\frac{t_{ref}}{E_c} + 2.5\frac{t_m}{E_m} + n\frac{t_a}{G_a}\right) \tag{2.63}$$

Here t_m is the thickness of the epoxy mortar, which was noted to vary between 2mm and 5mm depending on the size of irregularities on concrete surface, E_m is the modulus of elasticity of epoxy mortar and n_p is the number of layers of fabric reinforcement used. k is an empirical constant, and k_c is a parameter used to represent the level of concrete surface preparation which was dependent on the environment and workmanship, and ranged between 0.65 and 1.0. In a similar fashion, the expression for fracture energy, initially proposed by Holzenkämpfer (1994), was modified to include the above parameters such that;

$$G_f = k_b^2 k_c^2 C_f f_t \tag{2.64}$$

Where, values of C_f and k were determined through calibration with experimental results to be 0.40 mm and 1.47 mm, respectively, leading to

$$G_f = \frac{0.588(2-(b_p/b_c))}{1+(b_p/85)} f_t \tag{2.65}$$

The maximum transferable FRP force was determined as;

$$P_u = b_p\sqrt{2G_f E_p t_p} \tag{2.66}$$

Yuan and Wu (1999) and Yuan *et al.* (2000, 2001) studied the bond strength between FRPs and concrete for a pull push test using linear and nonlinear fracture mechanics. Their linear elastic fracture mechanics study resulted in the same equation as that proposed by (Täljsten 1994) but included the effect of widths of the plate and concrete member.

$$P_u = \sqrt{\frac{2E_p t_p G_f}{1+\alpha_T}} b_p \tag{2.67}$$

α_T above is replaced by α_γ given below.

$$\alpha_\gamma = \frac{b_p E_p t_p}{b_c E_c t_c} \tag{2.68}$$

The researchers also solved the nonlinear fracture mechanics equation for five different bond stress-slip relationships illustrated in Fig.2.8. Among them, the linearly ascending and then descending relationship (Fig.2.18.d) was considered to be the closest to reality. The maximum load carrying capacity for this case was developed by Yuan *et al.* (2001) to be:

$$P_u = \frac{\tau_u b_p}{\lambda_2} \frac{s_f}{(s_f - s_0)} \sin(\lambda_2 a) \tag{2.69}$$

Where, a is obtained by solving

$$\tanh[\lambda_1 (L - a)] = \frac{\lambda_2}{\lambda_1} \tan(\lambda_2 a) \tag{2.70}$$

Where, τ_u is the maximum stress on bond-slip curve;s_0 is the corresponding slip; $s_f$is the maximum slip; and λ_1 and λ_2 are defined below.

$$\lambda_1^2 = \frac{\tau_u}{s_0 E_p t_p}(1 + \alpha_\gamma) \tag{2.71}$$

$$\lambda_2^2 = \frac{\tau_u}{(s_f - s_0) E_p t_p}(1 + \alpha_\gamma) \tag{2.72}$$

In this solution, the relationship between P_u and L is an implicit function and is dependent on bond-slip coefficients λ_1 and λ_1, which are not easy to obtain.

Yuan *et al.* (2001) and Yoshizawa *et al.* (2000) defined the effective bond length as the value corresponding to 97% of the load carrying capacity when L is infinity. This gives;

$$L_e = a_0 + \frac{1}{2\lambda_1} \ln\left(\frac{\lambda_1 + \lambda_2 \tan(\lambda_2 a_0)}{\lambda_1 - \lambda_2 \tan(\lambda_2 a_0)}\right) \tag{2.73}$$

where

$$a_0 = \frac{1}{\lambda_2} sin^{-1}\left(0.97\sqrt{\frac{s_f - s_0}{s_f}}\right) \tag{2.74}$$

$$\alpha_\gamma = \frac{E_p t_p}{E_c t_c} \tag{2.75}$$

$$P_u = \begin{cases} \dfrac{\tau_u b_p}{\lambda} & if: L \geq L_e \\ \dfrac{\tau_u b_p}{\lambda_2}\dfrac{s_f}{s_f - s_0} sin(\lambda_2 a) & if: L < L_e \end{cases} \tag{2.76}$$

τ_u = maximum stress on the bond-slip curve; (considered as 8.0 MPa)

s_0 = slip corresponding to τ_u ; (considered as 0.05mm)

s_f= maximum slip (considered as 0.3mm)

subscripts p and c refer to plate and concrete.

The above concept was applied by Yuan *et al.* (2004), to investigate the full range of bond behaviour by employing a triangular bond-slip model. The researchers compared their analytical approach with experimental results and showed reasonably good correlations. That led them to the development of an iterative model and related parametric study.

Based on the work of Yuan *et al.* (2001), Chen and Teng (2001) concluded that typical values of slip at peak shear and failure for surface bonded FRP on concrete were 0.02 mm and 0.2 mm, respectively. Because the former was an order of magnitude smaller than the latter, a simple linearly decreasing bond–slip model was suggested.

Through a study of experimental data Yuan *et al.* (2001), Chen and Teng (2001) also agree that the ratio of the width of the bonded FRP to that of the concrete member, b_p/b_c, had a significant effect on stress development.

Chen and Teng (2001) used the Neubauer and Rostásy (1997) model, combining with the Yuan *et al.* (2001) approach. Although they applied the same relationship for effective length suggested by Yuan *et al.* (2001), the definition was related to the bond length that attracts 99% of the ultimate load as indicated below:

$$a_0 = \frac{1}{\lambda_2} arcsin\left(0.99\sqrt{\frac{s_f - s_0}{s_f}}\right) \tag{2.77}$$

With:

$$\lambda_1 = \sqrt{\frac{\tau_u}{s_0 E_p t_p}} \tag{2.78}$$

$$\lambda_2^2 = \frac{\tau_u}{(s_f - s_0) E_p t_p} \tag{2.79}$$

and

$$P_u = \beta_1 b_p \sqrt{2 E_p t_p G_f} \tag{2.80}$$

where

$$\beta_1 = \begin{cases} \left(\frac{L}{L_e}\right)\left(2 - \frac{L}{L_e}\right) & if : L > L_e \\ sin\left(\frac{\pi}{2}\frac{L}{L_e}\right) & if : L \le L_e \end{cases} \tag{2.81}$$

Through the regression analysis of experimental data, Chen and Teng (2001) proposed that;

$$P_{max} = 0.427 \beta_p \beta_L b_p L_e \sqrt{f_c'} \tag{2.82}$$

Where

$$\beta_p = \sqrt{\frac{2 - (b_p / b_c)}{1 + (b_p / b_c)}} \tag{2.83}$$

$$\beta_L = \begin{cases} 1 & if L \ge L_e \\ sin\frac{\pi L}{2 L_e} & if L < L_e \end{cases} \tag{2.84}$$

$$L_e = \sqrt{\frac{t_p E_p}{\sqrt{f'_c}}} \tag{2.85}$$

$$\varepsilon_{max} = 0.427 \sqrt{\frac{2-(b_p/b_c)}{1+(b_p/b_c)}} \sqrt{\frac{\sqrt{f'_c}}{E_p t_p}} \tag{2.86}$$

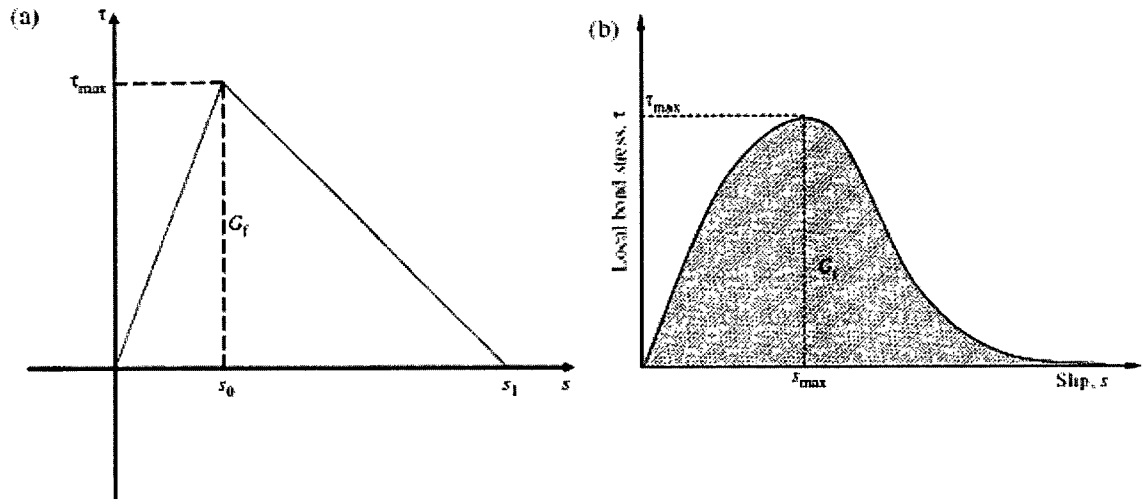

Fig. 2.12. (a) Schematics of bilinear bond stress–slip relationship between concrete and FRP and (b) Schematics of bond stress–slip relationship between concrete and FRP following Nakaba *et al.* (2001b).

Nakaba *et al.* (2001b) conducted a series of double-lap shear tests, with varying properties of concrete and FRP, and proposed that, rather than the triangular approximations shown in Fig.2.12(a) as suggested earlier by Holzenkämpfer (1994) and Neubauer and Rostásy (1997), a bond–slip relationship as shown in Fig.2.12(b) can be used. Using curve-fitting to experimental data, the relationship similar to that developed by Popovics (1973) was suggested. Indeed, Popovics' curve was accepted by several other researchers as well Ferracuti *et al.*(2006), and Kanakubo (2003). The following shows the suggested expression.

$$\tau = \tau_{max} \left(\frac{s}{s_{max}} \frac{n}{(n-1)+(s/s_{max})^n} \right) \tag{2.87}$$

Where, n is an empirical parameter, s and s_{max} are values of slip corresponding to local

bond stress and the maximum bond stress, respectively, both measured in millimeters. τ_{max} is the maximum bond stress measured in MPa as expressed below.

$$\tau_{max} = 3.5 f'^{0.19}_{c} \tag{2.88}$$

Over the range of concrete compressive strengths of 24–58 MPa, the values of s_{max} and n were determined to be 0.065 and 3 mm, respectively. This results in the following expression:

$$\tau = \tau_{max}\left(\frac{s}{s_0}\frac{3}{2+(s/s_{max})^3}\right) \tag{2.89}$$

Where; s_0= 0.065. The interfacial fracture energy, defined as the area below the bond stress–slip curve, can then be obtained as;

$$G_f = \int_0^\infty \tau ds = \int_0^\infty \tau_{max}\left(\frac{s}{s_{max}}\frac{3}{2+(s/s_{max})^3}\right)ds \approx 0.184\tau_{max} \approx 0.644 f_c'^{0.19} \tag{2.90}$$

Similarly, the effective bond length, Le, required to develop full stress transfer from concrete substrate to FRP can be approximated as;

$$L_e \approx \frac{P_{max}}{b_p \tau_{max}/2} \approx \frac{2b_p\sqrt{2G_f E_p t_p}}{b_p \tau_{max}} = \frac{0.6485\sqrt{E_p t_p}}{f_c'^{0.095}} \tag{2.91}$$

Wu *et al.* (2002) modified the above fracture mechanics model for different test setups, including pull and push tests for linear and bilinear bond slip curves. They also checked their results with the finite element method of analysis. For the case of push tests, the theoretical solutions was the same as that of Yuan *et al.* (2000), resulting in the following expression.

$$P_u = b_p\sqrt{\frac{2G_f E_p t_p}{\left(1+\frac{1}{\beta}\right)}} \tag{2.92}$$

For the pull tests, the solution was somewhat different, resulting in the following equation:

$$P_u = b_p \sqrt{2G_f E_p t_p \left(1 + \frac{1}{\beta}\right)} \tag{2.93}$$

Savioa *et al.* (2003) suggested the use of the bond slip curve suggested by Popovics with the empirical parameter n redefined as 2.86. They further suggested the use of $\tau_{max} = 3.5 f'^{0.19}_c$ (2.94) , and s_0= 0.051.

While the previous models were based primarily on the calibration of experimental data, Monti *et al.*(2003) conducted a parametric study using finite element analysis in conjunction with experiments to obtain equations for both anchorage bond capacity, σ_{max}, and effective bond length, L_e, as

$$\sigma_{max} = \beta \sqrt{\frac{E_p \tau_{max}}{3t_p}} \tag{2.95}$$

$$\text{where } \beta_L = \begin{cases} 1 & \text{if} L \geq L_e \\ \sin\dfrac{\pi L}{2L_e} & \text{if} L < L_e \end{cases} \text{ and} \tag{2.96}$$

$$L_e = \sqrt{\frac{t_p E_p}{\sqrt{4\tau_{max}}}} \tag{2.97}$$

The maximum bond stress was expressed as $\tau_{max} = 1.8 k_b f_t$, with k_b being the same as that defined by Brosens and Van Gemert (1999). The maximum strain in the FRP is determined as per Monti *et al.*(2003). The bond slip relationship is assumed to be bilinear (triangular) with the following expressions:

$$\tau = \begin{cases} \tau_{max}\left(\dfrac{s}{s_0}\right) & \text{if } s \leq s_0 \\ \tau_{max}\dfrac{s_f - s}{s_f - s_0} & \text{if } s > s_0 \end{cases} \tag{2.98}$$

and the maximum bond stress and the related slip is already suggested. The only section that is not mentioned in the previous expressions is the final slip.

$$\tau_{max} = 1.8\beta_w f_t \tag{2.99}$$

$$s_0 = 2.5\tau_{max}\left(\frac{t_a}{E_a} + \frac{50}{E_c}\right) \tag{2.100}$$

$$s_f = 0.33\beta_w \tag{2.101}$$

$$\beta_w = \sqrt{\frac{1.5(2 - b_p / b_c)}{1 + (b_p / 100)}} \tag{2.102}$$

Based on a set of double-lap shear tests, Ulaga *et al.* (2003) developed an expression for maximum load attainable based on whether the bond length was larger or smaller than the effective bond length. This is illustrated below:

$$\varepsilon_{max} = \sqrt{\frac{\tau_{max}}{3E_p t_p}} \tag{2.103}$$

$$P_u = \begin{cases} b_p\sqrt{\dfrac{2E_p t_p G_f}{(1+n\rho)}} & if: L \geq L_e \\ b_p\sqrt{\dfrac{E_p t_p G_f}{(1+n\rho)}}\sin\sqrt{\dfrac{(1+n\rho)\tau_{max}^2 l^2}{2E_p t_p G_f}} & if: L < L_e \end{cases} \tag{2.104}$$

Where; $n = \dfrac{E_p}{E_c}, \rho = \dfrac{A_p}{A_c}$ (2.105)

$$G_f = 0.045 f_c^{'2/3} \tag{2.106}$$

$$\tau_{max} = 0.4 f_c^{'2/3} \tag{2.107}$$

$$L_e = \frac{\pi}{2}\sqrt{\frac{2t_p E_p G_f}{(1+n\rho)\tau_{max}^2}} \tag{2.108}$$

Dai and Ueda (2003), Dai (2006) and Dai *et al.*(2005 and 2006) suggested a bond-slip model, as expressed below.

$$\tau_{max} = \frac{-1.575\alpha K_a + \sqrt{2.481\alpha^2 K_a^2 + 6.3\alpha\beta^2 K_a G_f}}{2\beta} \tag{2.109}$$

$$s_0 = \frac{\tau_{max}}{\alpha K_a} \tag{2.110}$$

$$\tau = \begin{cases} \tau_{max}\left(\frac{s}{s_0}\right)^{0.575} & \text{if : } s \le s_0 \text{ Ascendingbranch} \\ \tau_{max} e^{-\beta(s-s_0)} & \text{if : } s > s_0 \text{ Descendingbranch} \end{cases} \tag{2.111}$$

$$G_f = 7.55 K_a^{-0.449} (f_c')^{0.343} \tag{2.112}$$

$$\alpha = 0.028 (\frac{E_p t_p}{1000})^{0.254} \tag{2.113}$$

$$\beta = 0.0035 K_a (\frac{E_p t_p}{1000})^{0.34} \tag{2.114}$$

$$K_a = \frac{G_a}{t_a} \tag{2.115}$$

Ueda and Dai (2004) combined analytical and empirical approaches and developed the following relationships for effective length and ultimate load.

$$L_e = \frac{\sqrt{2E_p t_p}}{B\sqrt{G_f}} ln\left(\frac{1+\alpha}{1-\alpha}\right) \tag{2.116}$$

$$\alpha = \frac{exp\left(\frac{L_b B\sqrt{G_f}}{\sqrt{2E_p t_p}}\right) - 1}{exp\left(\frac{L_b B\sqrt{G_f}}{\sqrt{2E_p t_p}}\right) + 1} \tag{2.117}$$

$$P_u = \alpha P_{max}, P_{max} = (b_f + \Delta b_f)\sqrt{E_f t_f G_f} \tag{2.118}$$

Using regression analysis of experimental data, Ueda *et al.* (2003) proposed a new single curve bond–slip model, accounting for the effect of the adhesive through its shear modulus, G_a, and thickness, t_a. Bond stress development, as a function of slip, was expressed as:

$$\tau_{max} = 2BG_f(e^{-Bs} - e^{-2Bs}) \tag{2.119}$$

where:

$$G_f = 0.446\left(\frac{G_a}{t_a}\right)^{-0.352}(f_c')^{0.236}(E_p t_p)^{0.023} \tag{2.120}$$

$$2UG_f(e^{-Us} - e^{-2Us})/U = 6.846(E_p t_p)^{0.108}\left(\frac{G_a}{t_a}\right)^{0.833} \tag{2.121}$$

and the effective bond length, maximum bond stress, and maximum strain attainable by FRP are given as;

$$B = 6.846(E_p t_p)^{0.108}\left(\frac{G_a}{t_a}\right)^{0.833} \tag{2.122}$$

$$L_e = 38.1\frac{(E_p t_p)^{0.38}}{\left(\frac{G_a}{t_a}\right)^{0.657}(f_c')^{0.118}} \tag{2.123}$$

$$\tau_{max} = 0.5BG_f = 3.423(E_p t_p)^{0.108}\left(\frac{G_a}{t_a}\right)^{0.833}G_f \tag{2.124}$$

$$\varepsilon_{max} = \left(1+\frac{7.4}{b_p}\right)\sqrt{\frac{2G_f}{E_p t_p}} \tag{2.125}$$

In the development of the model, Ueda *et al.* (2003) used a microscope to measure the thickness of the adhesive after failure of the test specimens. Although the model clearly demonstrates the effect of the adhesive, it is difficult to assess this dimension a priori for field use and design. While there are definite significant differences in response due to the use of levels of adhesive which are thicker than that found to be structurally optimum, the differences within the practical range used in practice may be insignificant due to other local configurations and material variations. In the structures strengthened with FRP, the cracking of concrete decreases the relative effect of adhesive thickness (Hollaway and Leeming 1999).

Buyukozturk and Au (2004) applied the widely used analytical model of Sierra-Ruiz *et al.* 2002 that has the following form:

$$L_0 = \sqrt{\frac{E_p t_p t}{\mu_2}} \tag{2.126}$$

$$\varepsilon(x) = \frac{N}{b_p E_p t_p} \frac{sinh\left(\frac{L-x}{L_0}\right)}{sinh\left(\frac{L}{L_0}\right)} \tag{2.127}$$

Here, L represents the bond length, b_p the bond width, t_p the CFRP plate thickness, t the bond line thickness, E_p the elastic modulus of the plate, μ_2 the shear modulus of epoxy, and N the shear bond load. This analytical model was derived from the shear lag theory and it assumes elastic behaviour.

Savoia *et al.* (2003) used Popovic's equation for the nonlinear bond slip model. They applied the following iterative method for calculating slip, based on normal strains obtained from strain gauges.

$$s(x) = s(x_i) + \int_0^x \varepsilon(x)dx = s(x_i) + \frac{(\varepsilon_{i+1} - \varepsilon_i)}{(x_{i+1} - x_i)} \frac{x^2}{2} + \varepsilon_i x \tag{2.128}$$

The researchers used the experimental data generated by Chajes *et al.* (1996) and Miller *et al.* (2001) and conducted a regression analysis. This is shown in Fig.2.13.

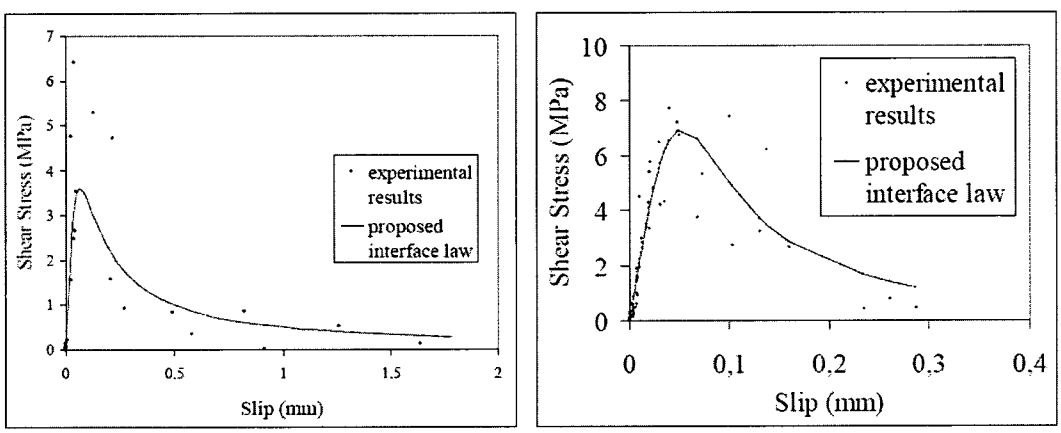

Fig. 2.13. The bond-slip curve developed by Savia *et al.* 2003, (a) Experimental data of Miller *et al.* (2001) and (b) Experimental data of Chajes *et al.* (1996)

The maximum bond strength associated with this model is $\tau_{max} = 3.5 f_c^{'0.19} (= 6.93MPa)$ for tests conducted by Chajes *et al.* (1996) and $\tau_{max} = 0.0184\sqrt{t_p E_p} = 3.6MPa$ for tests of Miller *et al.* 2001.

Analytical approach adopted by Faella et al. (2003) provides the effective length and ultimate load expressions that are shown below:

$$L_e = \sqrt{\frac{E_p t_p}{2.f_{xtm}}} \tag{2.129}$$

$$P_{max} = \tau_{max}.L.b_p \frac{\sin(\alpha_u L)}{\alpha_u L} with: L \le L_e = \frac{\pi}{2\alpha_u} \tag{2.130}$$

$$P_{max,L_e} = \tau_{max}\sqrt{\frac{E_p t_p}{k_u}}.b_p = \sqrt{2G_f E_p t_p}.b_p \tag{2.131}$$

Kanakubo1 *et al.*(2005) investigated the effect of local bond characteristics on macro-level bond behaviour by a numerical analysis based on the sequential integration method. The parameters investigated include; i) Bond slip (τ–s) relationships (Fig.2.14), ii) delamination fracture energy and iii) FRP stiffness as was suggested before by Täljsten (1994). It was analytically concluded that the influence of the shape of τ–s relationship is relatively small, and that macro-level bond strength is mainly influenced by the fracture energy and FRP stiffness. The researchers assumed a bond–slip relationship that was based on a perfectly rigid-plastic model with bond stress τ_y and ultimate slip s_u given as below.

$$L_e = s_u\sqrt{\frac{2t_p E_p}{G_f}} \tag{2.132}$$

$$G_f = \tau_y.s_u \tag{2.133}$$

$$s_u = \frac{\tau_y}{2E_f t_f}.L_e^2 \tag{2.134}$$

$$P_{max,} = b_p\sqrt{2G_f E_p t_p} \tag{2.135}$$

$$P_{max,} = 13.9\sqrt{G_f} = 2.39.\sqrt{t.E} \tag{2.136}$$

Where; l_e is the effective bond length, s_u is ultimate slip in local τ-s relationship (at point where bond stress = 0), $t.E$ is FRP stiffness and G_f is the delamination fracture energy which represents the anchorage condition of FRP.

Kanakubo *et al.* (2003) also used Popovic's model for bond stress-slip relationship. The effective length was derived as indicated below:

$$L_e = 0.7\sqrt{\frac{E_p t_p}{f_c^{0.2}}} \tag{2.137}$$

The related ultimate load was defined as:

$$P_u = \begin{cases} 1.1 f_c'^{0.2} b_p L_e & (L > L_e) \\ \left[0.7\cos\left(\frac{L}{L_e}\pi\right) + 1.8\right] f_c'^{0.2} b_p L & (L < L_e) \end{cases} \tag{2.138}$$

Daus (2004), also suggested a bilinear bond slip model based on Holzenkämpfer (1994) model. The researcher suggested the following expressions for ultimate bond strength T for the end of the plate, as well as the corresponding bond length l_t.

Ultimate bond strength:

$$P_{u,max} = 0.225 b_p \sqrt{E_p . t_p . \sqrt{f_c . f_{ctm}}} \tag{2.139}$$

b_p width of external reinforcement

f_c compressive cube strength of concrete

f_{ctm} surface tensile strength of concrete

L_e: bond length needed to transfer σ_{max} at the end of plate or laminate

E_p modulus of elasticity of external reinforcement,

t_p thickness of external reinforcement

$$L_e = 1.46\sqrt{\frac{E_p t_p}{\sqrt{f_c f_{ctm}}}} \tag{2.140}$$

$$\sigma_{max} = 0.225\sqrt{\frac{\sqrt{f_c f_{ctm}}.E_p}{t_p}} \qquad (2.141)$$

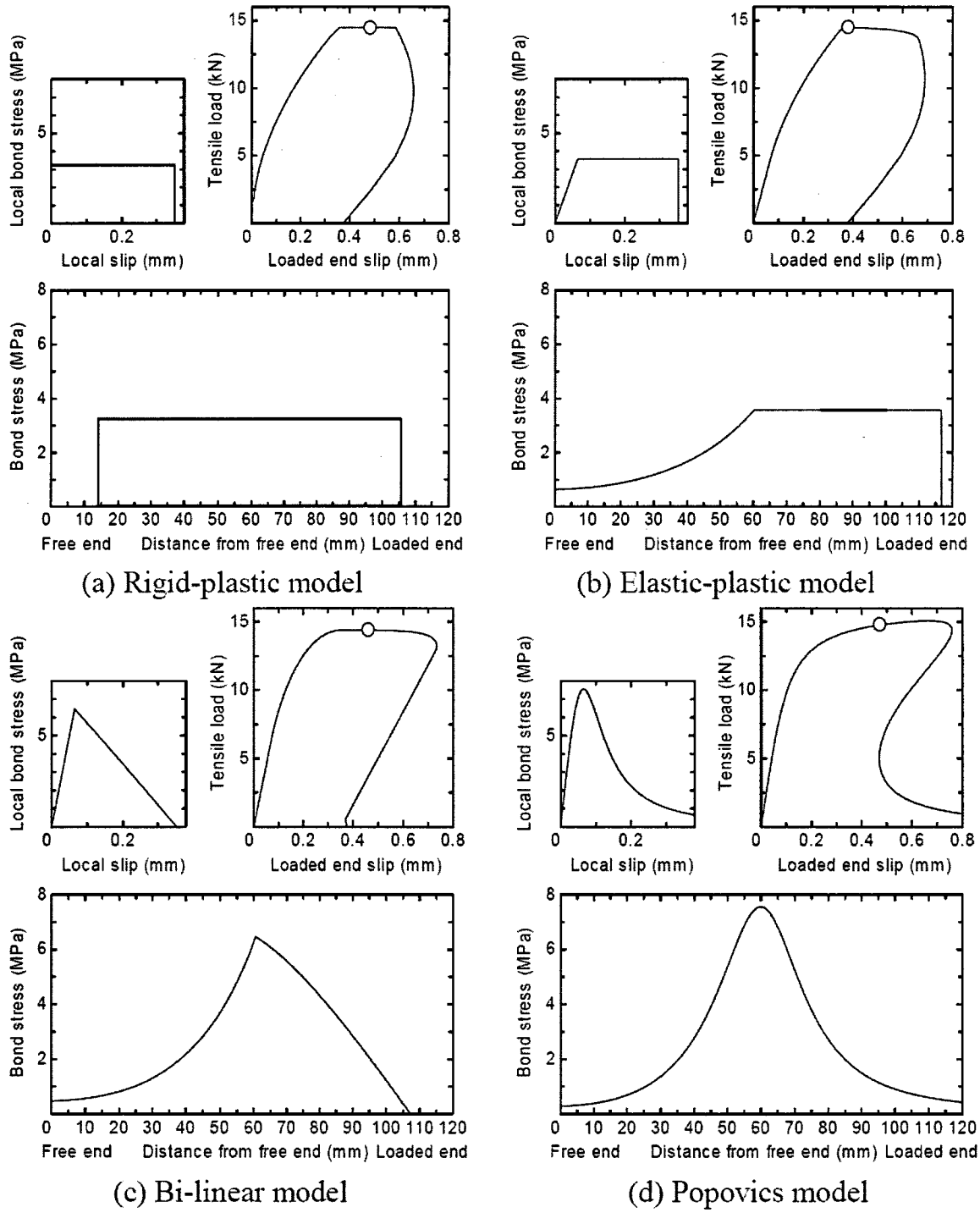

Fig. 2.14. Local τ– s relationships and macro bond behaviour Kanakubo *et al.*(2003)

The maximum fracture energy for external reinforcement that can be transferred at the end of the plate or laminate is expressed as shown below:

$$G_F = \frac{1}{2} . s_0 . \tau_u \tag{2.142}$$

Lu *et al.* (2004a,b ,and 2005a,b,c) suggested several models which are shown in Fig.2.15.

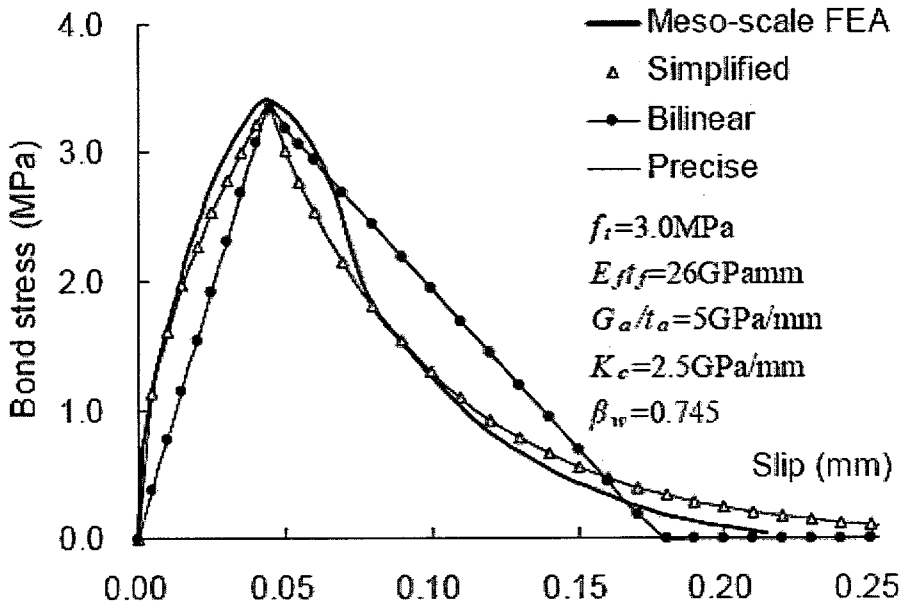

Fig. 2.15. Bond slip models suggested by Lu *et al.* (2005b)

The precise model, shown in the figure, is accurate but somewhat complicated. The precise model describes the ascending and descending branches separately using the following equations:

$$\tau_{max} = \alpha_1 \beta_w f_t \tag{2.143}$$

$s_e = \tau_{max}/K_0$ is the elastic component of s_0 and β_w is the FRP-to-concrete width ratio factor

$$s_0 = \alpha_2 \beta_w f_t + s_e \tag{2.144}$$

$$s_e = \frac{\tau_{max}}{K_0} \tag{2.145}$$

$$\beta_p = \sqrt{\frac{2.25 - (b_p / b_c)}{1.25 + (b_p / b_c)}} \tag{2.146}$$

$$\tau = \begin{cases} \tau_{max}\left(\sqrt{\left(\frac{s}{s_0 A} + B^2\right)} - B\right) & s < s_0 (Ascending.branch) \\ \tau_{max}\, exp\left[-\alpha\left(\frac{s}{s_0} - 1\right)\right] & s > s_0 (descending.branch) \end{cases} \tag{2.147}$$

Where;

$$A = \frac{s_0 - s_e}{s_0} \tag{2.148}$$

$$B = \frac{s_e}{2(s_0 - s_e)} \tag{2.149}$$

The parameter α controls the shape of the descending branch and is given by;

$$\alpha = \frac{1}{\frac{G_f}{\tau_{max} s_0} - \frac{2}{3}} \tag{2.150}$$

The fracture energy is defined as:

$$G_f = \alpha_3 \beta_w^2 \sqrt{f_t}\, f(K_a) \tag{2.151}$$

The coefficients α_1, α_2 and α_3 were determined through an iterative procedure, making use of both the finite element and the test results. The final values obtained from this process for these three coefficients are: $\alpha_1 = 1.50$, $\alpha_2 = 0.0195$, and $\alpha_3 = 0.308$. The term s_e above is equal to τ_{max}/K_0 and it represents the elastic component of s_0. β_w is the FRP-to-concrete width ratio factor. The initial stiffness of the bond–slip model is defined by;

$$K_0 = K_a K_c / (K_a + K_c) \tag{2.152}$$

Where,

$$K_a = G_a / t_a \tag{2.153}$$

$$K_c = G_c/t_c.\ G_c \tag{2.154}$$

G_a and G_c are the elastic shear modulus of the adhesive and concrete, and t_a and t_c are the effective thickness of the adhesive and concrete. A simplified model without a significant loss of accuracy can be easily obtained by noting that the initial stiffness of the bond–slip curve is much larger than the secant stiffness at the peak point.

$$\tau = \begin{cases} \tau_{max}\sqrt{\dfrac{s}{s_0}} & s \le s_0 (Ascending.branch) \\ \tau_{max}\, exp\left[-\alpha\left(\dfrac{s}{s_0}-1\right)\right] & s > s_0 (descending.branch) \end{cases} \tag{2.155}$$

Where:

$$s_0 = 0.0195\beta_w f_t \tag{2.156}$$

$$\alpha = \frac{1}{\dfrac{G_f}{\tau_{max} s_0} - \dfrac{2}{3}} \tag{2.157}$$

The fracture slip and energy can be obtained as:

$$s_f = \frac{2G_f}{\tau_{max}} \tag{2.158}$$

$$G_f = 0.308\beta_w^2\sqrt{f_t} \tag{2.159}$$

Further simplification can be introduced to the simplified model by adopting a bilinear bond–slip curve which can be used to derive a simple explicit design equation for the bond strength. This bilinear model has the same local bond strength and total interfacial fracture energy, so the bond strength is unaffected by this simplification if the bond length is longer than the effective bond length.

$$\tau(s) = \begin{cases} \tau_{max}\left(\dfrac{s}{s_0}\right) & if : s \le s_0 \\ \tau_{max}\left(\dfrac{s_f - s}{s_f - s_0}\right) & if : s_0 < s \le s_f \\ \tau = 0 & if : s > s_f \end{cases} \qquad (2.160)$$

Lu *et al.* (2005c) tested a meso scale Finite element model to control their models. They then compared several models and proposed modification on the models to propose precise and simplified models (Fig.2.16) and investigate the bilinear model. Their result was that using the bilinear model not only prevents using rigorous calculation but also is a very good estimate for design and research purposes. This observation was confirmed by Holzenkämpfer (1994), Täljsten (1997), Brosens and Van Gemert (1998), Yuan *et al.*(2001), and Wu *et al.* (2002).

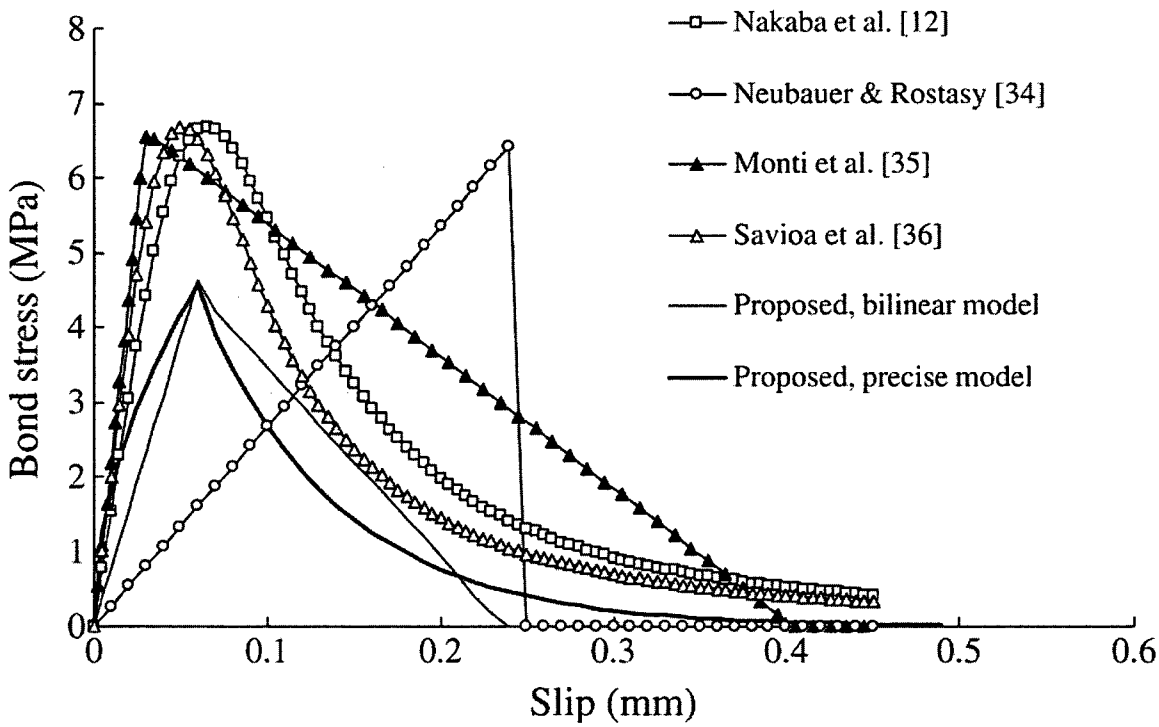

Fig. 2.16. Bond–slip curves from existing bond–slip models (Lu *et al.* 2005a,b)

Based on recent research Lu *et al.* (2004) suggested that the effective FRP strain at debonding can be calculated as:

$$L_{e-exp} = 1.33\sqrt{\frac{2E_p t_p}{f_t}} \tag{2.161}$$

The FRP strain $\varepsilon_{f,\inf}$ for an infinite bond length is given as (Lu *et al.* 2005a):

$$\varepsilon_{f,inf} = \beta_w \sqrt{\frac{0.616\sqrt{f_t}}{E_p t_p}} \quad \text{where} \quad \beta_p = \sqrt{\frac{2.25 - (b_p / b_c)}{1.25 + (b_p / b_c)}} \quad (2.146) \tag{2.162}$$

Chen et al.(2006) presented a similar model:

$$P_u = \begin{cases} b_p \sqrt{2E_p t_p G_f}\, \dfrac{1}{\sqrt{1-\beta^2}} & if: L > a_u \\ b_p \sqrt{2E_p t_p G_f}\, \dfrac{\sin(\lambda L)}{1-\cos(\lambda L)} & if: L \le a_u \end{cases} \tag{2.163}$$

$$a_u = \frac{1}{\lambda} \arccos \beta \tag{2.164}$$

2.2.3. Finite Element Models

Many researchers investigated the bond performance of FRP on concrete by using Finite Element Method (FEM). Included among them are: Jiang(1984), Kang (1996), Niu and Wu (2001), Chen *et al.*(2001), Yang *et al.* (2003), Chen *et al.* (2003), Teng *et al.* (2002), Wu and Yin(2003), Yin and Wu(2003), Yan *et al.* (2004), Chen and Pan (2004), Niu and Wu(2005) Chen and Pan (2006), Lu *et al.* (2005c, 2006), and Zhao *et al.* (2007).

Wu and Yin (2003), and Yin and Wu (2003) investigated the fracture behaviour of bond by both experimental and finite element approaches. They modeled a beam with an additional FRP sheet as reinforcement on the tension face. The objective was to investigate the effects of different types of interfacial debonding and concrete cracking on structural load-carrying capacity of the member.

Lu *et al.* (2004a) investigated eight different bond models for cracked concrete. They identified the following model developed at Dalian University of Technology (Kang, 1996) in China as the best performing model:

$$\tau_{max} = (0.543w^{-0.585} + 0.1999\sqrt{f_c'}\Delta^{0.72} \quad (2.165)$$

Where, w is the crack width in mm and Δ is the relative slip between cracked surfaces in mm. Eq.2.165 was therefore adopted to model the bond behaviour of cracked concrete in their study.

A meso-scale finite element model was first presented by Lu *et al.* (2004b) for simulating debonding behaviour of FRP-to-concrete joints in simple shear tests. In this model, both the FRP plate/sheet and the concrete were modeled using elements of mesoscopic sizes so that the shapes and paths of cracks during the entire debonding process could be appropriately captured. Results obtained from this model were presented to provide insight into the debonding failure process. Finally, based on a finite element parametric study and existing test results, three bond-slip models of different levels of sophistication were presented. The proposed models were claimed to be more accurate than all existing bond-slip models. The researchers implemented one of the models (the meso-scale finite element model) implemented in the MSC.MARC computer program to simulate interfacial debonding failure in a pull test. In this model, very small nearly square elements (0.25–0.5 mm in size) were used with fixed angle crack model (FACM) to capture the development and propagation of cracks in the concrete layer adjacent to the adhesive layer.

Lu *et al.* (2005a,b) investigated crack propagation during bond failure through FEM analysis, a phenomenon that cannot be clearly observed during testing. Their results conform to the experimental observations reported by McSweeney and Lopez(2005). The actual process of debonding is more complex than is predicted by the FEM model, as concrete is a non-homogeneous material. Nevertheless, the Lu *et al.* (2005c) meso-scale finite element results provide useful insight into the failure mechanism. The load–slip curve at the loaded end of specimen Wu-1 is shown in Fig. 2.17 as obtained from the FEM model. Representative points are marked as points A to F on this load–slip curve for the illustration of debonding process. Crack strain contours in concrete, corresponding to the load stages indicated in Fig. 2.17, are shown in Fig.2.19.

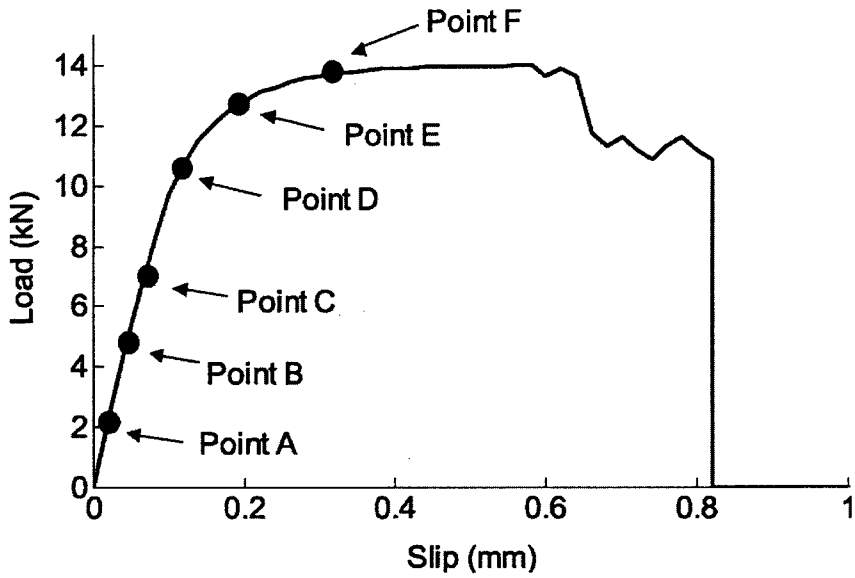

Fig. 2.17. Load–slip curve of specimen Wu-1 from the FE model. Lu *et al.* (2005c)

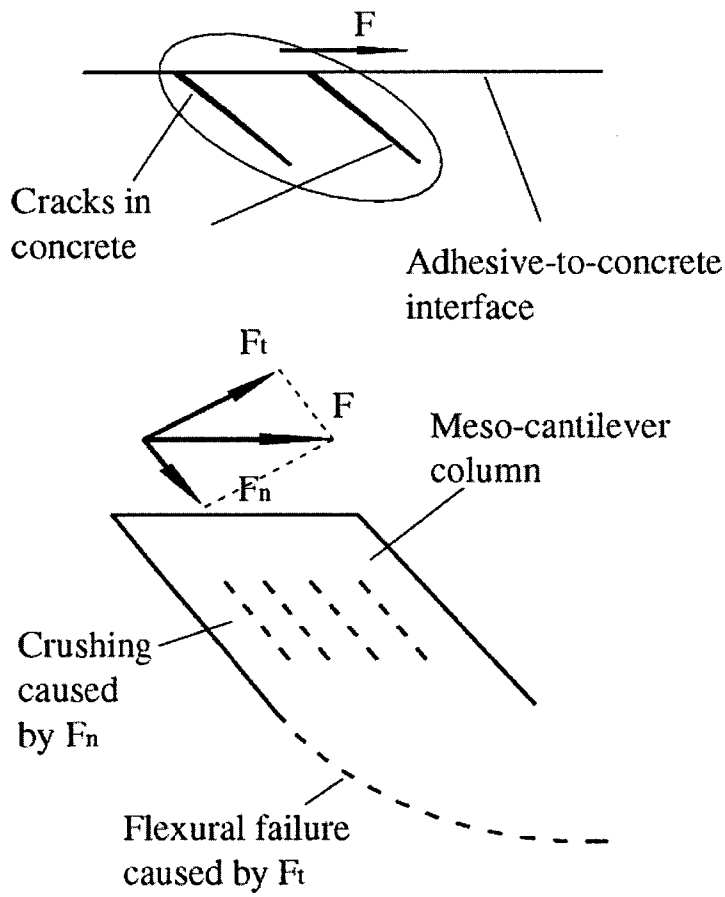

Fig. 2.18. Meso-cantilever column and its failure modes (Lu *et al.* 2005c)

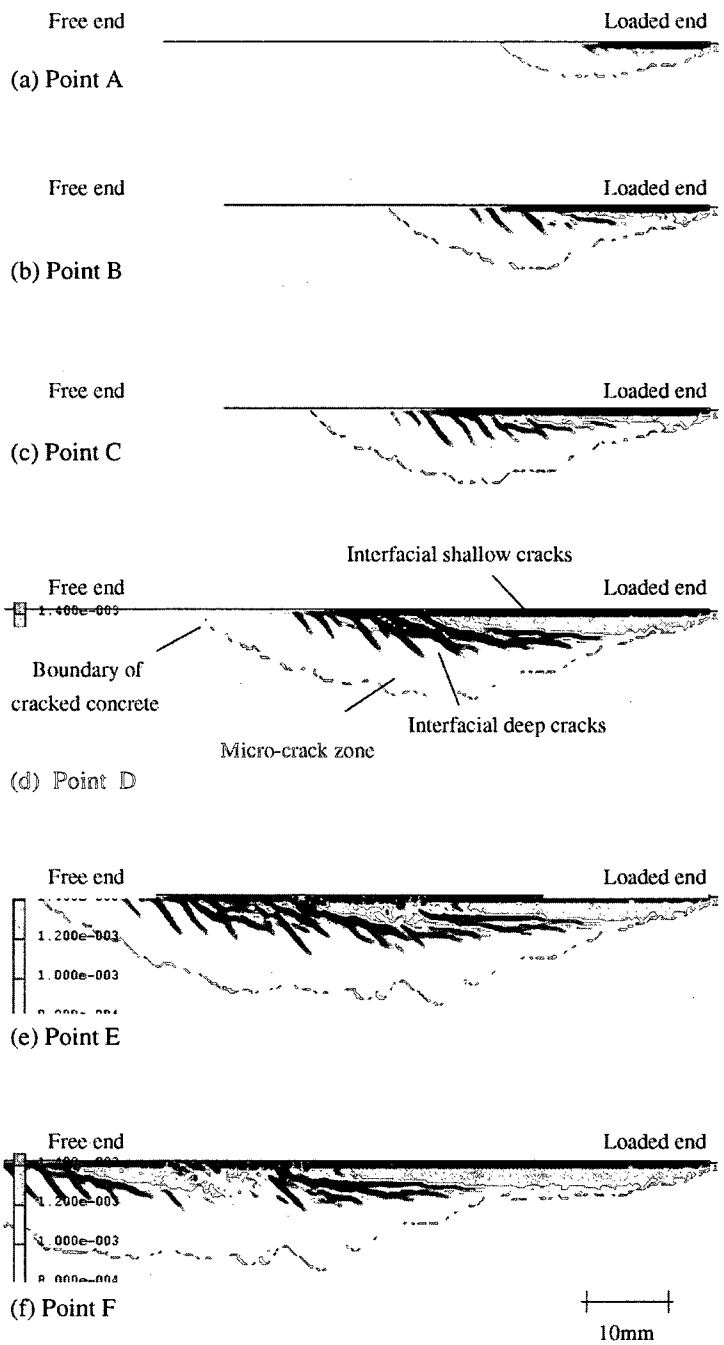

Fig. 2.19. Crack patterns in Wu-1 concrete prism as obtained by FE model.

(Lu *et al.* 2005c)

The researchers reported that, at a low level of loading, the formation of interfacial shallow cracks are at 45° to 60° to the interface, leading to the appearance of small cantilever columns (i.e. meso-cantilevers). With further increases in loading, these

cantilevers may grow longer as the shallow cracks grow into deep cracks, or may fail if the bond force acting on the cantilever reaches a critical value. The shear force F on the cantilever leads to axial compressive stresses which can cause crushing failure, or flexural tensile stresses at the root, which are responsible for flexural failure (Fig.2.18). An inspection of the finite element results reveal that debonding as observed in laboratory tests corresponds to the progressive flexural failure of meso-cantilevers, except near the loaded end where debonding is mainly due to the crushing of the mesocantilevers. Fig. 2.19(a) shows that in the early stages of loading, significant bond stresses are developed near the loaded end. As the load increases, bond stresses increase and the effective bond zone expands (Fig. 2.19.b). When the maximum bond stress reaches the local bond strength, softening (micro-cracking) of the interface commences. The bond stresses near the loaded end then decrease (Fig. 2.19c and d), and the effective bond zone continues to expand towards the free end. Finally, when full debonding is reached (Fig. 2.19.e), the bond stress close to the loaded end becomes very small, indicating the formation of a macro-crack. This macro-crack corresponds to the surface of the debonded concrete layer observed in a laboratory test. At this stage, the load–slip curve is already highly nonlinear. Afterwards, the effective bond zone moves away from the loaded end towards the free end as the macro-crack propagates towards the free end. During this stage the load increases much more slowly than the slip. After Point F, the load remains almost constant until the FRP plate is entirely debonded from the concrete prism. The same phenomenon was also explained by Yuan et al.(2004).

2.2.4. Design Proposals

A number of design procedures and expressions were developed by previous researchers to compute the effective bond length, maximum bond or maximum normal stresses. Van Gemert (1980) proposed a design expression for the ultimate bond capacity by assuming a triangular bond stress distribution along the full bond length, as shown below.

$$P_u = 0.5 b_p L f_{ctm} \tag{2.166}$$

The only material parameter in this equation is the concrete surface tensile strength f_{ctm}. According to Brosens and van Gemert (1997), the above formula provides the load at

concrete cracking in the initial force transfer zone, but it does not take into account the strength reserve after the first cracking. While this might be construed to mean that always provides a conservative prediction, such an interpretation is invalid, as the limit of the effective bond length is not included in the Equation. Therefore, the equation implies that the full tensile strength of the bonded plate can be carried by a sufficiently long bonded joint. This is conceptually misleading, as it contradicts with the well-established fact that any additional bond length beyond the effective bond length cannot increase the anchorage strength.

Volnyy and Pantelides (1999) attempted to derive the effective bond length using the above expression proposed by Van Gemert and fracture mechanics. Unfortunately, their concept of the effective bond length was incorrect, which introduced a number of errors. Therefore, the resulting approach may be viewed as an alternative expression of van Gemert's equation.

Chaallal *et al.* (1998) proposed a design expression based on the studies by Roberts (1989), and Varastehpour and Hamelin (1996). The expression is based on the assumption that bond behaviour resembles to that of a Mohr-Coulomb material. For bond strengthening, the researchers assumed that the maximum bond stress is twice the average stress τ_{avg} and the maximum bond stress does not exceed the Mohr-Coulomb strength equation given by Varastehpour and Hamelin (1996). This gives the following expression:

$$\tau_{avg} = \frac{\tau_{max}^{debonding}}{2} = \frac{2.7}{1 + k_1 \tan 33^\circ} \tag{2.167}$$

Where;

$$k_1 = t_p \sqrt{\frac{k_a}{4 E_p t_p}} \tag{2.168}$$

$$k_a = E_a \frac{b_a}{t_a} \tag{2.169}$$

The variables b_a, t_a, and E_a are the width, thickness, and Young's modulus of the adhesive, respectively. Because the relationship was based on limited experimental data and does not relate to the strength of concrete, its applicability is seriously limited. Another drawback of this proposal is that the effective bond length is not considered.

Khalifa *et al.* (1998) proposed a modification to the expression suggested earlier by Maeda *et al.* (1997), and included the effect of concrete strength so that it could be used for design. They used the relationship that bond strength between the FRP sheet and the concrete surface is a function of $(f'_c)^{2/3}$ (Horiguchi and Saeki 1997). Because the concrete strength was 42 MPa in the experiments carried out by Maeda *et al.* (1997), the modified equation assumed the following form:

$$\tau_u = \frac{110.2}{10^6}\left(\frac{f'_c}{42}\right)^{2/3} E_p t_p \tag{2.170}$$

Neubauer and Rostásy (1997) proposed the use of 75% of ultimate bond strength as a design value for design.

Chen and Teng (2001) suggested a design expression based on their model discussed earlier. Accordingly, the maximum design strength in FRP is as given below:

$$\sigma_{max,} = 0.315\beta_w\beta_L\sqrt{\frac{E_p}{t_p}\sqrt{f'_c}} \le f_p \tag{2.171}$$

Teng *et al.* (2003) modified the value of the numerical constant given in the above expression, based on the suggestion of Yuan *et al.* (2001), to account for intermediate crack-induced debonding in beams and slabs more accurately. The modified expression is presented below.

$$P_{max} = 0.48\beta_p\beta_L b_p L_e\sqrt{f'_c} \tag{2.172}$$

The researchers further suggested that the distance from the critical section to the plate end should be at least twice the effective bond length. This length is shown below as L_a.

$$L_a = 2\sqrt{\frac{t_p E_p}{\sqrt{f'_c}}} \tag{2.173}$$

Some of the above expressions were implemented in design codes and standards. For instance, both ACI440.2.R-08 and CSA *S806-02* adopted the expression suggested by Maeda *et al.* (1997) which was questioned by researchers recently(). Accordingly, the effective length defined in ACI440.2.R- 08 is:

$$L_e = \frac{23300}{(nt_p E_p)^{0.58}} \tag{2.174}$$

The ACI440.2.R- 08 also suggested that the bond capacity of FRP to be developed over a critical length l_{df}. Furthermore, to develop the effective FRP stress at a section, the available anchorage length of FRP should exceed the amount given bellow by Teng *et al.* 2001.

$$l_{df} = \sqrt{\frac{n_p E_p t_p}{\sqrt{f_c'}}} \tag{2.175}$$

Also, the effective strain in FRP reinforcement should be limited to the strain level at which debonding may occur. This level of strain, ε_{fd}, is defined below:

$$\varepsilon_{fd} = 0.41.\sqrt{\frac{f_c'}{n_p E_p t_p}} \leq 0.9\varepsilon_{fu} \tag{2.176}$$

CSA S806-02 adopted a similar expression for the effective length, as indicated below.

$$L_e = \frac{25350}{(t_f E_f)^{0.58}} \tag{2.177}$$

The anchorage length is defined as the shortest bond length required to develop the full capacity of external FRP reinforcement:

$$l_{fd} = \frac{b_p}{b_c}.\frac{E_p \varepsilon_u t_p}{k\sqrt{f_c'}} \tag{2.178}$$

That above expression does not conform to the concept of having an effective length for FRP.

2.3. Conclusions Based on Previous Research

As a result of the extensive literature review presented in this Chapter, the following conclusions can be drawn:

- The test variables that play significant roles in previous investigations can be summarized as; i) the properties of base or substrate material (type, strength, and surface roughness), ii) FRP (type, mechanical properties, thickness, number of layers, width), iii) epoxy adhesive (strength, elongation, thickness), iv) the loading history and the environmental conditions (moisture, temperature, frost, pollution). These variables have impact on the effective bond length, slip-bond curve, and rupture or fracture energy.

- For concrete substrates, the parameters that affect failure consist of the compressive and tensile strength, bond stress, and elastic modulus.

- Previously suggested expressions for the effective FRP bond length were primarily a function of the thickness and elastic modulus of FRP. In recent years, the parameters affecting concrete strength and FRP strip width have also been incorporated into the expressions suggested for bond length.

- The test method can also play a significant role on test results. Both numerical and experimental studies have shown that the use of different test set-ups can lead to significantly different test results (Yao *et al.* 2005). Furthermore, it has been reported that small variations in test setups within a selected method, such as the height of the support or pushing block may also have an effect on test data (Yuan *et al.* 2004).

- Researchers have recently agreed that there exists an effective bond length beyond which the ultimate load capacity does not increase. However, there are differences in opinions about the manner in which the relevant parameters were introduced in effective bond length expressions. The relationships suggested by Maeda *et al.* (1997) and adopted by design codes such as ACI440.2.R-08 and CSA S806-02 are being challenged by researchers in recent years. (Niedermeier 1996, Blaschko *et al.* 1996, Täljsten 1994, 1997, Yuan *et al.* ,2001) ,Yoshizawa *et al.*,2000, Yuan *et al.* 2001, Chen and Teng 2001, JCI. Report-2003, Kamel *et al.* 2004). The main variables affecting effective bond length in these formulations are the modulus of elasticity and thickness of FRP. These two

variables appear in the denominator of the suggested expressions, indicating that they are inversely proportional to the effective bond length L_e. More recent formulations, however, include the same two variables as multipliers in the numerator. Furthermore, the effective bond length in some of the more recent expressions is also dependent on concrete failure properties, such as the compressive and tensile strength, bond stress, bond-slip relationship, rupture energy, and concrete elasticity modulus. It was indicated that higher concrete strengths result in lower effective bond lengths. The parameters that are related to FRP and concrete dimensions are considered to be less important. The proportion of sheet width to concrete width is used as a parameter in many investigations.

- The development or anchorage length concept in describing surface bonded FRP is not longer valid. Instead the effective length concept has been shown to reflect test observations.

- The effect of cyclic loading on bond characteristics of surface bonded FRP has not been investigated through typical pull or push tests, other than the investigation of structural response of large scale structural components retrofitted by surface bonded FRP.

- Currently there are several test setups suggested for the experimental investigation of surface bonded FRP on concrete and masonry substrates. However, a better test setup may have to be developed to capture the effects of a number of test parameters that are currently overlooked. Consequently, the current Canadian standard pull out test may need to be revised.

Chapter 3

EXPERIMENTAL WORK

An experimental program was designed to investigate the surface bond characteristics of CFRP sheets on concrete and masonry substrates. The test program consisted of 72 prisms with surface bonded carbon CFRP sheets, subjected to axial tension. This included 58 concrete, 6 concrete block and 6 clay brick specimens. The test variables were; i) CFRP bond length, ii) number of CFRP layers, iii) width of CFRP strips iv) substrate material (concrete, concrete block, and clay brick), v) loading (monotonically increasing static loading and cyclic loading), vi) concrete strength, vii) test setup. The following sections provide a summary of test specimens, test setup, test procedure, instrumentation and data acquisition, as well as an extensive discussion of test results.

3.1. Test Specimens

Table 3.1 summarizes the properties of test specimens and test variables considered in the experimental program. The test program was initially designed to conform to the recommended test procedure outlined in CSA S806-02. Therefore, the specimen geometry was based on the recommendations of CSA S806-02. The concrete prisms had cross sectional dimensions of 150x150 mm. Each prism consisted of two halves, with surface bonded CFRP connecting the two. Each half had a length of 200 mm (total length of 400 mm), except when the bond length was a parameter. In the latter case

the total specimen length varied between 230 mm and 600 mm. The two halves of the prisms were always equal. In certain cases, the available machine headroom limited the specimen geometry. Also, the specimen weight and ease in handling was a consideration, since a large number of specimens were tested. The test program and the setup were revised as needed, during the test program, depending on the results of previous tests.

Table 3.1. Test program

(a) Summary of test program

				FRP			Substrate	
	# of			Width	Layers	Thickness	Material	Strength
Series	Spec.	Description	Setup	b_p(mm)	n_p	$n_p t_p$ (mm)		MPa
1	6	1 Layer	Push	100	1	0.165	Concrete	46
2	6	1 Layer+ Attached Steel Sheet	Push	100	1	0.165	Concrete	47
3	7	2 Layer	Pull	100	2	0.330	Concrete	46
4	3	Three different setups	Pull	100	1	0.165	Concrete	46
5	7	Incremental Cyclic Loading	Pull	100	1	0.165	Concrete	47
6	6	Concrete Blocks	Pull	100	1	0.165	Blocks	16
7	5	Low Strength Concrete	Pull	100	1	0.165	Concrete	30
8	5	Low Width	Pull	65	1	0.165	Concrete	52
9	5	Lower Width	Pull	30	1	0.165	Concrete	52
10	6	3 Layers	Pull	100	3	0.495	Concrete	54
11	6	Brick	Pull	100	1	0.165	Brick	~20
12	6	High Strength	Pull	100	1	0.165	Concrete	76
13	2	Long bond	Pull	100	1	0.165	Concrete	46, 68
14	2	High Strength, Lower Width	Pull	30	1	0.165	Concrete	68

Table 3.1.(b) Details of test program

Code #	Description	b_p mm	n_p	L_b mm	L_{spec} mm	f'_c MPa	P_u kN	Failure Mode
1-1	Push:Fig. 3.1(a)	100	1	35	400	46	11.23	Diagonal crack
1-2	Push:Fig. 3.1(a)	100	1	45	400	46	7.35	Within the epoxy layer
1-3	Push:Fig. 3.1(a)	100	1	57	400	46	14.13	Diagonal and Within the epoxy layer
1-4	Push:Fig. 3.1(a)	100	1	70	400	46	14.72	Diagonal and Within the epoxy layer
1-5	Push:Fig. 3.1(a)	100	1	80	400	46	14.68	Diagonal and over top layer of concrete surface
1-6	Push:Fig. 3.1(a)	100	1	90	400	46	15.57	Diagonal and over top layer of concrete surface
2-1	Push:Fig. 3.1(b)	100	1	35	400	47	9.98	Diagonal
2-2	Push:Fig. 3.1(b)	100	1	45	400	47	11.51	Diagonal and top 1-3 mm layer of concrete
2-3	Push:Fig. 3.1(b)	100	1	57	400	47	15.56	Diagonal and top 1-3 mm layer of concrete
2-4	Push:Fig. 3.1(b)	100	1	70	400	47	16.01	Diagonal and over top layer of concrete surface
2-5	Push:Fig. 3.1(b)	100	1	80	400	47	17.81	Diagonal and top 1-3 mm layer of concrete
2-6	Push:Fig. 3.1(b)	100	1	90	400	47	20.91	Diagonal and top 0-3 mm layer of concrete
4-1	Setup Fig.3.3.(a)	100	1	90	230	46	22.64	Bar anchorage failure
4-2	Setup Fig.3.3(b)	100	1	90	230	46	17.77	Diagonal and top 1-3 mm layer of concrete
4-3	Setup Fig.3.2(a)	100	1	90	230	46	14.13	Diagonal and bar anchorage failure
3-1	3 Layers	100	2	35	400	46	11.99	Diagonal
3-2	3 Layers	100	2	45	400	46	14.96	Diagonal and concrete failure within 30 mm of surface
3-3	3 Layers	100	2	57	400	46	19.04	Diagonal
3-4	3 Layers	100	2	70	400	46	22.51	Diagonal and concrete failure within 30 mm of surface
3-5	3 Layers	100	2	80	400	46	22.59	Diagonal and bar anchorage
3-6	3 Layers	100	2	90	400	46	25.50	Diagonal and bar anchorage
3-7	3 Layers	100	2	180	500	46	25.68	Bar anchorage failure and diagonal cracks

Table 3.1.(b) Cont'd. Details of test program

Code #	Description	b_p mm	n_p	L_b mm	L_{spec} mm	f'_c MPa	P_u kN	Failure Mode
5-1	Cyclic Loading	100	1	34	400	47	15.01	Diagonal and top 1-10 mm layer of concrete
5-2	Cyclic Loading	100	1	45	400	47	10.97	Diagonal and top 1-3 mm layer of concrete
5-3	Cyclic Loading	100	1	58	400	47	12.38	Diagonal and top 1-3 mm layer of concrete
5-4	Cyclic Loading	100	1	70	400	47	15.00	Diagonal and top 1-3 mm layer of concrete
5-5	Cyclic Loading	100	1	80	400	47	19.63	Diagonal and top 1-3 mm layer of concrete
5-6	Cyclic Loading	100	1	180	500	47	24.00	Diagonal and top 1-3 mm layer of concrete
5-7	Cyclic Loading	100	1	113	400	47	24.76	Diagonal and top 1-10 mm layer of concrete
6-1	Concrete Blocks	100	1	35	400	16		Diagonal
6-2	Concrete Blocks	100	1	45	400	16	10.35	Diagonal
6-3	Concrete Blocks	100	1	57	400	16	13.91	Tension failure of the walls of block masonry units
6-4	Concrete Blocks	100	1	70	400	16		Tension failure of the walls of block masonry units
6-5	Concrete Blocks	100	1	80	400	16	12.58	Tension failure of the walls of block masonry units
6-6	Concrete Blocks	100	1	90	400	16	15.99	Tension failure of the walls of block masonry units
7-1	Lower Strength	100	1	35	400	30	5.93	Diagonal
7-2	Lower Strength	100	1	70	400	30	12.26	Diagonal and top 1-3 mm layer of concrete
7-3	Lower Strength	100	1	105	400	30	15.48	Diagonal and top 1-10 mm layer of concrete
7-4	Lower Strength	100	1	140	400	30	18.78	Diagonal and failure within top 1 mm layer of concrete
7-5	Lower Strength	100	1	220	500	30	19.15	Diagonal and failure within top 1 mm layer of concrete
8-1	Low Width	65	1	40	400	52	9.33	Diagonal and top 1-3 mm layer of concrete
8-2	Low Width	65	1	55	400	52	11.58	Diagonal and top 1-10 mm layer of concrete
8-3	Low Width	65	1	79	400	52	15.05	Diagonal and top 1-5 mm layer of concrete
8-4	Low Width	65	1	100	400	52	16.34	Diagonal and failure within top 1 mm layer of concrete
8-5	Low Width	65	1	177	500	52	26.56	Diagonal and top 1-3 mm layer of concrete

Table 3.1.(b) Cont'd. Details of test program

Code #	Description	b_p mm	n_p	L_b mm	L_{spec} mm	f'_c MPa	P_u kN	Failure Mode
9-1	Lower Width	30	1	39	400	52	9.36	Diagonal and Within the epoxy layer
9-2	Lower Width	30	1	58	400	52	9.39	Diagonal and Within the epoxy layer
9-3	Lower Width	30	1	78	400	52	8.60	Diagonal and Within the epoxy layer
9-4	Lower Width	30	1	100	400	52	12.21	Diagonal and failure within top 1 mm layer of concrete
9-5	Lower Width	30	1	177	500	52	11.21	Diagonal and Within the epoxy layer
10-1	3 Layers	100	3	35	400	54	15.29	Diagonal
10-2	3 Layers	100	3	60	400	54	23.97	Diagonal deep to the rebar
10-3	3 Layers	100	3	85	400	54	25.18	Diagonal deep to the rebar
10-4	3 Layers	100	3	112	400	54	32.05	Diagonal deep to the rebar
10-5	3 Layers	100	3	150	400	54	22.60	Bar anchorage
10-6	3 Layers	100	3	280	610	54	38.21	Diagonal cracking and Bar anchorage
11-1	Clay Brick	40	1	35	400	20	5.62	Diagonal failure
11-2	Clay Brick	40	1	55	400	20	6.96	Diagonal failure
11-3	Clay Brick	40	1	80	400	20	7.62	Diagonal and Within the epoxy layer
11-4	Clay Brick	40	1	105	400	20	9.21	Diagonal and Within the epoxy layer
11-5	Clay Brick	40	1	140	400	20	10.91	Diagonal and Within the epoxy layer
11-6	Clay Brick	40	1	173	400	20	7.71	Diagonal and Within the epoxy layer
12-1	High Strength	100	1	30	400	76	17.25	Diagonal failure
12-2	High Strength	100	1	45	400	76	14.61	Diagonal failure
12-3	High Strength	100	1	65	400	76	20.74	Diagonal failure
12-4	High Strength	100	1	90	400	76	23.55	Diagonal deep faced to the rebar
12-5	High Strength	100	1	140	400	76	32.49	Diagonal and top 1-3 mm layer of concrete
12-6	High Strength	100	1	240	600	76	34.47	Diagonal and top 1-10 mm layer of concrete
13-1	Long Bond	100	1	240	600	68	49.03	Diagonal and failure within top 1 mm layer of concrete
13-2	Long Bond	100	1	240	600	46	20.16	Diagonal and top 1-10 mm layer of concrete
14-1	Check	30	1	25	400	68	4.65	Diagonal crack
14-2	Check 2	30	2	180	500	68	15.13	Diagonal and top 0-3 mm layer of concrete

- All specimens are concrete unless otherwise indicated.
- The setup shown in Fig. 3.5. was used for all specimens unless otherwise indicated.

The test series indicated in Table 3.1 refer to the batches of specimens prepared together to investigate the effects of test variables. In most series, the bond length was the only variable, having 5 to 7 different values. The reference bond length used was computed based on the expression suggested by Maeda *et.al.* (1997). The effect of test setup was investigated by comparing the specimens in Series 1, 2, and 4. Within each of these series the only variable considered was the bond length. Series 3 and 10 specimens were tested to investigate the effects of the number of FRP layers, consisting of 2 and 3 layers, respectively. The reference FRP width was selected to be 100 mm. This was changed in Series 8 and 9 to 65 mm and 30 mm, respectively to investigate the width effect. The FRP width was also changed to 30 mm in Series 14, but this series had a higher strength concrete. The effect of concrete strength was investigated by comparing the specimens of Series 7 and 12 which had lower (30 MPa) and higher strength (76 MPa) concretes, respectively. Most of the test specimens had concrete strength of approximately 46 MPa. Therefore, Series 1 specimens from this strength group were also included in the comparison. The effects of cyclic loading were investigated in Series 5 by applying incrementally increasing tensile force cycles. The specimens of series 6 and 11 were tested to investigate the performance of concrete blocks and bricks as different substrates, respectively.

3.2. Test Setup

The test method and test setup in the current investigation were adopted from the CSA Standard S806-02 with minor variations. Specifically, the setup described for determining the bond strength of CFRP sheets on concrete, recommended in Annex P, Method A of CSA S806-02 was adopted. The Standard recommends a special test frame instead of using a universal testing machine. In this research program, an existing universal testing machine in the Structures Laboratory of the University of Ottawa was used to apply the load. Fig. 2.2.a demonstrates the details of the CSA S806-02 requirements. The specimen length is governed by the development length of the rebar embedded in concrete to apply the tensile force.

The test setup was primarily designed to establish the effective bond length. The sheet length was taken as kL_{ea}, where L_{ea} represents the anticipated bond length estimated by using CSA S806-02 (2002), which is based on the expression developed by Maeda *et al.* (1997). The sheet length varied between 0.6 and 1.6 times the anticipated length in increments of 0.2 (k = 0.6, 0.8, 1.0, 1.2, 1.4, 1.6). It is suggested in Annex P, Method A of CSA S806-02 to conduct tests starting with the shortest length of CFRP and gradually increasing the length until the bond force does not change by more than 10% between the last three subsequent bond lengths. The average of these three bond lengths would then be taken as the effective bond length for the CFRP at hand. This method of establishing the effective bond length may result in a conservative estimate.

The following test setups were used in the current research, as minor variations of the method recommended in CSA S806.

3.2.1. Push Test Setups

In the initial phase of the research, it was conservatively assumed that the material rupturing capacity of CFRP could be developed. Consequently, the required development length of re-bars embedded in concrete, based on the CSA method, was found to translate into too long specimens. Therefore, as the distance between the heads of the universal testing machine did not allow long specimens, and handling very long specimens would be inconvenient, the CSA test setup was modified and the re-bars were welded to steel plates to develop sufficient anchorage. This allowed a reduction in the specimen length to 400 mm. The specimen geometry is illustrated in Fig. 3.1. The rebar size (diameter) was determined such that it would remain elastic when the CFRP reached its tensile rupturing capacity (assuming sufficiently high bond strength). A relatively thick steel plate was welded to maintain the elastic rigidity during testing. This resulted in a push test, since the concrete was pushed away by the steel plate (Fig. 3.1.b). Applying the push load through internally placed steel plates had not been done in previous experimental research.

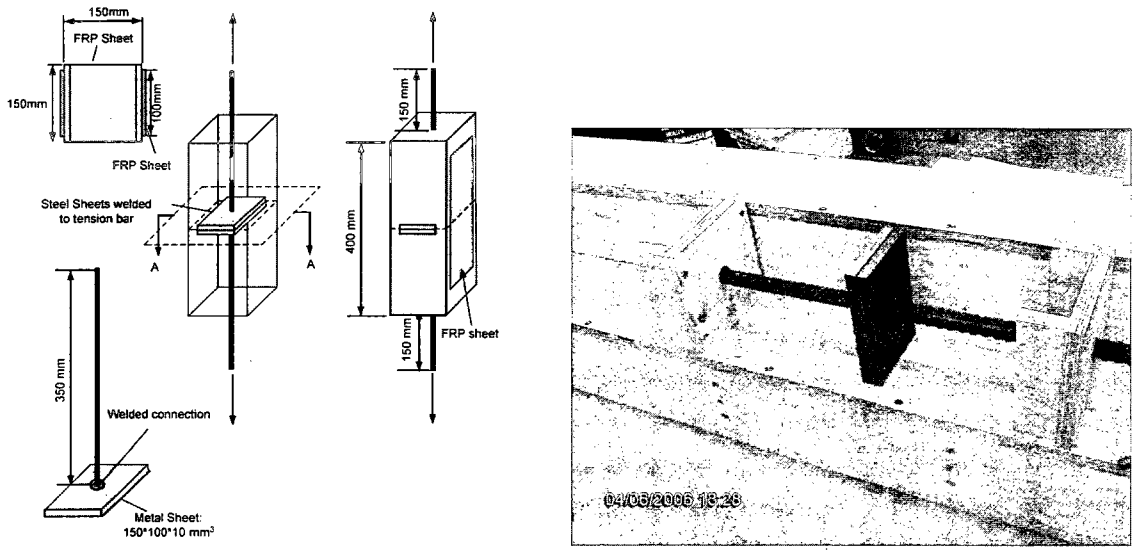

(a) (b)

Figure 3.1. Steel plates used to apply load (a) Schematic view; (b) Actual re-bar plate assembly in formwork

The specimens lacked the spiral reinforcement recommended by CSA S803-02 for controlling splitting tensile cracks, because they would not be generated in the method illustrated in Fig. 3.1. A side benefit of omitting the spiral reinforcement was that the specimen could be cast from concrete containing larger size aggregates. The presence of welded steel plates facilitated the alignment of bars in the formwork prior to casting, which was essential in eliminating accidental eccentricities (Shadravan *et al.* 2007). The concrete was cast with steel bars in the horizontal position as required by CSA S806-02. The CFRP sheets had a width of 100 mm, leaving 25 mm distance to the specimen edge on either side. The steel plate had 100 mm dimension perpendicular to the plane of the CFRP, positioned to be 25 mm short of reaching the surface bonded CFRP sheets on either side.

FRP strips were placed on two opposite faces of each specimen, crossing over the intentionally created weak section by the presence of steel plates representing the interface of two elements. Sheet length was taken as kL_{ea}, where L_{ea} represented the anticipated bond length, as explained above. The CFRP sheet length varied between 0.6 and 1.6 times the anticipated length, in increments of 0.2. Since the calculated effective length was only 56 mm, the length of CFRP was limited. That also affected the accuracy of the sheet length, which was cut to the desired length within 3 mm precision.

After the Series 1 tests, it was decided that the same specimens could be re-used with CFRP sheets bonded on the other two perpendicular faces. This resulted in an additional 6 specimens (Specimens 2-1 to 2-6). This time, however, the CFRP sheets were almost in contact with the edges of steel plates along their short sides, forming Series 2 tests. This is illustrated in Fig. 3.2(b).

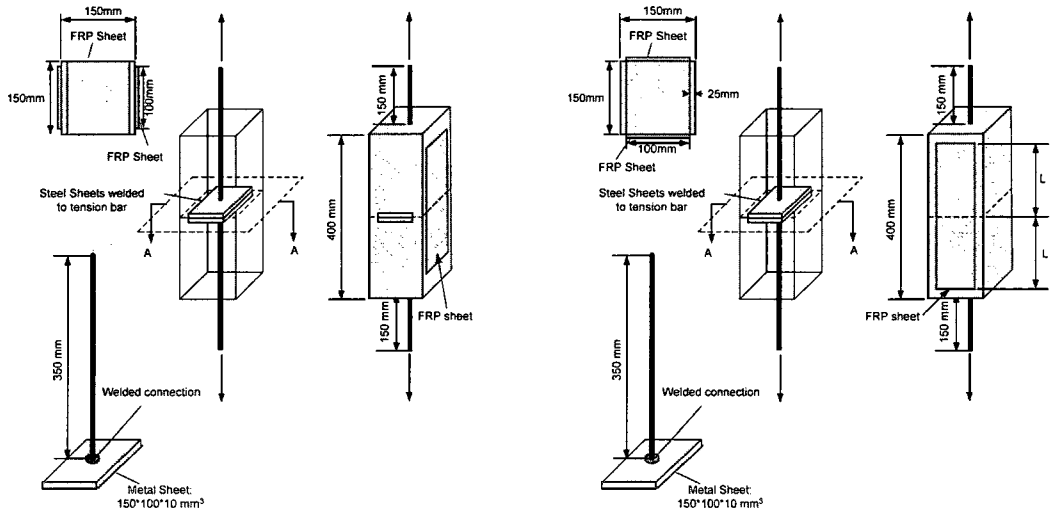

(a) Test series 1 (b) Test series 2

Figure 3.2. Schematic views of test setup used for Series1 and 2 specimens

The test setup used for Series 1 and 2 specimens can be applied as an appropriate push test. However, the perceived need for the steel plates could not be realized since the bond failure preceded the CFRP rupture, leaving the bond between rebars and concrete sufficient to conduct the test as pull tests. Therefore, the thick steel plates were not used in the following test setups.

3.2.2. Pull Test Setups

The majority of the specimens were tested under a direct pull, where the pull force was transmitted through bond between the embedded rebar and concrete, without the pushing plate. Initial three pilot tests had either a thin metal sheet in the middle to create a weak section, as suggested by CSA S805-02, or foam to induce a crack between the two halves of the specimen. These formed Series 4 specimens. The steel sheet had 100 and 150 mm by 150 mm cross sectional dimension. In one of the specimens the

CFRP was placed parallel to the long side of the sheet, and in the other specimen they were placed parallel to the short side. The specimens are illustrated in Fig. 3.3.

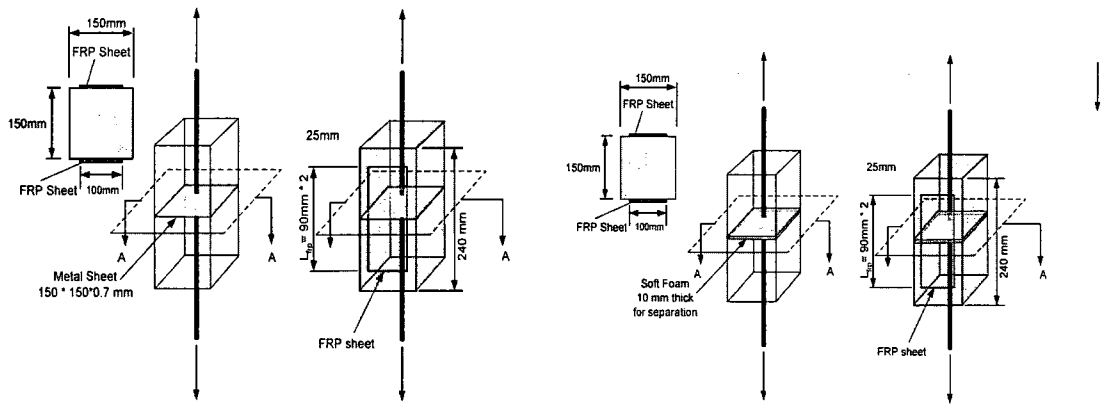

(a) (b)

Figure 3.3. The test specimens setup schematic view for: (a) Specimen #4-1 Entirely Separated thin Sheet +Wrapping(240mm) (b) Specimen #4-2- 10 mm Foam between Separated Sections(230mm)

One of the objectives of performing Series 4 tests was to see if the specimens could be made shorter to improve handling. The specimen length was selected to be 240 mm based on the effective bond length observed in earlier tests. Two of the 3 specimens failed through the bond failure of embedded re-bars, indicating that the specimen length was not sufficient. Therefore, longer specimens were used in subsequent tests.

When two separate but identical CFRP sheets are used, one on either side of the specimen, in actual fact four bond lengths are being tested until the weakest segment suffers from bond failure. In such a specimen, there is a rather high probability of introducing a defect in one of the four bond lengths (one in four), which governs the capacity. Furthermore, all four lengths have to be instrumented for elongation measurements. It is therefore preferable to reduce the number of bond lengths per specimen. Hence a new setup was implemented with U-shaped CFRP sheets, continuous on one side of the specimen, allowing two bond lengths to be tested at a time. This reduces the likelihood of introducing a defect (one in two) and also reduces the instrumentation to be used per specimen, while promoting a more accurate test procedure. Therefore, the new test setup, referred to it as; "U-shaped Pull Test," was implemented

for the remaining tests. Fig.3.4 illustrates schematics of a typical U-shaped pull test. The new setup allowed a reduction in the total number of strain gauges used, while permitting an increased number of gauges per bond length.

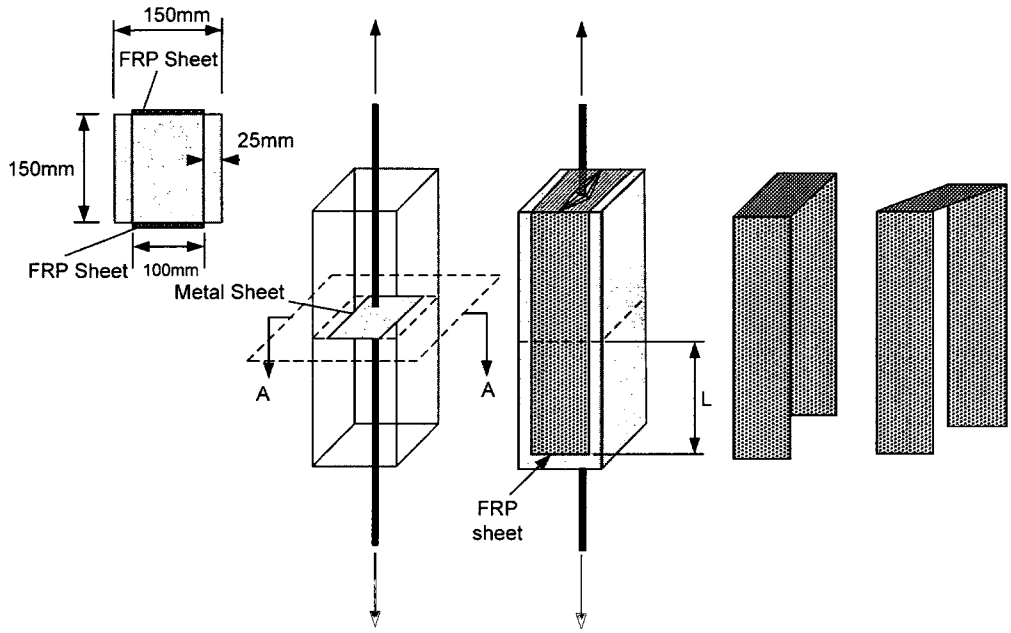

Figure 3.4. The schematic view of test specimens with U-shaped CFRP strips

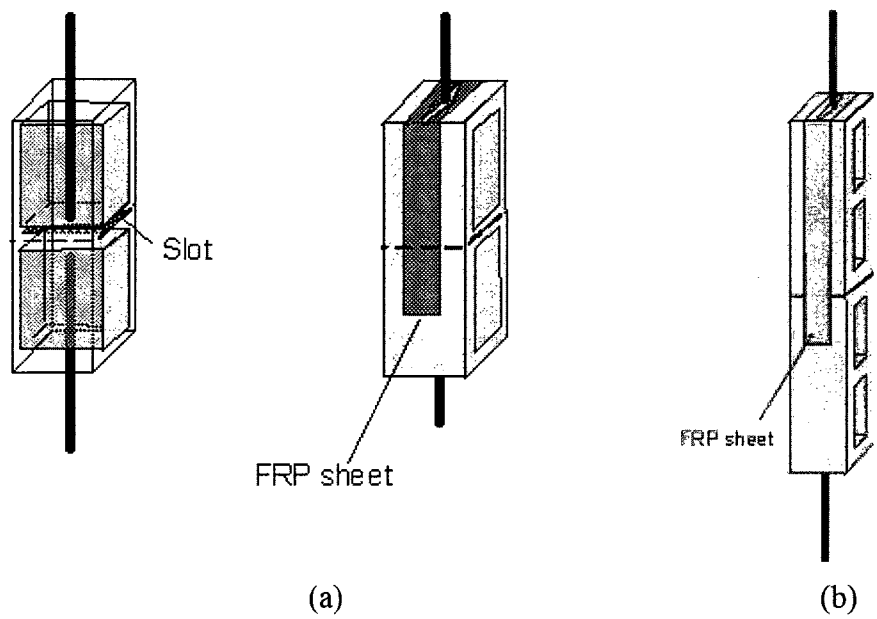

(a) (b)

Figure 3.5. The pull out bond test specimens, for (a)concrete block and (b)brick substrates

The U-shaped pull test setup was also applied to concrete block and clay brick tests. Fig.3.5 shows typical masonry test specimens. The blocks included separating slot, facilitates cracking between the two sides. In the case of concrete block tests, the hollow segments of units were filled with concrete to improve the bond strength of the embedded re-bars. For clay brick units, the filler material used was the polymer based putty that was also used to smoothen the substrate surface before the application of CFRP sheets.

3.3. Preparation of Specimens

The specimens were prepared in the Structures Laboratory of the University of Ottawa. They were prepared in phases. The characteristics of test setup and test parameters were established during the test program, and were based on the results obtained in previous tests.

3.3.1 Material Properties

The same CFRP material was used for all specimens. The specified tensile strength and modulus of elasticity of carbon CFRP were 4275 MPa; and E_t= 228,000 MPa, respectively (Shalouf 2005 and Wabo-Mbrace technical catalog). The matrix used to make the composite material was Wabo MBrace Saturant epoxy. The same material was used as adhesive to apply the CFRP sheets on the substrate material. Wabo Mrace Putty and primer was used to smoothen concrete and masonry substrates prior to the application of CFRP. Once saturated with epoxy, the CFRP composite sheets had tensile strength of approximately 700 MPa and elastic modulus of 60 GPa. The thickness of the CFRP composite sheet was approximately 0.9 mm (Saatcioglu et al. 2007)

Rebars and steel plates used in this research were of normal strength, with a nominal yield strength of f_y = 400 MPa.

Two different mix designs and a number of different batches of concrete were used for the preparation of concrete substrates. The concrete was mixed at the Concrete Laboratory of the University of Ottawa. The majority of the specimens had normal strength concrete, with an average concrete strength of 46 MPa. There were some variations in concrete strength at the time of testing, essentially resulting from differences in curing and the age of concrete. The lowest strength concrete substrate was tested when

the concrete strength was 30 MPa. Series 12 through 14 had high-strength concrete, with strengths ranging between 68 MPa and 72 MPa. Table 3.1 shows the concrete strength for each series of specimen. The concrete mix designs used are shown in Table 3.2. The maximum aggregate size was 20 mm.

Table 3.2 Concrete mix designs

Series	Water (kg)	Cement (kg)	SP*	Sand (kg) (0-5 mm)	Gravel (kg) (5 -10 mm)	Gravel (kg) (10 -20 mm)
1-11, 13,14	216	524	-	608	496	656
12	189	540	5.4(1%C)	609	496	657

*Super plasticizer, Type SPN, EUCON 37

3.3.2 Concrete Substrate

The concrete specimens were cast using the available steel formwork in the Concrete Laboratory of the University of Ottawa. Plywood dividers were added to the existing steel formwork to obtain the required specimen length, as illustrated in Fig. 3.6. No. 20 re-bars (19.6 mm diameter) were used to apply either the pull or through the attached steel sheets the push forces. Each rebar was cut to the required length such that they protruded from the ends of the specimens by about 150 mm to be able to grip on the bars. The steel plates for the push tests had 100 mm by 150 mm cross sectional dimensions and 10 mm thickness. The thin sheets used in pull tests also had the same cross-sectional dimensions, but their thickness was 0.7 mm. One of the pull specimens had a 10 mm thick Styrofoam separating the two halves of the concrete prism. All specimens were prepared in a similar fashion, except for some differences resulting from the use of different test setups. Figures 3.6 through 3.12 show various stages of specimen preparation.

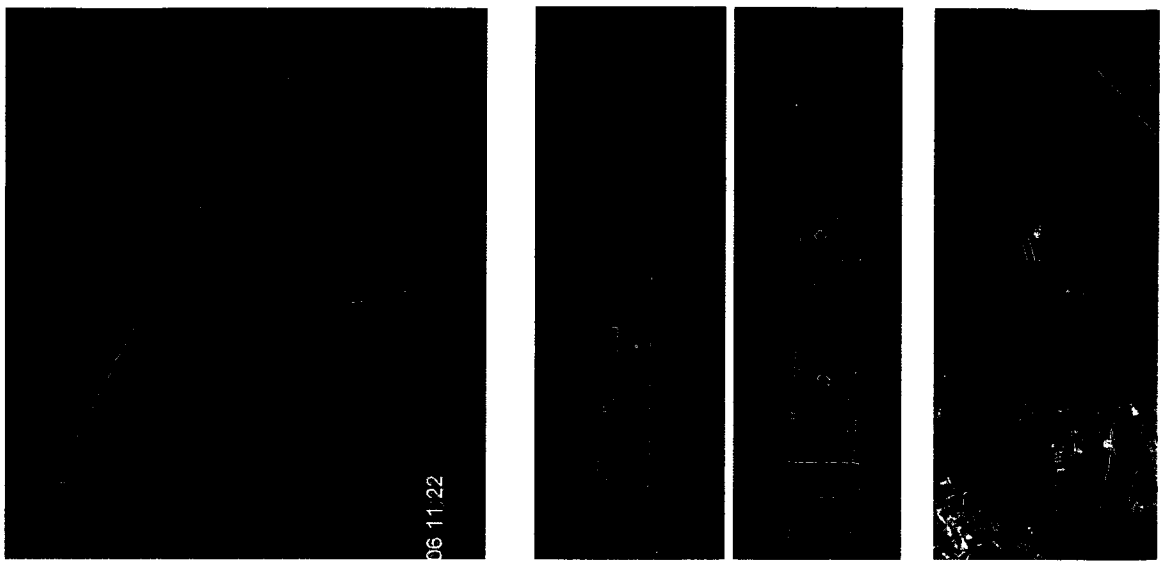

(a) (b) (c)

Figure 3.6. Formwork and Casting of concrete specimens in the lab(a) Existing steel formwork, (b)Modified formworks, (c) Cast specimens

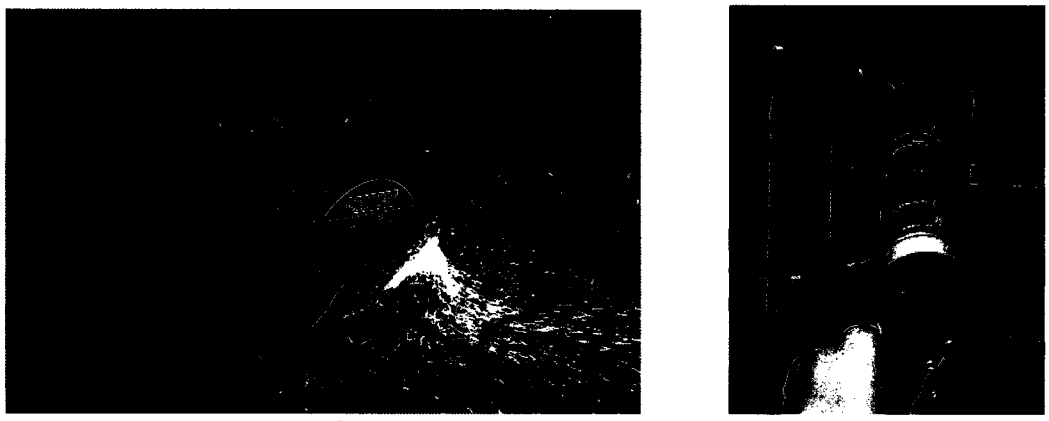

(a) (b)

Figure 3.7. Making specimens (a) Cutting rebars (20 mm for Concrete and 10 mm diameter for brick specimens, (b) Replacing the formwork sides.

The concrete was mixed in the laboratory using a concrete mixer, in 0.1 cubic meter batches. Fig. 3.9 illustrates the concrete mixing process. The specimens were released from their formwork at least 24 hours after casting. Those with a compressive strength of around 46 MPa were moist cured for three weeks in a curing room. The lower strength specimens (Series 7) had the same concrete mix but were cured only for one week. The high strength specimens had two mix designs. Series 12 had the high-strength concrete mix discussed earlier, and developed 76 MPa strength, whereas Series 13 and 14

had normal-strength mix designs but developed higher strengths because of longer time of curing. Upon the completion of curing, the specimens were removed and left at lab temperature and humidity.

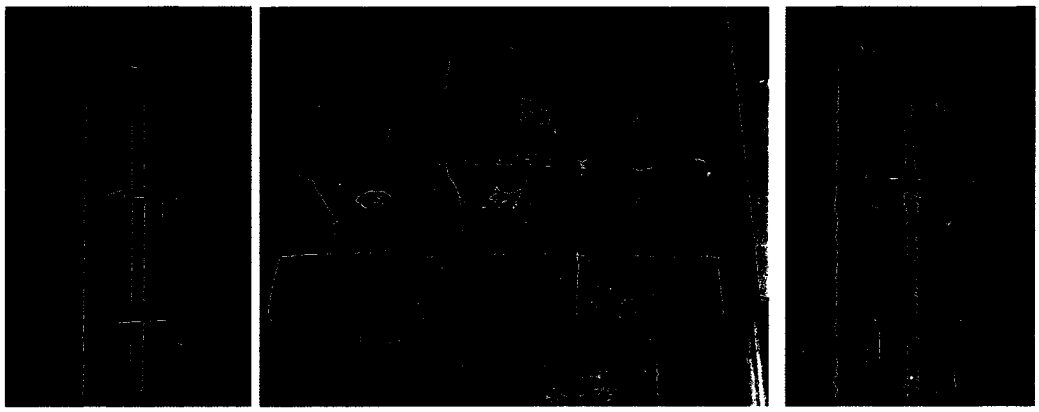

(a) (b) (c)

Figure 3.8. Formwork for different setups (a) Series 1, with pushing plates, (b) Series 4, i) with limited separating sheet, ii) with entire separating sheet, iii) with separating 10 mm foam , (c) Setup with the thin separating sheet

In order to gain uniform concrete strength and avoid possible strength reduction due to the bleeding of the concrete on the finished surface, the CFRP sheets were placed in the side faces. The concrete surface was smoothened by applying two coats of epoxy-based putty (Wabo-Mbrace type) before the application of CFRP. The surface was sanded before a single layer of 0.165 mm thick carbon fibre sheet strips were epoxy glued on opposite surfaces of each specimen in Series 1 and 2, as shown in Fig.3.10(c). All other specimens had U-shaped sheets that wrapped around one end of the specimen, as illustrated in Fig.3.11. The first layer was cured at lab temperature of about 25°C for a minimum of three days before additional layers were applied, as appropriate. Each CFRP sheet was instrumented with four to eight 10 mm long strain gauges (Tokyo Sokko type FLA-10-11).

(a) (b) (c)

Figure 3.9. Concreting (a) Concrete plant, (b) Vibration of fresh concrete, (c) Curing .

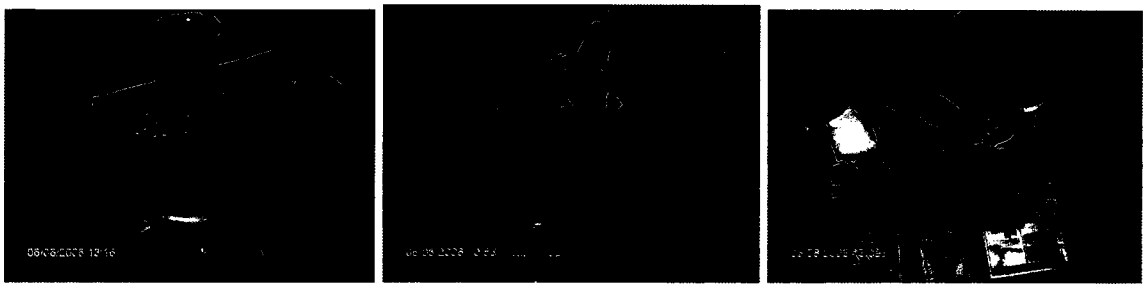

(a) (b) (c)

Figure 3.10. Preparation of specimens (a) Putty; (b) Sanding; (c) Placing CFRP sheets

(a) (b)

Figure 3.11. Preparing test specimens (a) One layer, (b) Preparing for second layer

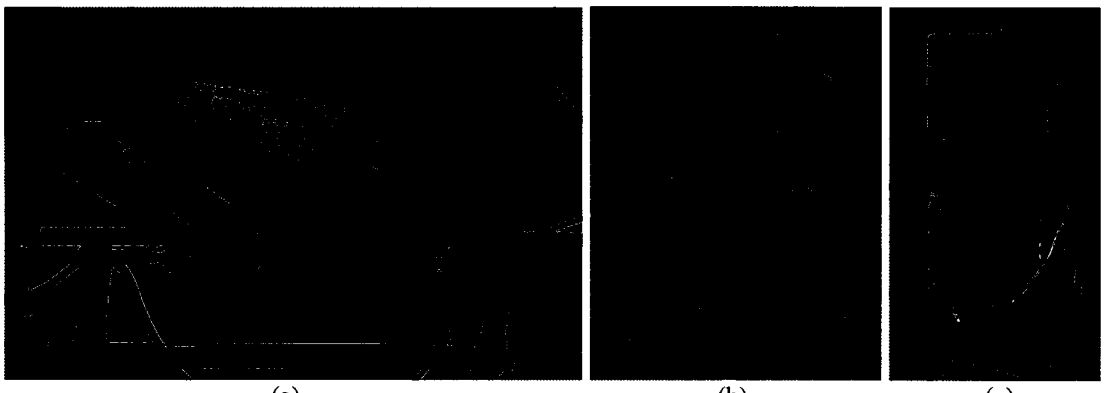

(a) (b) (c)

Figure 3.12. Preparation of test specimens Series 2 for testing in the perpendicular faces to the same specimens of Tests series 1 (a) Grinding the surface, (b) Putty covered, (c) A specimen ready for testing in the perpendicular face to Series 1 specimens.

3.3.3 Masonry Substrates

The masonry specimens were prepared to match standard sizes of concrete block and brick units. Concrete block specimens consisted of single blocks of 390 mm length. A weak section was created in the middle of each block to have controlled cracking during testing. A hole was drilled in the blocks to insert the rebar to facilitate the application of tensile force, and the cells were filled with concrete. Fig. 3.13 and 3.14 illustrate the preparation of concrete blocks for testing. The compressive strength of concrete masonry was established to be 16 MPa by testing half block portions. The blocks were manufactured using small size aggregates with a maximum size of 5 mm. The CFRP strips placed on block units was 100 mm wide. Each CFRP sheet was instrumented with four to eight 10 mm long strain gauges (TokyoSokko type FLA10-11).

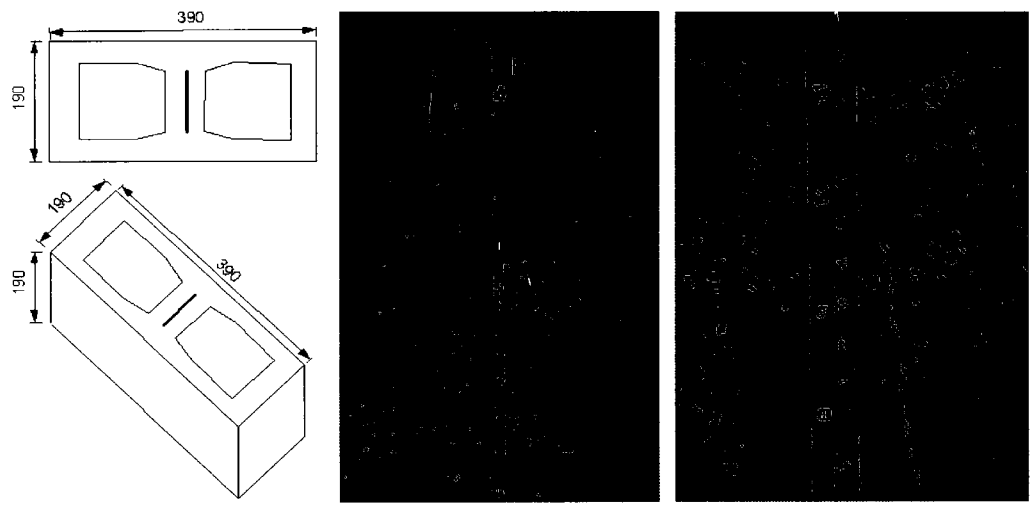

Figure 3.13. Concrete block (a) Dimension and shape (b) Crushed (c) Mixture

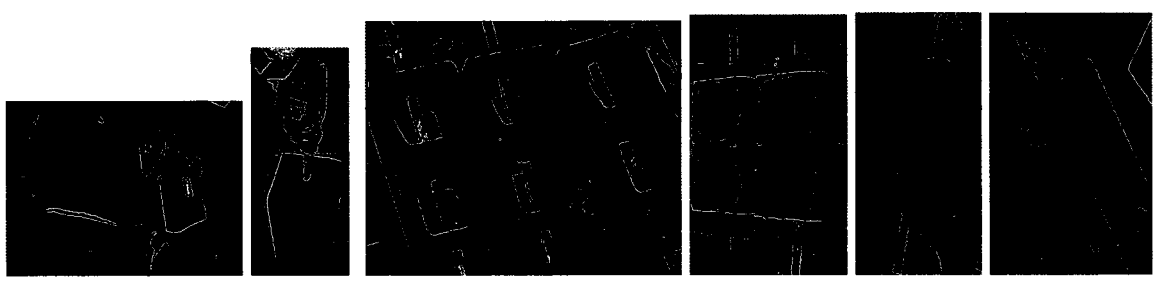

Figure 3.14. Concrete block test specimen preparation (a) Precutting cracking line (b) Drilling the centerline(c) Replacing the rebar No.20 (d) Blocks filled with concrete (e) Putty covered (f) Sandpapered and ready for CFRP layer

Brick masonry specimens consisted of two brick units with 255 x 90 x 90 mm dimensions with 5 cells of 35 x 30 x 80mm size each. The preparation of these specimens was similar to that followed to produce concrete block masonry specimens, except in these specimens 10Mrebars were used to apply axial tension. The brick cells were filled with epoxy based putty that was also used for surface preparation. TheCFRP strips placed on brick units were 40 mm. Each CFRP sheet was instrumented with four to eight 10 mm long strain gauges (Tokyo Sokko type FLA-10-11). The stages of specimen preparation are shown in figures 3.15 and 3.16.

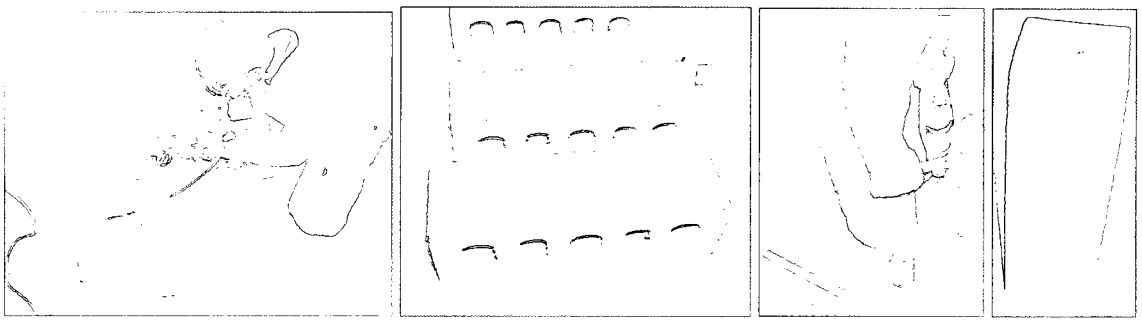

(a) (b) (c) (d)

Figure 3.15. Bricks preparing for specimens (a) Grinding, (b) Grinded, (c) Drilling, (d) Grinded and drilled.

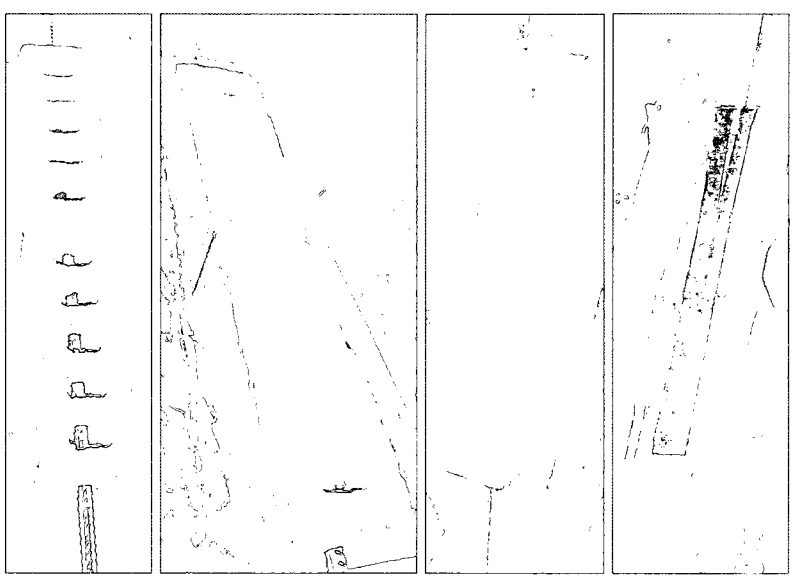

(a) (b) (c) (d)

Figure 3.16. Preparing Brick specimens (a) Inside setup, (b) Filled with putty, (c) Sandpapered, (d) WrappedCFRP

3.4. Test Procedure

A Galdabini universal testing machine with a tensile capacity of 600 kN was used to apply tensile forces on re-bars. All specimens were subjected to monotonically increasing axial tension except for Series 5, which were tested under cyclic loading. The rate of load application was 0.5 MPa/min as suggested by CSA S806-02(2002). The same rate was applied for the loading and unloading phases of the cyclic load as well. The magnitude of cyclic loading was increased in increments of 10 kN during each cycle, as illustrated in Fig.3.17, until failure.

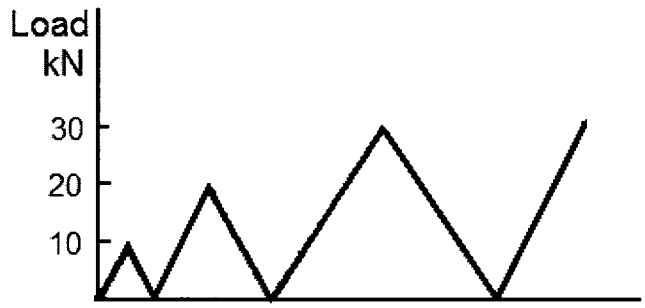

Figure 3.17. Cyclic loading in series 5 specimens

The test machine displayed and recorded the applied load and machine head movement during each test. A data acquisition system was used to record the strain data. In Series 1 and 2 different arrangements of strain gauges were used. It was then decided to place the gauges along the centerline of CFRP strip to obtain the strain profile along the bond length. For specimens with very short bond lengths, a lower number of strain gauges were used. The majority of specimens had 4 strain gauges on each side.

3.5. Observed Behaviour

The performance of specimens was observed during testing for potential damages. The strain data was also monitored during testing. It was observed that the strains on each of the two CFRP strips, one on either side, increased at approximately the same rate indicating the concentric nature of applied load. While the bond stress developed on each side was expected to be the same, the initial failure always took place on one side only, where the bond strength was weaker. This was also the case in other research programs.

Prior to the bond failure, the bond stress developed on each face was roughly equal, contributing one half of the total ultimate load resistance. The observed final failure of CFRP-concrete surface bond was sudden and extremely brittle, and was accompanied by a large release of energy and high level of noise. For short bonded length, there was little warning before the final failure. The longer CFRP bond lengths provided some warning in the form of cracking sound.

All but 5 (7%) specimens failed through CFRP surface failure. These 5 specimens suffered premature re-bar anchorage failures (pull out failure) due to insufficient bar development lengths. Two of the 5 specimens were intended to be pilot tests to establish the test setup. The other 3 re-bar anchorage failures were observed in specimens with long bond lengths with two or three layers of CFRP, resulting in high forces.

The failure mode in 24 (34%) of specimens was diagonal tension of the corner concrete (Fig. 3.18). This type of failure occurred either in specimens with short bond lengths, resulting in the dislodging of a small wedge of concrete near the corner; or specimens with longer but multiple layers of CFRP for which the bond strength was high enough to increase the bond strength, still triggering diagonal tension failure. This type of failure was also observed in some of the high-strength concrete specimens where the bond resistance was higher. A total of 42 (59%) specimens suffered bond failure, which initiated with diagonal tension cracking of corner concrete, followed by the delamination of CFRP strip due to insufficient bond capacity. This delamination was observed to occur either completely on the top paste layer of concrete surface (7 specimens, forming 10%) demonstrated in Fig. 3.19(b) or partly penetrating into the top layer of concrete for about 1 mm to 10 mm depth, hence pulling out of a thin layer of concrete along the entire bond length (18 specimens, 25%) shown in 3.19(a) or locally within a shorter segment (8 specimens, forming 11%). Some of the surface bond failure occurred partly between the putty and the CFRP sheet. Nine specimens (13%) suffered failure mostly within the epoxy adhesive. Fig.3.19(c) and 3.19(d) shows this failure in a concrete and a brick specimen respectively. One specimen showed bond failure along its entire length, without the formation of a diagonal crack and the separation of a concrete wedge. This was attributed to the low adhesive strength associated with short curing time of epoxy resin.

When the failure was not due to the surface bond, the results of the specimens were not used for bond failure analysis.

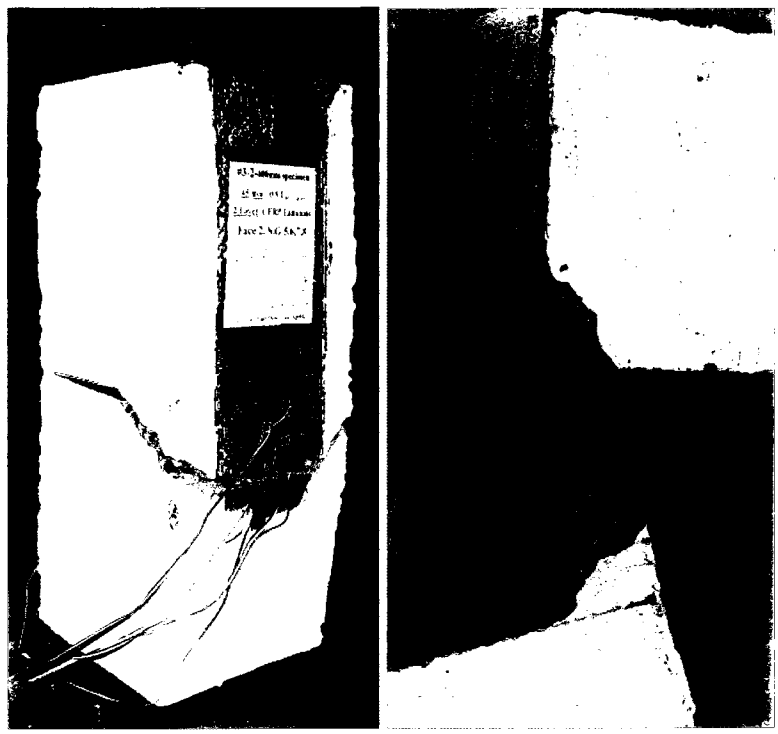

Figure 3.18. Concrete diagonal failure to the end of the specimens

A close inspection of the failure surface indicated the presence of micro columns in some specimens. The specimens tested under cyclic loading showed loose micro column concrete that could be separated from the failure surface. Fig.3.20 illustrates the failure surface and the concrete micro columns observed.

In some specimens with long bond length, segments of CFRP strips were damaged by the energy released near failure, exhibiting splitting in the direction of fibers (longitudinal direction). Epoxy in some specimens developed transverse cracking due to the sudden release of energy at failure. The concrete surface was always rough, with numerous microcracks oriented in a manner indicative of the direction of bond failure.

When the diagonal crack occurs away from the spliced end of the specimen, it is intercepted by the re-bar embedded in concrete to apply the tensile force. The presence of reinforcement does affect the diagonal tension capacity of the section. However, the crack crosses the re-bar near its end. The short development length of the bar is believed

to reduce its effectiveness considerably, thereby having a limited effect on specimen performance. This phenomenon was observed in Series 3 and 10 with double and triple layers of CFRP, and Series 12 with high strength concrete. Fig.3.21 shows the location of embedded re-bar, relative to the diagonal crack.

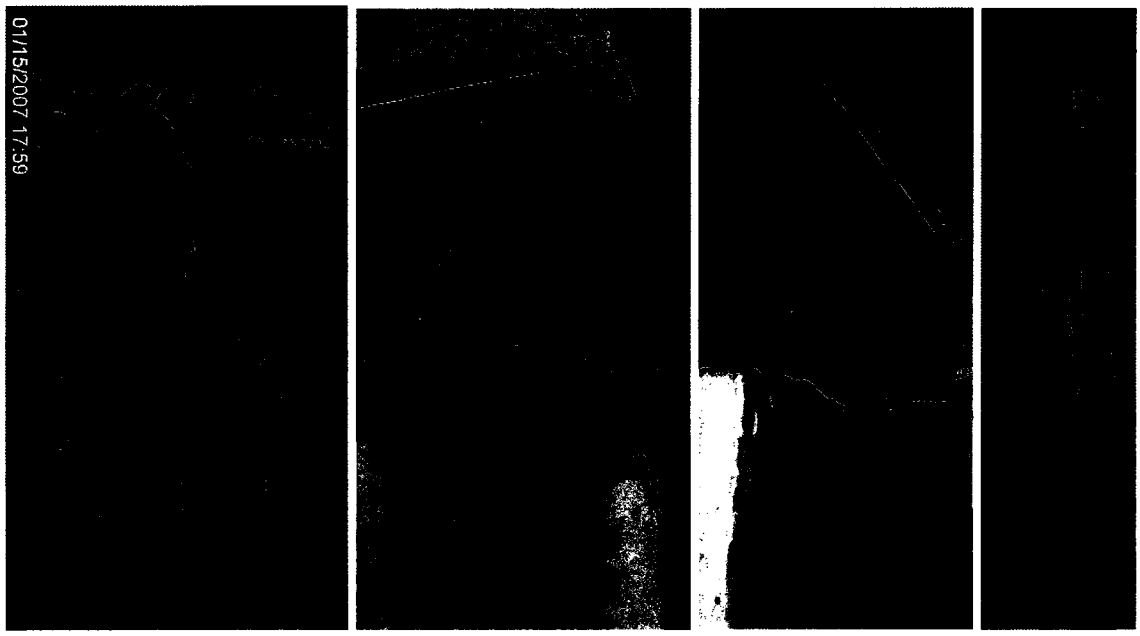

(a) (b) (c) (d)

Figure 3.19. Failure in specimens (a)In 1-10 mm of the concrete near surface (b)In top layer of concrete surface (c) On epoxy surface (d) On epoxy surface in a brick specimen

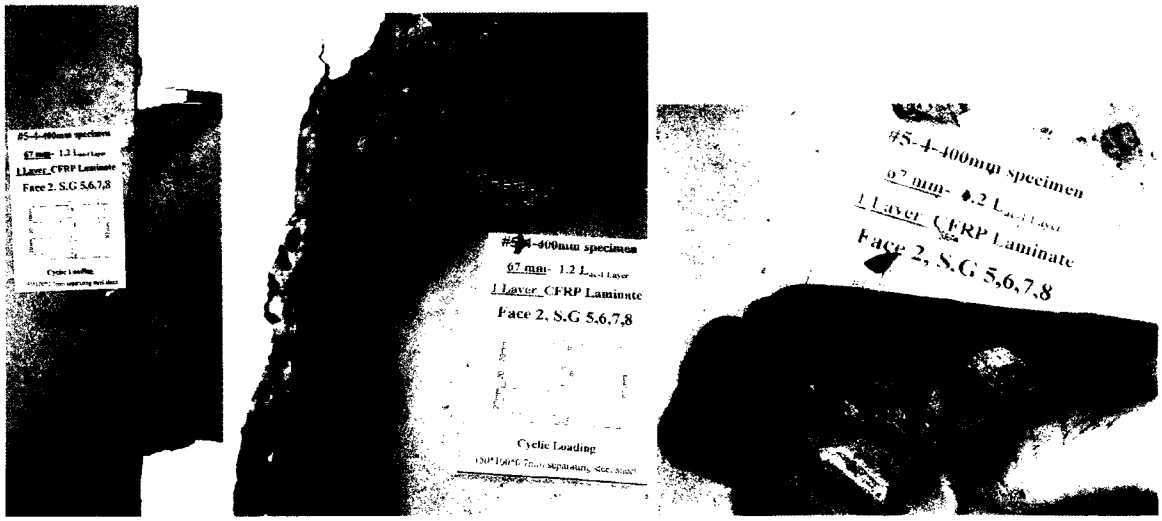

Figure 3.20. The failure and cracking pattern and the dental cracking or micro-cantilever columns in the specimen subjected to cyclic loading

Figure 3.21. Governing the rebar when deep diagonal cracking happened in Specimen #12-5 with high strength concrete (76 MPa) and 140mm bond length

A unique aspect of failure in Series 2 tests was the development of self-hardening after failure, which resulted in a slight and temporary post-failure resistance. The force deformation of such a failure in Specimen#2.3 is shown in Fig.3.22. Therefore, the failure may be perceived to occur in two stages. The two-stage failure is attributed to the presence of the steel plate, which provides a secondary support against the dislodging of concrete wedge that has resulted from diagonal tension failure. This resulted in the crushing of concrete near the end of the CFRP strip, which has caused the complete loss of load resistance. This is illustrated in 3.23 and 3.24.

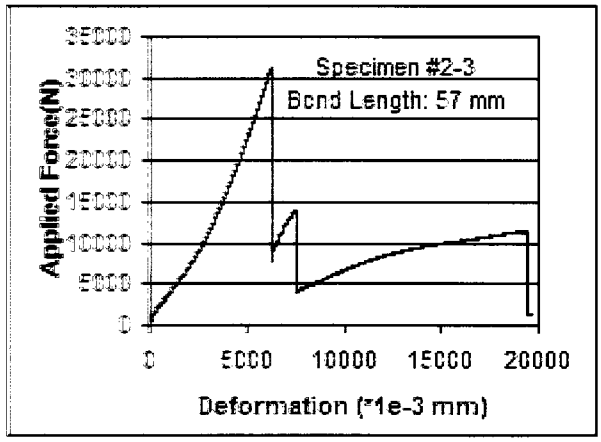

Figure 3.22. Two stage failure in concrete Specimen #2-3

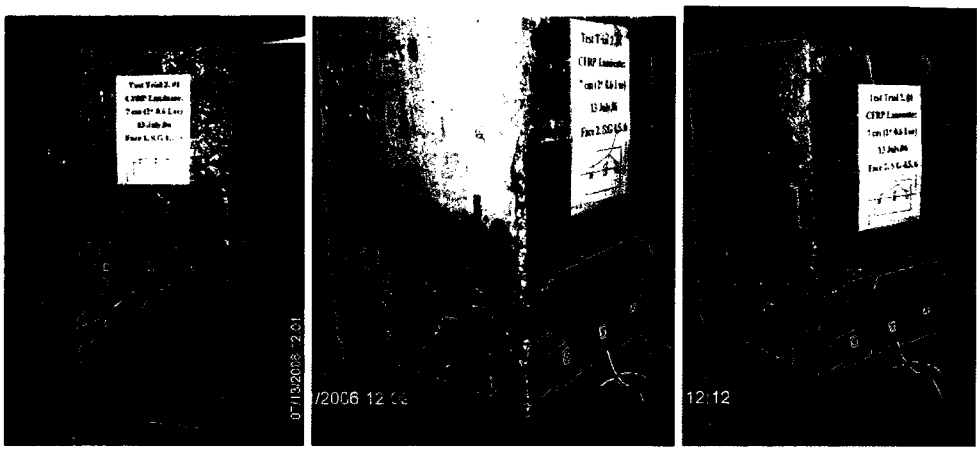

Figure 3.23. Series 2 typical specimen bond failure in Specimen #2.1. (a) Before failure, (b) The first stage failure, (c) Total bond failure.

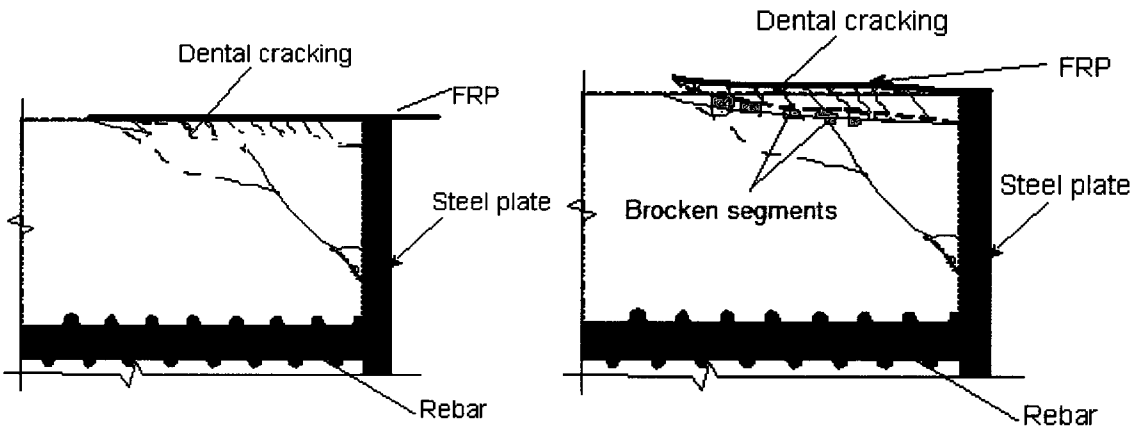

(a) (b)

Figure 3.24. Cracking pattern of the Series 2 specimens with pushing setup (a) Configuration of the diagonal and cantilever column cracking (b) After first stage of failure, secondary support of pushing steel plate and substituting broken segments

During testing the failure always occurred in one of the two CFRP strips crossing the weak section. After the failure of the first strip, the two halves of specimens, started to separate and rotate, while maintaining contact on one side. The load resistance dropped significantly at this stage of loading as axial deformations increased rapidly. This stage of loading is shown in Fig.3.25 and the load deformation curve is shown in Fig.3.27. The secondary load resistance was only a fraction of the ultimate load capacity. The second face failure was also a brittle failure that occurred as the CFRP started peeling of the concrete surface. Although sometimes, diagonal cracks were observed on the second

face, it can be speculated that they have formed along with the fracture surface of the first face, and simply propagated upon the stripping of the CFRP from the surface.

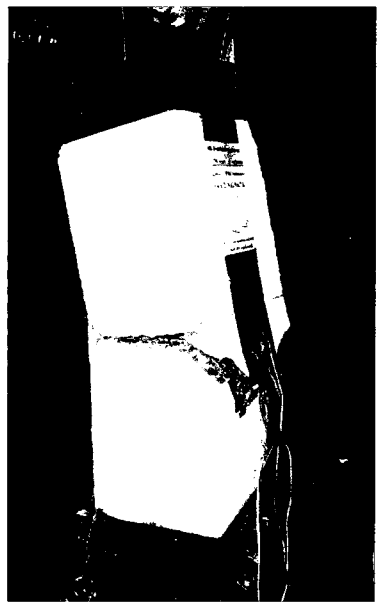

Figure 3.25. The loading of Specimen #8-3 after the failure of first face CFRP strip.

In concrete block specimens, the shape of the block affected the cracking pattern. Because the concrete in block masonry was of low strength, diagonal tension capacity of concrete governed the failure. Irrespective of the long bond length, the failure always occurred due to diagonal tension. Fig.3.26 illustrates the failure mode.

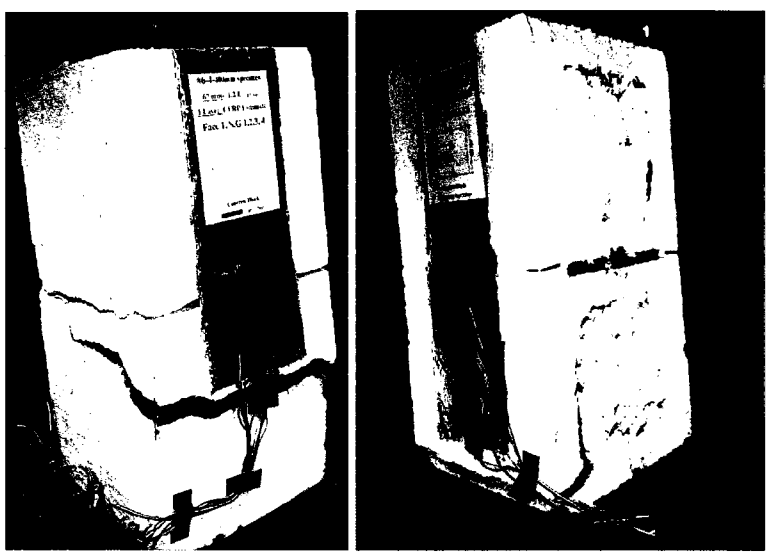

Figure 3.26. Typical failure of concrete block Specimens #6-3 and #6-6

3.6. Test Results

The test results are summarized in this section in terms of force-deformation relationships and the CFRP strain data. The specimen strength, longitudinal displacement and the elongation of CFRP strips are discussed as the effects of test variables are investigated.

- **Force- Deformation Relationships**

All the specimens failed due to either CFRP bond or diagonal tension failure for the edge concrete. There was no failure of CFRP recorded. The stress in CFRP at failure ranged between 7% and 58% of the tensile rupturing capacity. The observed failure was extremely brittle, accompanied by a large release of energy and a high noise level. Fig.3.27 demonstrates a typical curve for the load-deformation relationship recorded during testing. It indicates an almost linear behaviour up to failure. The brittle failure observed is reflected on the force-deformation relationship by a sudden loss of load resistance. The effect of the second face CFRP strip is seen as a slight post-failure increase in load at approximately 30% of the initial resistance.

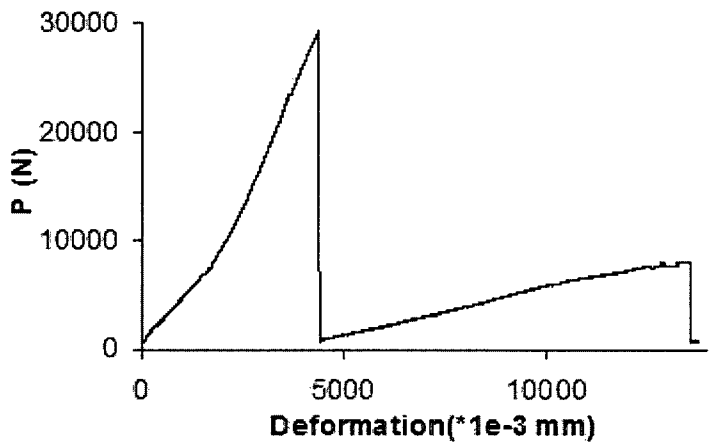

Figure 3.27. Typical Measured Load-Deformation curve in Specimen #1-5

- **Strain Results**

Strain gauge data provided useful information in assessing bond-slip characteristics of surface bonded CFRP. Fig.3.28 shows typical strain variations with applied tension. The results consistently showed highest strains at mid-length where the

interface of two specimen halves is located. The maximum strain at ultimate load varied between 0.23% and 0.33% depending on the length of CFRP strip. The relationship between these two variables was found to be linear, as shown in Fig.3.29(a). The variation of failure displacement with bond length is plotted in Fig.3.29(b), also illustrating a linear relationship.

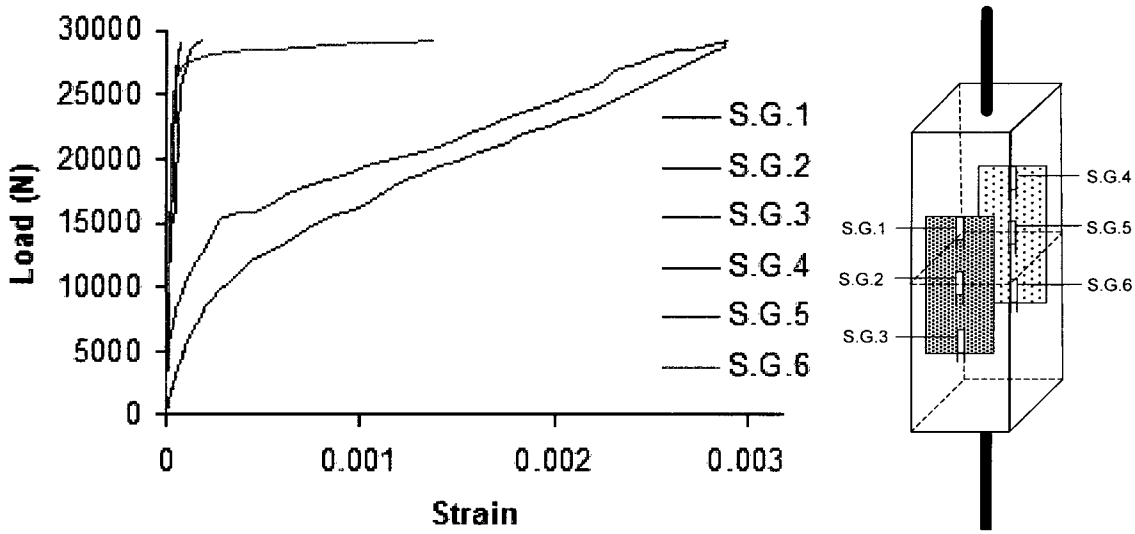

Figure 3.28. Typical load-strain relationship (Specimen #1-5)

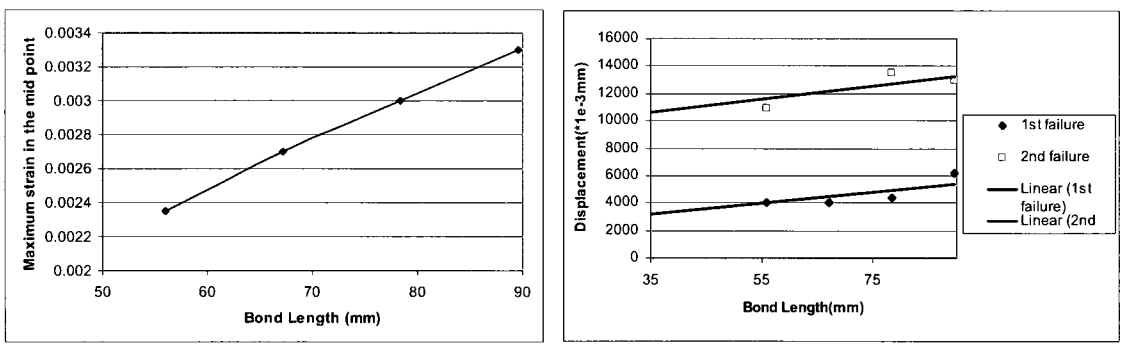

(a) (b)

Figure 3.29. Typical variations of recorded strains and displacements in test series #1

The variation of maximum-recorded strain measured at the critical section with bond length is shown in Fig. 3.29(a). Accordingly, the maximum strain increases with increasing bond length. Fig. 3.29(b) shows that the displacement at which the first bond failure of the first CFRP strip occurs is significantly below the value recorded at the failure of the second the strip.

The normal stresses in CFRP reflect the bond stresses in the substrate material. The maximum strain in CFRP is normally in the range of 0.003 to 0.005. The strain values are summarized in Table 3.3. The table indicates higher strain values in high-strength concrete specimens, as well as specimens tested under cyclic loading. Furthermore, the recorded strains become smaller as the number of CFRP layers increase, reflecting the reduced average strains. Cyclic loading tends to produce increased cracking, resulting in higher recorded strains, producing strains in the range of 0.006 to 0.007. Narrower strip widths also result in higher strains of up to 0.009 because of increased stress in CFRP.

Table 3.3. Measured maximum strain in 1×10^{-3} when ultimate load is applied

	L(mm)											
f'_c	**30**	**35**	**45**	**57**	**65**	**70**	**80**	**90**	**105**	**140**	**220**	**240**
16			1.86	2.48			2.92	3.30				
30		1.27				3.82			3.12	5.78	4.41	
46				3.60		2.80	3.00	3.30				
46								5.80				
46								4.70				
46								3.70				
47		2.40	3.40	3.30		4.10	5.50	6.00				
68												8.00
76	3.79				5.10			5.00		7.20		8.80

The strain values recorded along the bond length are plotted in Fig.3.30 for one of the specimens (Specimen #3-5). Fig. 3.30(a) indicates the variation of strains under increasing load. The strains approach zero at the far end of the bond length, and increase significantly near the critical section. Initially, under small amounts of load, the increase in strains near the critical section shows exponential variation with distance with very small strains at the far end. As the applied force increases, rate changes. As the ultimate load is approached, significant micro cracking occurs near the critical section. This yields almost constant strain within this region with a sharp increase of strains within the far end region where there remains strong bond between the CFRP and concrete. The observed pattern of strain variation agrees well with the expected behaviour. Fig.3.30(a) shows the strain readings for a specimen where the bond length is higher than the effective length.

The figure clearly distinguishes the effective bond length, where the strains increase sharply within a segment and locations of dental cracking where the strain variation is nearly zero.

Fig. 3.30(b) shows the strain variation in the second CFRP strip crossing the critical section. This is the strip that maintained its integrity as the first strip developed bond failure. The strains in this strip initially showed a similar variation, but kept developing bond, as indicated by increases observed in strains near the critical section. This is different than the behaviour observed in the first strip under the same load, which showed nearly constant strains over a segment that had developed micro cracking. This is an indication of reserve bond capacity in the second strip, which helped maintain its bond resistance.

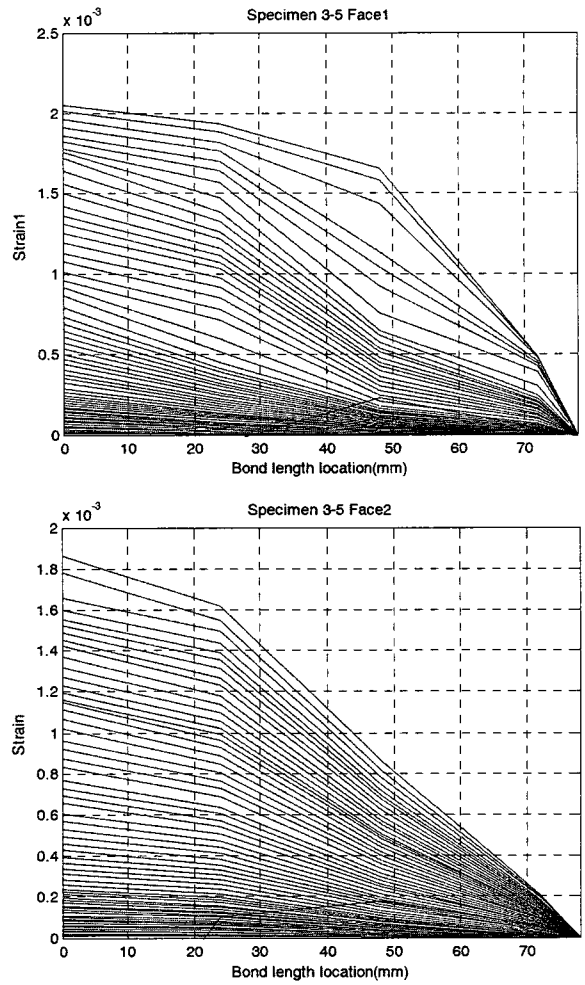

Figure 3.30. Strain variation through the bond length in Specimen #3- 5 (a) Face 1 leading the failure, (b) Face 2, without failure.

Since the strain readings reflect localized effects, they do not necessarily capture sudden jumps in strains that may occur at crack locations. Another example is selected to illustrate this point. Specimen #13-1, with a long bond length (240 mm) was instrumented to have one of the highest numbers of strain gauges used per side (8 gauges) to attain a better understanding of the strain behaviour. Fig.3.31 demonstrates the strain gauge arrangement and its cracking and failure stages. The strain versus time curves are shown in Fig.3.32(a) for different gauges at different locations. The strain at the critical section (SG1) shows the highest values as expected. The force versus time curve is shown in Fig.3.32(b). The occurrence of a crack is indicated in these graphs by a sudden drop in strain values.

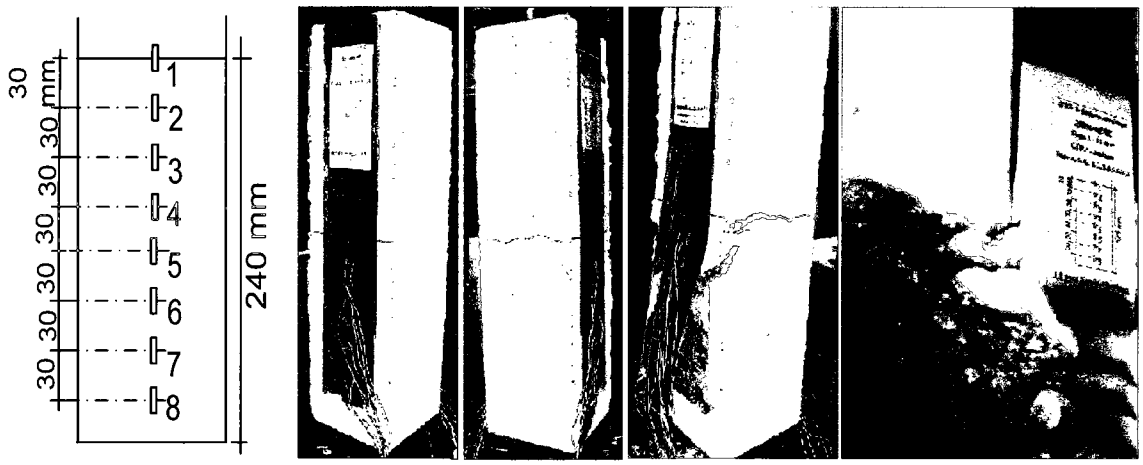

Figure 3.31. The arrangement of the strain gauges and the failure cracking stages of specimen #13-1.

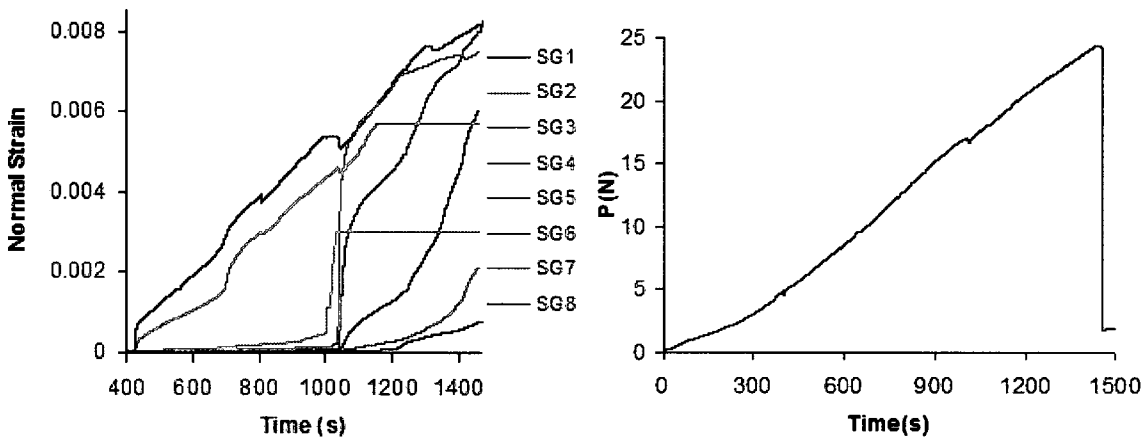

Figure 3.32. Results of #13-1 test (a) Strain versus time in different locations, (b) Loading versus time.

The strains at different load levels are plotted in Fig.3.33. The behaviour is very similar to that shown earlier in Fig.3.30 for another specimen. However, this time the formation of a major diagonal crack near failure was captured with a sudden drop in readings. Without this drop, the Figure shows the same trend near the critical section with almost a flat variation, indicating a low rate of variation in strains over a segment of micro-cracking.

The trend observed in the above two examples was also observed in other concrete specimens, as well as brick and concrete block specimens. Therefore, the same effective length concept and stress release at cracks apply to masonry elements with externally bonded CFRP sheets.

The observed behaviour of strains signifies the characteristics of bond behaviour in specimens with different bond length. The specimens with longer bond lengths exhibited relatively gradual bond failure, as the constant strain region shifted towards the end of the strip, eventually causing bond failure. In cases where the bond length was not long enough to permit such shift, the failure was more sudden and brittle.

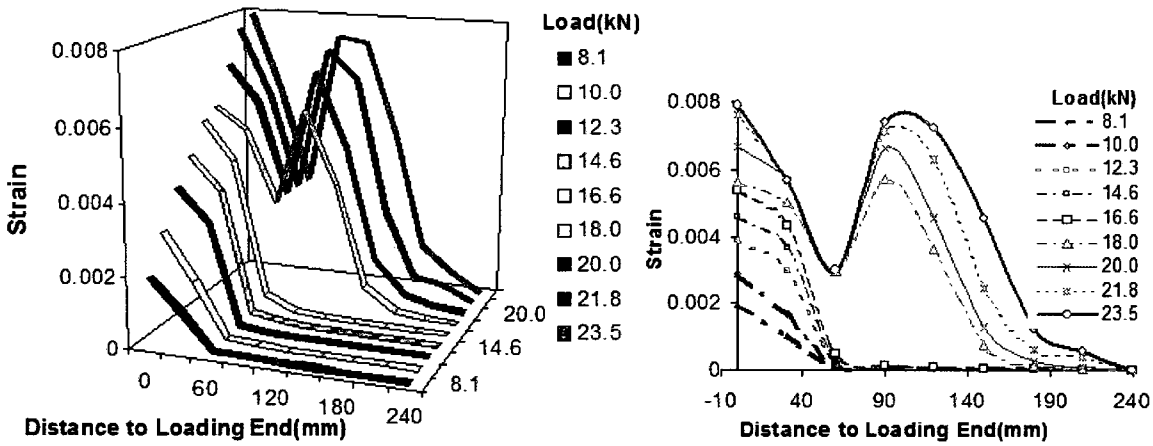

Figure 3.33. The strain location for different load levels

- **The Effect of Bond Length**

Different specimens were tested with similar properties but different bond length to investigate the effect of bond length on ultimate force capacity. Most of the test specimens demonstrated that they had an effective bond length beyond which further increase in bond length could not improve the load capacity. This length, for the

specimens tested in the current investigation, varied approximately between 40 mm and 120 mm depending on other test variables. It was observed that increased bond length, beyond the effective bond length, could not be justified in terms of increasing bond and/or tensile load capacity.

Fig.3.34 provides a summary of some of the ultimate load resistances recorded as a function of bond lengths. The specimens in the same diagram have the same properties except for bond length, which was changed as the only variable. When relatively short CFRP bond length was used, the strength increased with bond length. Once the bond length reached "effective bond length," the load resistance remained approximately constant and any further increase in bond length did not generate substantially increased capacity. Though this general pattern was observed in test results, the strength, as well as the actual shape of these relationships varied with other test parameters, as further discussed in subsequent sections.

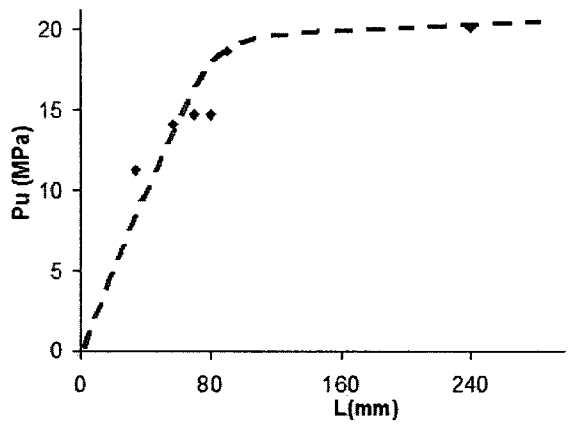

(a) f'_c=46 MPa,1 layer CFRP, b_p= 100 mm

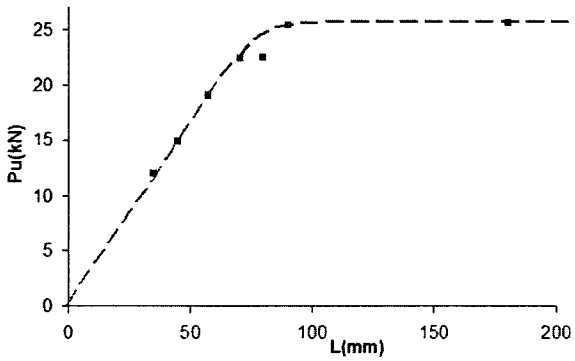

(b) Two layers of CFRP

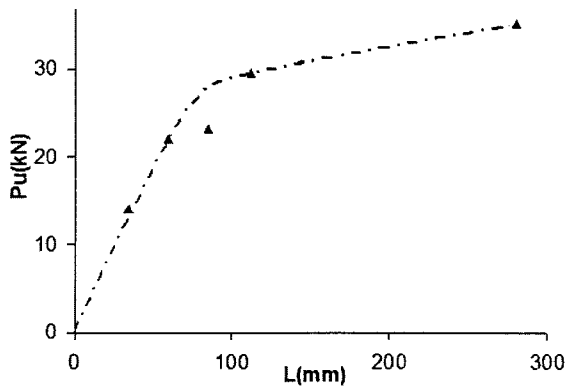

(c) Three layers of CFRP

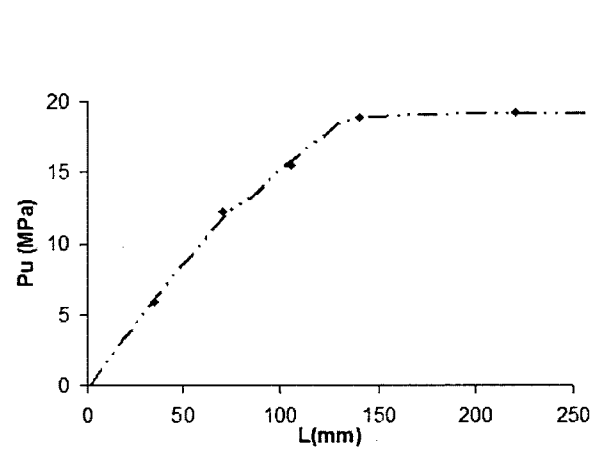

(d) Concrete with Lower strength (f'_c=30MPa)

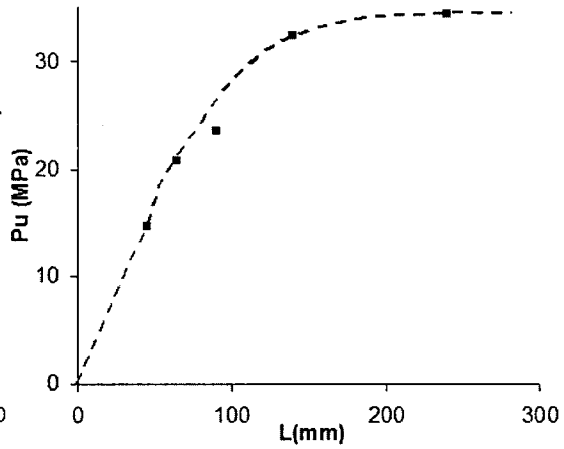

(e) High strength concrete (f'_c=76MPa)

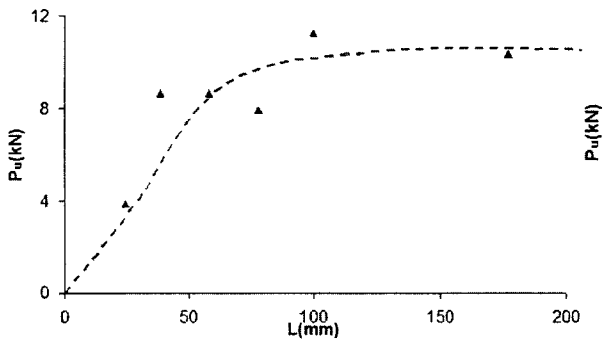

(f) CFRP width of 30mm

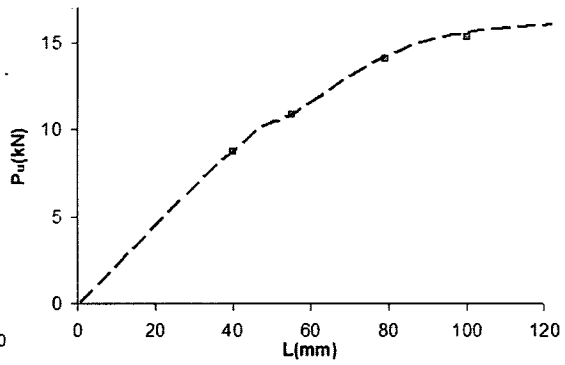

(g) CFRP width of 65mm

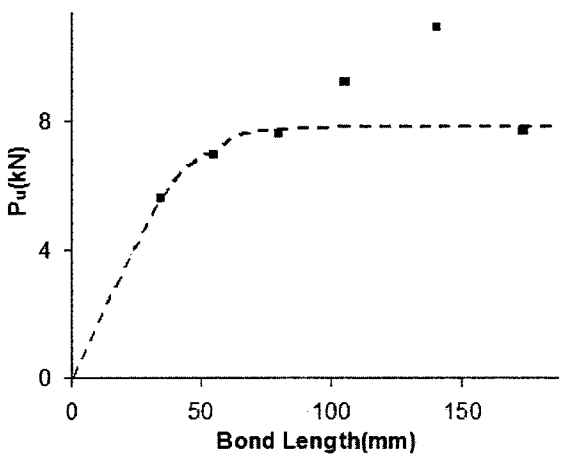

(g) Brick specimens

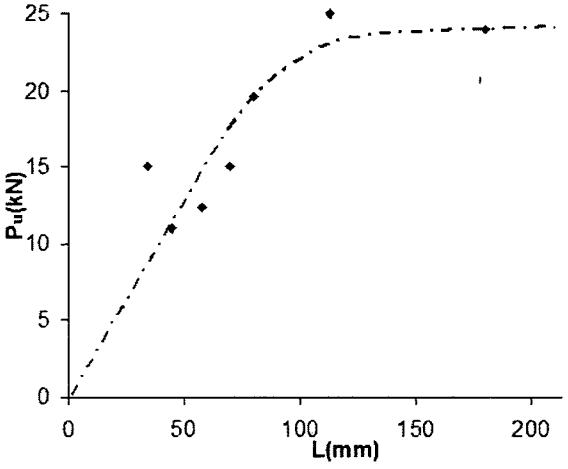

(h) Cyclic loading

Figure 3.34. The Load-bond length curves for the different Surface bond failure Testing Series

- **The Effect of Concrete Strength**

The bond failure of CFRP depends on surface bond stress and diagonal tension capacity of concrete near the interface. Therefore, the effect of concrete capacity was investigated by testing specimens with different concrete compressive strengths. The concrete strength for each specimen was established through testing standard cylinders with 200 mm length and 100 mm diameter. Fig.3.35 demonstrates the relationship between ultimate load and concrete strength for different bond lengths. The results show that the ultimate load capacity increases with concrete strength.

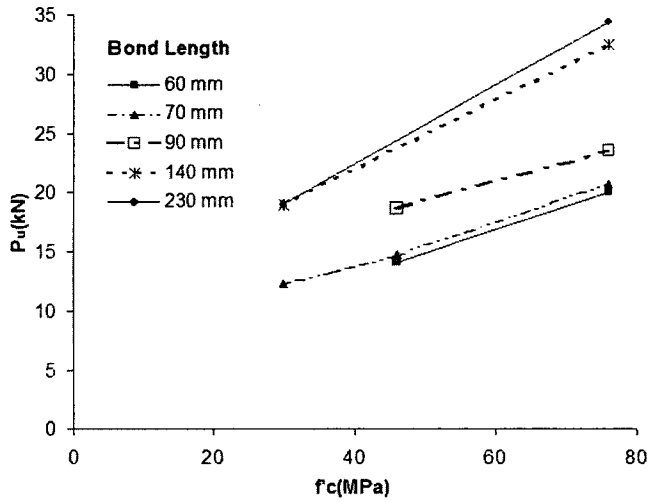

Figure 3.35. The relationship of ultimate load versus unconfined compressive strength of concrete in different bond lengths

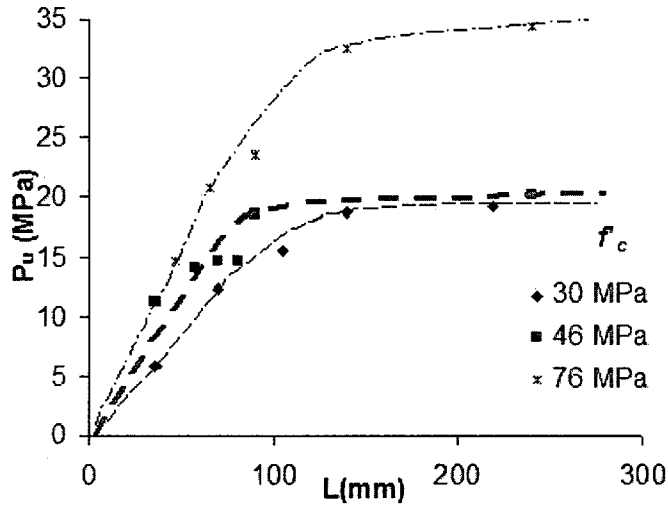

Figure 3.36. The ultimate load versus bond length, in concrete specimens with different compressive strength

- **The Effect of CFRP Layers**

Different number of CFRP layers may be used in practice to strengthen structures. Therefore, this parameter was investigated by testing specimens with different number of layers of CFRP strips. Fig.3.37 shows the variation of ultimate load with the number of CFRP layers. It indicates that the ultimate load capacity increases with the number of layers, though much less than the increase in cross-sectional area of material or the material rupturing strength. Fig.3.37 (b) shows the effect on effective bond length. The effective length under higher pull forces also increases with the number of CFRP layers, albeit in a very marginal manner.

Fig.3.38 illustrates experimentally measured strains for two specimens; one with two layers and the other with three layers of CFRP. When more layers are used, the strains are lower even though the applied force is higher, mainly because the strain measurements were taken on the top layer of CFRP, which is located away from the interface. This implies that the first layer that is in contact with the substrate may have strained more, but the top layer tends to strain less.

- **The Effect of Width of CFRP Sheet**

Specimens with three different CFRP sheet widths of 30, 65 and 100 mm were tested. The results were governed by the tensile strength of surface concrete and the bond width as dictated by the strip width. Fig.3.39 demonstrates the effect of CFRP width on effective length and ultimate load. Ultimate load is related to the cross sectional area of CFRP sheets and hence showed an improvement with CFRP width, however the change of the effective length is negligible. The strain measurements recorded at the centerline of each trip is plotted in Fig.3.40 for two specimens, for comparison. The specimen with 65 mm CFRP width showed somewhat lower strains in the centre of the strip than the specimen with 30 mm strip. This may be attributed to the stress distribution in the transverse direction, which tends to be more uniform in wider strips.

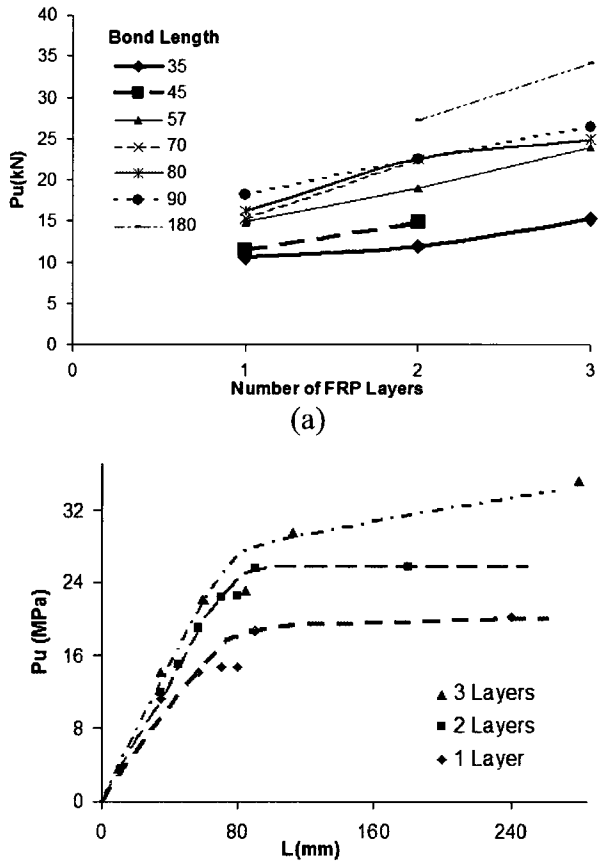

Figure 3.37. The effect of number of layers of CFRP sheet on ultimate bond load, and effective length in concrete specimens

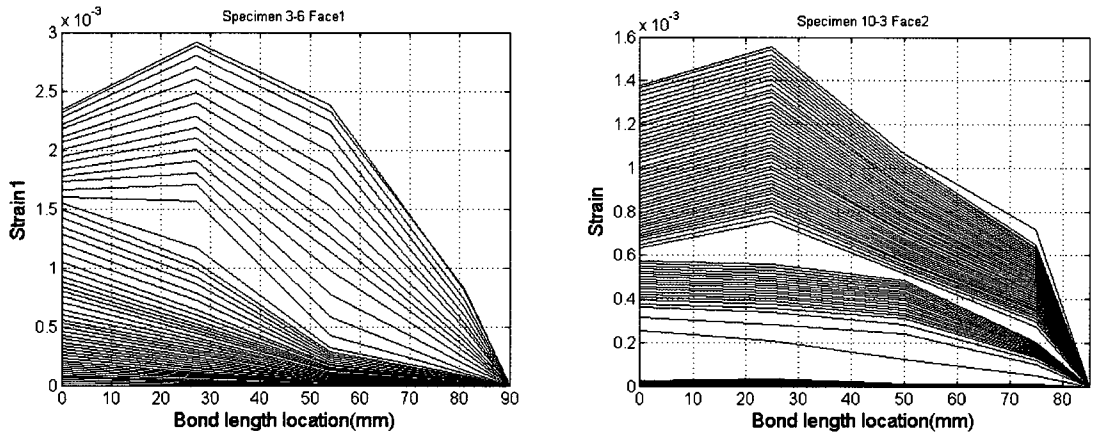

Figure 3.38. Strain versus location in concrete Specimen (a) #3-6 with 2 layers of CFRP sheet and and 90 mm bond length (b) #10-3 with 3 layers of CFRP sheets and 85mm bond length.

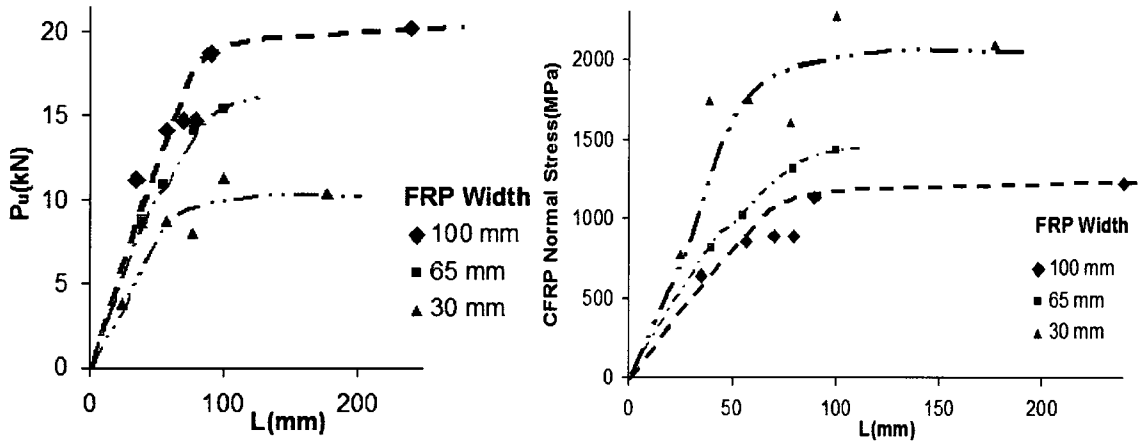

Figure 3.39. The effect of width of CFRP sheet on ultimate bond load, CFRP sheet maximum normal stress, and effective length

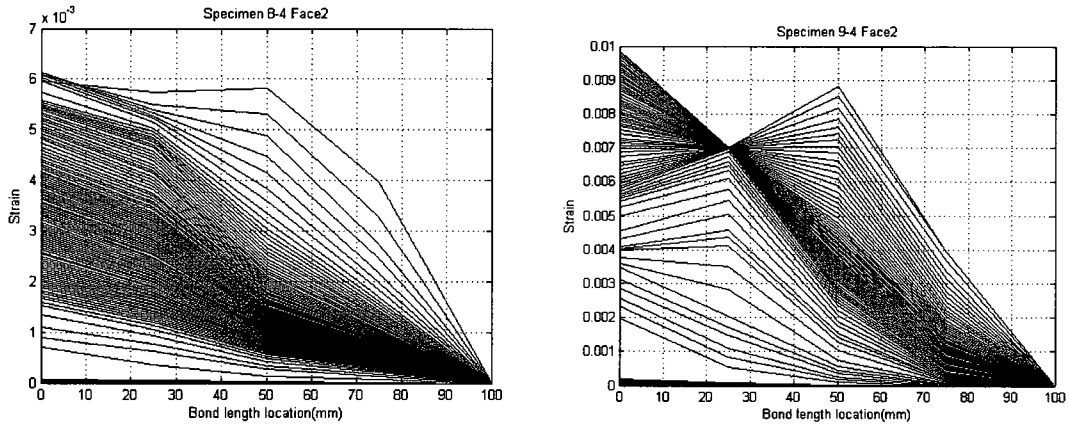

(a) (b)

Figure 3.40. Strain versus location in concrete Specimen (a) #8-4 with 65mm width and 100 mm CFRP length (b) #9-4 with 30mm width and 100 mm length

The distribution of the strains along the width of CFRP was established for specimens with different widths. The strain gauges located in the critical sections of specimens with short bond length did not produce consistent results. They amplified the effects of accidental eccentricities, showing non-symmetrical readings. That is shown schematically in Fig.3.41.

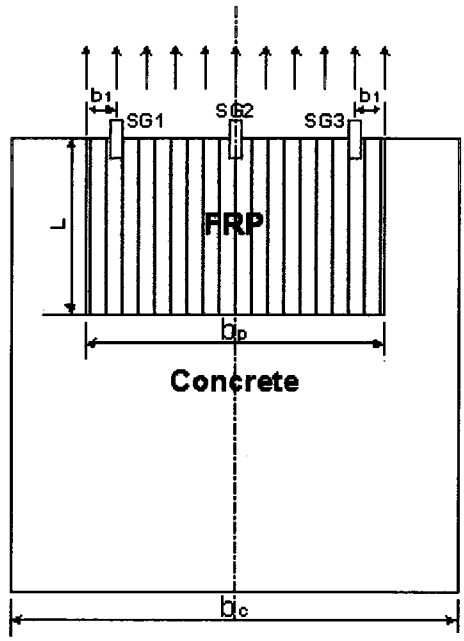

Figure 3.41. Arrangement of strain gauges in the critical cross section

Fig.3.42 indicates the maximum normal strains measured in critical section of different specimens. Each graph shows the strain distribution obtained from strain gauges for a particular width. It can be clearly concluded that the strain distribution across the width is more uniform for narrower strip widths. Fig.3.43 illustrates this point schematically.

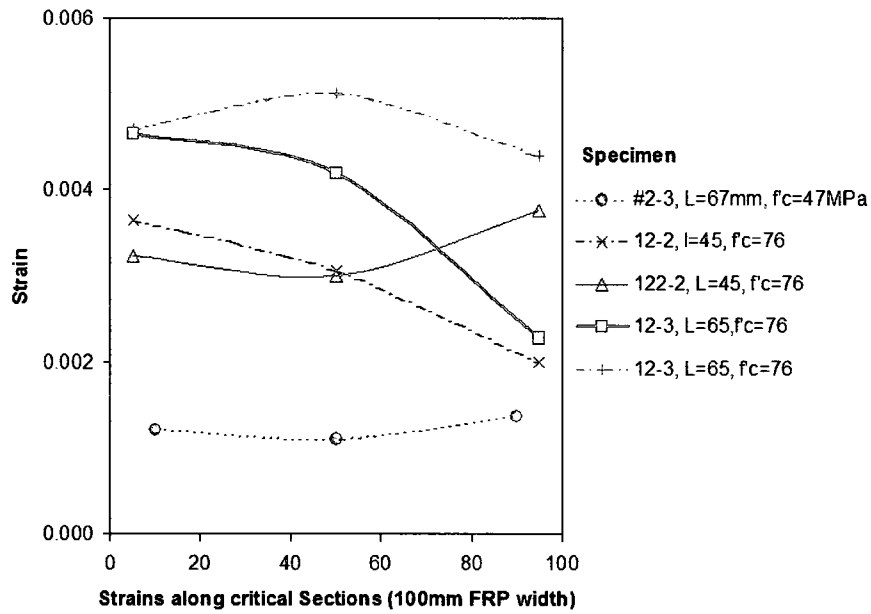

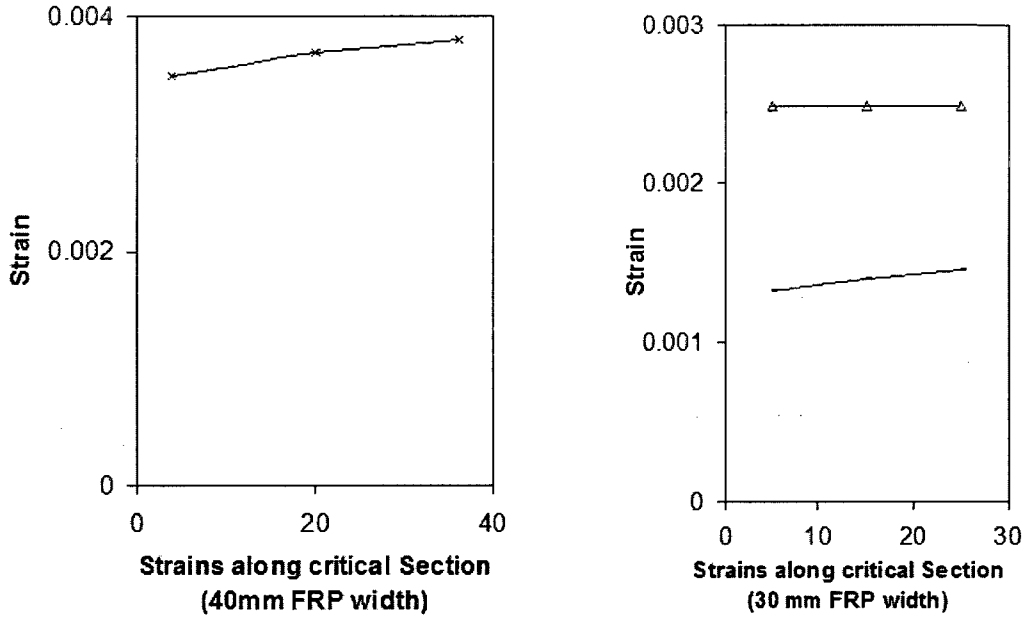

Figure 3.42. Strain in critical sections of specimens with different CFRP width

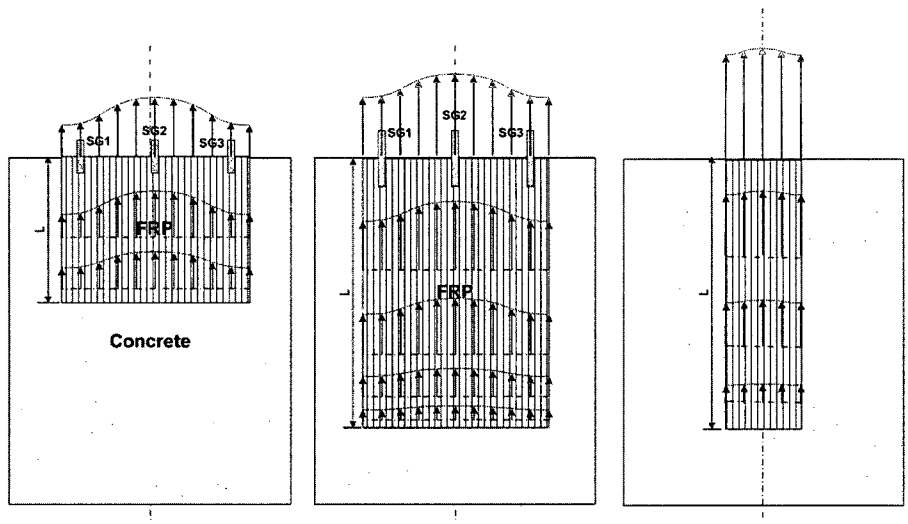

Figure 3.43. Schematic view of stress distribution in CFRP sheet

- **The Effect of Loading**

Two types of loading used were, i) monotonically increasing direct tension, and ii) cyclic loading between a load increment and zero under incrementally increasing tensile forces. The cyclic loading improved bond behaviour while decreasing the brittleness of failure. This can be attributed to the realignment of micro columns between dental cracks along the failure plane. The cyclic loading resulted in more gradual damage at the interface, allowing the micro columns to be more pronounced and visible. This resulted

in higher strength in specimens subjected to cyclic loading. The load versus bond length relationships for monotonic and cyclic loading cases is compared in Fig.3.44.

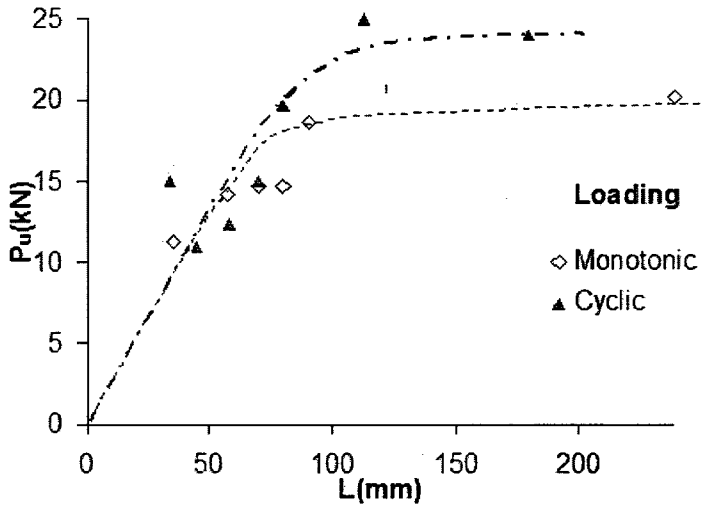

Figure 3.44. Comparison between static and cyclic loading.

Fig.3.45 shows a typical force-deformation relationship obtained from a cyclic test. It was observed that the relationship under monotonic loading provided an envelope for cyclic loading, with reloading branches under cyclic loading merging with the monotonic curve with a slight reduction in slope. The variation of strains along the bond length is illustrated in Fig.3.46 for Specimen #5-7 for different stages of loading. It demonstrates that the distribution of strains and the pattern of variation under increasing load are similar to those observed in specimens tested under monotonic loading.

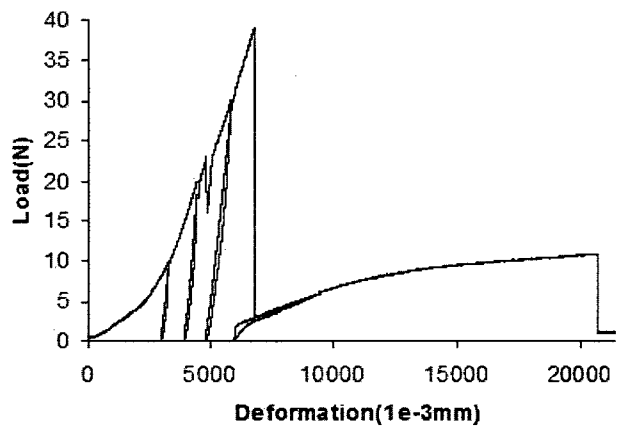

Figure 3.45. Typical load versus deformation result of Specimen #5-5 subjected to cyclic loading.

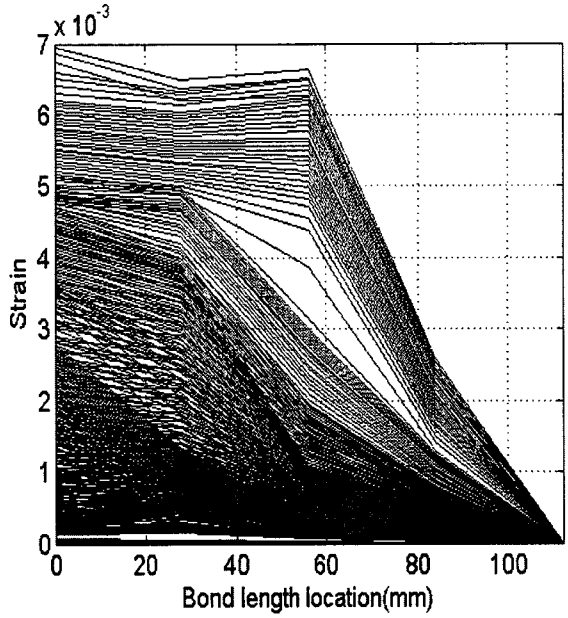

Figure 3.46. Strain variations in the concrete Specimen #5-7 with 110 mm CFRP length subjected to cyclic loading

- **The Effect of Substrate**

The ultimate strength versus bond length relationships for specimens with different substrates are shown in Fig.3.47. The relationships are presented in terms of CFRP stress, instead of the applied load, since the strip width in brick specimens was different (narrower) than that used in concrete and block specimens. The comparison indicates lower bond capacity in block specimens. This can be explained by the difference in failure patterns. Both concrete and brick masonry specimens suffered surface bond failures, whereas the concrete block specimens failed prematurely through the failure of the walls of block masonry units. This can be attributed to the lower strength of concrete block units, as compared with brick masonry. The higher bond strength of CFRP on brick masonry is attributed to the narrower strip width. As discussed earlier, narrow widths of strips tend to develop higher bond strengths than wider strip, though wider strips may results in higher tensile force capacity. The CFRP strain variation for Specimen #11-6 with brick substrate is shown in Fig.3.48. Brick specimens showed similar strain patterns under different stages of loading as those for concrete specimens.

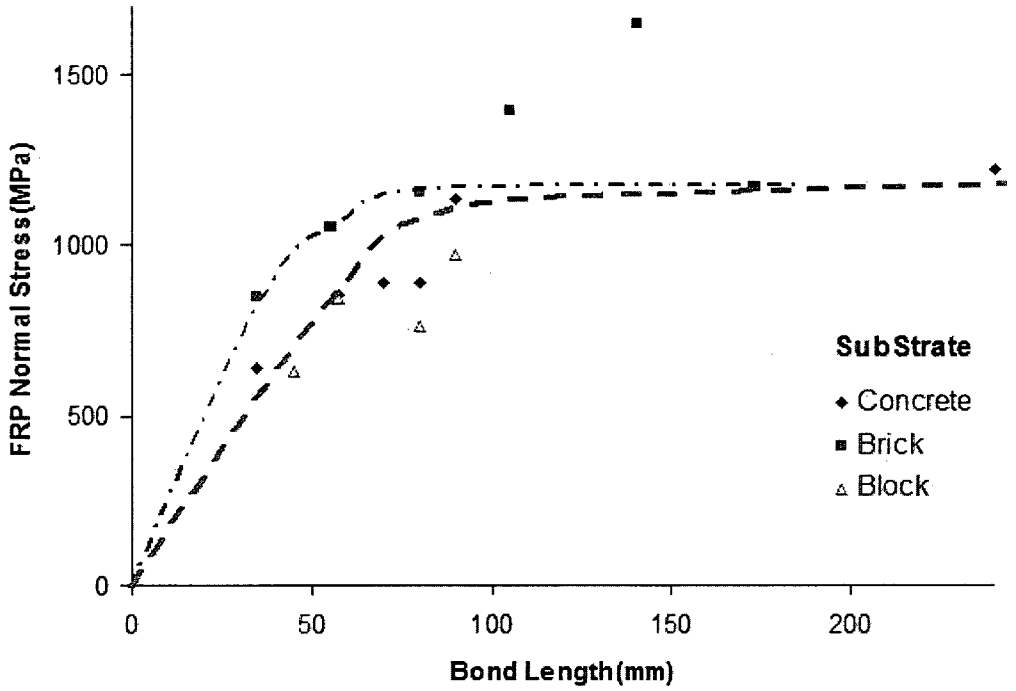

Figure 3.47. Comparing maximum normal stress in CFRP strips in the specimens with different substrates

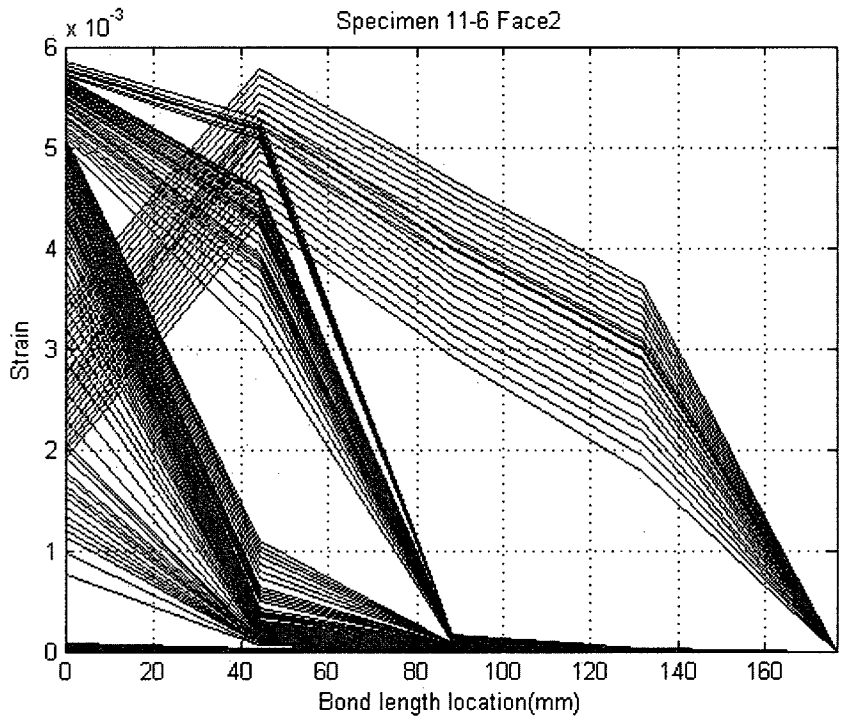

Figure 3.48. Strain versus location in the Brick Specimen #11-6 with 173 mm CFRP length and 40 mm CFRP width

3.7. Conclusion

The following conclusions may be drawn from the experimental research reported in this Chapter, which involved tests of 72 small scale specimens.

- The test setup for bond-pull tests that involved the use of U-shaped CFRP strips showed better and consistent results, and hence it is recommended for future tests.
- Most of the test specimens demonstrated an effective bond length beyond which the load resistance remained approximately constant, indicating that surface bond capacity of CFRP is limited by the bond strength associated with a specific length. The strain values recorded during the tests agree with the concept of effective length, as the strains cannot be increased beyond a specific limit.
- The failure pattern commonly observed during experimental research was that due to surface bond failure associated with the failure of the interface. The interface failure often initiated with micro cracking (dental cracking) that resulted in cantilever micro columns. The strains measurements confirm this observation with sudden jumps at the locations of cracks. Depending on the test setup, however, some specimens experienced diagonal tension cracking at corners of the critical section.
- The load deformation relationship of pull-test specimens showed linear behaviour until failure, followed by a sudden loss of load resistance (brittle failure).
- The effect of increasing concrete strength is to increase the bond strength slightly, with little or no change in effective bond length.
- The effect of the number of layers of CFRP (thickness of CFRP) is to increase both the bond strength and the effective bond length.
- The CFRP stress at bond failure increases with reduced strip width. As the strips become narrower, the stress (and strain) distributions across the width become more uniform, increasing the effectiveness of CFRP, as opposed to wider strips that tend to develop higher stress near the centre, with reduced stresses near the edges.
- Cyclic loading improves bond behaviour, while decreasing brittleness of the failure mode and increasing the effective bond length.

- The type of substrate material (concrete, concrete block and clay brick masonry) does not appear to have a significant effect on bond performance provided that the specimens do not suffer from other forms of failure. In the tests conducted here, concrete and brick masonry performed equally well, with failure taking place on the surface. The block masonry units suffered the failure of thin masonry walls around the cells, and could not develop their full bond capacities.
- Bond failure was observed to occur at longitudinal CFRP strains of 0.003 to 0.005 on the surface. As the number of CFRP layers increased, the strains measured on the surface decreased to approximately 0.001. For high-strength concrete specimens, the failure strain increased up to about 0.009, reflecting the importance of concrete strength on the mechanism of crack formation on the surface. Similarly high strains were also measured in narrow strips. Cyclic loading resulted in gradual formation of cracks, with increased strains up to about 0.007.

Chapter 4

ANALYTICAL RESEARCH

4.1. General

Analytical research consists of two parts; i) development of a new bond-slip model for surface bonded FRP sheets and ii) development of design methodology and design expressions for surface bonded FRP applications. The work in the first part was completed by evaluating the test data. This was done to assess the significance of each parameter and to conduct regression analyses to generate analytical expressions. These expressions were then used to describe the effects of test parameters on bond stress-bond slip relationships. The same expressions were also used in developing a design procedure, which formed the second part of the analytical research. The details of the process followed are presented in this chapter.

4.2. Analytical techniques used in evaluating test data

The test data obtained as part of the current research project was processed using the computer software MATLAB. The resulting relationships identified the significance of each parameter on bond-slip characteristics of surface bonded FRP.

The slip of FRP on the substrate was computed through the integration of measured strains over the bond length, as shown below.

$$s(x) = s(0) + \int_0^x \varepsilon(x)dx \tag{4.1}$$

where s(0) is the slip at the far end of the FRP laminate. This quantity may be assumed to be equal to zero. The next step involved the estimation of bond stress between the substrate and FRP. This was done as illustrated below.

$$\tau(x) = n_p.t_p.E_p.\frac{\Delta\varepsilon}{\Delta x} = n_p.t_p.E_p\,\frac{\varepsilon_{n+1} - \varepsilon_n}{x_{n+1} - x_n} \tag{4.2}$$

The bond stress and corresponding slip were used to quantify the effects of test variables. This procedure allowed the incorporation of relevant test parameters into the bond-slip model.

The measured values of strains obtained on the surface of the FRP strip are not representative of the average stress across the FRP cross-section. The difference may be explained by localized readings provided by strain gauges and the non-uniform nature of strain distribution across the depth and width of FRP strips. Therefore, it was necessary to apply a modification factor to recorded strains to arrive at average values of strains in FRP strips. This factor was obtained from equilibrium of forces. Accordingly, the average strain near the loading end of a strip was computed from recorded load and elastic modulus of FRP, because the measured strains varied approximately linearly in this region. Fig. 4.1 shows the linearity of experimentally recorded strains under increasing load. Then, the ratio of average to recorded strains at the loading end was computed as the modification factor. The same modification factor was applied to strain readings at other locations. The difference between computed average strains and recorded localized strains was found to vary between 5% and 35% at ultimate load level. Usually, specimens with multiple layers of FRP showed more divergence from the computed average strain as the measurement taken on the surface was not representative of the strain condition across the depth. The following expression illustrates the computation of the modification factor k:

$$k = \frac{P}{\varepsilon_{g,max}.E.b_p.n_p.t_p} \tag{4.3}$$

The modified strain can then be computed as below:

$$\varepsilon = k.\varepsilon_g \tag{4.4}$$

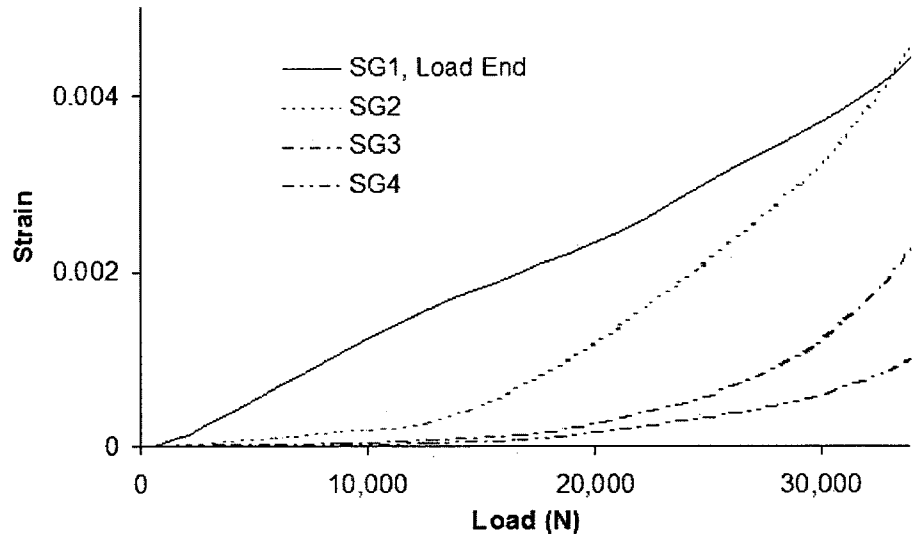

Fig. 4.1 Strain data recorded at the loading end of Specimen #4.2

Once the bond-slip relationship was established as described above, the area under this relationship was computed to find the fracture energy, which was used to establish the ultimate bond capacity, as well as the effective length of FRP. The following is the expression used for computing the fracture energy.

$$G_f = \int_0^\infty \tau ds \tag{4.5}$$

Sample Evaluation of a Test Specimen

The analysis procedure described above is applied to Specimen #4.2 to illustrate the evaluation of test data. The following steps are used to compute bond and slip quantities for the specimen at hand.

i. Compute modification factor "*k*" from Eq. 4.3 to establish strains at material interface from recorded surface strain values.

ii. Compute strains at material interface from Eq. 4.4.

iii. Use surface strain values to compute slip from Eq. 4.1.

iv. Use surface strains to compute bond stress from Eq. 4.2.

v. Construct the bond-slip relationship.

Fig. 4.2 shows measured (surface) strains and corrected (interface) strains for Specimen # 4.2. The strains increase exponentially towards the loading end, with maximum strain occurring at the loading end of FRP strip. This continues until the onset of surface cracks and associated slippage. Once the substrate surface begins to deteriorate within the high strain region, local bond stresses start decreasing as the high-strain region of FRP propagates towards the far end, generating a uniform strain zone. This zone extends towards the far end of FRP under relatively constant load as the material continues delaminating.

The variation of bond (surface shear) stress in FRP at different stages of loading is illustrated in Fig. 4.3. The figure indicates a gradual increase in bond with applied load. As surface cracks develop, bond stress decreases near these locations. The loss of bond eventually takes place near the loading end as the FRP delaminates from the surface of the substrate. As the applied load is increased, high bond regions start shifting away from the loading end, while showing sharp declines at locations of surface cracking.

Bond-slip relationships computed from experimental strain values are shown in Fig. 4.4. Fig. 4.4(a) illustrates the bond-slip relationships measured at different strain gauge locations under increasing loading. These gauges were placed at different locations along the centre-line of the FRP strip. Theoretically, the bond-slip relationship recorded at each strain gauge location should be the same if material imperfections and non-uniform cracking of concrete did not occur. Furthermore, the strain distribution between the recorded data is interpolated, resulting in linear variations among these points, introducing inaccuracies in the curves. Nevertheless, the curves do show the expected trend, with the majority showing similar behaviour. Fig. 4.4(b) depicts bond-slip relationships along the length of FRP, where each curve corresponds to a different load stage.

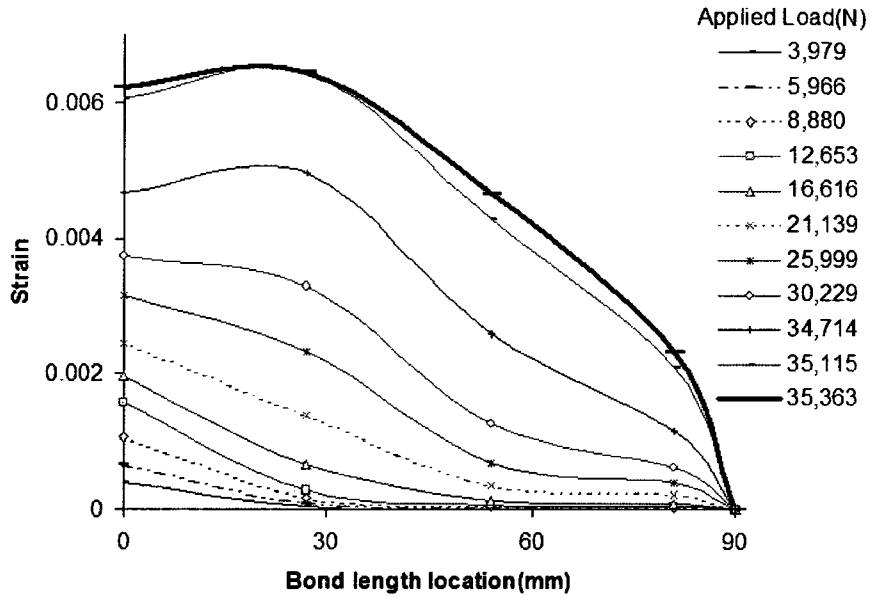

(a) Measured (surface) strains

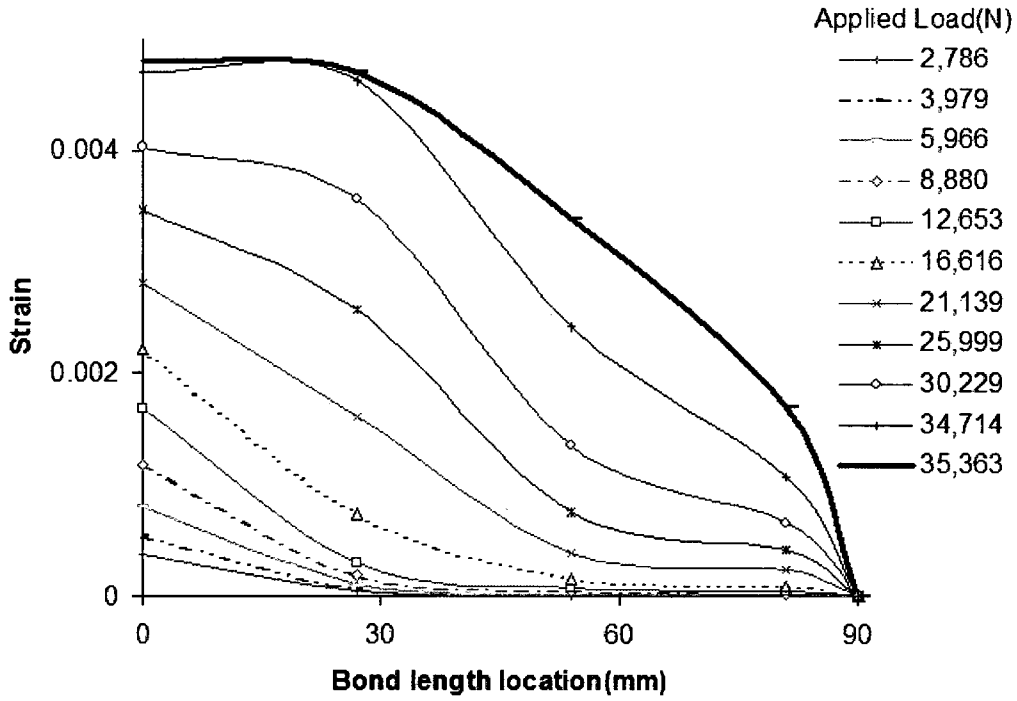

(b) Corrected (interface) strains

Fig. 4.2 Longitudinal strains along the bond length of Specimen #4-2

(f'_c=46 MPa; L_b=90mm; n=1; b_p=100 mm)

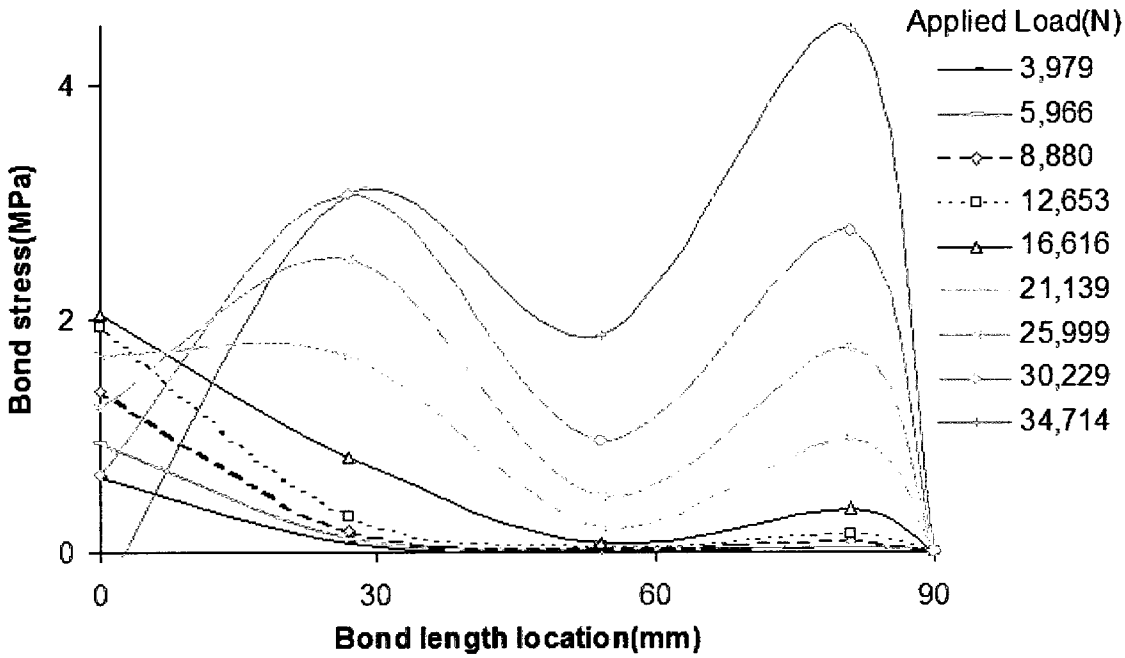

Fig. 4.3 Calculated bond stress along the bond length of Specimen #4.2

Bond-slip relationships computed from experimental strain values are shown in Fig. 4.4. Fig. 4.4(a) illustrates the bond-slip relationships measured at different strain gauge locations under increasing loading. These gauges were placed at different locations along the centre-line of the FRP strip. Theoretically, the bond-slip relationship recorded at each strain gauge location should be the same if material imperfections and non-uniform cracking of concrete did not occur. Furthermore, the strain distribution between the recorded data is interpolated, resulting in linear variations among these points, introducing inaccuracies in the curves. Nevertheless, the curves do show the expected trend, with the majority showing similar behaviour. Fig. 4.4(b) depicts bond-slip relationships along the length of FRP, where each curve corresponds to a different load stage.

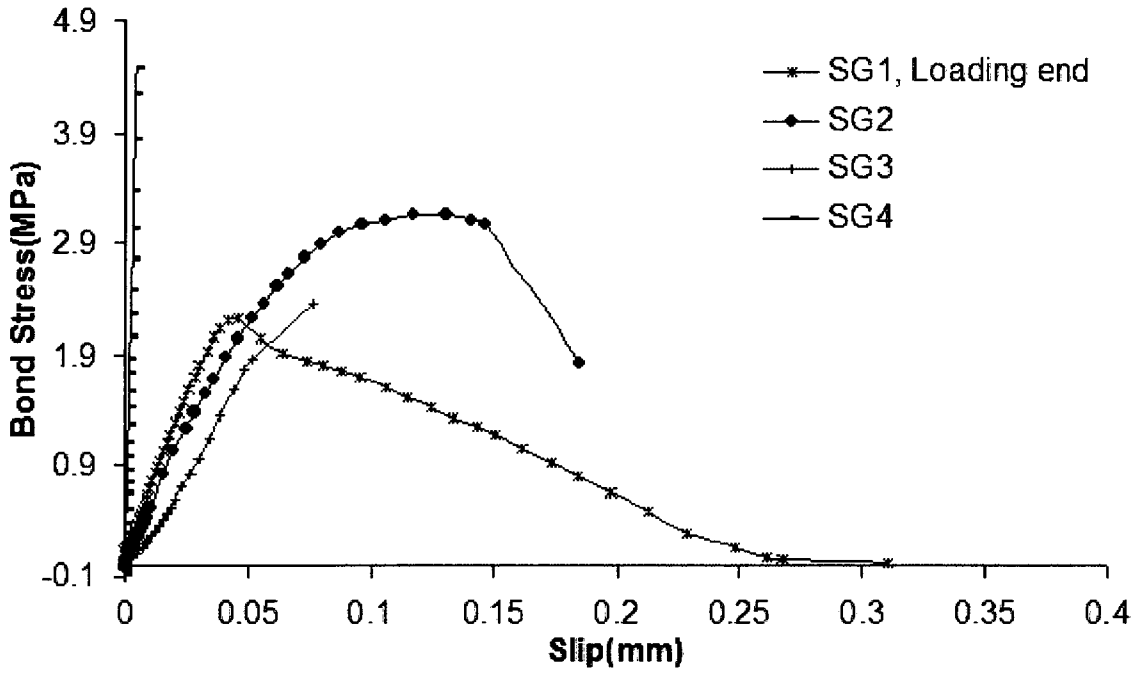

(a)

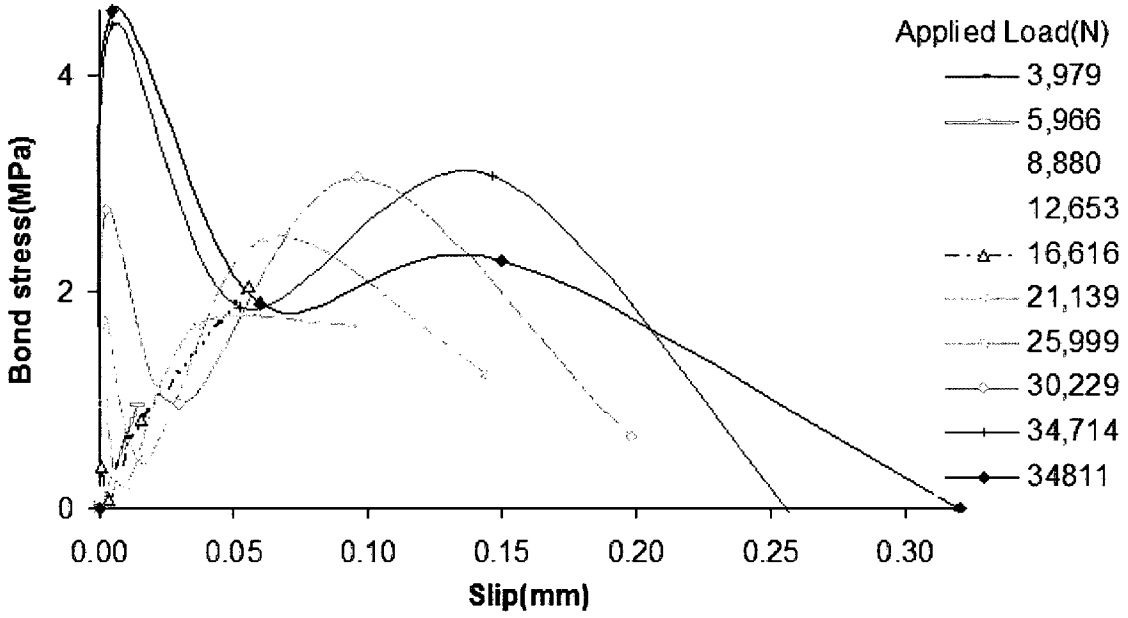

(b)

Fig. 4.4 Bond-slip relationships for Specimen #4.2; a) Bond-slip calculated using each strain gauge; b) Bond-slip calculated for each load stage

The strain data presented above and the computed bond slip relationships can be presented as three-dimensional plots if the load data is incorporated in the same plots. This is shown in Fig. 4.5, which depicts strain-load-bond length, and bond stress-load-slip relationships. These types of plots were used in deriving the bond-slip model presented later in this Chapter.

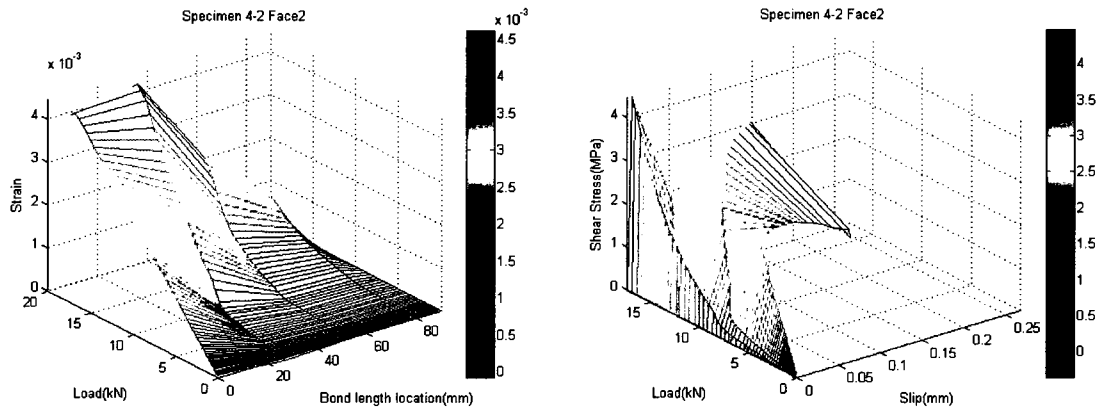

(a) (b)

Fig. 4.5 Three-dimensional plots for Specimen #4.2; (a) Strain-load-bond length, and; (b) Bond-slip-load relationships

An analytical bond-slip model is often built based on the quantification of certain primary features. These include; i) maximum bond, ii) slip at maximum bond and iii) maximum slip, as well as iv) the variation of bond-slip characteristics between these points. The maximum bond stress is often obtained from experimental data recorded near the end segment of a delaminating FRP strip, because the bond stress continues increasing beyond the local bond failure near the loading end. Therefore, the maximum bond stress quantity was obtained from recorded strains by the last strain gauge near the far end of the strip. The results for Specimen #4.2 indicated 4.6 MPa as the approximate maximum bond value as shown in Fig. 4.4. The maximum slip s_f attained after the degradation of the entire bond (i.e., zero bond stress) upon failure is estimated to be s_f = 0.32 mm. The third important modeling parameter is the slip corresponding to maximum bond stress, s_0. Fig. 4.4(a) shows significantly different s_0 values, depending on the strain gauge used, ranging between 0.005 and 0.105, with an average value of 0.05.

4.3. Effects of variables on bond behaviour

The experimental investigation consisted of a parametric study to assess the significance of modeling parameters. The effects of test parameters were plotted, and regression analyses were conducted to generate analytical expressions characterizing the importance of each variable. The data indicated that the relationships between the test variables and bon slip characteristics could be best expressed using power relationships as explained in the following sections.

4.3.1. Concrete Strength

Companion specimens with different concrete strengths were tested to investigate the significance of concrete strength on bond-slip characteristics of surface bonded FRP. Fig. 4.6 indicates the effect of concrete strength on ultimate bond capacity as characterized by the ultimate pull force. Accordingly, the ultimate bond strength consistently improved with increasing concrete strength. This could be attributed to improved diagonal tension capacity of higher strength concretes, which resisted higher forces before surface cracks were formed, leading to bond deterioration. The increase in ultimate load capacity showed approximately the same rate in all groups of specimens having different bond lengths. The regression analysis of test data indicated that concrete strength was related to ultimate load capacity through the power expression shown below, with a coeficient of variation of 0.09.

$$P_u \propto f'_c{}^{0.58} \tag{4.6}$$

The same relationship can also be used for ultimate strain because the ultimate strain is proportional to ultimate load through elastic modulus and the material remains elastic until failure.

$$\varepsilon_u \propto f'_c{}^{0.58} \tag{4.7}$$

The bond stress is obtained from FRP strains by using Eq. 4.2 and hence bond and concrete strength are also related through the same trend indicated in Eq. 4,7. This is shown below.

$$\tau_u \propto f'_c{}^{0.58} \tag{4.8}$$

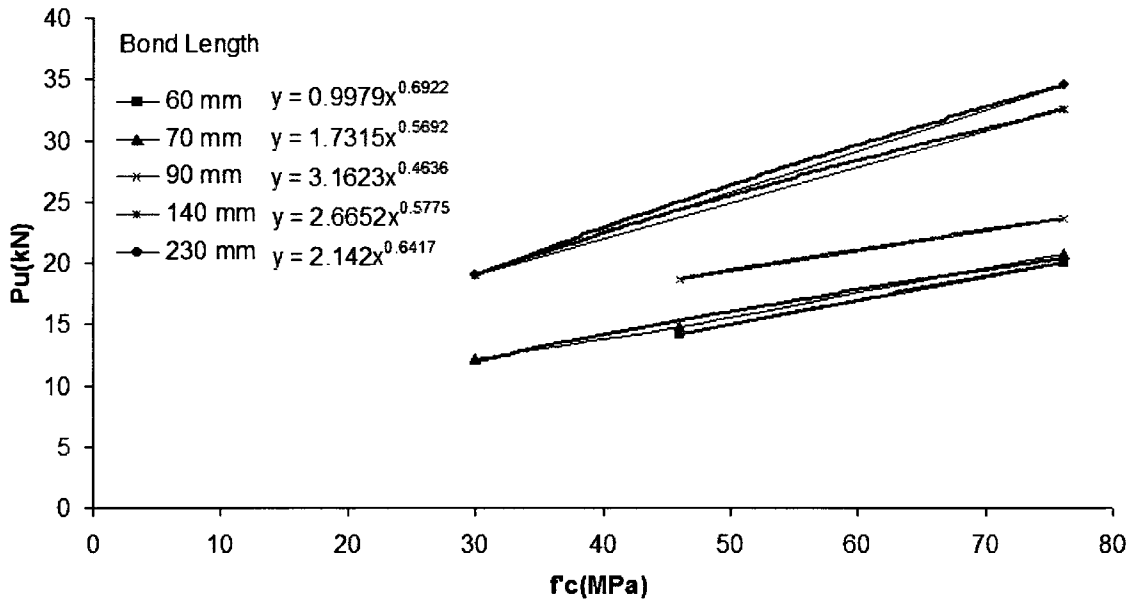

a) Test data with the same properties except for concrete strength

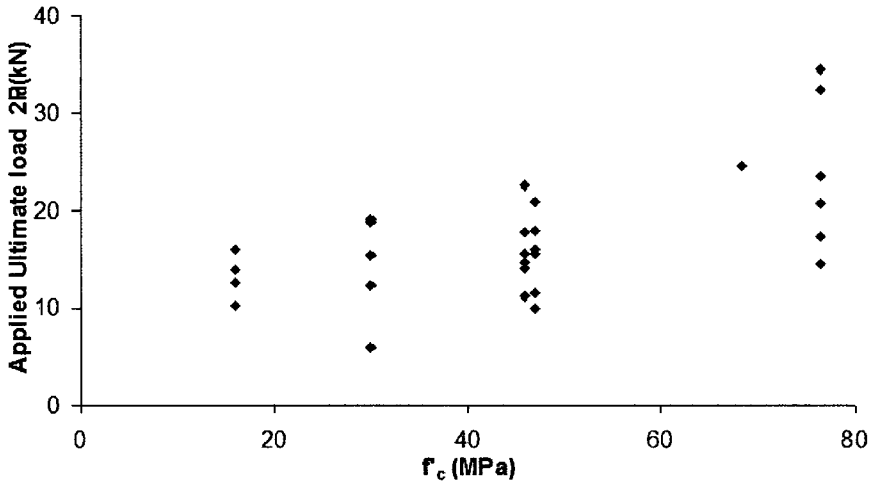

b) Tests data with different concrete strengths

Fig. 4.6 The ultimate load versus compressive strength relationships

The effect of concrete strength on slip can be investigated by computing slip from the strain data using Eq. 4.1. Because the ultimate strain increases with concrete strength linearly, the slip is also expected to follow the same trend. This is indicated below for slip at maximum bond and maximum slip at failure.

$$s_o \propto f'^{0.58}_c \tag{4.9}$$

The influence of concrete strength on effective bond length was discussed in Chapter 3 and the test data was shown in Fig. 3.36. The limited test data that was generated indicated little or no appreciable influence of concrete strength on effective bond length. Therefore, for the purpose of developing a design procedure it was assumed that concrete strength did not influence the effective bond length.

4.3.2. Number of layers of FRP

Different numbers of layers of FRP sheets are used in practice to attain different strength levels for retrofitting structural elements. Therefore, it is important to investigate the bond characteristics of FRP sheets as affected by the number of layers (or thickness). This was done in the experimental program.

The relationship between ultimate load and the number of FRP layers is shown in Fig. 4.7. Higher number of layers results in slightly higher ultimate load capacity. The regression analysis of test data shows the following relationship between the ultimate load capacity and the number of layers, with a coeficient of variation of 0.10.

$$P_u \propto n_p^{0.42} \tag{4.10}$$

The number of layers also represents the stiffness of FRP (nt_pE_p) when the same FRP material is used in each layer. Therefore, the relationship derived above can also be used to denote the effect of FRP stiffness on ultimate load capacity. It is noteworthy that the increase in strip stiffness leads to a more uniform distribution of bond stress. This results in higher ultimate load capacity.

$$P_u \propto \left(n_p t_p E_P\right)^{0.42} \tag{4.11}$$

The above relationship shows that the ultimate load capacity increases at a rate less than the increase in FRP stiffness. This implies that the use of several layers of FRP may not be as effective as one may assume, and the capacity does not increase in proportion to the number of layers employed.

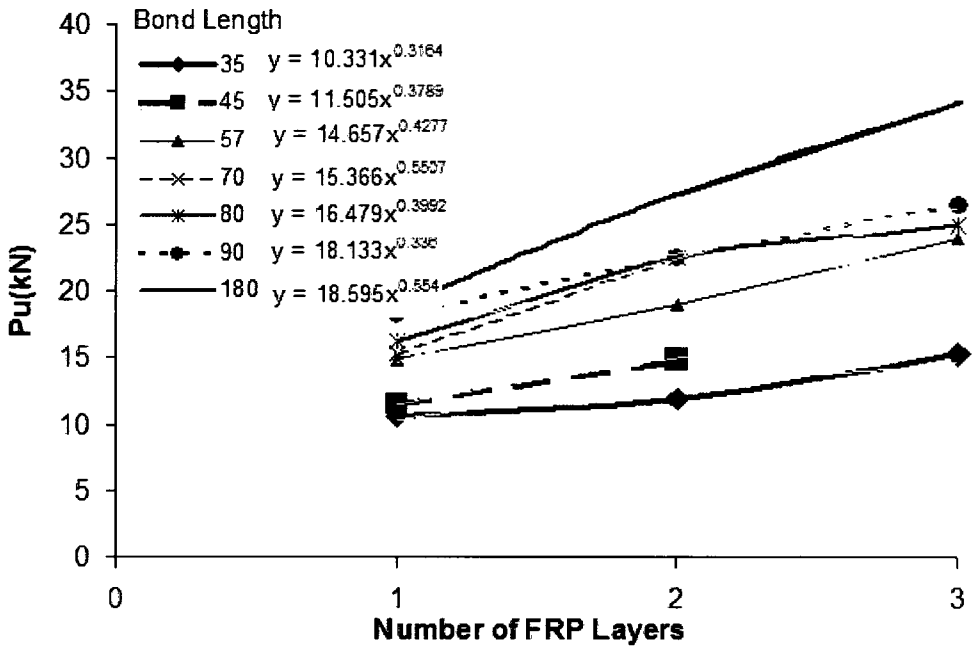

Fig. 4.7 Ultimate load as affected by the number of layers

Expressing Eq. 4.12 in terms of ultimate strain gives the following relationship.

$$\varepsilon_u = \frac{P_u}{n_p t_p b_p E_P} \tag{4.12}$$

$$\varepsilon_u \propto (n_p t_p E_P)^{-0.58} \tag{4.13}$$

The ultimate bond stress follows the same trend as that for ultimate load given in Eq. 4.12, relative to the number of FRP layers (or FRP stiffness).

$$\tau_u \propto \left(n_p t_p E_P\right)^{0.42} \tag{4.14}$$

Slip can be obtained from the integration of strains as per Eq. 4.1 Therefore, slip and longitudinal strains are related through the same proportionality established earlier. Hence;

$$s \propto \left(n_p t_p E_P\right)^{-0.58} \tag{4.15}$$

An important design parameter is effective bond length for FRP. This parameter was found to increase slightly when additional layers of FRP are used. This is illustrated in Fig. 3.37. Fig. 4.8 demonstrates the relationship between the effective length as estimated from test data and the number of layers. It is suggested that the relationship given below may be representative of the trend observed experimentally.

$$L_e \propto (n_p E_p t_p)^{0.23} \tag{4.16}$$

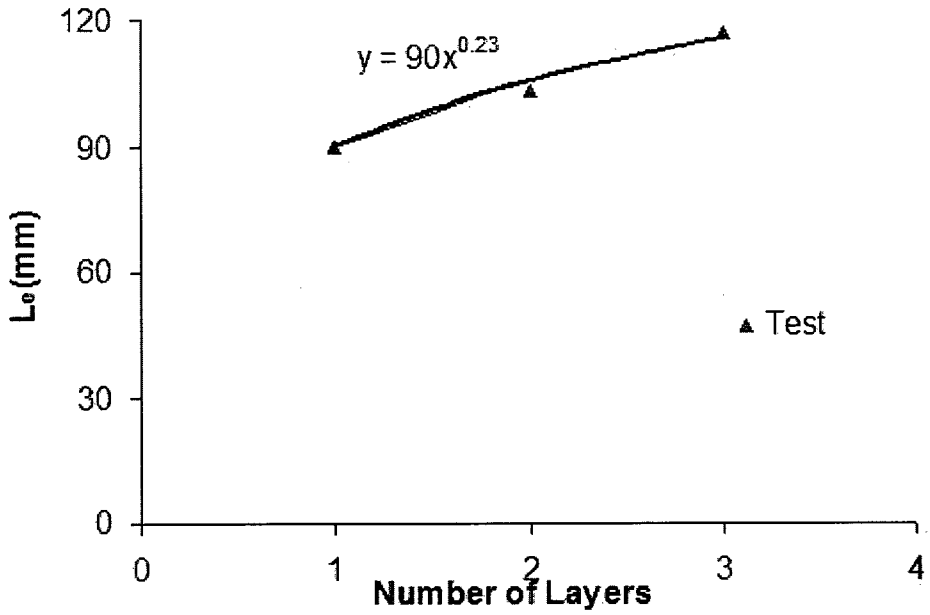

Fig. 4.8 Effective lengths versus number of layers

4.3.3. Width of FRP Sheet

It was observed experimentally that wider FRP strips resulted in higher ultimate load capacity because of the increased surface area. However, the rate of increase in ultimate load capacity was not proportional to the increase in strip width. Fig. 4.9 illustrates this point. The following relationship can be obtained from the experimental data with a coeficient of variation of 0.16.

$$P_u \propto (b_P)^{0.42} \tag{4.17}$$

The relationship for ultimate strain can be obtained from the above expression as shown below.

$$\varepsilon_u = \frac{P_u}{n_p t_p b_p E_P} \tag{4.18}$$

$$\varepsilon_u \propto (b_P)^{-0.58} \tag{4.19}$$

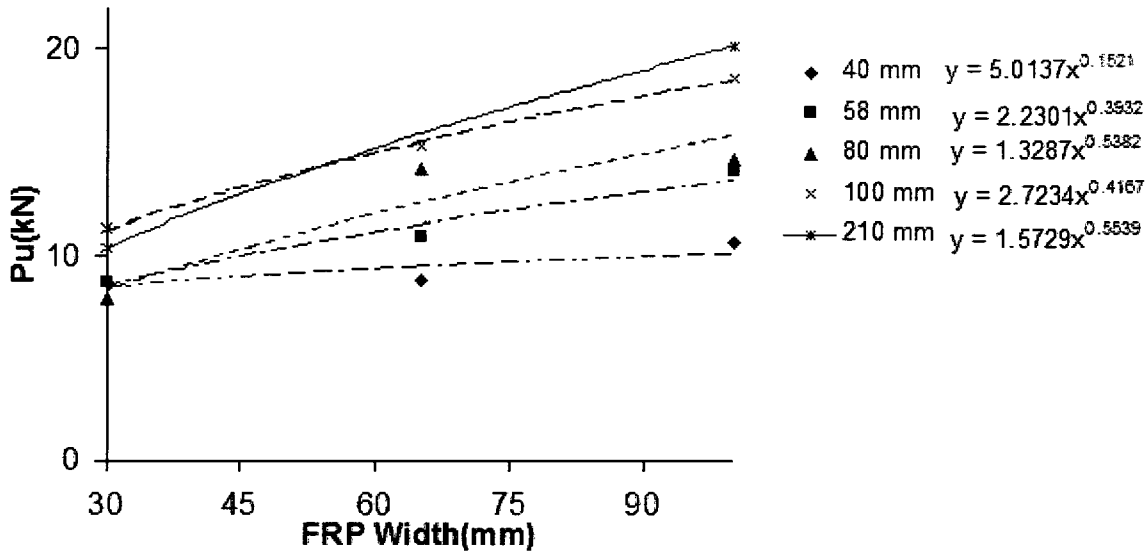

Fig. 4.9 Ultimate load as affected by width of FRP

The bond stress is anticipated to follow the same trend as normal strain, as one is obtained from the other. This is indicated below.

$$\tau_u \propto (b_P)^{-0.58} \tag{4.20}$$

Similarly, slip corresponding to ultimate bond stress is obtained through the integration of ultimate strain, and hence shows the same trend as that given in Eq. 4.21.

$$s_o \propto (b_P)^{-0.58} \tag{4.21}$$

The effect of strip width on effective length was investigated experimentally, and discussed in Chapter 3. Fig. 3.39 shows that the strip width did not show a clear effect on effective length and hence can be ignored as a design variable.

4.3.4. Cyclic loading

Fig. 3.42 demonstrates the force-deformation relationship recorded for a typical specimen under cyclic loading. The force-deformation relationship indicates that the reloading branches reach almost the previous unloading points, merging with the initial curve.

Comparing cyclic load tests with companion specimens under monotonic loading assessed the significance of cyclic loading on effective bond length. This comparison is plotted in Fig. 3.41 for ultimate load capacity, and indicates improved bond strength under cyclic loading because of the more gradual failure observed during testing. The cyclic loading resulted in more gradual damage at the interface, allowing the formation of micro columns to be more pronounced and visible. The consequence was to attain approximately 20% higher load capacity under cyclic loading as shown in Fig. 4.10. This is expressed below.

$$(P_u) = c.(P_u)_{montonic} \begin{cases} c = 1.2 & CyclicLoading \\ c = 1.0 & Monotonicloading \end{cases} \tag{4.22}$$

Similarly, factor of c=1.2 can be applied to the ultimate strain, as well as bond and slip quantities to introduce the effect of cycling the load.

$$(\varepsilon_u)_{cyclic} = c.(\varepsilon_u)_{montonic} \tag{4.23}$$

$$(\tau_u)_{cyclic} = c.(\tau_u)_{montonic} \tag{4.24}$$

$$(s_o)_{cyclic} = c.(s_o)_{montonic} \tag{4.25}$$

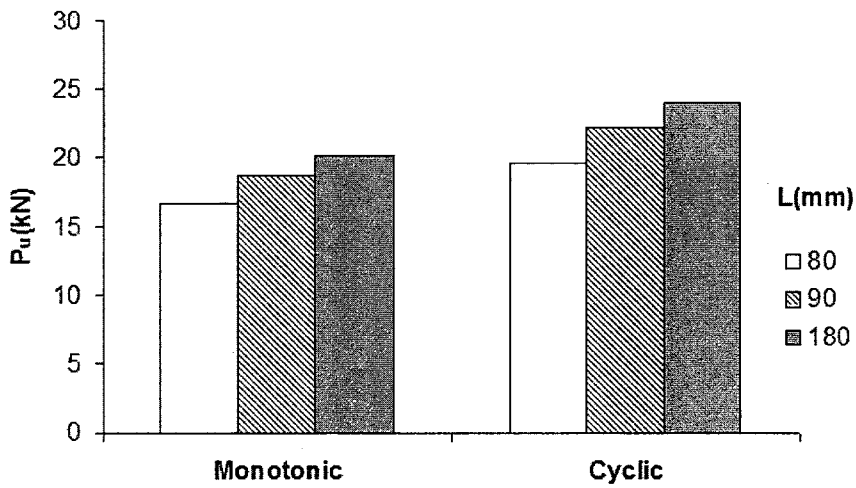

Fig. 4.10 The effect of cyclic loading on ultimate load

Bond capacities of specimens with different bond lengths were compared to assess the significance of cyclic loading. Fig. 4.11 shows that cyclic loading result in an increase of about 20% in the effective bond length. This is indicated below.

$$(L_e)_{cyclic} = c.(L_e)_{montonic}\ ,\ c=1.2 \tag{4.26}$$

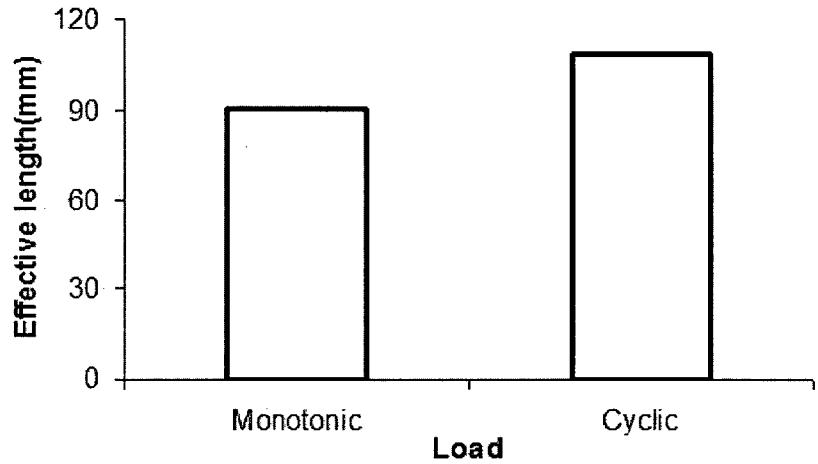

Fig. 4.11 The effect of cyclic loading on effective bond length

4.3.5. Substrate material

The effect of substrate material was investigated experimentally to investigate the suitability of bond-slip information developed for concrete to brick and block masonry. A limited number of tests were conducted using clay brick and concrete masonry block units. The blocks developed failure of the cells once the tensile capacity of concrete was reached prior to developing FRP bond failure. These specimens did show similar bond-slip characteristics as others until the failure of concrete has occurred. However, they never developed bond failures and hence their results could not be used in assessing strength and deformation capacity associated with bond.

The brick specimens showed a similar trend for the variation of ultimate load as that obtained for concrete provided all other parameters remained the same. The correlation between normalized ultimate capacity for specimens with brick and concrete substrates is shown in Fig. 4.12. This figure is based on experimental values for ultimate load capacity, normalized by other test parameters that are known to affect the capacity.

$$r = \frac{\{P_u/[c \times f_b^{0.58}(n_p t_p E_p b_p)^{0.42}]\}_{Brick}}{\{P_u/[c \times f_c^{0.58}(n_p t_p E_p b_p)^{0.42}]\}_{Concrete}} \quad (4.27)$$

where, f_b is the compressive strength of brick. The similarity observed in the behaviour of ultimate load capacity can also be applied to ultimate bond and corresponding slip as both of these quantities are computed from the ultimate load capacity. Therefore, the trends observed for these parameters in concrete specimens can be applied to those observed in brick specimens as well. Similarly, the observations made for effective FRP bond length on concrete and brick specimens indicated similar trends. This is summarized below for the brick specimens.

$$P_u \propto c \times f_s^{0.58}(n_p t_p E_p b_p)^{0.42} \quad (4.28)$$

$$s_0 \propto c\left(\frac{f_s}{n_p t_p E_p b_p}\right)^{0.58} \quad (4.29)$$

$$\tau_u \propto \left(\frac{f'_c}{b_p}\right)^{0.58}(n_p t_p E_p)^{0.42} \quad (4.30)$$

$$L_e \propto (n_p E_p t_p)^{0.23} \quad (4.31)$$

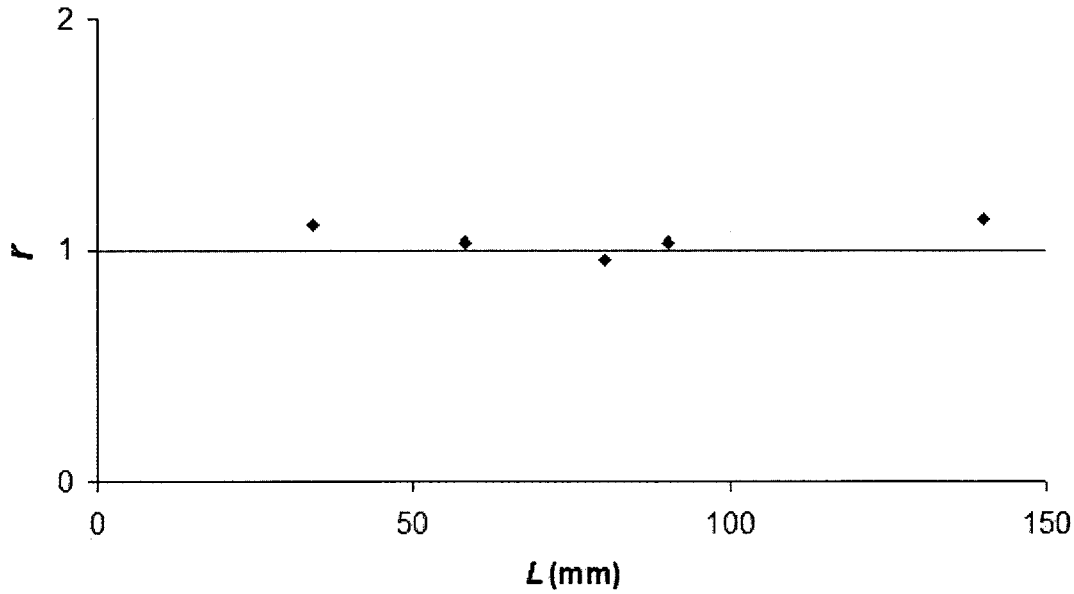

Fig. 4.12. The correlation of test data between concrete and brick specimens as indicated by normalized ultimate strength ratio, r.

4.4. Development of bond slip model

4.4.1 Bond-slip phenomenon for surface bonded FRP sheets

When a surface bonded FRP sheet is subjected to direct tension, tensile stresses are transferred to the substrate through surface bond stresses. The progression and distribution of bond stresses depend on the bond length. It was experimentally observed that, for a given bond length, bond stresses progressively increase under increasing direct tension of FRP. The distribution of bond stress is not uniform. Fig. 4.3 illustrates the distribution of bond stress along the bond length of a test specimen under increasing load. The bond stress increases until the ultimate bond stress τ_u is attained. As the applied load continues to increase, the stressed region spreads over the effective bond length while beginning to form a bell-shaped distribution. As the load approaches the ultimate load, the bond stress distribution assumes a complete bell-shaped distribution with the peak stress equal to the ultimate bond stress. Further increase in applied load results in the detachment of FRP over the effective bond length and the propagation of stresses towards the far end of the bond length while maintaining the same shape of stress distribution. This continues as the bell-shaped bond stress distribution moves until the end of the bond length, at which time the complete bond failure occurs. Fig. 4.13 illustrates the propagation of bond stresses along the bond length. It also shows the distribution of longitudinal strains on FRP that corresponds to bond stress distribution.

4.4.2 Model Development

The foregoing discussion highlights the bond-slip phenomenon between surface-bonded FRP sheets and concrete or masonry substrate. This phenomenon was modeled by developing an analytical bond-slip relationship. This was done on the basis of the experimental data recorded within the effective bond length. Hence, the parameters of the bell-shaped bond-slip relationship were derived for the effective length, based on the premise that the shape of the bond-slip model corresponding to the effective bond length remains the same for any segment within the bond length. This implies that the parameters of the bond-slip model are a function of the effective length, L_e. Fig. 4.14 shows the idealized bond-slip relationships over the effective length.

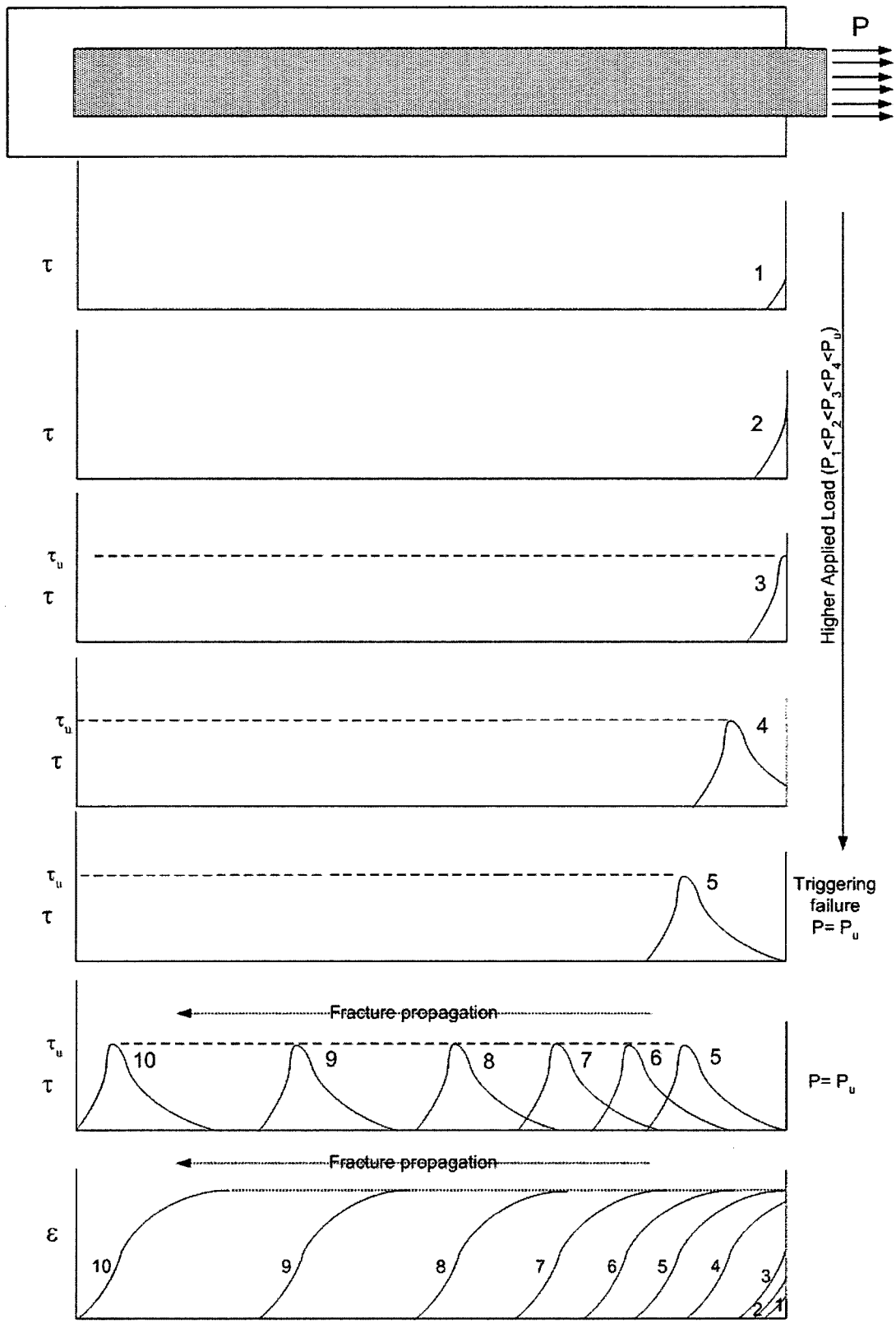

Fig. 4.13 Propagation of bond stresses and associated strains along FRP length

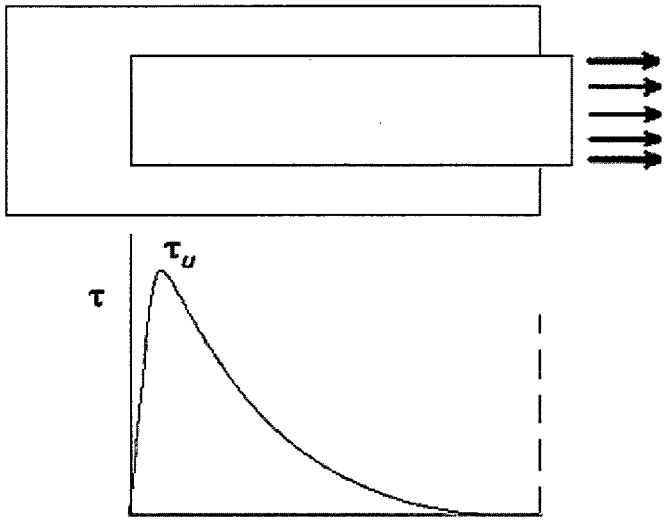

Fig. 4. 14 Idealized bond stress distribution over the effective length at ultimate

If the bond length is very small, the substrate material failure may precede the bond failure. As the bond length increases, the bond stresses distribute over the available bond length. It was experimentally observed that the ultimate bond stress τ_u and the corresponding slip s_o both change with bond length. This is shown in Figs. 4.15 and 4.16. The following expressions give the trend observed in these relationships using a power fit.

$$\tau_u \propto L_b^{-0.5} \tag{4.32}$$

$$s_0 \propto L_b \tag{4.33}$$

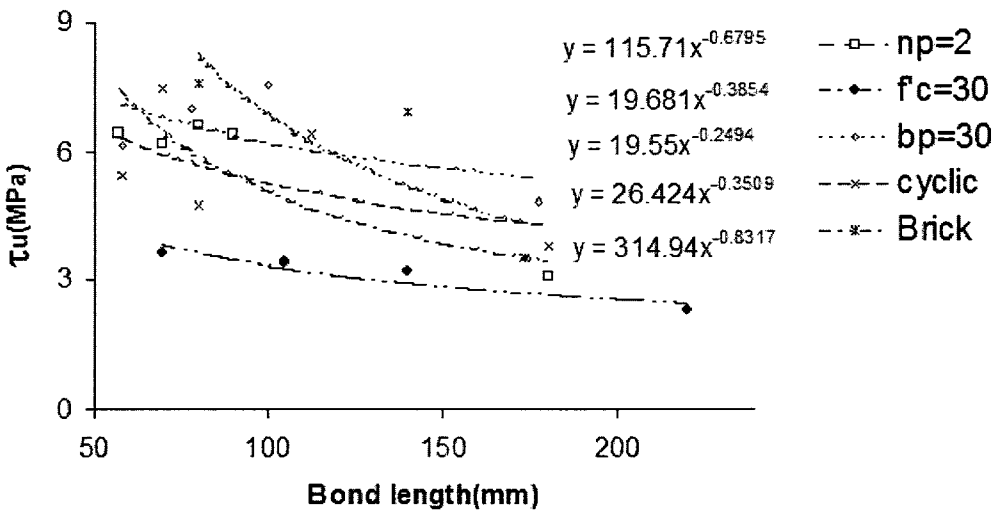

Fig. 4.15 Bond at ultimate load versus bond length

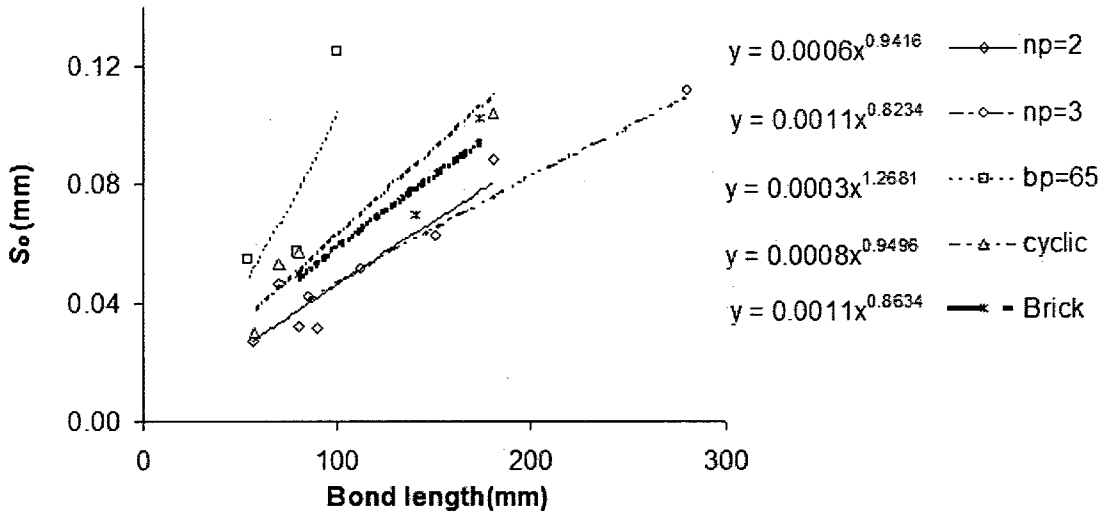

Fig. 4.16 Slip at ultimate load versus bond length

For the purpose of developing a bond-slip model, it was assumed that the bond stress distribution, including τ_u and s_o, remain constant over a bond length equal to the effective bond length, as illustrated in Fig. 4.13. The above relationships are then used to incorporate the effect of bond length on τ_u and s_o within the effective length. Substituting $L_b = L_e$, and combining with the contributions of other test variables as previously established in Eqs. 4.6 to 4.29, the following expressions can be written.

$$\tau_u \propto c\left(\frac{f'_c}{b_p}\right)^{0.58} (n_p t_p E_p)^{0.42} \times L_e^{-0.5} \propto c^{0.5}\left(\frac{f'_c}{b_p}\right)^{0.58} (n_p t_p E_p)^{0.305} \tag{4.34}$$

$$s_0 \propto \left(\frac{f_c'}{n_p t_p E_p b_p}\right)^{0.58} \times L_e \propto c\left(\frac{f'_c}{b_p}\right)^{0.58} (n t_p E_p)^{-0.35} \tag{4.35}$$

4.4.3. Shape of the bond-slip model

The shapes of bond-slip models proposed by previous investigators were examined before a shape was formulated for the proposed model. The models proposed by others consisted of either continuous or discrete functions for ascending and descending branches, including a linear descending segment or a complete bilinear ascending and descending segments. The experimental observations indicate that the relationship that was suggested earlier by Popovics for the stress-strain relationship of

concrete is also suitable for representing the bond-slip relationship of surface bonded FRP sheets. This relationship is shown below:

$$\tau = \tau_{max}\left(\frac{s}{s_0} \times \frac{n}{(n-1)+(s/s_0)^n}\right) \tag{4.36}$$

where, n is a constant. Each parameter in the above expression was derived from experimental data using the relationships discussed previously in this chapter. These parameters consist of s_0, τ_{max}, and the fracture energy G_f, which is used to define constant n.

In addition to the continuous function given in Eq. 4.36, a simplified bilinear model is also suggested for more approximate calculations of bond and slip that may be more suitable for structural design purposes. This is shown below.

$$\tau = \begin{cases} \tau_{\max}\left(\dfrac{s}{s_0}\right) & ifs \le s_0 \\ \tau_{\max}\dfrac{s_f - s}{s_f - s_0} & ifs > s_0 \end{cases} \tag{4.37}$$

The parameters of the above two models are discussed in the following section.

4.4.4 Parameters of models

The power functions that were developed earlier to express the effects of test variables on modelling parameters are used to derive expressions for the parameters of the model. Figs. 4.17 and 4.18 demonstrate the expressions developed for s_o and τ_u respectively. The resulting expressions from these figures are given below.

$$s_0 = 3.5c^2\left(\frac{f'_c}{b_p}\right)^{0.58}\left(n_p t_p E_p\right)^{-0.35} \tag{4.38}$$

$$\tau_u = 0.30c^{0.5}\left(\frac{f'_c}{b_p}\right)^{0.58}\left(n_p t_p E_p\right)^{0.30} \tag{4.39}$$

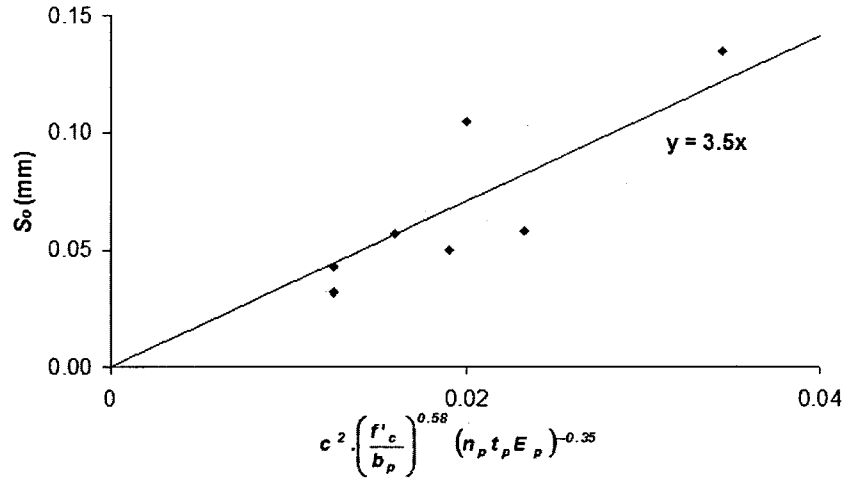

Fig. 4.17 Slip at ultimate bond versus related variables

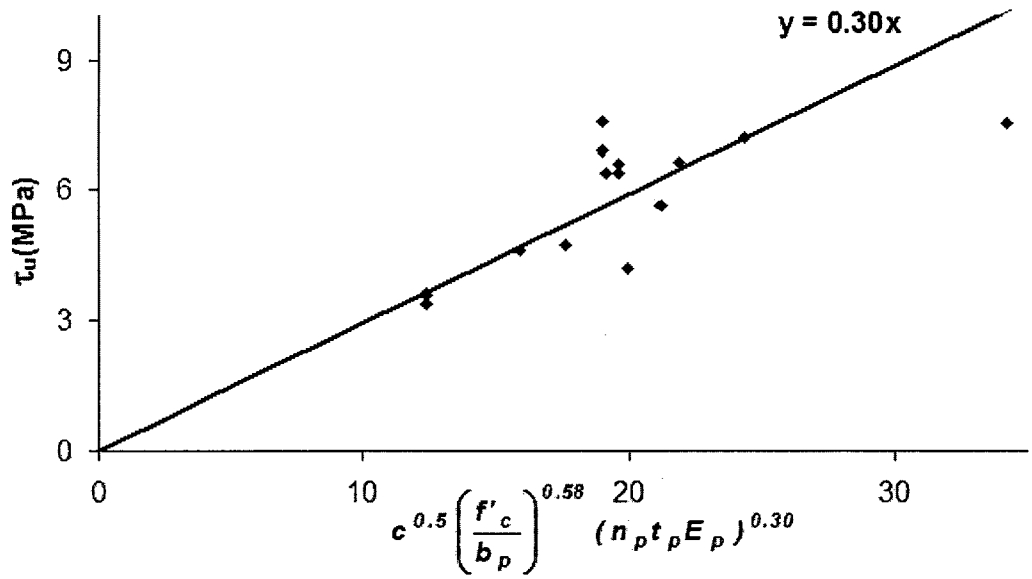

Fig. 4.18. Ultimate bond stress versus related variables

The Popovics constant n was established through the fracture energy G_f, which is the area under the bond-slip relationship, reflecting the shape of the model. The following outlines the steps that were followed to derive an expression for parameter n.

- Experimental data was used to plot bond-slip relationships for specimens with bond length approximately equal to the effective bond length. This was done because specimens with an effective length were selected as reference specimens in establishing the shape of the model, as discussed earlier.

- Area under each bond-slip relationship was computed to find the fracture energy.
- The experimental fracture energy computed above was set equal to the area under the Popovics curve based on the empirically computed values of τ_u and s_o using Eqs. 4.34 and 4.35 and the unknown parameter "n." This resulted in the computation of "n" for each case.
- The effects of experimental variables on parameter "n" were investigated.
- Those experimental variables that did not show significant effects on "n" were eliminated.
- An expression was developed for "n" as a function of the most significant test variable, FRP strip width.

Fig. 4.19 shows the comparison of "n" with test variables. The figure clearly indicates that the only test variable that shows a significant influence on "n" is the width of FRP strip b_p. Fig. 4.20 was then used to derive an expression between "n" and b_p, using a power fit to test data. This expression is shown below.

$$n = \frac{20}{(b_p)^{0.42}} \tag{4.40}$$

Whereas Popovics curve, with the proposed expressions for τ_u, s_o and n, can define the model, another parameter is needed to simplify the model in the form of a bilinear bond-slip relationship. This new parameter is the maximum slip s_f that takes place at the end of the linearly descending branch of the bi-linear relationship. This quantity can be related to fracture energy through the following expression.

$$s_f = \frac{2G_f}{\tau_{max}} \tag{4.41}$$

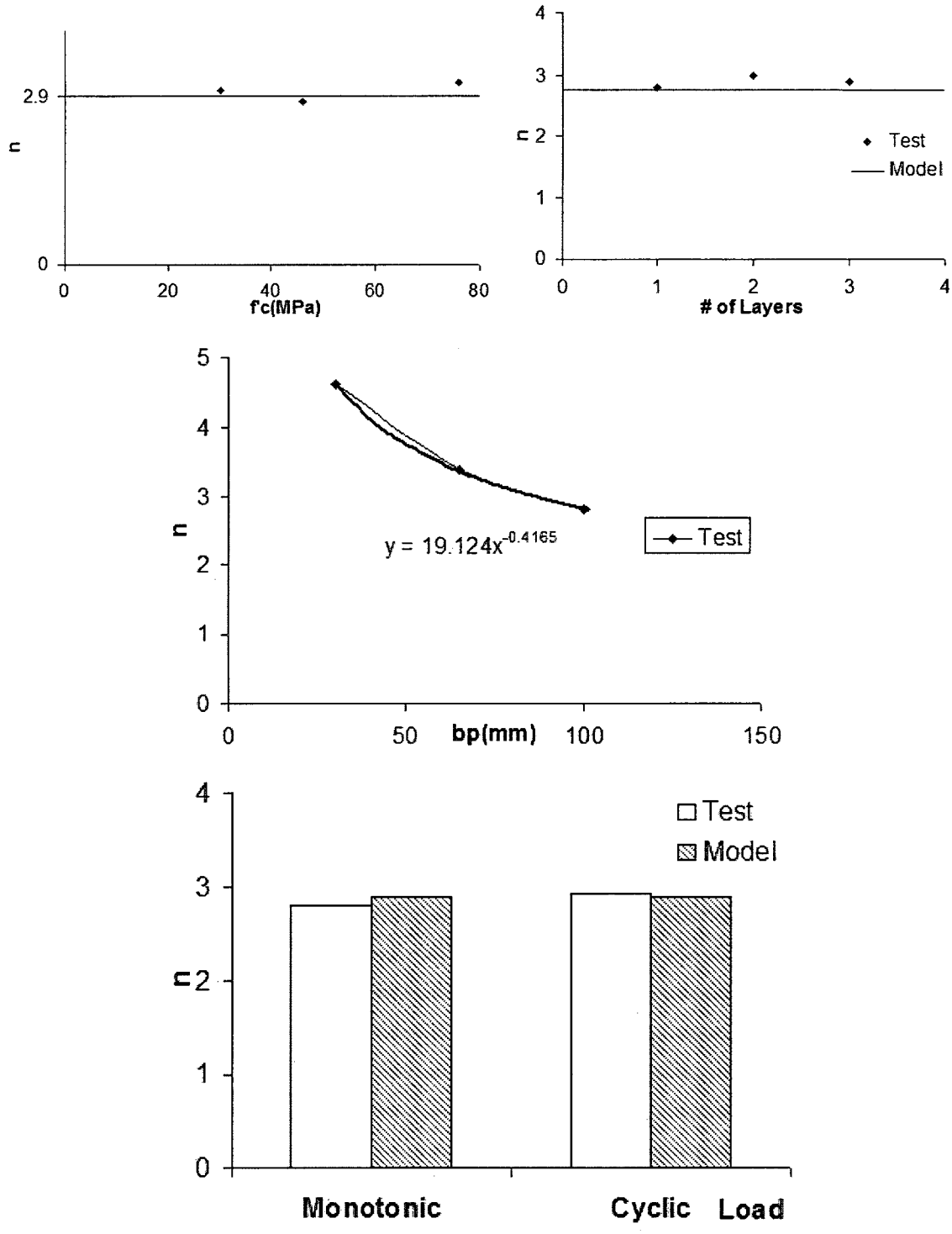

Fig. 4.19. Comparison between test and model results for the Popovics coefficient, n, for each variable

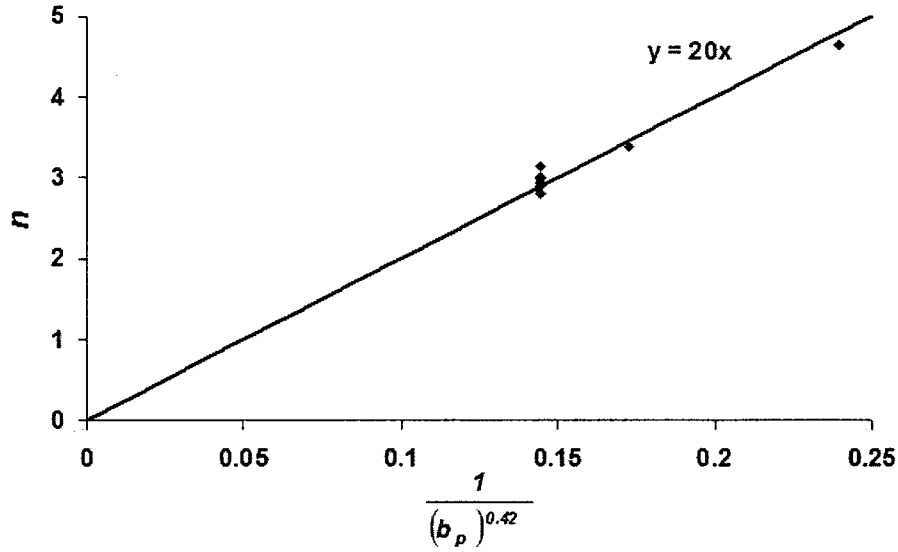

Fig. 4.20. Relationship for Popovics coefficient, n

Fracture energy G_f computed from experimental data is plotted in Fig. 4.21 as a function of different test variables. The figure helps establish the effect of each variable on G_f. Accordingly, except for the number of layers of FRP, which does not affect G_f significantly, all other variables were found to have effects on the fracture energy. Fig. 4.22 can be used to derive an empirical expression for G_f.

$$G_f = 0.13 cf'_c \left(b_p\right)^{-0.45} \tag{4.42}$$

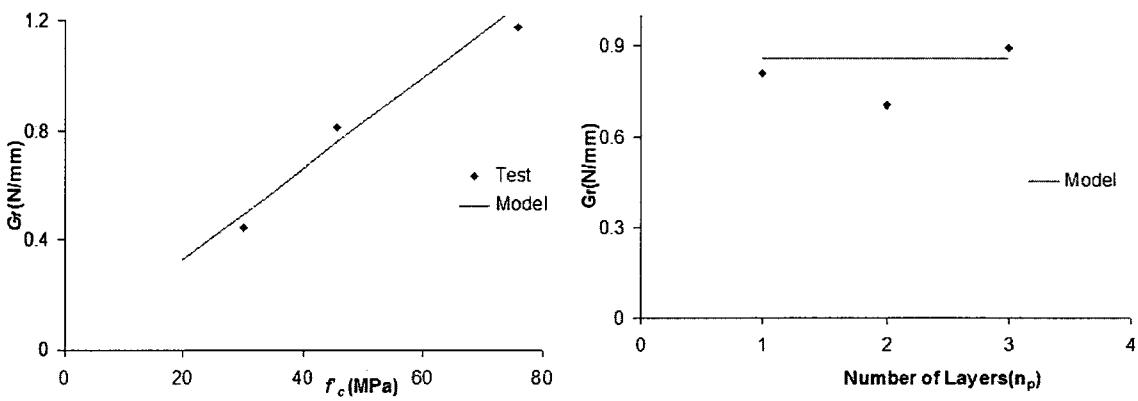

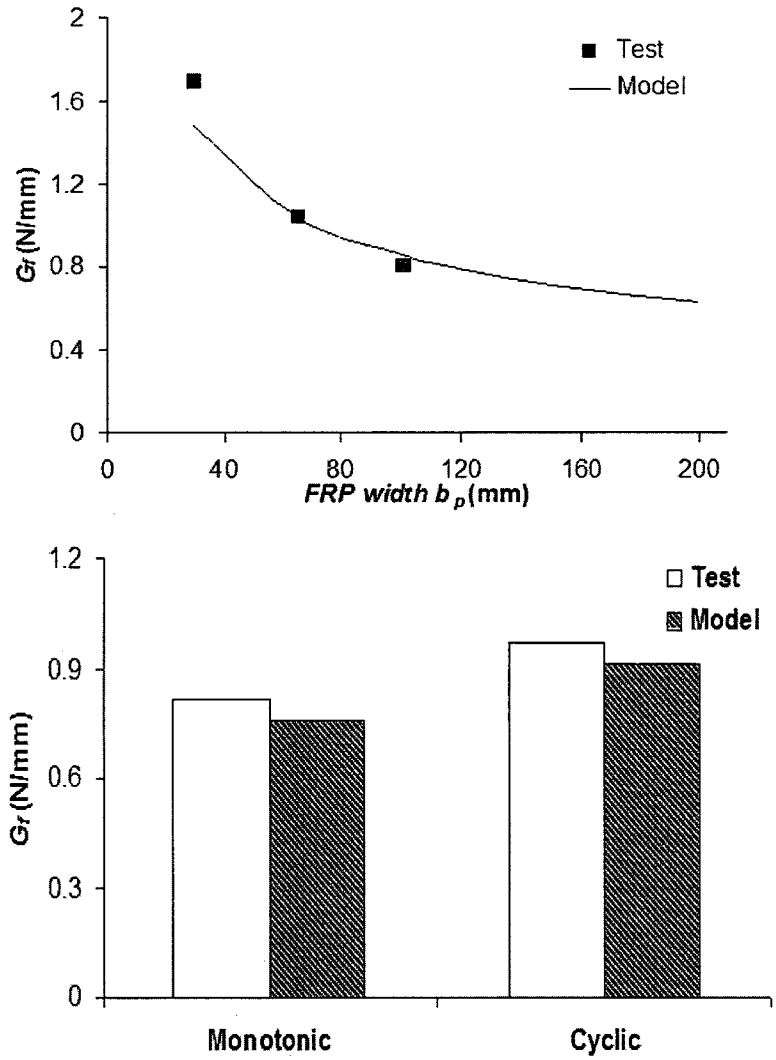

Fig. 4.21. Fracture energy versus test variables

Substituting Eq. 4.42 into 4.41 results in the following expression for s_f.

$$s_f = \frac{2G_f}{\tau_{max}} = 0.9c^{0.5}(f'_c)^{0.42}(b_p)^{0.13}(n_p t_p E_p)^{-0.3} \tag{4.43}$$

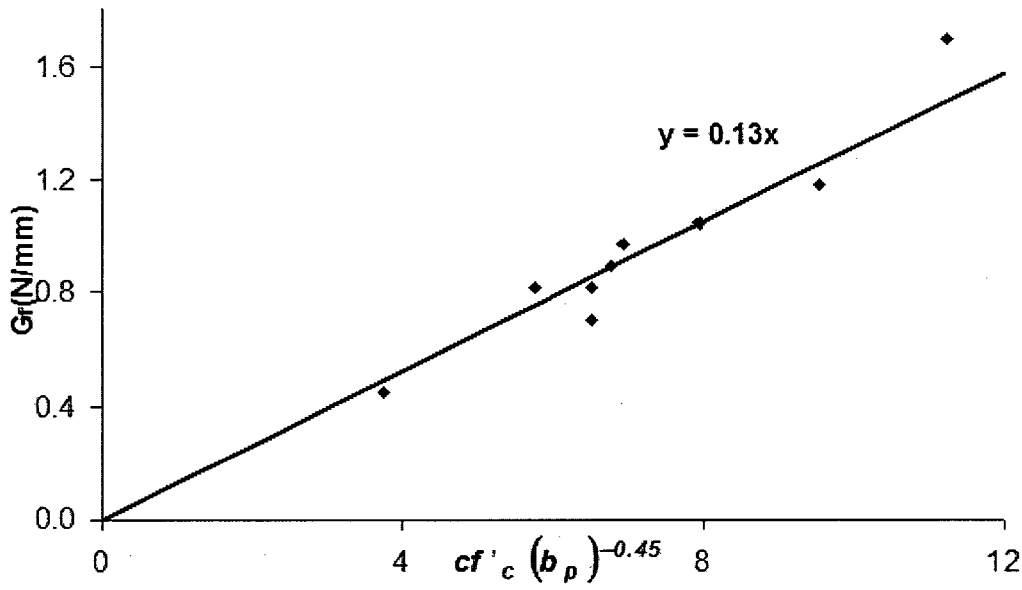

Fig. 4.22. Fracture energy as a function of test variables

4.4.5 Verification of the model

The bond-slip model that was developed in Section 4.4.4 was verified against experimental data generated in the current investigation, as well as those reported by other researchers. The model was also compared with analytical models developed by others.

The verification conducted in this section includes the comparisons of model parameters and complete bond-slip relationships with the experimental data generated as part of the current investigation. The modeling parameters used in the comparison include ultimate bond stress, τ_u, slip at maximum bond, s_o, the Popovics coefficient, n, and fracture energy per area, G_f. The comparisons are illustrated in figures 4.23 through 4.25. The results show reasonably good correlations of modeling parameters with experimental data, with coefficients of variation of 28%, 40% and 33% for ultimate bond strength, corresponding slip and fracture energy, respectively. In view of the imperfection nature of experimental surface bonded FRP fracture mechanism, these values indicate reasonably good correlation.

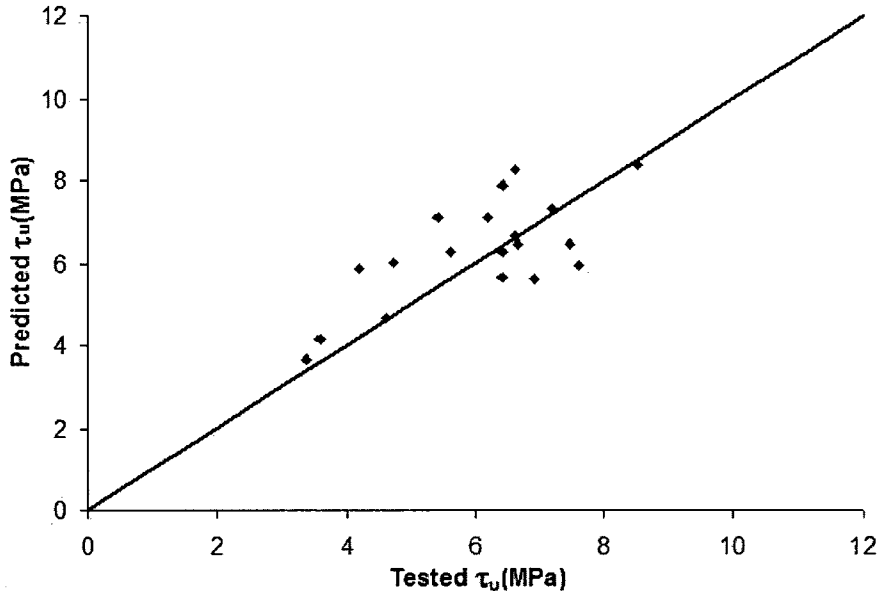

Fig. 4.23. Comparison between test and model results for ultimate bond stress

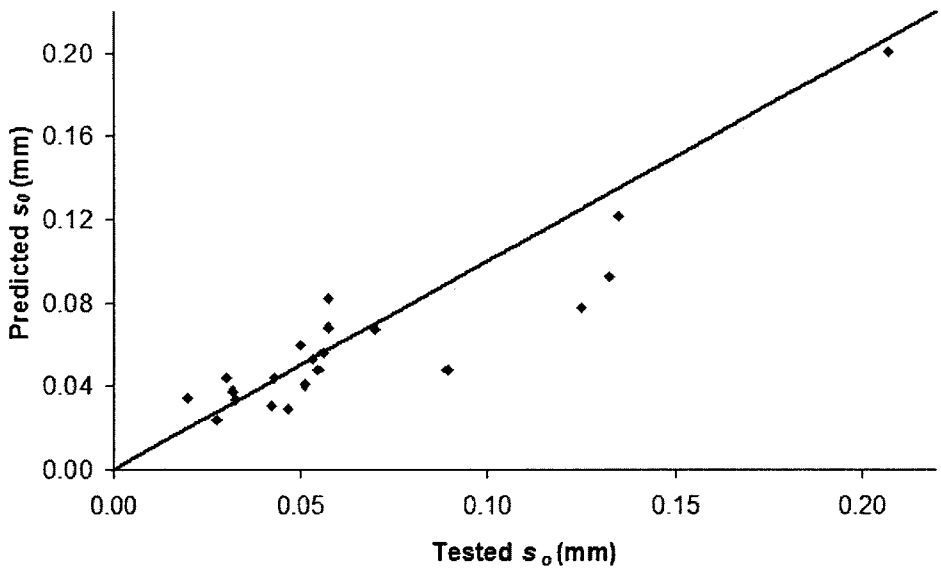

Fig. 4.24. Comparison of the computed and test values for s_o

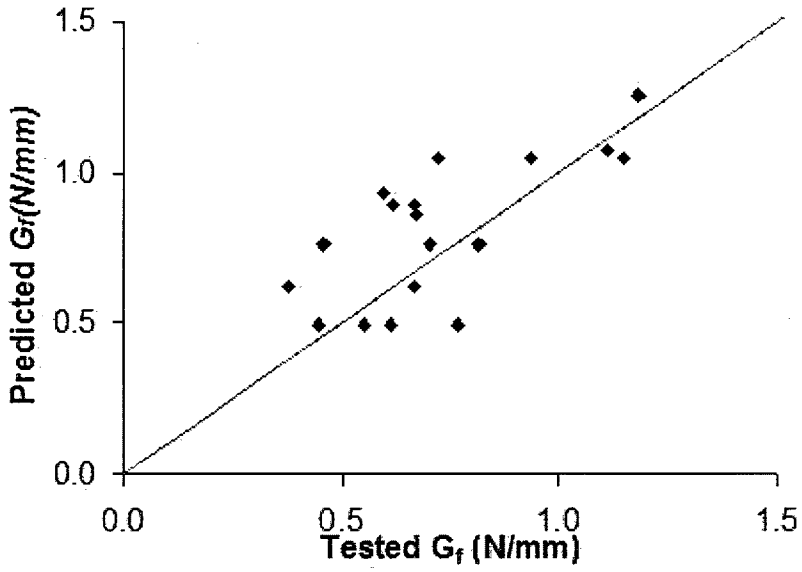

Fig. 4.25. Comparison of G_f computed from the analytical model and test data

The verification is extended to cover comparisons of complete bond-slip relationships along the effective length of test specimens. Fig. 4.26 shows the comparisons at ultimate when the ultimate bond stress is attained and the fracture over the effective length occurs. The comparisons show very good correlation for specimens with different concrete strengths, FRP strip widths, number of FRP layers (thickness), cyclic versus monotonic loading and different substrates (concrete and brick).

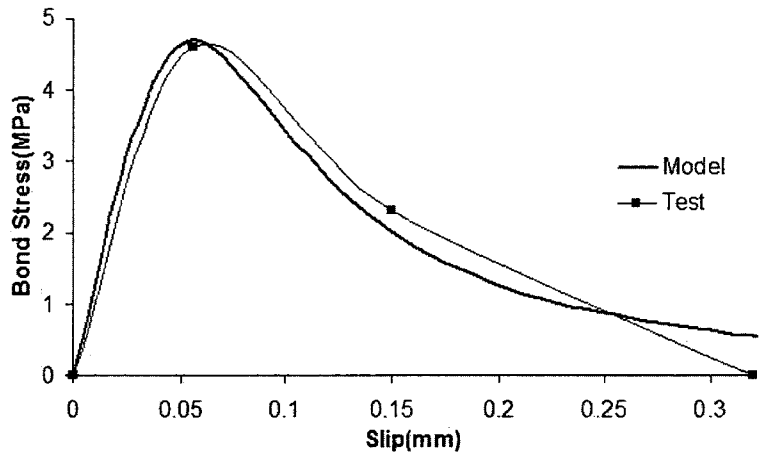

(a) Reference Specimen #4-2 (f'_c=46MPa, n_p=1, b_p=100mm, L=90mm)

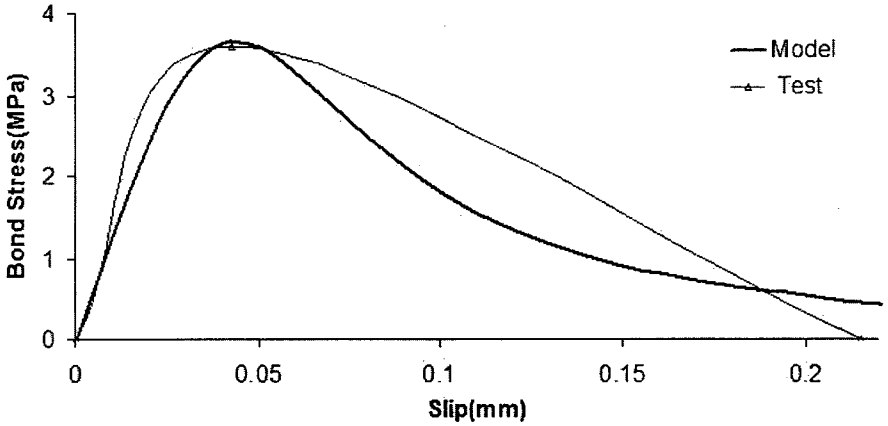

(b) Specimen #7.3 with lower strength of (f'_c =30MPa, n_p=1, b_p=100mm, L=105mm)

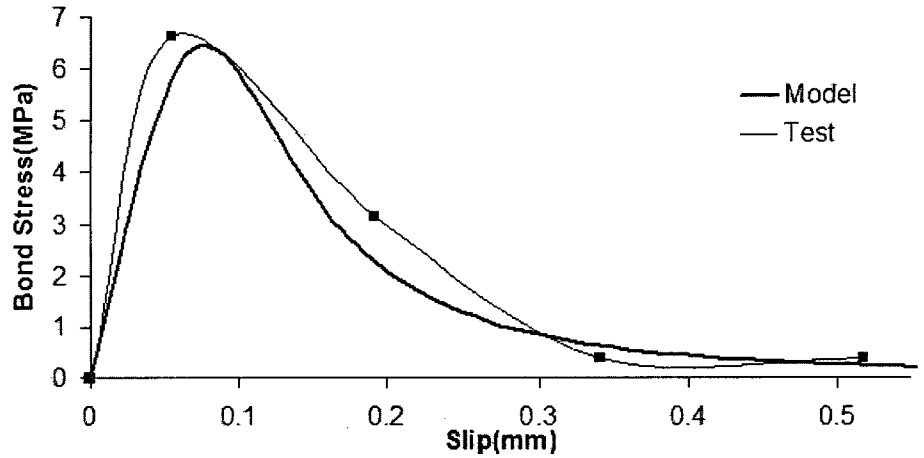

(c) Specimen #8.3 with low FRP width of (f'_c =52MPa, n_p=1, b_p=65mm, L=80mm)

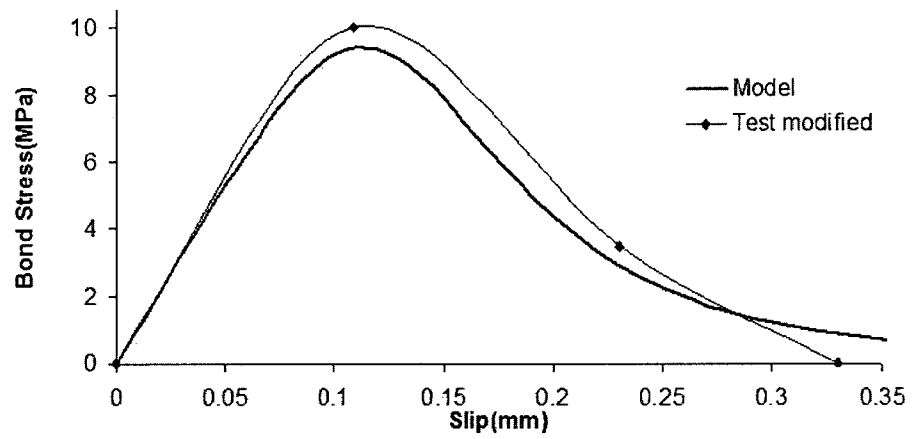

(d) Specimen #9.3 with lower FRP width of (f'_c =46MPa, n_p=1, b_p=30mm, L=78mm)

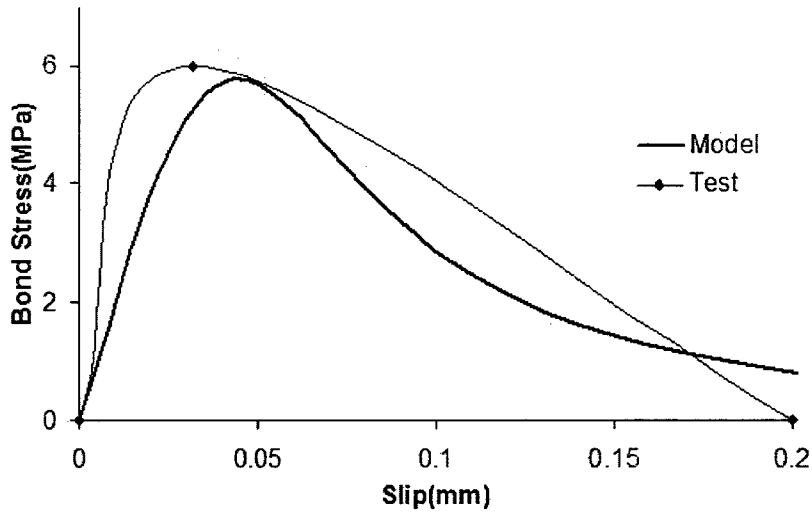

(e) Specimens with two layers of FRP strip (f'_c =46MPa, n_p=2, b_p=100mm, L=90mm)

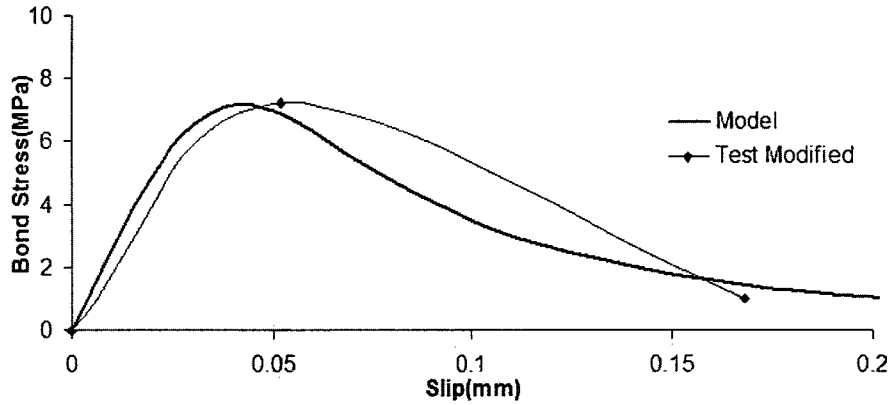

(f) Specimen with three layers of FRP strip (f'_c =54MPa, n_p=3, b_p=100mm, L=85mm)

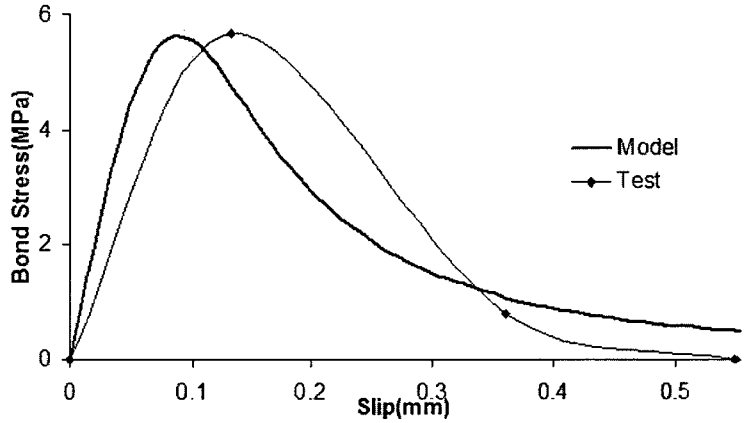

(g) Specimen subjected to cyclic loading(f'_c =54MPa, n_p=1, b_p=100mm, L=113mm)

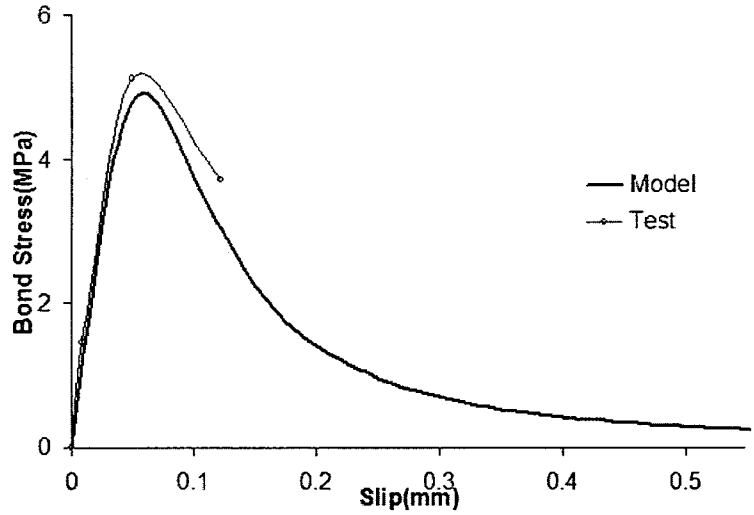

(h) Specimen with brick substrate(f=20MPa, n_p=1, b_p=40mm, L=80mm)

Fig. 4.26. Test bond slip in different points and suggested bond-slip model for specimens applied to effective bond length

4.4.6. Comparisons with previous experimental data and analytical models

A thorough literature review was conducted, as reported in Chapter 2, to find the available experimental data generated by previous researchers. Over 100 research publications were studies to collect as much test data as possible. The majority of test data in the literature was reported from pull-out tests in the form of ultimate force capacity. Few experimental results are available in the literature for slip and maximum bond stress values. This was attributed to the wide scatter of test data typically obtained from the types of tests conducted in the area. The majority of researchers did not compare these test quantities with the models that they developed. A total of 31 pairs of test data could be found with results on τ_u and s_o. Fig. 4.27 compares these results reported by Nakaba et.al (2001), Chajes *et al.* (1996), Miller *et al.* (2001),Chajes *et al.* (1995), Yuan *et al.*(2004), Bizindavyi and Neale (1999), Lorenzis and Nanni 2002, Van Gemert (1980), Dai *et al.* (2005), Ferracuti *et al.* (2006), Leung and Pan (2005), and Ueda and Dai (2005) with the proposed expressions, i.e., τ_u from Eq. 4.34 and s_0 from Eq. 4.35. The comparison shows more scatter than the earlier comparisons with experimental data generated in the current investigation.

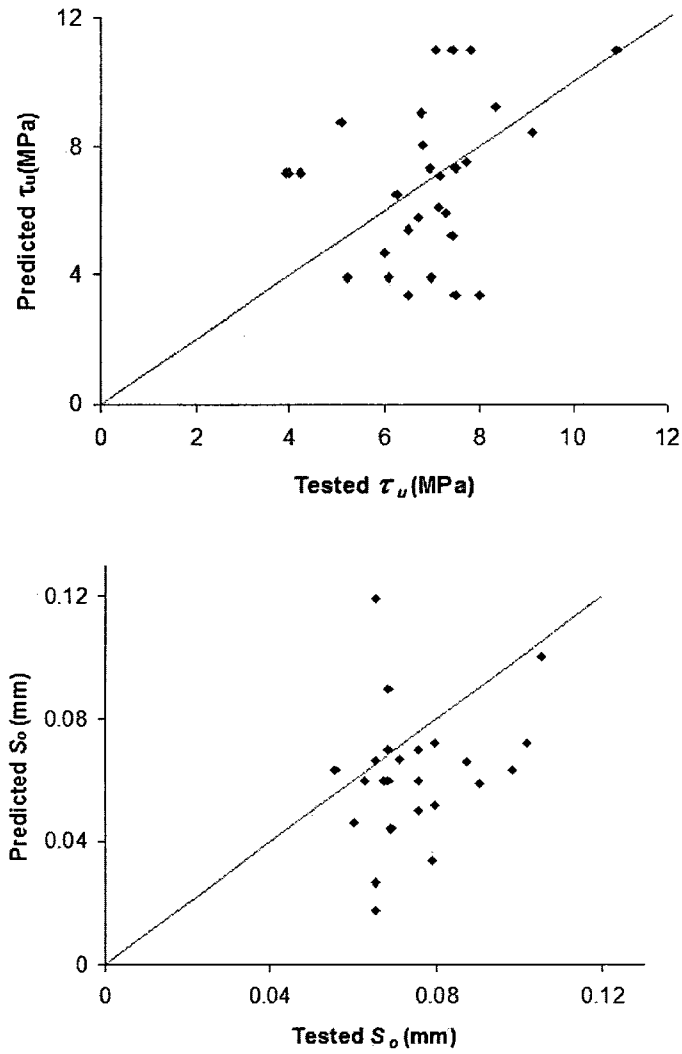

Fig. 4.27. Comparison of the model parameters including ultimate bond stress and related slip for tests reported by other researchers

The proposed model and its parameters were also compared with those suggested by others. The comparisons covered different cases with different FRP and concrete properties. Three variables were shown for: i) concrete strength, ii) number of layers of FRP and iii) width of FRP strip. A reference case was taken as 30 MPa concrete with a single layer of 100 mm wide strip, and each of these parameters were then varied one at a time. Fig. 4.28 shows the comparison of the expressions suggested for s_0. In this figure, the expression used for the proposed model is Eq. 4.35. Most of the previous researchers suggested a constant value for s_0. These constant values ranged between 0.02 and 0.12. The proposed expression has resulted in a range of values between 0.02 and 0.11

depending on other variables, as this expression incorporates the effects of other variables that were shown to play important roles during the experimental research. The proposed expression appears to provide values between the extremes predicted by other models.

The comparison for ultimate bond stresses, τ_u, is presented in Fig. 4.29. The values computed by the proposed model have resulted in values that fall between the values suggested by others, but more in line with those proposed more recently. Similar comparison is made for the fracture energy in Fig. 4.30, with similar results, where the proposed model produced energy values that fall almost half way between the two extremes predicted by previous researchers.

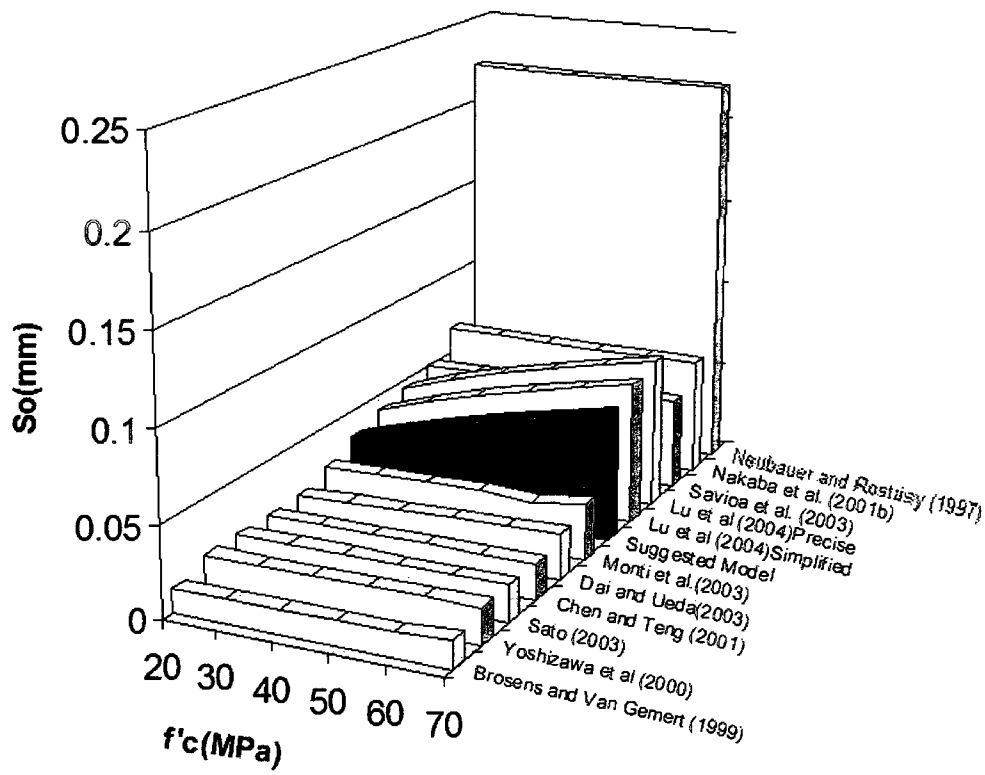

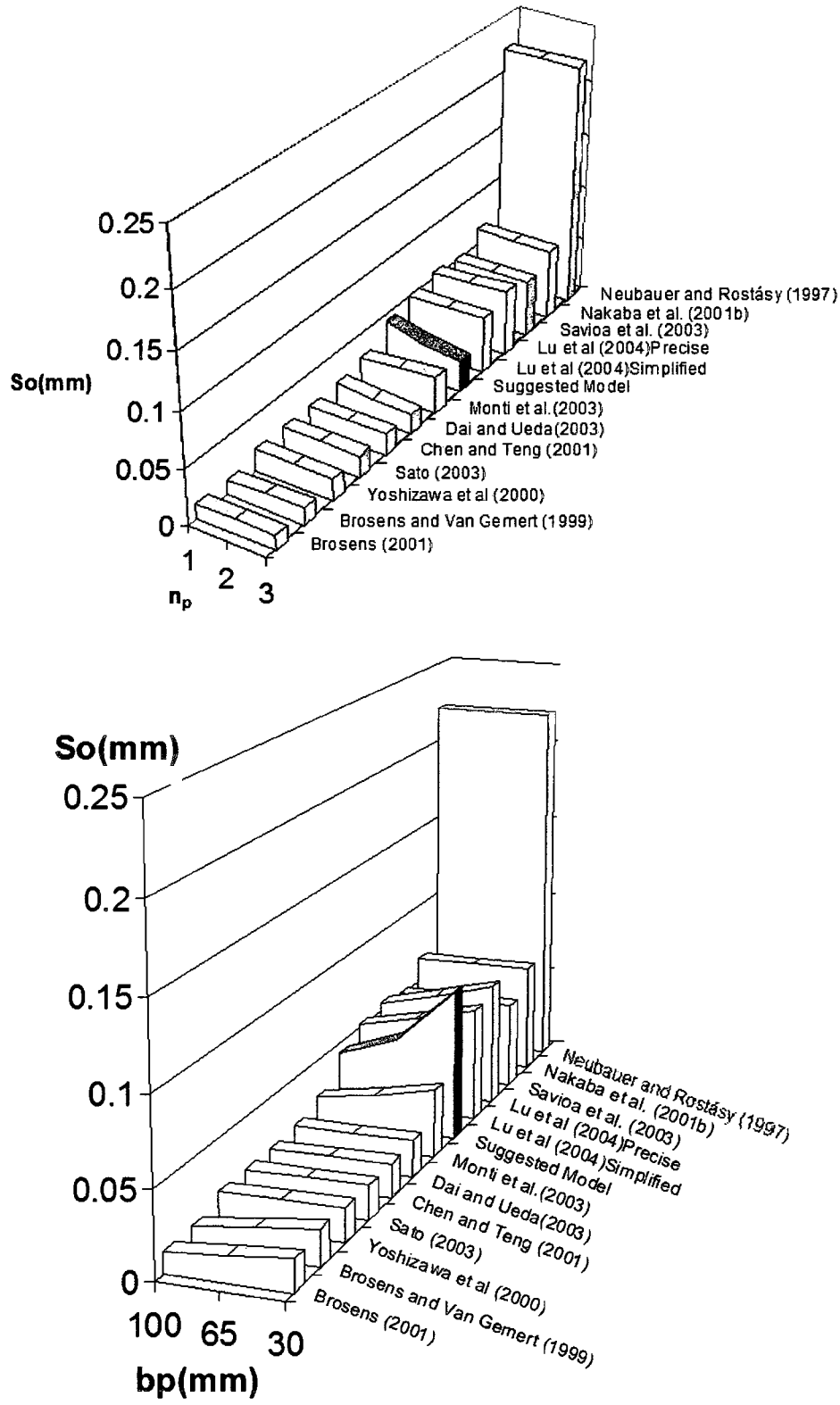

Fig. 4.28. Comparison of the s_0 expressions (b_c=150 mm, t_p=0.165 mm, E_p=228000 MPa, E_c =23650 MPa, G_a=1920 MPa, G_c =10200 MPa, f_t=2.65 MPa)

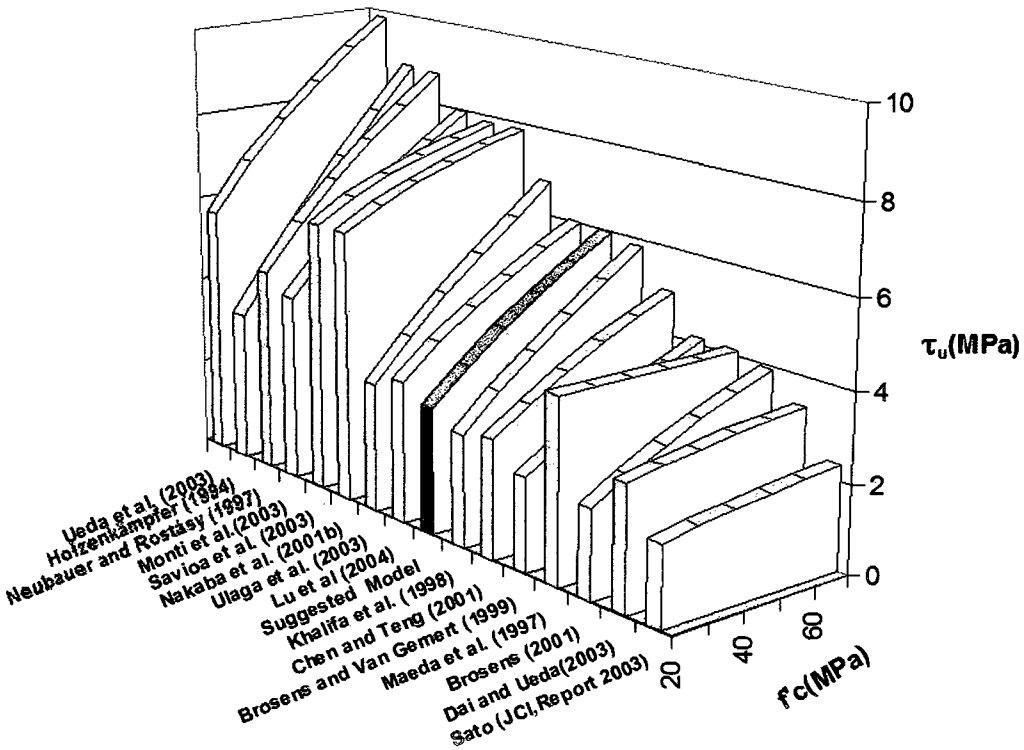
10
8
6
4
2
0
τu(MPa)
Ueda et al. (2003)
Holzenkämpfer (1994)
Neubauer and Rostasy (1997)
Monti et al.(2003)
Savioa et al. (2003)
Nakaba et al. (2001b)
Ulaga et al. (2003)
Lu et al (2004)
Suggested Model
Khalifa et al. (1998)
Chen and Teng (2001)
Brosens and Van Gemert (1999)
Maeda et al. (1997)
Brosens (2001)
Dai and Ueda(2003)
Sato (JCI,Report 2003)
20
40
60
f'c(MPa)

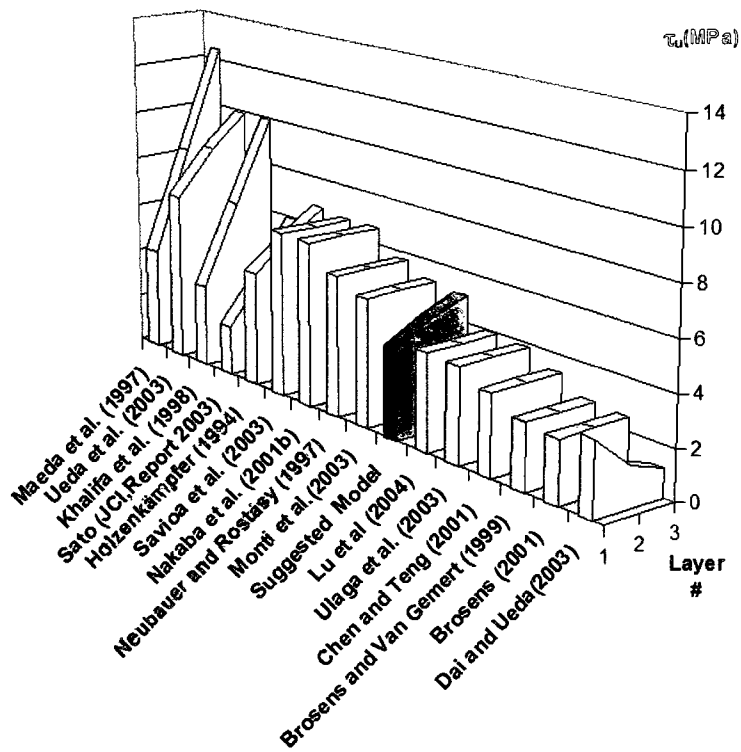
τu(MPa)
14
12
10
8
6
4
2
0
Maeda et al. (1997)
Ueda et al. (2003)
Khalifa et al. (1998)
Sato (JCI,Report 2003)
Holzenkämpfer (1994)
Savioa et al. (2003)
Nakaba et al. (2001b)
Neubauer and Rostasy (1997)
Monti et al.(2003)
Suggested Model
Lu et al (2004)
Ulaga et al. (2003)
Chen and Teng (2001)
Brosens and Van Gemert (1999)
Brosens (2001)
Dai and Ueda(2003)
1
2
3
Layer #

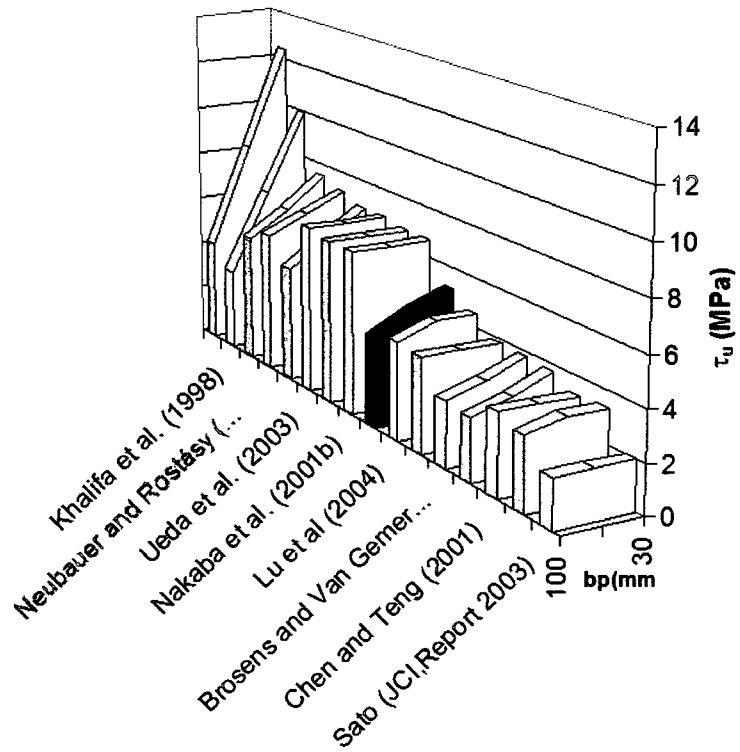

Fig. 4.29. Comparison of the τ_u expressions (b_c=150 mm, t_p=0.165 mm, E_p=228000 MPa, E_c =23650 MPa, G_a=1920 MPa, G_c =10200 MPa, f_t=2.65 MPa)

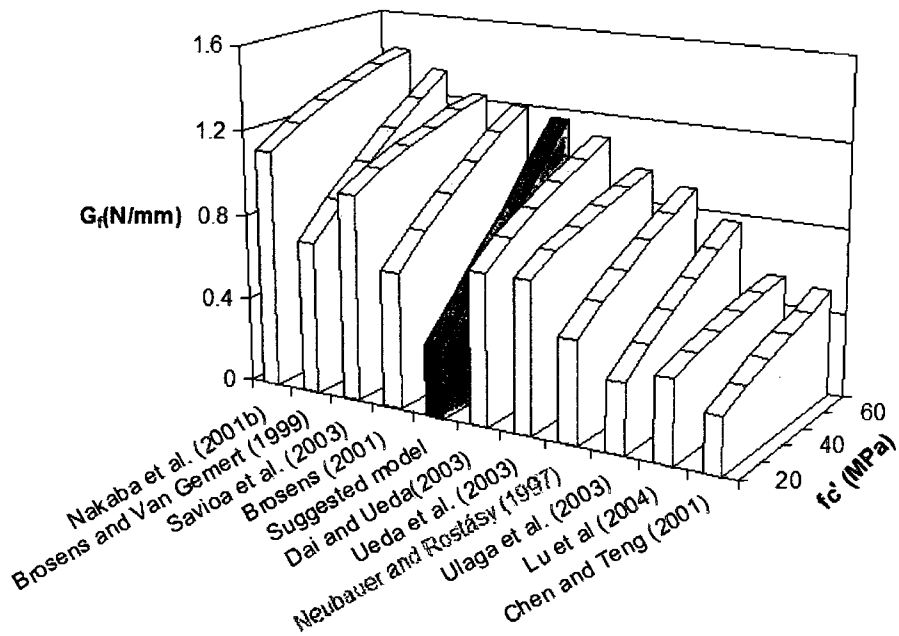

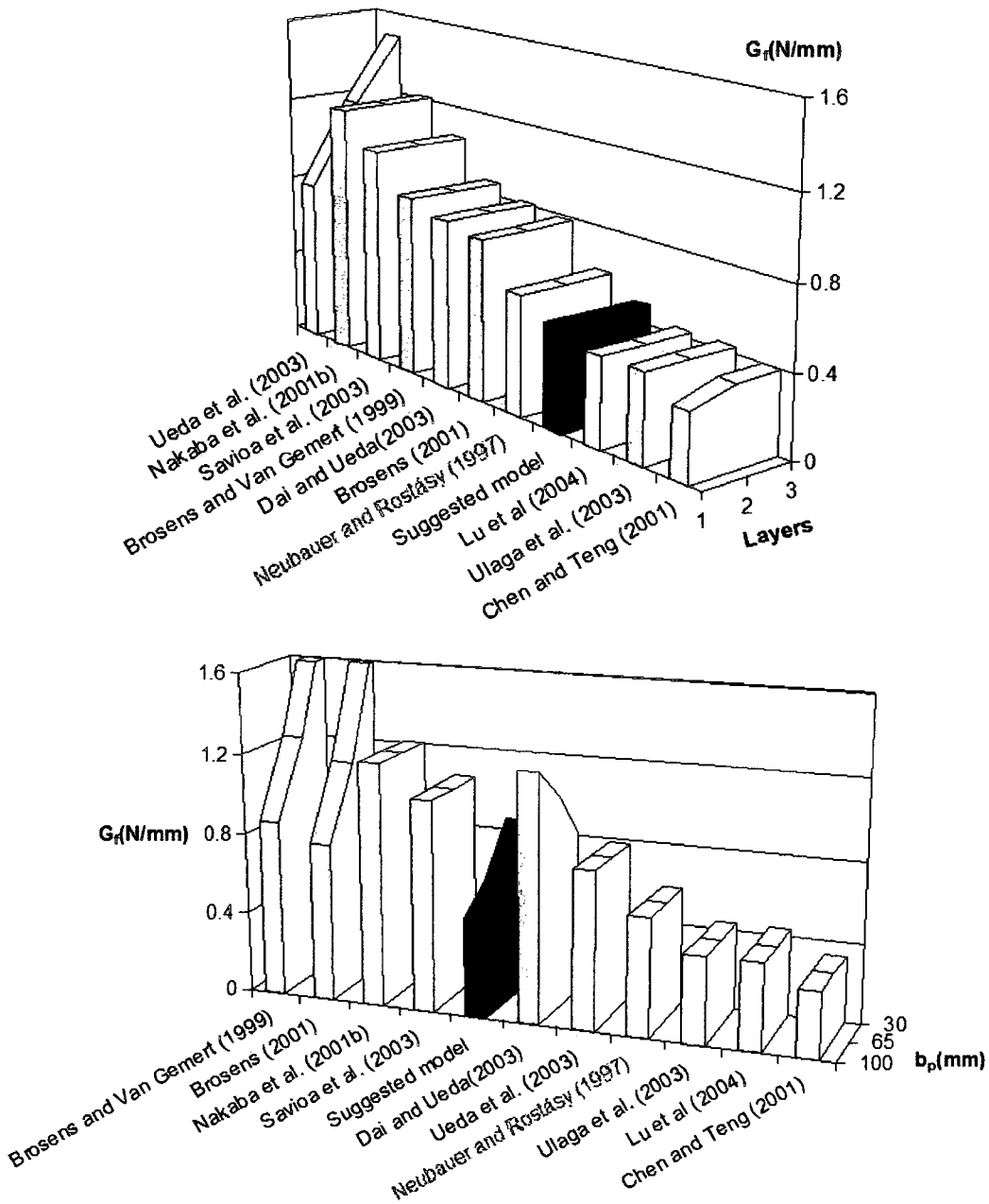

Fig. 4.30. Comparison of the G_f expressions (b_c=150 mm, t_p=0.165 mm, E_p=228000 MPa, E_c =23650 MPa, G_a=1920 MPa, G_c =10200 MPa, f_t=2.65 MPa)

The proposed model is also compared with others in its entirety. This permits the comparison of the shapes of bond-slip relationship. Some of the previous researchers also

used the Popovics' curve that was adopted in the proposed model. The coefficient "n" that defines the curve was taken as a constant value by all of the previous researchers. The majority used a value of n = 3. The proposed model, on the other hand, expressed "n" as a function of FRP strip width, as this was observed to play a significant role on the shape of the bond-slip model. This value varied between 3.87 and 1.97 for strip widths of 50 mm to 250 mm. The comparisons are made in Fig. 4.31 for a combination of three parameters, i.e., concrete strength, number of FRP layers and strip width. As can be seen in the figure, the proposed model falls in between those suggested earlier by others.

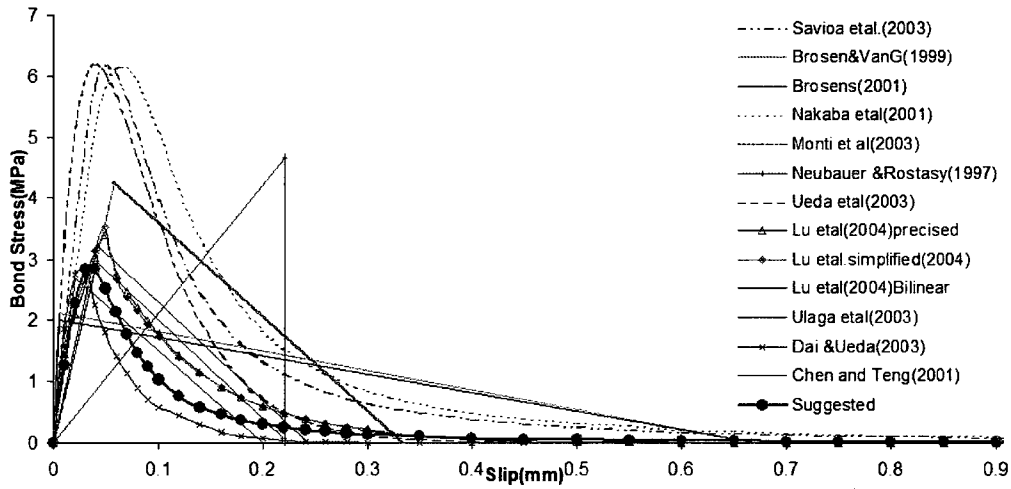

(a) n_p=1, b_p=100mm, f'_c=**20 MPa**, f_t=2.37 MPa, E_c =21150 MPa , G_c =9120 MPa

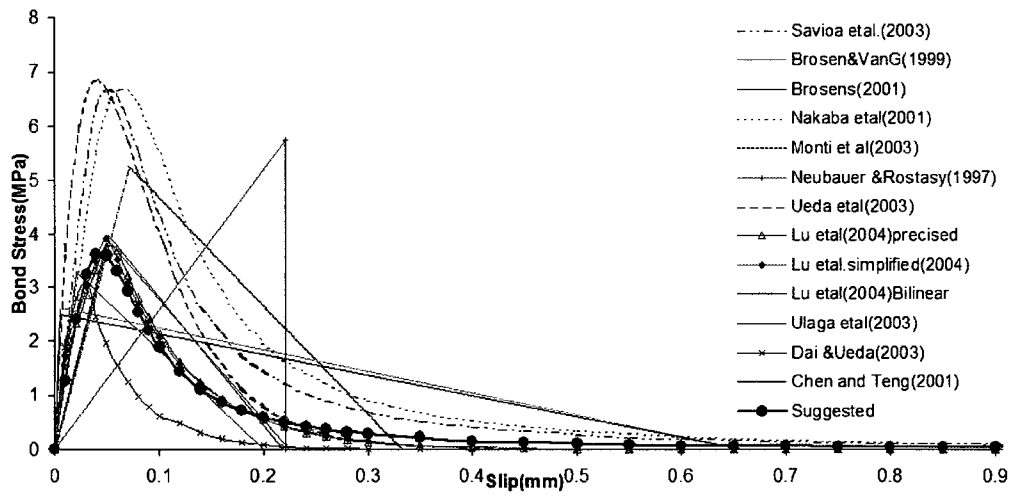

(b) n_p=1, b_p=100mm, f'_c=**30 MPa**, , f_t=2.90 MPa, E_c =25900 MPa, G_c =11150 MPa

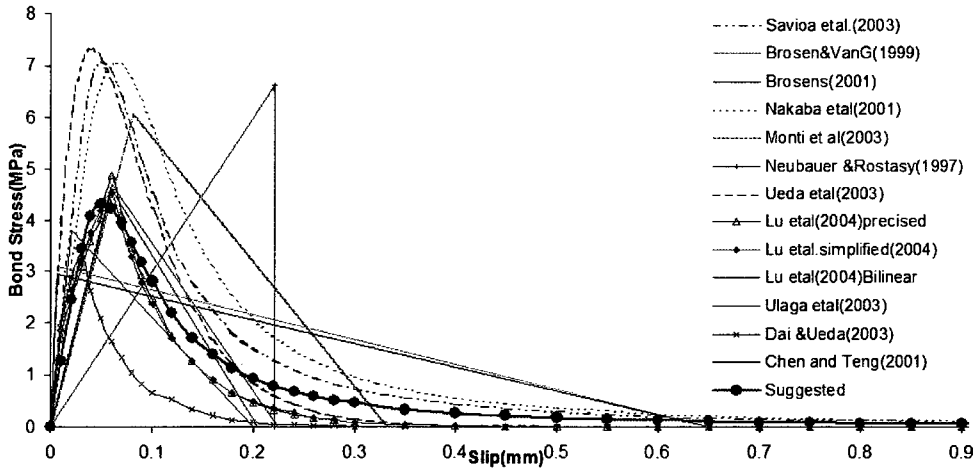

(c) n_p=1, b_p=100mm, $\boldsymbol{f'_c}$**=40 MPa**, f_t=3.35 MPa, E_c =29900 MPa, G_c =12900 MPa

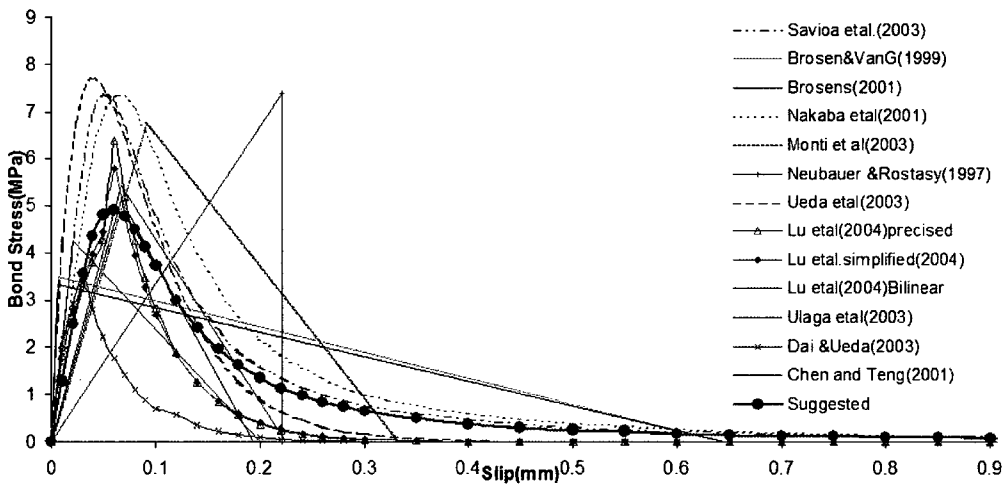

(d) n_p=1, b_p=100mm, $\boldsymbol{f'_c}$**=50 MPa**, f_t=3.75 MPa, E_c =33450 MPa, G_c =14400 MPa

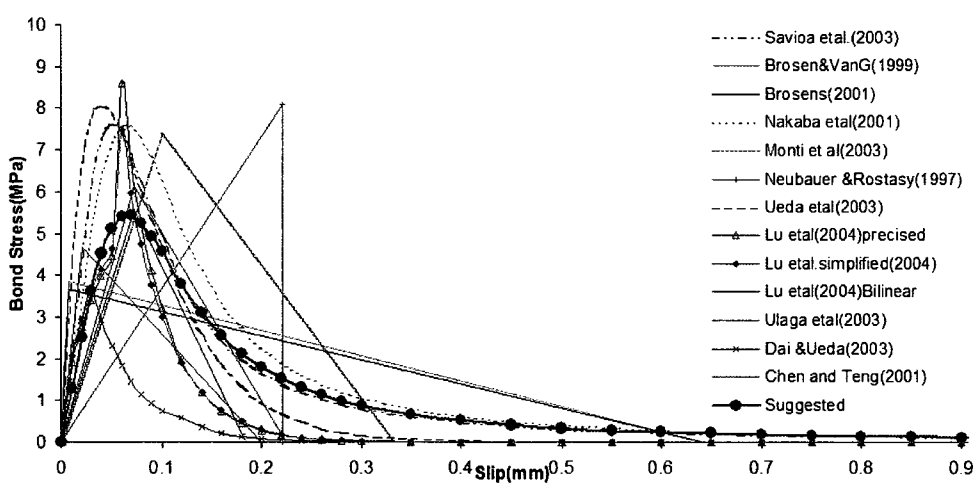

(e) n_p=1, b_p=100mm, $\boldsymbol{f'_c}$**=60 MPa**, f_t=4.1 MPa, E_c =36650 MPa, G_c =15800 MPa

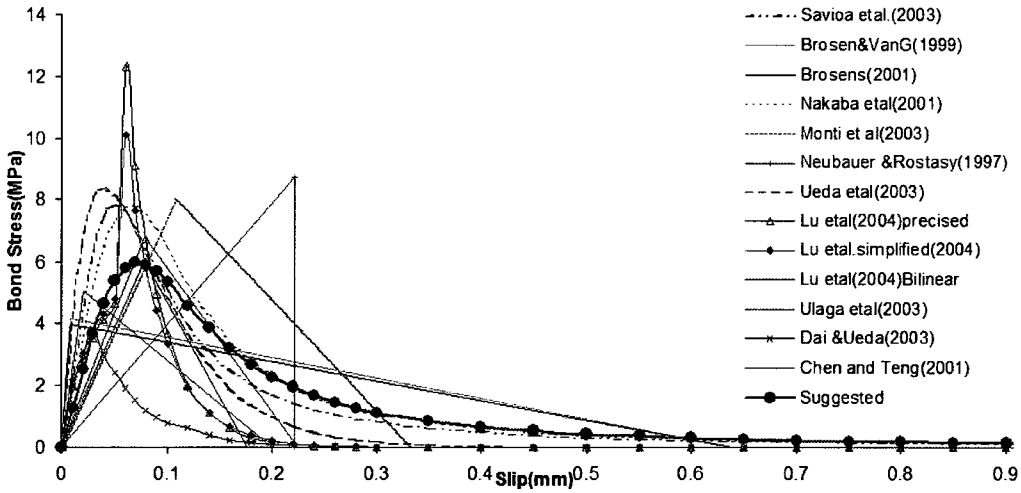

(f) n_p=1, b_p=100mm, ***f'c*=70 MPa**, f_t=4.43 MPa, E_c =39600 MPa, G_c =17050 MPa

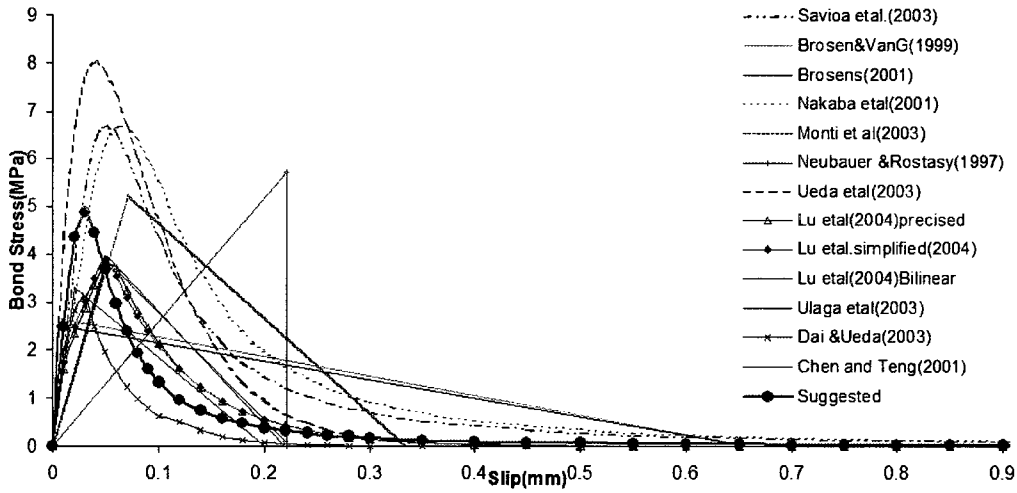

(g) ***n*p=2**, b_p=100mm, f'_c=30 MPa, , f_t=2.90 MPa, E_c =25900 MPa, G_c =11150 MPa

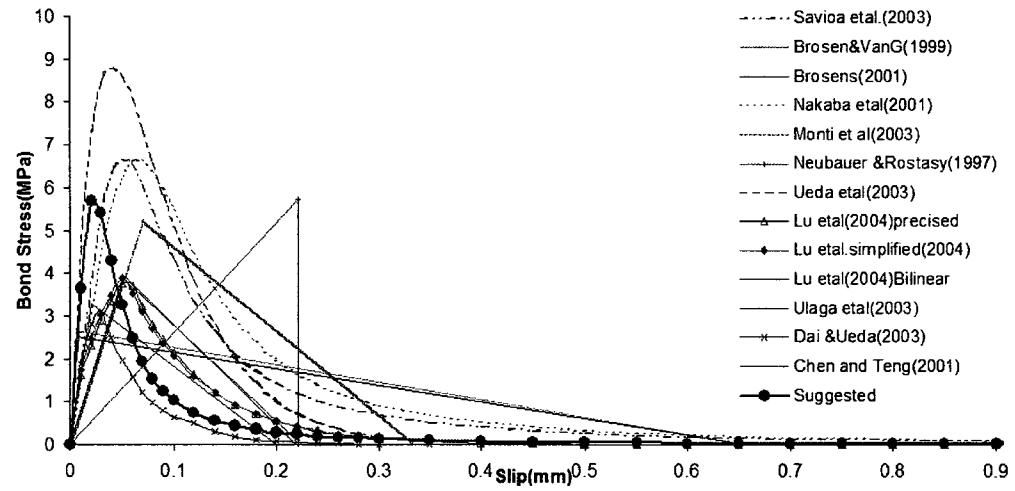

(h) ***n*p=3** b_p=100mm, f'_c=30 MPa, , f_t=2.90 MPa, E_c =25900 MPa, G_c =11150 MPa

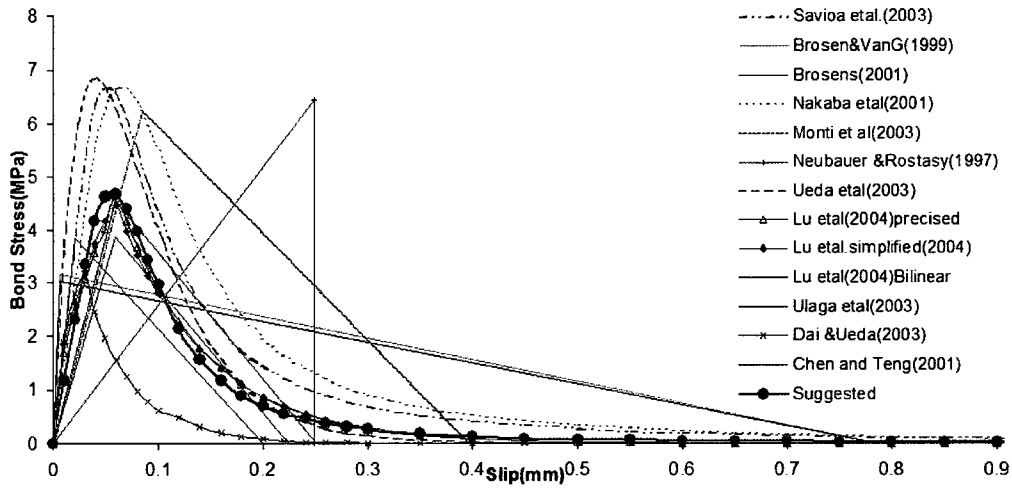

(i) n_p=1, $\boldsymbol{b_p}$**=65mm**, f'_c=30 MPa, , f_t=2.90 MPa, E_c =25900 MPa, G_c =11150 MPa

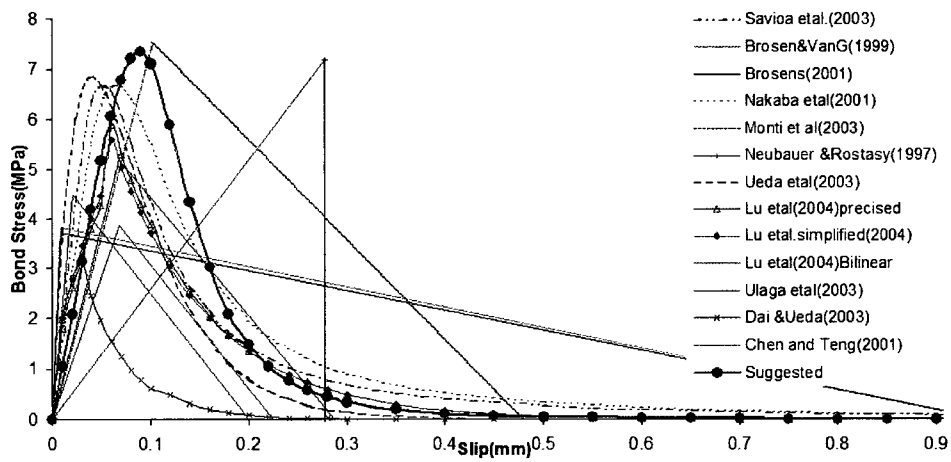

(j) n_p=1, $\boldsymbol{b_p}$**=30mm**, f'_c=30 MPa, , f_t=2.90 MPa, E_c =25900 MPa, G_c =11150 MPa

Fig. 4.31. Comparison of bond slip models (b_c=150 mm, t_p=0.165 mm, E_p=228000 MPa, and G_a=1920 MPa)

4.5. Development of a Design Procedure for Surface Bonded FRP

Designing surface bonded FRP on concrete and masonry substrates involves the computation of strength as expressed in the form of direct tensile force capacity of FRP strip, required bond length, and possibly the deformation of FRP in the form of extension and slippage. The bond-slip model developed above serves as a fundamental tool to allow

the computation of the slip of surface bonded FRP sheets. The ultimate capacity P_u and the required bond length (expressed in terms of effective bond length) can be established from the experimental data. Expressions are developed for the latter two design parameters, i.e., P_u and L_e, in the following sections.

4.5.1. Effective bond length

Effective bond length is defined as length of FRP beyond which the ultimate load does not increase significantly, even if more of it is provided. Fig. 4.32 shows schematically the commonly observed tensile force-bond length relationship. As the Figure illustrates, a certain bond length is necessary to develop the maximum tensile capacity indicated by P_u. This length is defined as the "effective bond length of FRP." The effective length was established by plotting experimentally obtained ultimate tensile forces against bond length. The point at which the rate of change in ultimate force resistance has decreased significantly is taken as the effective bond length. This length can also be established from the strain gauge data. This was done here as confirmation of the former approach. Fig. 4.13 illustrates the relationship of longitudinal strains, bond and the effective length.

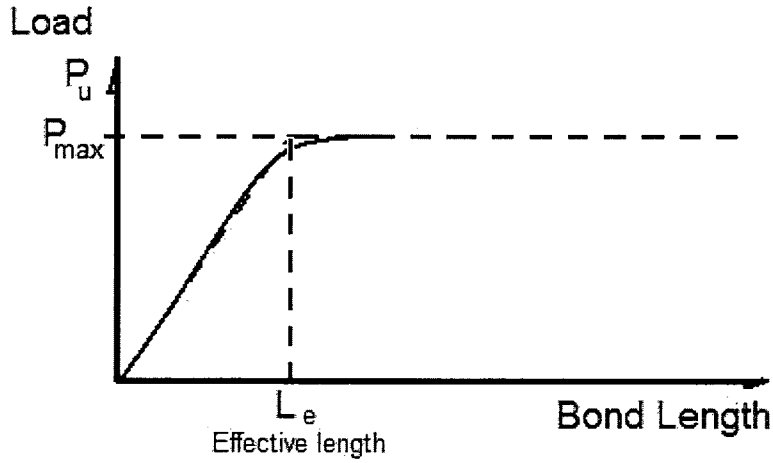

Fig. 4.32. Idealized tensile force-bond length relationship

It was demonstrated in Section 4.2 that, of all the test variables considered, the most significant two parameters that affected the effective length were, i) number of FRP layers (thickness), and ii) nature of loading (monotonic versus cyclic). The rate of change

in effective length with these parameters was also established in the same section. Fig. 4.33 shows a plot of these variables against effective length, and the derivation of the expression for effective bond length. This expression is given below. Eq. 4.44 and Fig. 4.33 indicate that the effective bond length varies between 90 and 115 mm for the test specimens considered in this investigation.

$$L_e = 8.c.(n_p.t_p.E_p)^{0.23} \tag{4.44}$$

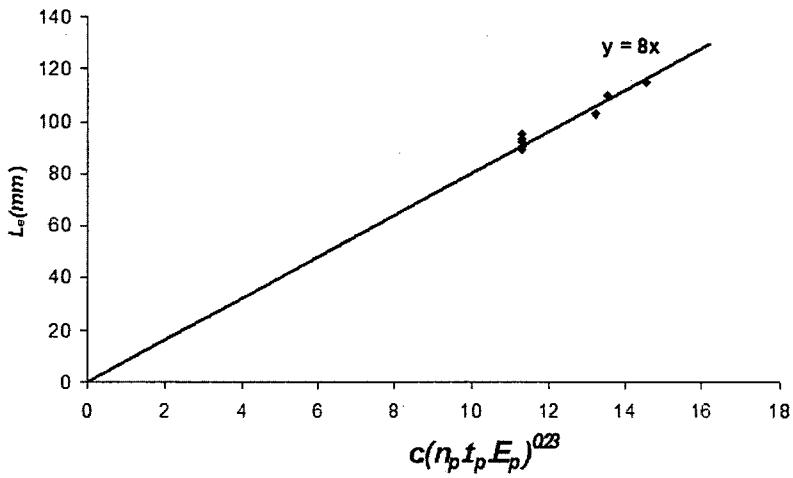

Fig. 4.33. Effective length versus related variables

The above expression provides an estimate for the effective length, based on the assumption that there is no increase in ultimate load capacity when the bond length increases beyond the effective length. However, though this assumption may be used as a lower-bound approach, the test results did show a small increase in ultimate load capacity with increasing bond length, as illustrated in Fig. 4.34. This was attributed to the contribution of friction forces that develop within the effective length beyond the formation of surface cracking. As the bond length increases, the resistance provided by friction in regions where maximum bond stress has been exceeded and hence substantial slippage has already taken place, contributes to the increase in ultimate load resistance while improving the ductility of the failure mechanism. To capture this phenomenon, the relationship between the ultimate load and bond length for all specimens tested in the current investigation was investigated. After many trials, the following best-fit relationship was found to represent the trend between P_u and L_b.

$$P_u \propto [1-exp(-0.02L_b)] \quad (4.45)$$

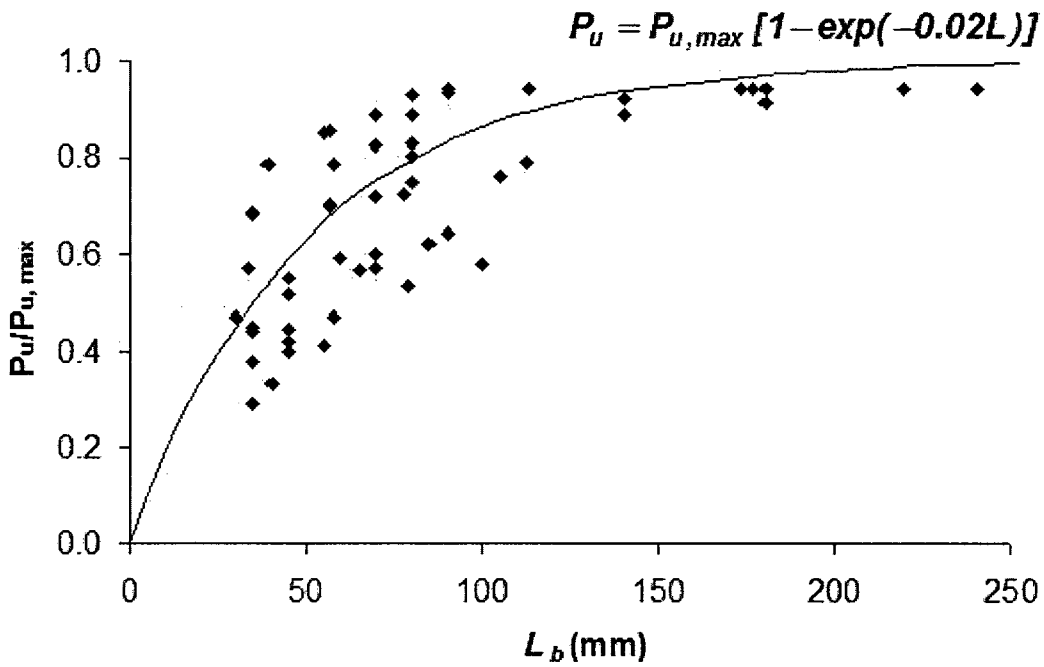

Fig. 4.34. Tensile force-bond length relationship

For a specific case, with constant test parameters, Eq. 4.45 can also be written in the following form.

$$P_u = P_{u,max}[1-exp(-0.02L_b)] \quad (4.46)$$

$P_{u,max}$ in the above expression is the maximum ultimate load that can be attained. This quantity is theoretically obtained when the bond length L_b approaches infinity and the slope of the relationship given in Eq. 4.46 becomes zero. Designing FRP for this theoretical maximum load for very little increase in capacity is obviously not warranted. It was found that the use of $2L_e$ in place of L_b, for the range of effective length values obtained in the experimental investigation (90 mm to 115 mm), leads to a design bond length that ranges between 97% and 99% of the theoretical $P_{u,max}$., as illustrated in Fig. 4.35. This length (2Le) is recommended for use in design, with the following design expression for effective bond length.

$$L_{e-design} = 2.L_e = 16.c.(n_p.t_p.E_p)^{0.23} \quad (4.47)$$

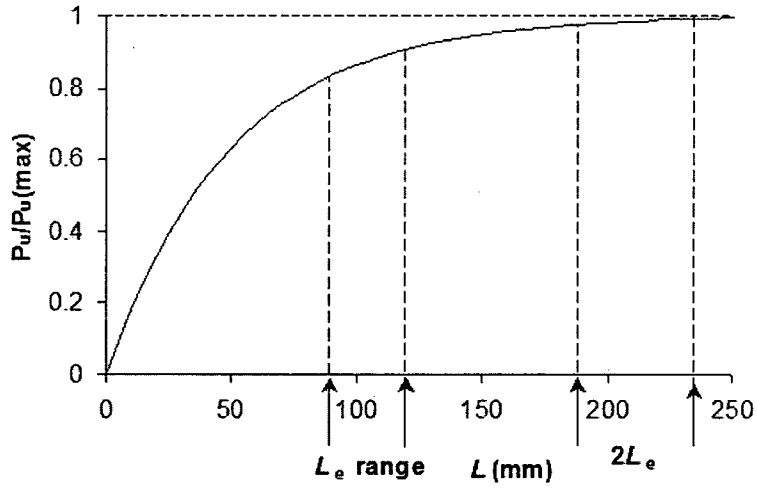

Fig. 4.35. Idealized relationship between ultimate load and bond length

4.5.2. Ultimate capacity

The relationship between test variables and ultimate load capacity P_u was established earlier in Section 4.2. The effect of bond length on P_u was discussed in the preceding section. Combining these parameters for the test data, results in Fig. 4.36, which leads to an expression between design variables and ultimate load capacity P_u.

$$P_u = 4.2 \times c \times f'^{0.58}_c (n_p t_p E_p b_p)^{0.42} [1 - exp(-0.02 L_b)] \quad (4.48)$$

Where; c = 1.0 for monotonic loading and 1.2 for cyclic loading; f'_c is concrete cylinder strength in MPa; n_p, t_p, b_p, E_p and L_b are the number of layers, thickness per layer, strip width, modulus of elasticity, and, bond length of FRP respectively, expressed in units of mm and Newton.

Eq. 4.48 can be expressed in terms of ultimate normal stress that corresponds to bond capacity, by dividing P_u by the area of FRP strip. This is shown below.

$$\sigma_u = 4.2 \times c \times \left(\frac{f'_c}{n_p t_p b_p} \right)^{0.58} (E_p)^{0.42} [1 - exp(-0.02 L_b)] \leq f_p \quad (4.50)$$

While f_p is the tensile strength of FRP sheet.

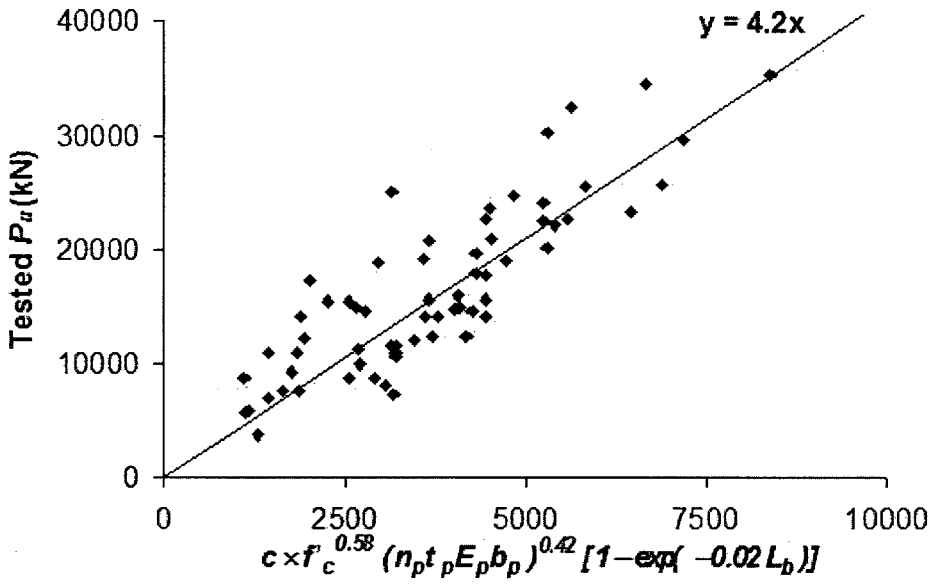

Fig. 4.36. Relationship between ultimate load and related variables

4.5.3. Verification of the design expressions

The expression for the effective length of FRP was compared with experimental data earlier in Fig. 4.33, and shows good correlations. The ultimate load expression given in Eq. 4.48 is used to compare analytical and experimental strength values in Fig. 4.37. The correlation between the two is also good, with a coeficient of variation of 19% for 64 specimens.

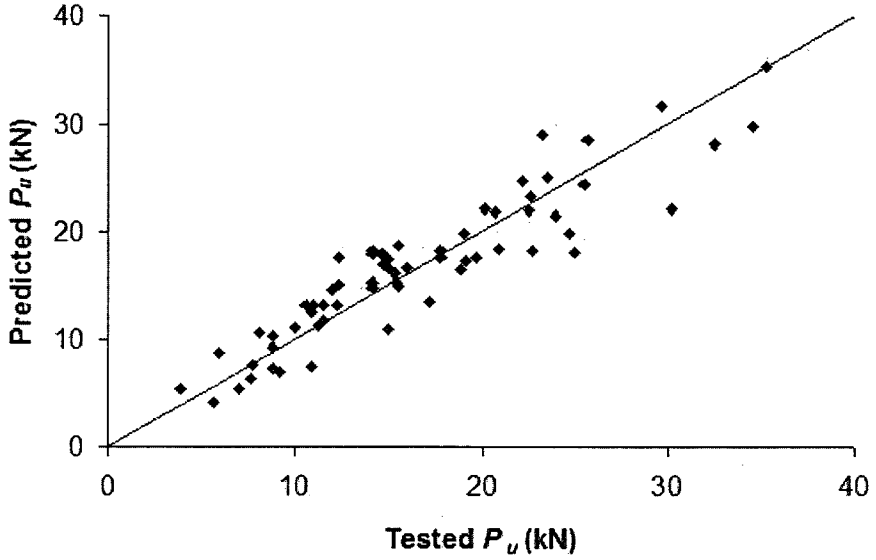

Fig. 4.37. Ultimate load test versus the predicted results

4.5.4. Comparisons with previous test data and recommendations

The test data reported by previous investigators are used in this section to compare against the analytical expressions derived for effective length and the ultimate load. The experimental data for effective length comparison consists of 46 tests reported by Maeda *et al.* (1997), Bizindavyi and Neale (1999), Täljsten (1997), Dai *et al.* (2006), Kamel et.al (2004), Wu *et al.* (2003), Ueda *et al.*(1999), Tan(2002). Fig. 4.38 presents the comparison between the experimental and analytically computed values. Both the effective length L_e and the design effective length ($L_{e\text{-design}} = 2L_e$) are used for the comparison. The results show a significant scatter of data. Though the average of the effective length is only 2% more than that computed based on the suggested expression, the coefficient of variation of tested/predicted is 57%. This can be explained by the subjective nature of selecting the effective length from test data and the nature of different types of tests conducted. Others have reported similarly wide scatters of test data in comparing with analytically computed effective lengths.

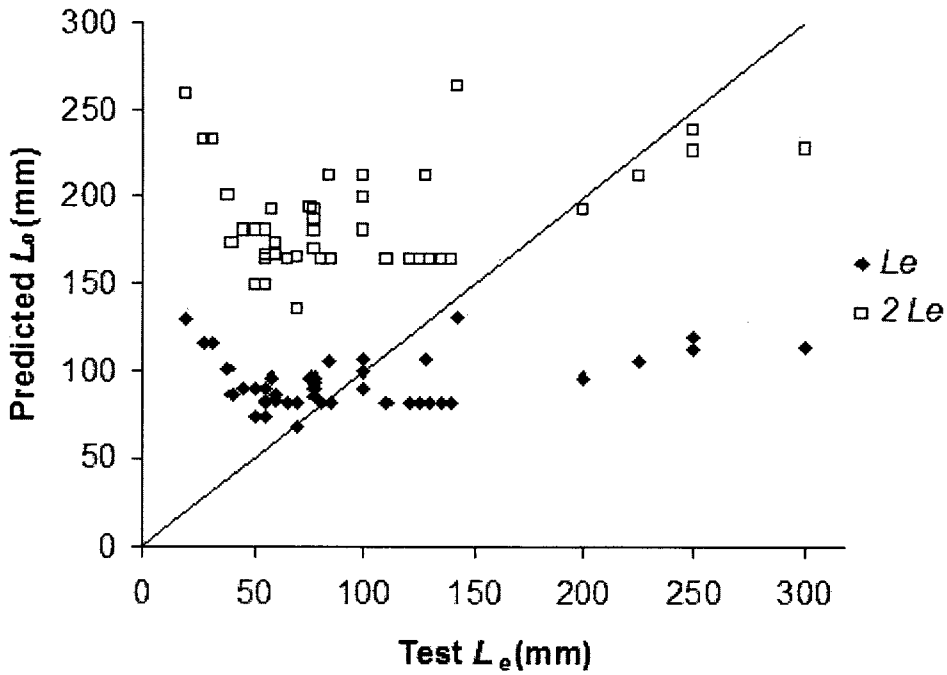

Fig. 4.38. Effective length predicted versus others' test

The expression suggested for ultimate load (Eq. 4.47) is also verified against test data reported by others. A total of 235 test data reported by Bizindavyi and Neale (1999), Chajes *et al.* (1996), Maeda *et al.* (1997), Ren (2003), Tan(2002), Takeo *et al.* (1997),

Ueda *et al.* (1999), Wu *et al.* (2001), Wu *et al.* (2002), Yuan *et al.* (2004), Zhao *et al.* (2000), Nakaba et.al (2001), Miller *et al.* (2001), Lorenzis and Nanni (2002), Dai *et al.* (2005), Ferracuti *et al.* (2006), Leung and Pan (2005), and Ueda and Dai (2005), involving CFRP and GFRP strips were used for this purpose. This is shown in Fig. 4.39. The results indicate good correlations, even with GFRP strips, though the analytical expression was developed for CFRP. The average of computed values is about 8% higher than that of test results. The coeficient of variation of test values over computed ultimate load values is about 32%.

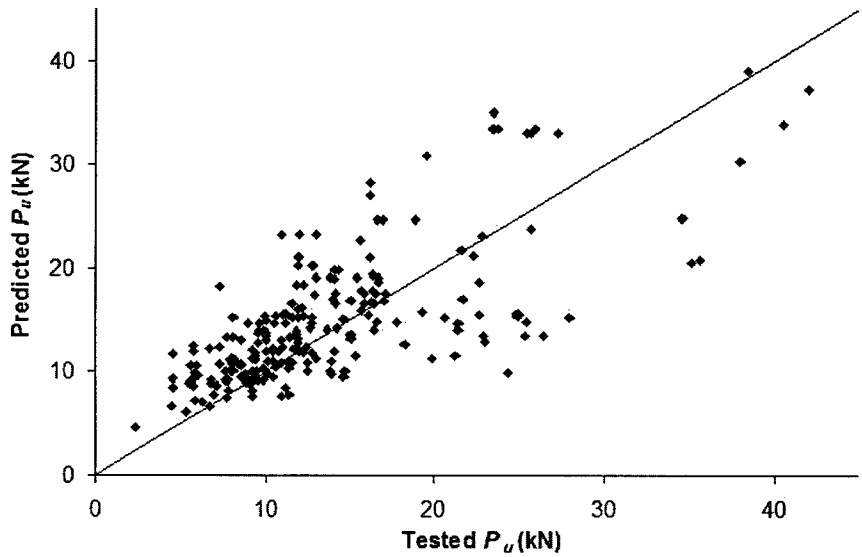

Fig. 4.39 Correlation of suggested with experimental data obtained by others

The comparisons for computed effective length and ultimate load capacity are extended to include analytical expressions suggested by other researchers. The comparison for effective length is shown in Fig. 4.40. Of particular importance is the model suggested by Maeda *et al.* (1997), which forms the basis for the design expressions that appear in ACI 440 (2008) and CSA S806 (2002) design guidelines. These design expressions include the number of FRP layers, representing thickness and stiffness of FRP, in the denominator, unlike the expression suggested in the current research program, as well as those suggested more recently by others. The comparisons between analytical expressions suggested by previous researchers and the current research are shown in Fig. 4.41 for ultimate load. The results indicate that the value computed by the suggested expression provides an average value of the computed values by other expressions.

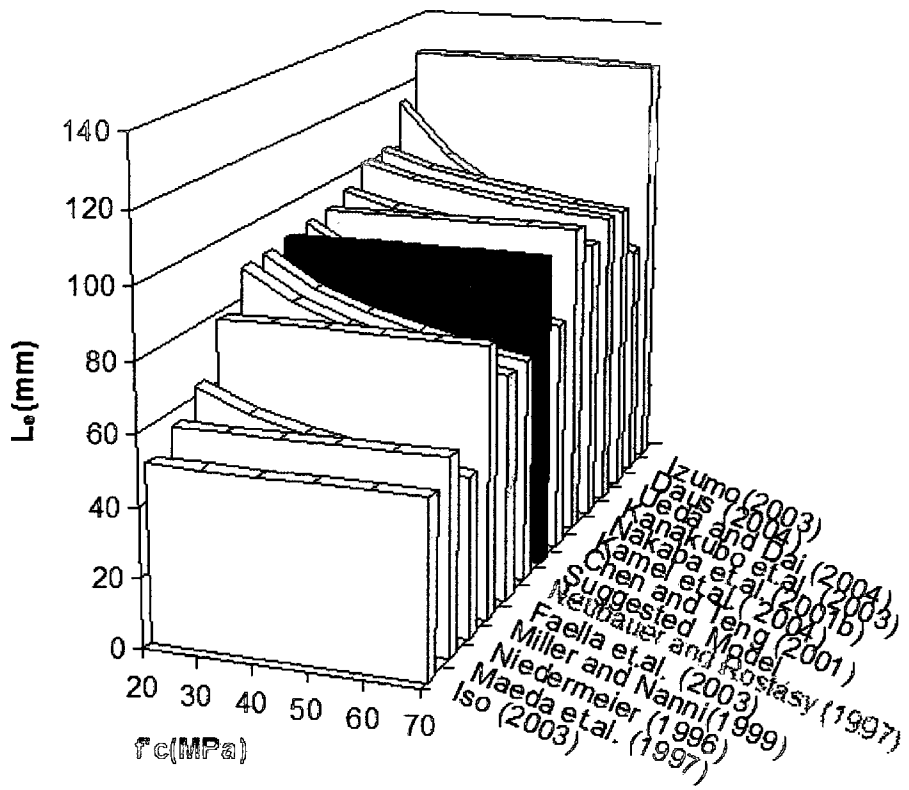
Le(mm)
140
120
100
80
60
40
20
0
20 30 40 50 60 70
f'c(MPa)
Izumo(2003)
Daus (2004)
Ueda and Dai (2004)
Kanakubo et.al (2003)
Nakaba et.al.(2001b)
Kamel et.al. (2004)
Chen and Teng (2001)
Suggested Model
Neubauer and Rostasy (1997)
Faella et.al. (2003)
Miller and Nanni(1999)
Niedermeier (1996)
Maeda et.al. (1997)
Iso (2003)

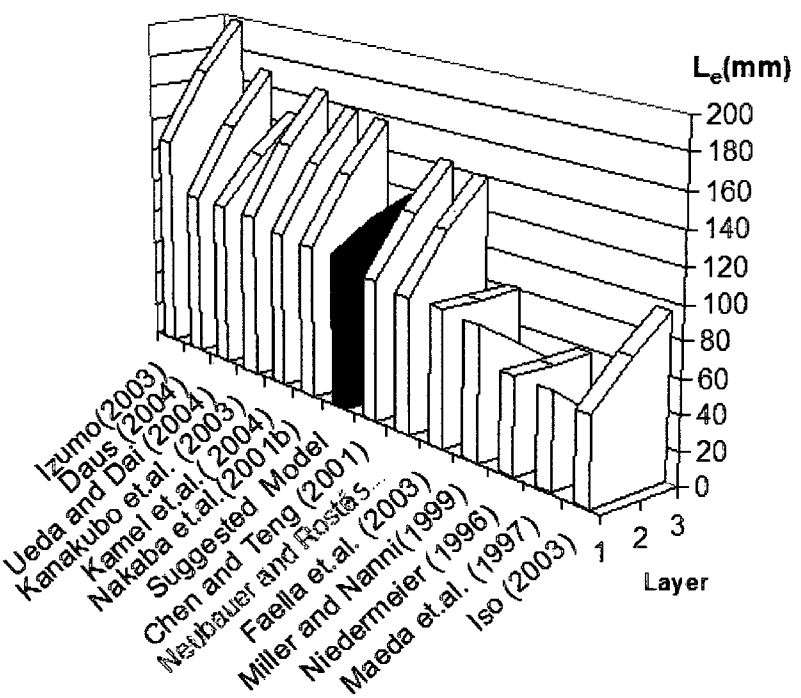
Le(mm)
200
180
160
140
120
100
80
60
40
20
0
1 2 3
Layer
Izumo(2003)
Daus (2004)
Ueda and Dai (2004)
Kanakubo et.al. (2003)
Kamel et.al.(2004)
Nakaba et.al.(2001b)
Suggested Model
Chen and Teng (2001)
Neubauer and Rostas...
Faella et.al. (2003)
Miller and Nanni(1999)
Niedermeier (1996)
Maeda et.al. (1997)
Iso (2003)

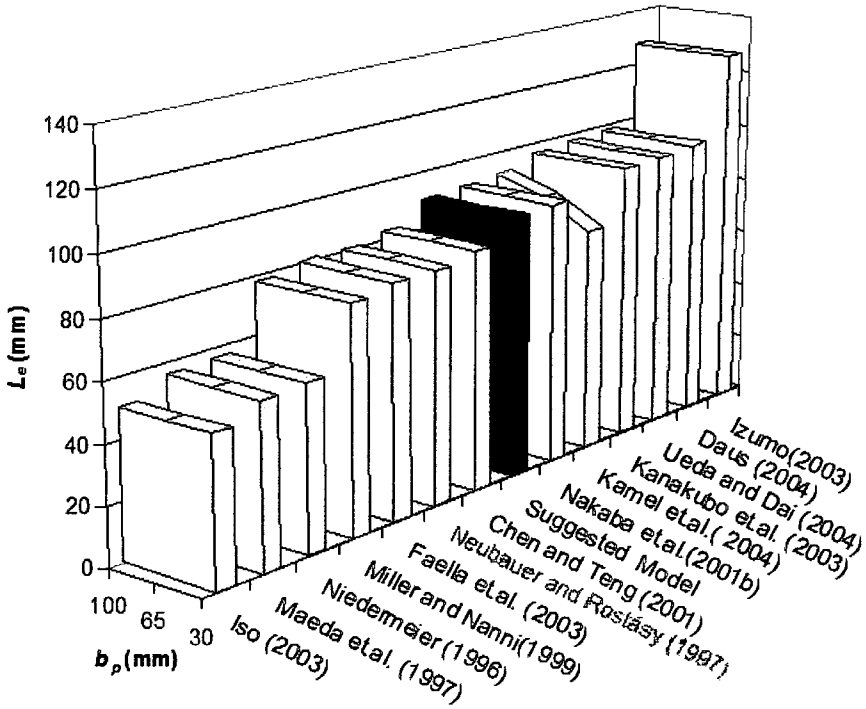

Fig. 4.40. Suggested L_e in the literature (b_c=150 mm, t_p=0.165 mm, n_p=1, E_p=228000 MPa, G_a=1920 MPa)

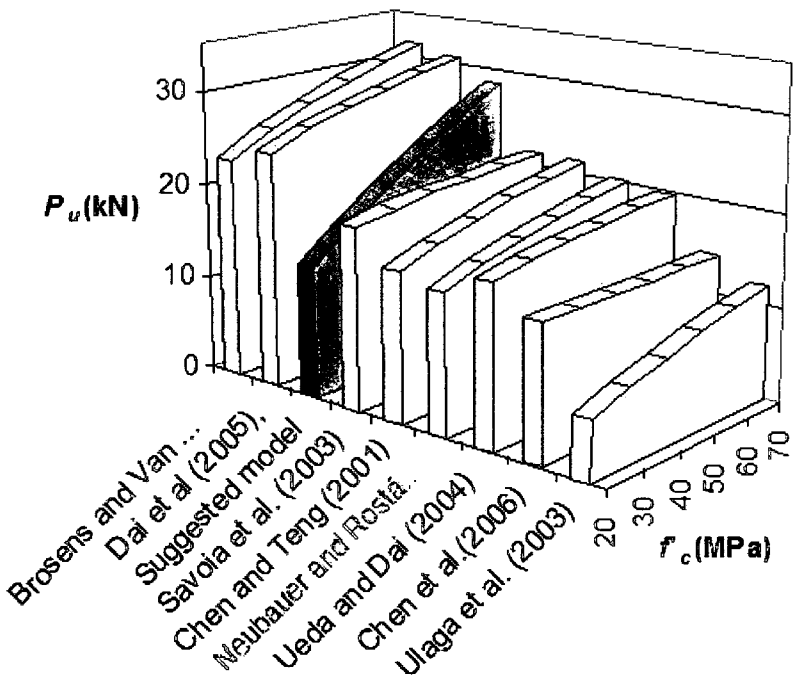

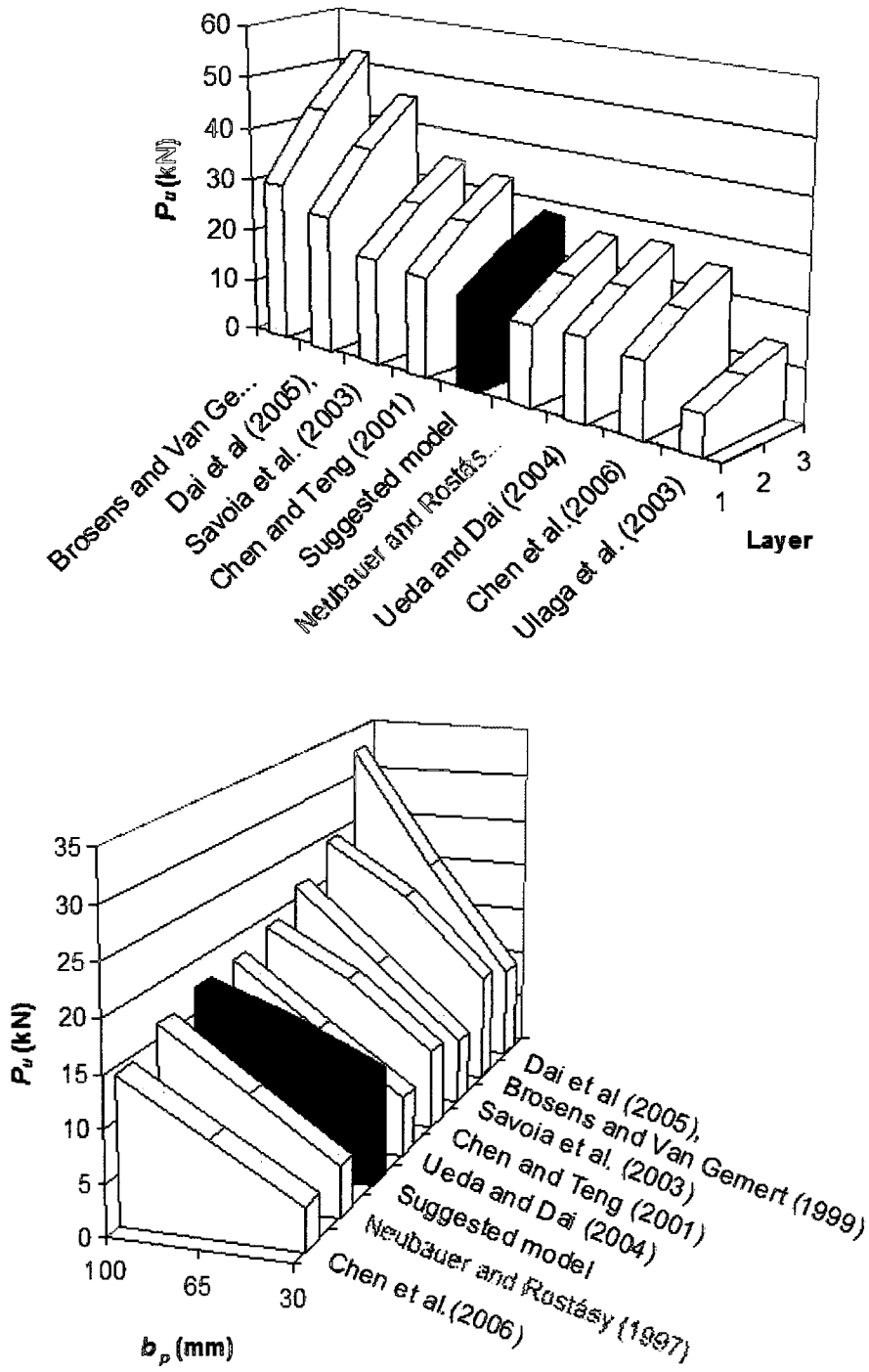

Fig. 4.41. Suggested P_u in the literature (b_c=150 mm, t_p=0.165 mm, n_p=1, E_p=228000 MPa, G_a=1920 MPa)

Chapter 5

SUMMARY AND CONCLUSION

The research program and its findings are summarized in this Chapter. Both experimental and analytical research is included, with relevant conclusions drawn from the entire research program. Where appropriate, the information gathered from the comprehensive literature review conducted is incorporated in arriving some of the conclusions.

5.1. Summary

Surface bond characteristics of FRP sheets on concrete and masonry substrates is not well established. The current research was undertaken to contribute towards the knowledge gap in the area. The research program consists of both experimental and analytical tasks. An extensive literature review was conducted as the first task. Over 125 technical literatures were scrutinized to assess the state of the art in the field and the research needs before the experimental program and the analytical approach were established.

The experimental research consisted of seventy-one small-scale test specimens to undertake pull-out surface bond tests. The test variables included, the width, length, and the number of layers of CFRP strips; concrete compressive strength; substrate material consisting of concrete, brick and concrete blocks; and loading conditions as monotonic

and cyclic loading. The test program was categorized into 12 series. Each series of test specimens had identical properties with different bond length. Each series was designed and prepared after testing the previous series of specimens. A number of different test setup were used, including the setup suggested by CSA S806 (2002) and the setup developed as part of the current investigation with U-shaped FRP strips. The latter setup proved to produce consistent results, and it is recommended for future tests.

The cross-sectional dimension of square concrete specimens was 150 mm. Each specimen consisted of two halves, attached by CFRP strips. The specimen length varied between 300 mm and 600 mm. The FRP strip with changed between 30 mm to 100 mm and the bond length changed between 30 mm to 240 mm. The majority of specimens had a single layer of FRP but some had two and three layers. The concrete strength varied between 30 MP and 76 MPa. The tests were conducted under slowly increasing monotonic loading, using Galdabini universal testing machine. The FRP strips were instrumented with strain gauges. The force and displacement in the longitudinal direction were measured at different time intervals during testing until failure occurred.

The test results were plotted in terms of force-displacement relationships, as well as ultimate strength versus bond length. Strain gauge data was also plotted to compute surface bond stress and slippage of FRP on the substrate. The test data provided invaluable information for illustrating the effects of test variables, as well as for the development of an analytical bond-slip model and design expressions. The experimental data was used to generate and validate a new bond-slip model. Design expressions, in terms effective bond length and ultimate load capacity were derived from experimental data. Comparisons were made between the analytical results and experimental and analytical data reported in the literature.

5.2. Conclusions

The following conclusions can be drawn from the combined experimental and analytical research reported in this thesis:

- Surface bonded FRP strips on concrete and masonry substrates develop limited strength, as governed by bond failure. The bond stress on the interface shows a bell-

shaped distribution spread over an effective bond length with a maximum bond stress that varies between 3.0 MPa and 7.0 MPa for the type of specimens considered in the current investigations, depending on the parameters of bond.

- The surface bonded FRP has an effective length beyond which any further increase in bond length does not result in substantial increase in bond strength. This length was determined to vary between 90 mm and 115 mm for the specimens tested in this investigation.
- The effect of increased concrete strength on surface bond characteristics of FRP is to increase ultimate bond capacity and corresponding slip marginally, without much influence on the effective length.
- The effect of increased number of layers of FRP is to increase ultimate bond while decreasing slippage, with a small increase in effective bond length. The significance of the number of FRP layers (or thickness) on effective bond length is in contradiction with that suggested by ACI 440 and CSA S806, both of which suggest reductions in effective bond length with increased FRP thickness.
- The effect of the increase in FRP strip width is to increase ultimate bond resistance, while decreasing ultimate bond strength and the corresponding slip, without much influence on effective bond length. The effect of strip width was found to be more pronounced than what was reported by previous researchers.
- Cyclic loading improves surface bond characteristics of FRP, increasing ultimate load resistance by approximately a factor of 1.2 while also resulting in increases in ultimate bond stress and effective bond length.
- Surface bond characteristics of FRP on concrete and clay brick substrates are similar. Concrete block masonry tends to fail prematurely due to the material failure of block cell walls prior to developing bond failures.
- The revised test setup for pull-out tests used in the current investigation with U-shaped FRP strips provides more consistent results and hence it is recommended as a standard test setup for future tests.

- The analytical bond-slip model developed as part of the current investigation provides good estimates of experimentally recorded bond behaviour.
- The design expressions developed for the computation of ultimate load capacity and the effective bond length can be used to design surface-bonded FRP applications on concrete and brick substrates. The expressions show good correlation when compared with test data.
- The ultimate load capacity continues to increase, all be it marginally, with an increase in bond length between the effective length and twice the effective length. Therefore, it is recommended to use $2L_e$ as the design effective length.

5.3. Recommendations for Future Research

The following are recommended for future research:

- Tests of longer specimens with longer bond lengths to establish the effect of bond length on ultimate force, effective bond length and the propagation of bond fracture within the bond length, with a large number of closely spaced strain gauges.
- Experimental research involving more sophisticated instrumentation, involving fibre optic sensors and image processing to better asses the bond phenomenon within the bond length.
- Investigation of surface bond characteristics under high strain rates (eg., blast shock waves) and fatigue loading.
- Experimental and analytical research on the use of different types of FRPs, including GFRP and AFRP.
- The investigation of environmental conditions on surface bond behaviour of FRP, including high temperature, fire, frost, and high humidity conditions.
- Further research on the effect of different concrete block masonry units, with different sizes and different wall thicknesses.
- Conduct large-scale tests to establish possible size effect and the verification of suggested design expressions.

NOTATION

a, a_0	Coefficients of bond models
A_p	($b_p.L_b$) Bond Area of FRP sheet (mm^2)
A_c	($b_c.L_c$) Area of Concrete (mm^2)
B	Coefficient of bond model
b_p	Width of FRP (mm)
Δb_p	Effected Width of FRP (mm)
b_c	Width of Concrete (mm)
c	Loading coefficient (1.0 for monotonic loading, 1.2 for cyclic loading)
c_f	Constant in a linear regression of the results of double shear or similar tests
f_c	Compressive strength of concrete cube (MPa)
f_{ctm}	Surface tensile strength of concrete determined in a pull-off test according to DIN1048 (Deutsches, 1991);
f_t , f_{ct}	Tensile strength of concrete (MPa)
f_p	Tensile strength of FRP sheet (MPa)
f_s	Compressive strength of concrete (MPa)
f_{st}	Surface tensile strength of concrete (MPa)
f'_c	Compressive strength of concrete cylinder (MPa)
E_a	Modulus of elasticity of adhesive material (MPa)
E_c	Modulus of elasticity of concrete (MPa)
E_m	Modulus of elasticity of epoxy mortar(MPa)
E_p	Modulus of elasticity of FRP sheet (MPa)
G_a	Shear modulus of adhesive (MPa)
G_c	Shear modulus of concrete (MPa)
G_f	Fracture energy ($N.mm/mm^2$)
K_a	Shear modulus over thickness of adhesive $\left(\frac{G_a}{t_a}\right)$
K_b , k_p	Geometric factors related to b_p and b_c
k_c	Constant which represents the level of concrete surface preparation
k_0	Initial stiffness of the bond–slip model

L_b, L	FRP bond length (mm)
L_{Spec}	Length of the concrete specimen(mm)
L_e	Effective bond length (mm)
N	Shear bond load
n	Popovics constant
n_p, n	Number of layers of FRP
P	Bond Load (N)
P_u	Ultimate bond load (N)
P_{max} , $P_{u,max}$	Maximum
s	Slip (mm)
s_o ,s_{max}	Slip in ultimate bond (mm)
s_f	Maximum slip (mm)
t_a	Thickness of (mm)
t_m	Thickness of the epoxy mortar
t_p	Thickness of FRP layer (mm)
t_{ref}, t_c	Reference bond thickness of concrete (mm)
U	Coefficients of bond models
w	Crack width (mm)
α, α_1, α_2	Coefficients of bond models
α_T, α_Y	Stiffness FRP to concrete proportion
β_p, β, β_w	Geometric factors related to b_p and b_c
β, β_1	Coefficients related to bond length
Δ	Relative slip between cracked surfaces(mm)
ε	Longitudinal Strain of FRP strip
ε_u , ε_{max}	Ultimate longitudinal strain of FRP strip
μ_2	Shear modulus of epoxy
ρ	Area proportion $\left(\frac{A_p}{A_c}\right)$
σ	Longitudinal Stress of FRP strip (MPa)
σ_u , σ_{max}	Ultimate longitudinal strain of FRP strip (MPa)

τ	Bond stress (MPa)
τ_u, τ_{max}	Ultimate bond stress (MPa)
ν_a	Poisson's ratio of adhesive material
ν_c	Poisson's ratio of concrete
λ	Coefficient related to slip amounts of s_o and s_f
λ_1 and λ_1	bond-slip coefficients
ω	Coefficient related to s_o, s_f, τ_{max} and stiffnes proprtaionof FRP to concrete

REFERENCES

ACI440.2.R- 02 (2002,2008), *Guide for the design and construction of externally bonded FRP systems for strengthening concrete structures.*

Ahmad and van Gemert (1999), *Effect of longitudinal carbon fiber reinforced plastic laminates on shear capacity of reinforced concrete beams*, Proceedings of the fourth International Symposium on Fiber Reinforced Polymer Reinforcement for Reinforced concrete structures, Baltimore, Maryland, USA, edited by C.W. Dolan, S.H.Rizkalla and A.Nanni, pp. 33-943, ACI, Farmington Hills, Michigan,USA.

Bizindavyi L, Neale KW. (1997) *Experimental and theoretical investigation of transfer lengths for composite laminates bonded to concrete.* In: Proceedings, Annual Conference of Canadian Society for Civil Engineering, Vol 6, Structures–Composite Materials, Structural Systems Telecommunication Towers, Sherbrooke, Que´bec, Canada;, pp. 51–60.

Bizindavyi L, Neale KW. (1999) *Transfer lengths and bond strengths for composites bonded to concrete.* J Compos Construct ASCE;3(4):153–60.

Blaschko, M., Niedermeier, R., and Zilch, K. (1996), *''Bond failure modes of flexural members strengthened with FRP.'' Fiber Compos. In Infrastruct., Proc., 2nd Int. Conf. on Compos. in Infrastruct.*, H. Saadatmanesh and M. R. Ehsani, eds., 315–327.

Brosens, K. (2001). *Anchorage of Externally Bonded Steel Plates and CFRP Laminates for the Strengthening of Concrete Elements.* PhD Dissertation, Department of Civil Engineering, Katholieke Universiteit Leuven.

Brosens, K. and Van Gemert, D. (1999). *Anchorage Design for Externally Bonded Carbon Fiber Polymer Laminates,* In: Dolan, C. W., Rizkalla, S. H. and Nanni, A. (eds), Proceedings of the 4th International Symposium on Fiber Reinforced Polymer Reinforcement for Concrete Structures, Baltimore, USA, pp. 635–645.

Brosens K, van Gemert D. (1998), *Plate end shear design for external CFRP laminates.* Proceedings of FRAMCOS-3. Freiburg, Germany: Aedificatio Publishers;, p. 1793–804.

Brosens K. and Van Gemert, D. (1997). "*Anchoring Stresses between Concrete and Carbon Fibre Reinforced Laminates*," Non-Metallic (FRP) Reinforcement for Concrete Structures, Vol. 1, Japan Concrete Institute, Japan, pp. 271-278.

Canadian Standard Association, (2002) *S806-02 Design and construction of Building Components with Fibre-Reinforced Polymers*, Toronto, ON, Canada, 2002, 178p.

Buyukozturk, O., Au, C. (2004) *Failure behaviour of FRP bonded concrete affected by interface fracture, Part 2. Moisture Degradation in FRP Bonded Concrete Systems: An Interface Fracture Approach*, , IST Group.

Buyukozturk O., Gunes O., E. Karaca (2004) *Progress on understanding debonding problems in reinforced concrete and steel members strengthened using FRP composites*, Construction and Building Materials 18 (2004) 9–19

Buyukozturk, O., and Hearing. B. (1998): *"Failure Behaviour of Precracked Concrete Beams Retrofitted with FRP.*" Journal of Composites for Construction 2 pp. 138-144.

Casareto M., Oliveri A., Romelli A., Lagomarsino S. (2003) *Bond behaviour of FRP laminates adhered to masonry 2 Advancing with Composites*, Plast, - rb2c.mst.edu

Chaallal O, Nollet MJ, Perraton D. (1998) *Strengthening of reinforced concrete beams withexternally bonded fibre-reinforced-plastic plates: design guidelines for shear and flexure*. Can J Civil Engng , 25(4):692–704.

Chajes, M.J.; Finch, W.W.Jr.; Januszka, T.F.; and Thomson, T.A. (1996). "*Bond and Force Transfer of Composite Material Plates Bonded to Concrete*", ACI Structural Journal, ACI, Vol. 93, No. 2, pp. 295-303.

Chajes MJ, Januszka TF, Mertz DR, Thomson TA, Finch WW. (1995) *Shear strengthening of reinforced concrete beams using externally applied composite fabrics.* ACI Struct J ;92(3):

Chen JF, Teng JG. (2001) *Anchorage strength models for FRP and steel plates bonded to concrete*. ASCE Journal of Structural Engineering, ASCE;127(1):784–791.

Chen JF, Yang ZJ, Holt GD. (2001) *FRP or steel plate-to-concrete bonded joints: effect of test methods on experimental bond strength*. Steel Compos Struct;1(2):231–44.

Chen JF, Teng JG. (2003), *Shear capacity of FRP strengthened RC beams: FRP debonding*. Construct Build Mater;17(1):27–41.

Chen JF, Pan WK. (2004) *Stresses in simple shear test specimens for steel or FRP-to-concrete bond strength a 3D finite element study*. In: Proceedings of the advanced composites in construction; 20–22 April 2004, Surrey. p. 473–82

Chen J.F., W.K. Pan (2006), *Three dimensional stress distribution in FRP-to-concrete bond test specimens*, Construction and Building Materials 20 (2006) 46–58

Comite′ Euro-International du Be′ton, CEB-FIP Model Code 1990(1993) (CEB-FIP MC90), Bulletin D'Information No. 215, Lausanne.

Dai J.G.,(2006) *Interfacial models for fiber reinforced polymer (FRP) sheets Externally bonded to concrete*, http://www.civil.hokudai.ac.jp/egpsee/alumni/abstracts/Dai.pdf

Dai JG, Ueda T. (2003) *Local bond stress slip relations for FRP sheets concrete interfaces. In: Proc. of 6th international symposium on FRP reinforcement for concrete structures*. Singapore: World Scientific Publications;. p. 143–52.

Dai, J.G., Saito Y., Ueda, T., and Sato, Y., (2006) *Static and Fatigue Bond Characteristics of Interfaces between CFRP Sheets and Frost Damage Experienced Concrete* SP-230—86 , 1515-1530

Dai, J.G., Ueda, T., and Sato, Y., (2006) *Unified Analytical approaches for determining shear bond characteristics of FRP concrete interfaces through pullout tests,* Journal of Advanced concrete technology V4 n 1, 133-145.

Dai, J.G., Ueda, T., and Sato, Y., (2005) *Development of the Nonlinear Bond Stress-Slip Model of Fiber Reinforced Plastics Sheet-Concrete Interfaces with a Simple Method* ASCE, Journal of Composites for Construction, 9(1, 52-62.

Darby J.J. (1999) *Role of bonded fibre reinforced composites in strengthening of structures'*, Strengthening of Reinforced Concrete Structures: Using Externally-Bonded FRP composites in Structural and civil engineering, edited by L.C. Hollaway and M.B. Leeming , Woodhead publishing Cambridge, UK.

Daus, S. (2004), "*Verification of a Design concept for the bond strength of externally bonded reinforcement on RC members*", *Darmstadt Concrete* 19, 17p.

Di Tommaso, A. Neubauer, A. Pantuso, U. and Rostasy, F. S. (2001), *"Behaviour of adhesively bonded concrete CFRP joints at low and high temperatures"*, *Mechanics of Composite Materials*, 37, n4, pp327-338.

Deutsches Institut für Normung, e.V. (1991). "*DIN1048, Augsgabe 6.91, Teil 2: Prüfverfahren für Beton, Festbeton in Bauwerken und Bauteilen.*" Beuth Verlag, Berlin (in German).

Eligehausen, R., Popov, E.P., and Bertero, V.V. (1983). *Local bond stress-slip relationships of deformed bars under generalized excitations. Report Nº 83/23, Envir. Engrg. Res.Council*, University of California, Berkeley, California.

Ferracuti B. Savoia M. Mazzotti C. (2006), *A numerical model for FRP–concrete delamination*, Composites: Part B 37 356–364

FORCA tow sheets technical notes. (1994). Autocon Composites Inc.,New York

Fuzukawa K, Numao T, Wu Z, Yoshizawa H, Mitsui M. (1997) *Critical strain energy release rate of interface debonding between carbon fibre sheet and mortar.* Non-Metallic (FRP) Reinforcement for Concrete Structures. Proceedings of the 3rd International Symposium, Vol. 1 Tokyo, Japan. Japan Concrete Institute;, p. 295–302.

Hiroyuki Y, Wu Z. (1997), *Analysis of debonding fracture properties of CFS strengthened member subject to tension*. Non-Metallic (FRP) Reinforcement for Concrete Structures. Proceedings of the 3rd International Symposium, Vol. 1 Tokyo, Japan. Japan, Concrete Institute; p. 287–94.2{5})

Hollaway L.C. and Leeming M.B. (1999) *Review of materials and techniques for plate bonding,* Strengthening of Reinforced Concrete Structures: Using Externally-Bonded FRP composites in Structural and civil engineering, edited by L.C. Hollaway and M.B. Leeming , Woodhead publishing Cambridge, UK.

Holzenkämpfer O. (1994). *Ingenieurmodelle des Verbundes geklebter Bewehrung für Betonbauteile. Dissertation, TU Braunschweig*, Germany.

Horiguchi, T. and Saeki, N. (1997). *"Effect of Test Methods and Quality of Concrete on Bond Strength of CFRP Sheet,"* Non-Metallic (FRP) Reinforcement for Concrete Structures, proceedings of the third international symposium, vol. 1; Vol. 1, Japan Concrete Institute, Japan, pp. 265-270.

Izumo, K., Saeki, N., Asamizu, T., and Shimura, K. (1997). *''Strengthening reinforced concrete beams by using prestressed fiber sheets.''* Proc., 3rd Int. Symp., Non-Metallic (FRP) Reinforcement for Concrete Struct., Vol. 1, Japan Concrete Institute, Tokyo, 379–386.

JCI Report,(2003) *"Technical report of technical committee on retrofit technology"*. Proc., international symposium on latest achievement of technology and research on retrofitting concrete structures.

Jiang JJ. (1984). *Nonlinear finite element analysis of RC structures*. Xian_an: Shanxi Science and Technology Press.

Kamel A., Elwi A.E. and Cheng R.J.J. *(2004), Bond model for FRP sheets bonded to concrete,* Emirates Journal for Engineering Research, 9 (2), 77-82

Kanakubo, T. Wu, Z.S. and Ueda T.(2005), "*Influence of local Bond characteristics in FRP-concrete bond behaviour*" http://www.kz.tsukuba.ac.jp/~kanakubo/4292.pdf

Kanakubo, T., Furuta, T., and Fukuyama, H., (2003) *Bond Strength between Fiber-Reinforced Polymer Laminates and Concrete*, Proceedings of FRPRCS-6, Edited by K.H Tan, Singapore, 8-10, July, 2003, 134-143, 12.

Kang, Q L.(1996), Finite element analysis for reinforced concrete, Beijing, China Water Power Press, 120-126

Kang Q L (1996) *Finite element analysis for reinforced concrete*, Beijing, China Water Power Press, 120-126

Karbhari V.M., Niu H., and Sikorsky C.(2006) *Review and Comparison of Fracture Mechanics-based Bond Strength Models for FRP-strengthened Structures* Journal of Reinforced Plastics and Composites; 25; 1757

Khalifa A, Gold WJ, Nanni A, Aziz A. (1998) *Contribution of externally bonded FRP to shear capacity of RC flexural members*. J Compos Construct ASCE;2(4):195–203.

Kobatake Y, Kimura K, Ktsumata H. (1993) *A retrofitting method for reinforced concrete structures using carbon fibre*. In: Nanni A, editor. Fibre-reinforced-plastic (FRP) reinforcement for concrete structures: properties and applications. Amsterdam: Elsevier;, p. 435–50.

Leung C. K.Y. and Pan J. (2005) *Effect of concrete composition on FRP/concrete bond capacity*, Proceedings of the International Symposium on Bond Behaviours of FRP in Structures (BBFS 2005)Chen and Teng (eds), 2005 International Institute for FRP in Construction

Lopez, M.M. (2000)."*Study of the Flexural Behaviour of Reinforced Concrete Beams Strengthened by Externally Bonded Fiber Reinforced Polymeric (FRP) Laminates*." Ph.D. Thesis University of Michigan,

Lopez, M.M., and A.E. Naaman. (2003) "*Concrete Cover Failure or Tooth Type Failure in RC Beams Strengthened with FRP Laminates.*" Fiber-Reinforced Polymer Reinforcement for Concrete Structures, Proc. of the Sixth International Symposium on FRP Reinforcement for Concrete Structures, 8-19 Jul. 2003, Singapore. Ed. Kiang Hwee Tan. River Edge: World Scientific Publishing Co., pp. 317 - 326.

Lorenzis, L., B. Miller, And A. Nanni, (2001) "*Bond of FRP Laminates to Concrete*", ACI Materials Journal, Vol. 98, No. 3, May -June 2001, pp. 256-264

Lorenzis, L. and Nanni, A., (2002) "*Bond Between Near Surface Mounted FRP Rods and Concrete in Structural Strengthening,*" *ACI Structures Journal*, 99, n2, March-April,pp. 123-133.

Lu X.Z. Jiang J.J. Teng J.G. Ye L.P., (2006), *Finite element simulation of debonding in FRP-to-concrete bonded joints*, Construction and Building Materials 20 (2006) 412–424

Lu X.Z. Ye L.P., Teng J.G., Ye L.P., Jianga, J.J., (2005a) *Bond–slip models for FRP sheets/plates bonded to concrete*, Engineering Structures 27 (2005) 920–937

Lu, X. Z., Teng, J. G., Ye, L. P. and Jiang, J. J. (2005b). *"Bond-slip models for FRP sheets/plates externally bonded to concrete*", Engineering Structures, 27(6), 938-950.

Lu X.Z. Ye L.P., Teng J.G., Jianga, J.J. (2005c) *Meso-scale finite element model for FRP sheets/plates bonded to concrete*, Engineering Structures 27 564–575

Lu, X.Z. Teng, J.G. Ye L.P. and Jiang J.J. (2004a) "*Bond–slip models for FRP sheets/plates bonded to concrete*" Proceedings of 2nd international Conference of advanced polymer composites for structural applications in construction (ACIC2004).Hollaway L C, Chryssanthopoulos M K, Moy S S J, eds.Cambridge, England : Woodhead Publishing Limited, pp152-161.

Lu XZ, Yan JJ, Wei H, Ye LP, Jiang JJ. (2004b) *Discussion on the key difficulties of finite element analysis for the interface between FRP sheet and concrete*, Proceedings of the 2nd National Civil Engineering Forum of graduate students of China; 2004. p. 134–7.

Maeda, T.; Asano, Y.; Sato, Y.; Ueda, T.; and Kakuta, Y. (1997). *"A Study on Bond Mechanism of Carbon Fiber Sheet," Non-Metallic (FRP) Reinforcement for Concrete Structures*, Vol. 1, Japan Concrete Institute, Japan, pp. 279-286.

MATLAB (2007)

McSweeney B.M. and M.M. Lopez, (2005) *FRP-Concrete Bond Behaviour: A Parametric Study Through Pull-Off Testing*, 441-459, FRPRCS-7

Meier, U. (1997). *''Post-strengthening by continuous fiber laminates in Europe.''* Proc., 3rd Int. Symp., Non-Metallic (FRP) Reinforcement forConcrete Struct., Vol. 1, Japan Concrete Institute, Tokyo, 41–56.

Miller, B. and Nanni, A., (1999) *"Bond Between CFRP Sheets and Concrete,"* Proceedings, ASCE 5th Materials Congress, Cincinnati, OH, L.C. Bank, Editor, May 10-12, pp. 240-247.

Miller, B., Nanni, A., and Bakis, C. E. (1999) *"Analytical Model for CFRP Sheets Bonded to Concrete," Proc. 8th Int Structural Faults and Repair Conf.*, M.C. Forde, Ed., Engineering Technics Press, Edinburgh, Scotland, 10 pp. CD-ROM version.

Miller B., Nanni A. and De Lorenzis L., (2001) *"Bond of FRP laminates to concrete"*, *ACI Material J.*, Vol. 98(3, pp. 246-254.

Monti, G., Renzelli, M. and Luciani, P. (2003). *FRP Adhesion in Uncracked and Cracked Concrete Zones*, In: Proceedings of the Sixth International Symposium on FRP Reinforcement for Concrete Structures(FRPRCS-6), Vol. 1, pp. 183–192. Singapore: World Scientific Publications;

Nakaba K, Toshiyuki K, Tomoki F, Hiroyuki Y. (2001a) *Bond behaviour between fiber-reinforced polymer laminates and concrete.* ACI Structural Journal;98(3):359–67.

Nakaba, K. Kanakubo, T., Furuta, T. and Yoshizawa, H. (2001b) *"Bond Behaviour between Fiber-Reinforced Polymer Laminates and Concrete"*, ACI Structural journal, no. 98-S34, May-June 2001, 9p.

Neubauer, U. and Rostasy, F.S., (1997) "*Design Aspects of Concrete Structures strengthened with Externally Bonded CFRP Plates*", Concrete and Composites, Proc. 7'h Int. Conf. on Structural Faults and Repair, ECS Pub. Edinburgh, Scotland ., V. *2*, pp.109-1 18

Niu, H. Wu, Z. (2005) "*Analytical modeling on debonding failure of FRP strengthened RC flextural structures*" Computer-Aided Civil and Infrastructure Engineering, 20, 2005, pp354–368.

Niu H, Wu Z. (2001) *Interfacial debonding mechanism influenced by flexural cracks in FRP-strengthened beams*. J Struct Engng JSCE A 2001;47:1277–88.

Oehlers, D.J.and Seracino, R. (2004), *Design of FRP and steel plated RC structures*, Adelaide, Australia, 2004, Elsevier, 228p.

Ouyang Z. AND Wan B. (2008) *Experimental and Numerical Study of Moisture Effects on the Bond Fracture Energy of FRP*/Concrete Joints Journal of reinforced plastics and composites, Vol. 27, No. 2/2008

Popovics, S. (1973). *A Numerical Approach to Complete Stress–Strain Curve of Concrete*, Cement and Concrete Research, 3(5): 583–599.

Saatcioglu M., Serrato F. and Foo S. (2007), Seismic Performance of Masonry Infill Walls Retrofitted with CFRP Sheets., Seventh International Symposium on Fibre Reinforced Polymer Reinforcement for Concrete Structures. ACI, SP 230, Paper No. 20, American Concrete Institute, pp. 341-354.

Sato, Y., Vecchio, F. J (2003)"*Tension stiffening and crack formation in reinforced concrete members with fiber reinforced polymer sheets*", ASCE, Journal of structural engineering, 129 (6) , 717-724.

Sato, Y., Asano,Y. and Ueda,T(2001)."*Fundamental study on bond mechanism of carbon fiber sheet*", concrete library International, JSCE, 37, 97-115.

Sato, Y., Ueda, T., Kakuta, Y., and Ono, S. (1997a) *''Ultimate shear capacity of reinforced concrete beams with carbon fibre sheet.''* Non-Metallic (FRP) Reinforcement for Concrete Structures, Proc., 3rd Int.Symposium, Vol. 1, Japan Concrete Institute, Sapporo, Japan, 499–505.

Sato, Y., Katsumata, H., and Kobatake, Y. (1997b) *''Shear strengthening of existing reinforced concrete beams by CFRP sheet.''* Non-Metallic (FRP) Reinforcement for Concrete Structures, Proc., 3rd Int. Symposium, Vol. 1, Japan Concrete Institute, Sapporo, Japan, 507–513.

Sato, Y., Kimura,K, and Kobatake,Y(1997c).*"Bond behaviours between CFRP sheet and concrete"* Journal of structural construction engineering, AIJ, No.500, 75-82.J

Sato, Y., Ueda, T., Kakuta, Y., and Tanaka, T. (1996). *''Shear reinforcing effect of carbon fibre sheet attached to side of reinforced concrete beams.''* Proc., 2nd Int. Conf. on Advanced Compos. Mat. in Bridges and Struct., M. M. El-Badry, ed., Canadian Society for Civil Engineering, Montreal, 621–627.

Savioa M, Farracuti B, Mazzotti D. (2003) *Non-linear bond–slip law for FRP concrete interface. In: Proc. of 6th international symposium on FRP reinforcement for concrete structures*. Singapore: World Scientific Publications; 2003. p. 163–72.

Serrato F.(2002) *Seismic retrofit of URM Infill Panels in reinforced concrete frames using FRP sheets*, MASC Civil Engineering, university of Ottawa.

Shadravan B., Saatcioglu M. (2009), The effect of cyclic loading on performance of surface bonded FRP sheets on concrete, 9th International Symposium on Fiber Reinforced Polymer Reinforcement for Concrete Structures, Sydney, Australia, Under Publish.

Shadravan B. , Saatcioglu M. and Foo S., (2007) *An investigation on the bond length of FRP sheets on concrete substrate*, 8th International Symposium on Fiber Reinforced Polymer Reinforcement for Concrete Structures, University of Patras, Patras, Greece, July 16-18.

Shalouf F, (2005) *Seismic Retrofit of Reinforced concrete Frames with diagonal Prestressing to FRP Strips*, PhD Thesis, Dep. Of Civil Eng., Univ. of Ottawa, 190p.

Swamy, R. N., Jones, R., and Charif, A. (1986). ''Shear adhesion properties of epoxy resin adhesives.'' *Proc., Int. Symp. on Adhesion between Polymers and Concrete*, Chapman and Hall, London, 741–755.

Täljsten, B. (1994). "*Plate Bonding. Strengthening of existing concrete structures with epoxy bonded plates of steel or fiber reinforced plastics*", Doctoral Thesis, Luleå University of Technology, Sweden.

Täljsten, B. (1996). *Strengthening of Concrete Prisms using the Plate-bonding Technique*, International Journal of Fracture, 82(3): 253–266.

Täljsten, B. (1997). "*Defining Anchor Lengths of Steel and CFRP Plates Bonded to Concrete*," Int. Journal of Adhesion and Adhesives, Vol. 17, No. 4, pp. 319-327

Takeo K, Matsushita H, Makizumi T, Nagashima G. (1997) *Bond characteristics of CFRP sheets in the CFRP bonding technique*. In: Proc. of Japan concrete institute, vol. 19, no. 2. June,p. 1599–604.

Tan Z. (2002) *Experimental research for RC beam strengthened with GFRP*. Master degree thesis, Tsinghua University, Beijing;

Teng JG, Yuan H, Chen JF. (2006) FRP-to-concrete interfaces between two adjacent cracks: theoretical model for debonding failure. Int J Solid Structures.

Teng JG, Smith ST, Yao J, Chen JF. (2003) *Intermediate crack-induced debonding in RC beams and slabs*. Construct Build Mater;17(6–7):447–62.

Teng J. G., Chen J. F., Smith S. T., Lam L.(2002a), *FRP-strengthened RC Structures: Strengthened RC Structures*, John Wiley and Sons.

Teng JG, Zhang JW, Smith ST. (2002b) *Interfacial stresses in reinforcedconcrete beams bonded with a soffit plate: a finite element study*. Constr Build Mater;16(1):1–14.

Teng JG, Chen JF, Simth ST, Lam L. (2002c) *FRP-strengthened RC structures.* UK: John Wiley and Sons.

Teng, J.G. Chen, J.F. Smith, S.T. and Lam, L. (2001) *FRP Strengthened RC structures,* John Wiley and Sons, Sussex, England , 2001, 245p

Teng JG, Lam L., Chan W. and Wong J. , (2000) *Retrofitting of deficient RC cantilever slabs using GFRP strips.* J Compos Constr, ASCE 4 2 ,pp. 75–84.

Triantafillou TC, Plevris N. (1992) *Strengthening of RC beams with epoxy-bon ded fibre-composite materials.* Mater Struct 1992;25:201–11.

Tripi J. M., Bakis C. E., Boothby T. E. and Nanni, A. (2000) *Deformation in concrete with external CFRP sheet reinforcement,* ASCE Journal of Composites for construction, May 2000/ 85-94.

Ueda T., and Dai J., (2005) "*Interface bond between FRP sheets and concrete substrates: properties, numerical modeling and roles in member behaviour*", *rog. Struct. Engng,* 7, pp27-43.

Ueda, T., and Dai, J.G., (2004) *New Shear Bond Model for FRP-Concrete Interface-from modeling to application,* Proceedings of the Second International Conference on FRP Composites in Civil Engineering-CICE, Adelaide, Australia, 69-81.

Ueda T, Dai JG, Sato Y. (2003) *A nonlinear bond stress–slip relationship for FRP sheet–concrete interface.* In: Proc. of international symposium on latest achievement of technology and research on retrofitting concrete structures. p. 113–20.

Ueda, T., Sato, Y., and Asano, Y. (1999) "*Experimental study on bond strength of continuous carbon fiber sheet.*" Proc., 4th Int. Symposium on Fiber Reinforced Polymer for Reinforced Concrete Structures, American Concrete Institute, Detroit, Mich., 407–416.

Ulaga, T., Vogel, T. and Meier, U. (2003). *Bilinear Stress–Slip Bond Model: Theoretical Background and Significance*, In: Proceedings of the Sixth International Symposium on FRP Reinforcement for Concrete Structures (FRPRCS-6), Vol. 1, pp. 153–162.

Van Gemert D. (1980) *Force transfer in epoxy-bonded steel–concrete joints.* Int J Adhes Adhesives , 1:67–72.

Vilnay O. (1988) *The analysis of reinforced concrete beams strengthened by epoxy bonded steel plates*, The Intematlonal Joumal of Cement Composites and Lightweight Concrete, Volume I0o Number2 May.

Wu Z.S., Yin J (2003) *Fracturing behaviours of FRP-strengthened concrete structures,* Engineering Fracture Mechanics 70 1339–1355.

Wu, Z.S., Yuan, H. and Niu, H. D. (2002). *Stress Transfer and Fracture Propagation in Different Kinds of Adhesive Joints*, ASCE Journal of Engineering Mechanics, 128(5): 562–573.

Wu Z.S., Yuan H, Hiroyuki Y, Toshiyuki K. (2001) *Experimental/analytical study on interfacial fracture energy and fracture propagation along FRP-concrete interface.* ACI International SP-201-8. p. 133–52.

Yang ZJ, Chen JF, Proverbs D. (2003) *Finite element modelling of concrete cover separation failure in FRP plated RC beams.* Constr Build Mater 2003;17(1):3–13.

Yang YX, Yue QR, Hu YC. (2001) *Experimental study on bond performance between carbon fiber sheets and concrete.* Journal of Building Structures 2001;22(3):36–42

Yao, J. Teng, J.G. and Chen, J.F. (2005) "*Experimental study on FRP to concrete bonded joints*", Composites, 36 Part B 2005, pp99-113.

Yoshizawa, H.; Wu.Z., Yuan H, Kanakubo T ,(2000)."*Study on FRP-concrete interface bond performance*", transactions of JSCE, 49 (662), 105-119.

Yoshizawa, H.; Myojo, T.; Okoshi, M.; Mizukoshi, M.; and Kliger, H. S. (1996). "*Effect of Sheet Bonding Condition on Concrete Members Having Externally Bonded Carbon Fiber Sheet*," Fourth Materials Engineering Conference, ASCE Annual Convention, Washington D.C.

Yuan H, Teng JG, Seracino R, Wu ZS, Yao J. (2004) *Full range behaviour of FRP-to-concrete bonded joints: a closed-form analytical solution.*, Engineering Structures 2004;26(5):553–64.127(7):784–91

Yuan, H., Wu, Z. S. and Yoshizawa, H. (2001). *Theoretical Solutions on Interfacial Stress Transfer of Externally Bonded Steel/Composite Laminates*, JSCE Journal of Structural Mechanics and Earthquake Engineering, 18(1): 27–39.

Yuan, H., Wu, Z. S., and Yoshizawa, H. (2000) ''*Theoretical solutions on interfacial stress transfer of externally bonded steel/composite laminates.*''J. Struct. Mech. Earthquake Eng., Japan Society of Civil Engineers, *Tokyo,* 18~1, 27–39.

Yuan H, Wu Z. (1999) *Interfacial fracture theory in structures strengthened withcomposite of continuous fiber.* In: Proceedings, Symposium of China and Japan, Science and Technology of 21st Century, Tokyo, Japan; pp. 142–55.

Zhao M., Dong Y., Zhao Y., Tennant A, and Ansari F. (2007) *Monitoring of Bond in FRP Retrofitted Concrete Structures,* Journal of Intelligent material systems and structures, Vol. 18—August 2007.

Zhao HD, Zhang Y, Zhao M. (2000) *Research on the bond performance between CFRP plate and concrete.* Proc. of 1st conference on FRP concrete structures of China. p. 247–53.

Ziraba YN, Baluch MH, Basunbul AM, Azad AK, Al-Sulaimani GJ, Sharif IA. (1995) *Combined experimental–numerical approach to characterization of steel–glue–concrete interface.* Mater Struct;28:518–25.